MULTIAXIAL FATIGUE CHARACTERIZATION OF SELF-REINFORCED POLYLACTIC ACID-CALCIUM PHOSPHATE COMPOSITE

Zaleha Binti Mustafa

Submitted in fulfilment of the requirement for the
Degree of Doctor of Philosophy (PhD)

Biomedical Engineering Division
School of Engineering
College of Science and Engineering
University of Glasgow

October 2012

ABSTRACT

The majority of failures of mechanical components are caused by fatigue. Unlike many conventional engineering components, implants in the body are subjected to complex multidirectional loading patterns, thus fatigue not only occurs under axial, fully or partly reversed loading, but also under torsional loading.

The fatigue behaviours of self-reinforced poly lactide composite (PLA) of unidirectional PLA fibres in PLA matrix containing tricalcium phosphates (TCP), (PLA-PLA-TCP) produced via pre-pregging technique has been investigated. Quasi-static test results indicated that PLA-PLA-TCP is stronger in tension than in compression and torsion and is significantly influence by moulding temperature. Uniaxial fatigue testing at 37° C in saline solution established S-N (Wöhler) curves for both axial and torsional loading for two moulding temperatures (140°C and 150°C). Compression loading showed significant effect on the axial fatigue behaviour. Biaxial fatigue results showed that the addition of torsion to axial loading significantly reduced the fatigue life. Out-of-phase loading was less detrimental to the fatigue life than in-phase. Fatigue development was evaluated by reduction in secant modulus and increase in energy absorbed. The threshold number of cycles at which damage starts to accumulate in the composite was found to be load ratio and direction dependent.

The effects of the degradation process in saline solution on the fatigue behaviour of the composite were also studied at 25% of the ultimate tensile and shear stresses. The specimens were immersed for 8, 12, 16 and 20 weeks periods before testing. The results indicated that even though immersion in saline solution reduced the static and cyclic properties of the composite, it still had good strength retention and comparable to the cortical bone at the end of 20 weeks of degradation period.

Microscopy examination on the fracture surface indicated that in uniaxial tension-compression fatigue, the failure was dominated by compression and failed via microbuckling mechanism. Biaxial fatigue failure was dominated by shear mechanisms with evidence of interfacial failure and fatigue striations.

TABLE OF CONTENTS

LIST OF TABLES

LIST OF FIGURES

TO:

MY FATHER

MUSTAFA SIDEK

ACKNOWLEDGEMENTS

All praise is due to Allah. May Allah's peace and blessings be upon the one after whom there is no other prophet.

It takes more than determination and hard work for the completion of this dissertation. Support I received from many people throughout my years here at University of Glasgow has undeniably played an important role. For that, I am forever grateful to the many individuals that assisted along the way.

First, I would like to thank Professor Elizabeth Tanner, my wonderful supervisor. Her unwavering patience, kindness and mentorship guided me through the process, her easily understood explanations and open mind allowed me to grow and learn in such a way that I am now a better researcher.

Very special thanks to the Ministry of Higher Education of Malaysia and University Technical Malaysia Melaka (UTeM) for the opportunity for further study as well as financial support.

Needless to mention, experimental obstacles might not able to be coped without the assistance of the technical staff. Hereby I would like to express my sincere appreciation to Mr. John Davidson, Mr. Brian Robb, Mr. Walter Robinson, Mr. Peter Chung and others for their help and patience in providing me the resources in completing this dissertation.

To my family and friends, my greatest treasures and gifts in my life, thank you. I am forever grateful to my father and my mum for instilling in me a desire to achieve my goals and a commitment to finish what I start, to the best of my ability, no matter what it takes. To my sisters, thank you for being such a strong pillar to our family these years while I away to complete this mission.

With all my heart, I would like to thank my friends Norilmi Ismail, Rainah Ismail, Aqilah Aziz, Adilah Azhari, Rafidah Cusairi, Siti Hajar Fadzullah, Salwahidayah Othman and Weamm Jaafar very warmly for their continuous help and encouragement. To Ross Colquhoun, a dear and understanding friend that anyone could wish for, thank you and I shall treasure our friendship forever.

For myself, this dissertation has been a personal accomplishment, which I hope will benefit others as much as it has me.

AUTHOR'S DECLARATIONS

I hereby declare that the thesis which follows is my own composition, that it is a record of the work done myself, and that it has not been presented in any previous application for a higher degree.

Zaleha Binti Mustafa

NONMENCLATURE

θ	Angle of shear (°)
°	Degrees
δ	Elongation (mm)
E	Young's modulus (GPa)
G	Shear modulus (GPa)
ν	Poisson's ratio
τ	Shear stress (MPa)
τ_{max}	Maximum shear stress (MPa)
ε	Longitudinal strain
γ	Shear strain
σ	Axial stress
$\sigma_{1,2}$	Maximum/minimum principal stress (MPa)
$\sigma_{C,T}$	Compressive/Tensile stress (MPa)
A	Cross sectional area of specimen (mm^2)
ρ	Density (Mgm^{-3})
$d_{g,s}$	Diameter in gauge length, shoulder of specimen (mm)
HA	Hydroxyapatite
I_F	Tsai-Wu value
L,l	Length of test section (mm)
$l_{s,g}$	Length of gauge section, shoulder of specimen (mm)
M_N	Molecular weight-number average
M_W	Molecular weight- weight average
N	Number of cycles
N_f	Number of cycles to failure
P	Applied force (N)
PGA	Polyglycolic acid
PLA	Polylactic acid
PLLA	Poly-L-lactic acid
PDLA	Poly-D-lactic acid
PLDLA	Poly-L-D-lactic acid
TCP	Tricalcium phosphate
α-TCP	α-tricalcium phosphate
am-TCP	am-tricalcium phosphate
ap-TCP	ap-tricalcium phosphate
B-TCP	B-tricalcium phosphate

BCP	Biphasic calcium phosphate
r	Radius of gauge section (mm)
$_{r.a}$	Real/apparent (correction factor)
T	Applied torque (Nm)
UCS	Ultimate compressive strength (MPa)
USS	Ultimate shear strength (MPa)
UTS	Ultimate tensile strength (MPa)
$V_{f,m}$	Volume fraction of fibre/matrix
X_t, X_c and X_s	Yield strengths under tensile, compression and torsion respectively (MPa)

CHAPTER 1 - INTRODUCTION

"Bone is power. It is bone to which the soft parts cling, from which they are, helpless, strung and held aloft to the sun, lest man be but another slithering earth-noser. What is this tissue that has double the strength of oak?"

Richard Selzer.

The development of bioresorbable and simultaneously bioactive PLA-based composites has progressed from partially absorbable PLA composites reinforced with carbon fibres to totally absorbable composites reinforced with calcium phosphates, such as hydroxyapatite (HA) (Wright-Charlesworth et al., 2006) or tricalcium phosphate (TCP), particles or fibres or bioactive glass particles (Cool et al., 2007) and with PLA fibres (Bleach et al., 2002) in fracture fixation applications. Biodegradable implants have many advantages compared to metallic implants, as they are able to provide adequate fixation during fracture healing but also degrade slowly in the body thus eliminating the need for a removal operation. As the implant slowly degrades during application, this allows gradual stress transfer from the implant to the healing bone, not only reduces the risk of osteoporosis but also stimulates bone growth and remodelling (Viljanen et al., 2001).

However, as most applications in the body are subjected to cyclic loads, with 1 million cycles per annum estimated for finger joints while in hips, it ranges from 0.5 to 2 millions cycles per annum depending on the patient's age and activity levels (Wallbridge and Downson, 1982). Thus if self reinforced polylactides acid – tricalcium phosphate filled composite (PLA-PLA-TCP) is to be used in cyclically loaded implants, its fatigue behaviour needs to be investigated. Another challenge of using degradable polymer such as polylactides as internal fixation devices is when used alone, they do not have adequate mechanical properties for use in load-bearing application. However, a self-reinforcing manufacturing method is adopted in this study in order to improve the mechanical properties of the polymer. Incorporating fillers such as calcium phosphate has not only

increased the bioactivity of the polymer but also altered the degradation behaviour of the matrix polymer.

This thesis is divided into 7 chapters. Chapter 2 is a comprehensive review of the literature, which includes description of the bone structure and some representative polymeric based biomaterials as well as a brief comparison of their mechanical properties. The background of uniaxial and multiaxial fatigue theory is also considered. Chapter 3 outlines the materials of interest and experimental technique used to characterize the materials, including the methods of post-testing analysis such as stress analysis and microscopic examinations. The results and discussion accompany the finding are presented in three chapter; Chapter 4 covers the physical, quasi-static testing, uniaxial fatigue as well as consideration of the effect of moulding temperature on the mechanical properties of the unidirectional composite. Chapter 5 deals with the alterations on fatigue properties in effect of the combination of different loading level as well as phase angle. Chapter 6 explores the effect of the fatigue properties of the composite in regards to degradation activities by saline solution. In this study the composite were immersed for up to 20 weeks prior to the testing. Failure modes are illustrated with fractography of the fracture surfaces to provide in depth understanding of the failure. Chapter 7 summarises the finding of the project together with future research, which should lead on from this project.

The aims of this thesis were to:

1. to study the effect of moulding temperature on the uniaxial fatigue life of PLA-PLA-TCP composite

2. to study the biaxial fatigue behaviour of PLA-PLA-TCP composite

3. to study the effect of the degradation on the uniaxial fatigue behaviour of the composite

Within the first aim, the specific objectives were to:

1. investigate the effect of the compression moulding temperature on the mechanical testing of the composite both tensile, compressive and torsion properties of the PLA-PLA-TCP composite.

2. gain greater understanding the fatigue behaviour of the composite under uniaxial loading by establishing an S-N curve in order to provide better estimation of the fatigue lives, observing the degradation on the mechanical properties of the composite due to fatigue via by reduction in secant modulus and increase of energy absorbed with respect to different moulding temperature

3. investigate the effect of compressive loading mode on the fatigue life of the composite

Within the second aim, the specific objectives were to:

1. investigate the effect of combined stresses on the fatigue life on PLA-PLA-TCP composite

2. investigate the effect of phase angle on the fatigue life of the PLA-PLA-TCP composite

Within the third aim, the specific objectives were to:

1. investigate the effect of the in vitro degradation of the composite on the tensile and torsion properties as well as uniaxial fatigue behaviour at fully reversed tension-compression and torsional loading at low level stress (25% of ultimate strengths)

CHAPTER 2 - BONE AND BIOMATERIALS

2.1 STUCTURE AND MECHANICS OF BONE

Bone describes both the structures and the materials of which they are made. The system has a complex structure and function at the macroscopic, microscopic and ultramicroscopic levels and has various chemical and physiological interrelations. Bone is a composite that composes of three major components which are a tough collagen fibre matrix, a natural polymer (around 20 wt.%), stiffened by calcium phosphate mineral (69 wt.%), while the rest consists of a mixture of water (9 wt.%) and other organic compound such as mucopolysacchrides and protein polysaccharides (Currey, 1998, Park and Lakes, 2007).

2.1.1 Bone structure

2.1.1.1 Primary Bone

Mammalian bone exists in two fairly distinct forms which are woven bone and lamellar bone, also known as primary bone. Woven bone is laid down very quickly, reported more than 4 μm thickness per day, and is usually found in foetuses and the callus which is produced in early stages of fracture repair. The collagen fibres are randomly orientated, fine, being around 0.1 μm in diameter. In comparison with woven bone, lamellar bone is laid down much more slowly in more precise arrangement with less than 1 μm thickness deposited a day. On the molecular scale, the bone mineralcrystals and collagen are arranged in sheets known as lamellae (Currey, 1998). The collagen found in bone mainly type I, twisted in a helicoidal structure that consist of two α_1 and one α_2 amino acid chains. These chains are then coiled in a right handed super helix to form 30 nm long tropocollagen molecules. These molecules then are stacked together with a substantial overlap to form microfibrils. Under the electron microscopy, regular transverse striations are observed on the microfibrils resulting from the staggered arrangement of the tropocollagen (Vaughan, 1975).

The bone mineral apatite crystals have a hexagonal lattice and similar chemical formula to hydroxyapatite, $Ca_{10}(PO_4)_6(OH)_2$. The crystals are aligned parallel to

the collagen fibrils and act as reinforcements to provide a very strong and tough composite (Hench, 2005). The stoichiometric ratio of calcium to phosphorus in human bone is 1.67 but it has been reported to vary from 1.37 to 1.91 usually with the lowest values from young children and in elderly bone (Boskey, 2004).

Ion substitution occurs; therefore the apatite in bone is not exactly stoichiometric hydroxyapatite. Sodium, strontium and lead ions can substitute for the calcium ions and fluoride or chloride can substitute for the hydroxyl ions and carbonates for the hydroxyl or phosphate ions. While other ions that cannot be accommodated by apatite lattice such as potassium, it is believed that they are absorbed onto the surface (Martin, 1999).

On the microscope scale, collagen fibres are arranged into lamellae, which can be in the form of sheets or be organized around a Haversian canal to form a Haversian system or osteon. The central Haversian canal, containing blood vessels, is surrounded by concentric lamellae of circumferentially arranged osteocytes making up the Haversian system. Adjacent lamellae within the osteon have preferred collagen fibre orientations with alternating directions, but the osteons are arranged so their long axes are aligned with the long axis of the bone. The diameter of an osteon is limited by the need for lamellae to be within diffusion distance of the Haversian canal to allow effective transport of nutrients in and waste products out. Communications between the osteons and the medullary cavity is achieved by the presence of Volkmann's canals, which run transversely. The osteons pack together to form cortical bone, the most organised mineralised tissue in the body. They are surrounded by lamellar bone laid down in sheets and on the endosteal (inner) and periosteal (outer surfaces) of cortical bone, a layer of osteogenic cells exist (Hench, 2005).

The location of cortical bone in a femur, a typical long bone, is shown in Figure 2.1, which also shows that on the microstructural levels, a second type of lamellar bone known as trabecular or cancellous bone is situated at the bone ends, found below the joint surface. Trabecular or cancellous bone consists of a branched network of bony tissue surrounded by marrow with the thickest trabeculae orientated in the direction of maximum stress. The trabeculae are made of lamellar bone, but with virtually no internal blood vessels as the

nutrients are received from the intratrabecular spaces. This structure provides mechanical strength without excessive weight and allows concentrated loads to be dispersed. For example, where tendons and ligaments are attached to the bone or below joint surfaces, cancellous bone allows impact loads to be resisted. It also gives a large reaction area for metabolic activities. Bone remodelling takes place directly on the surface of the trabeculae and this is much more active than in cortical bone (Vaughan, 1975; Black, 1988; Revell, 1998).

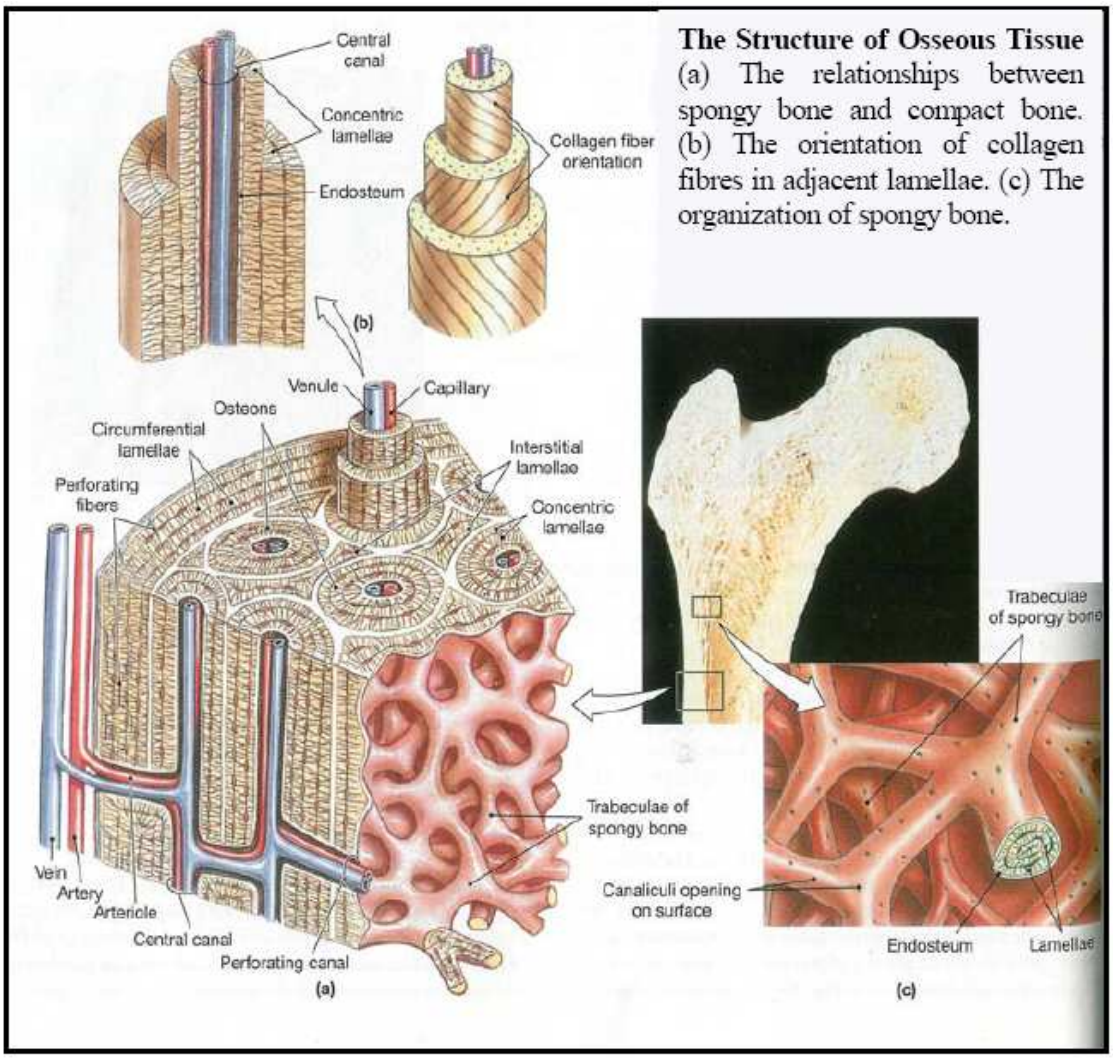

Figure 2.1 Typical bone structures (from Martini, 2004)

2.1.1.2 Secondary Bone

In cortical bone, there are variations in the degree of mineralization of the osteons as results from remodelling of the primary bones, forming secondary bone. Remodelling process can be understood as the adaptation ability of the bone to changes to its mechanical conditions. Wolff first postulated in late 19th Century “the law of bone remodelling” which is the law according to which

“alterations of the internal architecture are clearly observed and following mathematical rules, as well as secondary alterations of the external form of the bones following the same mathematical rules, occur as a consequence of primary changes in the shape and stressing or in the stressing of bones” (Brand and Claes, 1989).

There are three major types of cells present in bone namely osteoblasts, osteocytes and osteoclasts. Osteoblasts are normally located on the surface of bone, are mononucleate and their functions are to make osteoid and manufacture hormones, such as prostaglandins. Osteoblasts produce alkaline phosphatase, a type of hydrolase enzyme that responsible to remove phosphate groups, and has important role in bone mineralization as well as many matrix proteins (Davies, 1999).

Osteocytes are mature bone cells, originate from osteoblasts which have migrated into and become trapped in lacunae that is pores in bone. Osteocytes have many function including formation of bone, matrix maintenance and calcium homeostasis. They also act as mechanosensory receptors regulating the bone’s response to stress (Martini, 2004).

Osteoclasts are large, multinucleated cells located on bone surfaces in resorption pits, known as Howship’s lacunae and are responsible for bone resorption. Osteoclasts tunnel through the bone to form cylindrical spaces through which blood vessels grow. Osteoblasts follow behind laying down new lamellar bone circumferentially around the blood vessels, forming secondary osteons. As the bone tissue is laid down, the osteon becomes mineralized. Since the rate of remodelling is variable, so will be the degree of mineralization in different osteons. A layer of cement separates both the lamellae within the osteon and osteons themselves. Between the Harversian systems, interstitial bone, areas of mineralized matrix left by earlier remodelling processes remain. The structure of a secondary osteon is shown in Figure 2.2.

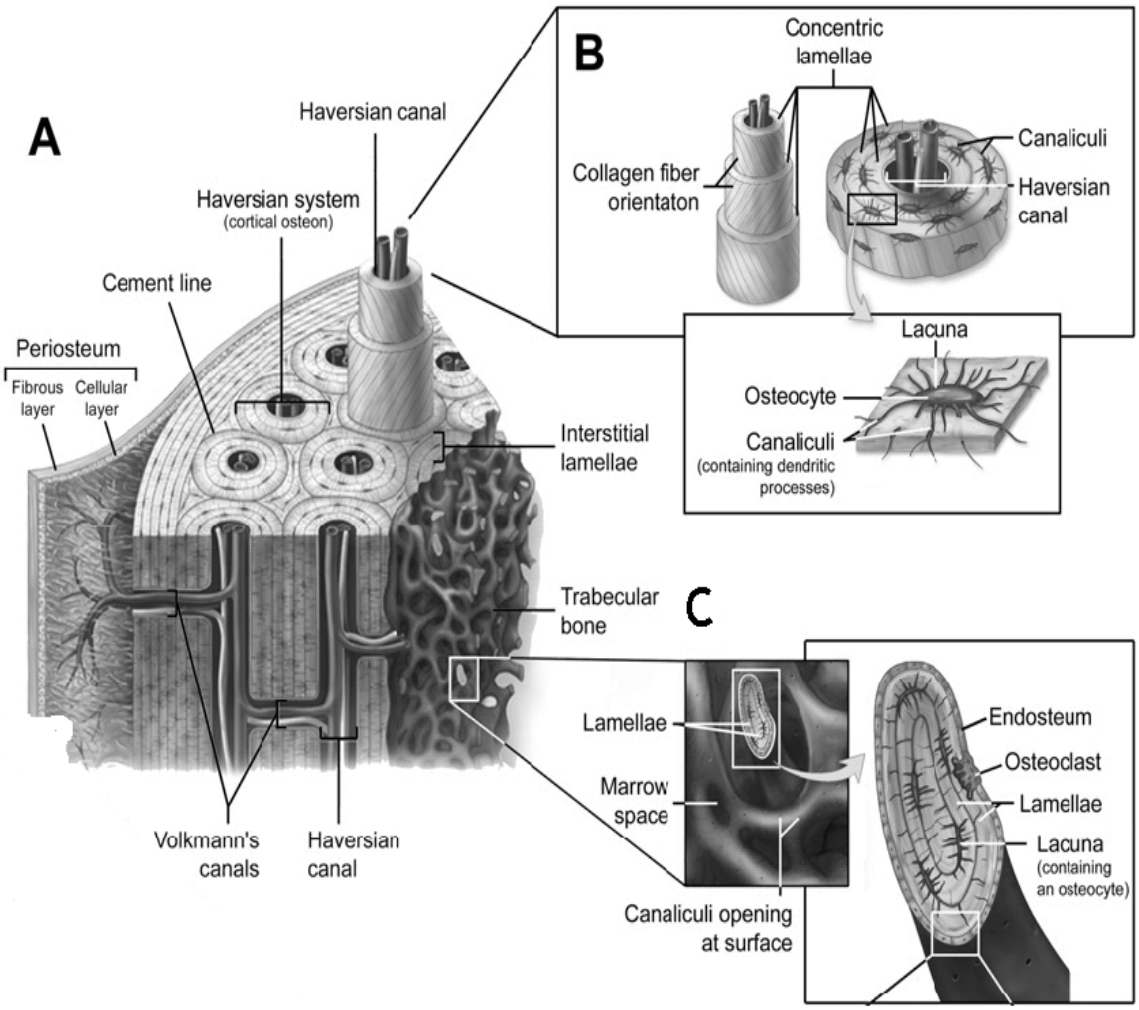

Figure 2.2 The microstructure of secondary cortical bone

(a) schematic of bone microstructure (b) cortical bone osteon or Haversian system with central Haversian canal, concentric lamellae, and uniformly spaced lacunae (c) trabeculae shown in cross section with lamellae of bone, lacunae, and outer covering of endosteum (from McKinley and O'Loughlin, 2008)

2.1.2 Mechanical Properties

Bone is linear elastic and brittle in nature, at the same time an anisotropic and viscoelastic material. Thus, the mechanical properties of bone cannot be stated simply since there are many factors that will affect its strength and stiffness such as porosity, degree of mineralization, the orientation of the collagen fibres and others (Martin, 1999). Test condition such orientation of samples with respect to the long axial axis of the bone, loading mode as well as strain rate also can influence the outcome of their mechanical properties. However, in order to aid with the design of osteoimplants, it is necessary to establish the range of mechanical properties of bone, as summarized in Table 2.1. Cortical

bone is stronger and stiffer than cancellous bone. Cancellous bone is porous and this leads to the lower mechanical properties (Gibson and Ashby, 1997).

Table 2.1 Some mechanical properties of human bone

(from Currey, 1998; Hench and Wilson, 1993)

	Cortical Bone	Cancellous Bone
Compressive strength (MPa)	100-230	2-12
Flexural , tensile strength (MPa)	50-150	10-20
Young's (tensile) modulus (GPa)	7-30	0.05-05
Fracture toughness (MPa $m^{1/2}$)	2-12	-
Strain to failure (%)	1-3	5-7

2.2 MATERIALS FOR BONE REPLACEMENT

In the last few decades, rapid progress in materials engineering research has lead to vast changes in materials development and utilization. Biomaterial applications span from total replacement of tissues and organs to improve function, corrective and repairs device to restore the function of the traumatized or degenerated tissues, to help in correct abnormalities and healing of the damaged tissue in order to improve the quality of the patient's life. As early as 1900s, biomaterials have been studied and the first breakthrough was made when steel was used to assist fracture fixation. However, in these early years, due to lack of understanding of material behaviour and mechanical forces, many of these bone plates failed. Over time, the understanding of the requirement for the biomaterials increased, resulting in accelerating of growth in development in biomaterials field. Metals, ranged from stainless steel, cobolt-chrome alloys to tantalum and titanium alloys are now used successfully. Beside metallic based materials, ceramics and glasses, classified as either inert such as alumina and zirconia or active (calcium phosphate and bioglasses) have also been discovered to have a good potential for use as biomaterials. They can be used both alone in dense or porous form or in combination with another material in form of composites.

Biomaterials usually refer to the synthetic materials used to replace part or function of living system and have an intimate contact with living tissue. Over

the years, numerous definitions have been proposed. The Clemson University Advisory Board for Biomaterials has officially defined a biomaterial to be “a systemically and pharmacologically inert substance designed for implantation within or incorporation with living systems” (Park and Lakes, 2007). Black (1992) defined biomaterials as “a nonviable material used in a medical device, intended to interact with biological system”. Other authors such as Bruck (1980) define biomaterials as “materials of synthetic as well as of natural origin in contact with tissue, blood, and biological fluids…. without adversely affecting the living organism and its component”. Williams (1999) define biomaterials both as “non-viable materials used in a medical device, intended to interact with biological systems” and “materials intended to interface with biological systems to evaluate, treat, augment or replace any tissue, organ or function of the body”.

In comparison, a biological material is a material such as skin or artery produced by a biological system. In general, biomaterial shall be used in this thesis to denote a man made material that is used in the biological situation.

The success of biomaterials in the body depends of many factors such as materials properties, design, biocompatibility, reliability, ease of manufacture and others. Consequently, even if only one of these factors is perfectly controlled, for example the mechanical design, so that the corresponding reliability is unity, other factors such as biocompatibility can severely affect the utility represented by the total reliability of the implants. Table 2.2 summarizes the number of requirement for the biomaterials.

Table 2.2 The requirement for biomaterials performance

(adapted from Williams, 1999)

Requirement	Implications
Materials properties	Strength and stiffness similar to the tissue or organ that it going to replace. Must have sufficient fatigue properties so failure will not occur prematurely
Design	Proper design that will give the adequate mechanical properties during application to avoid failure due insufficient strength
Biocompatibility	Non-toxic, non-irritant, non-carcinogenic, non-allergic
Reliability	Several different failure modes may be operating that control the probability of failure of the implant such as mechanical or biological deficiencies.
Ease of manufacturing	The materials should be relatively inexpensive and easy to mass produce, able to be sterilised without altering their mechanical properties and easy to use by surgeon

Biomaterials can be classified into three major groups based on their response in the host, which are bioinert, bioactive and biodegradable. The bioinert are considered to be inert in biological environment (Williams, 1999). Thus the materials should not cause any significant response with the host when implanted. However, in practice, totally inert materials do not exist. Thus it will be more appropriate to call this group as “nearly bioinert group”. Most of the bioinert materials are metal, but some ceramics and polymers are also included. The normal biological response to nearly bioinert materials is a thin and stable fibrous layer. Bioactive materials are materials that “show the ability to interact beneficially with the host or induce specific biological activity with the surrounding tissue in a specific application or function” (Williams, 1999). These materials are commonly ceramics and glasses. Biodegradable materials will breakdown in the body after a period of time and are then replaced by new tissue as they degrade (Williams, 1987). The materials in this group are mainly

polymers and certain calcium phosphate based ceramics or such as tricalcium phosphate (TCP) or glass.

One of the main issues when dealing with biomaterials is biocompatibility since a metal implant can corrode or release ions in an in vivo environment (Williams, 1982). It involves the acceptance of artificial implants by the surrounding tissue and by the body as a whole. In the early years of biomaterials development, biocompatibility meant that the materials should be totally inert in the biological environment, not provoke any abnormal inflammatory response, be non-toxic, non-carcinogenic, non-allergenic and not cause cancer. However, since later research showed that no material is totally inert in the body, the view of the biocompatibility has become more complex. In vivo studies suggest that most foreign materials are treated as harmful and provoke adverse reaction such as inflammation, fibrous tissue formation, infections and blood clotting (Huskins et al., 1999). In the past, for example materials such as vanadium steel, was chosen for its good mechanical properties, corroded rapidly in the body. Titanium is one of the most corrosion resistant metals but still traces of it found in tissues remote to where it has been implanted. This finding suggested that it does break down or degrade in some way in the body. Therefore, it is inappropriate to base biocompatibility on an inert response alone. Therefore, Williams (1999) has defined biocompatibility as "as the ability of a material to perform with an appropriate host response in a specific application".

A different viewpoint was taken by Black (1992) using the term "biological performance" as the interaction between materials and living systems in defining biocompatibility. This interaction involves consideration of various host responses such as local and systematic responses, other than the intended therapeutic response, of the living systems to the material and the material's response to the body. This is particularly crucial when evaluating the effect of degradation characteristics on biological performance of the degradable polymers. Several tissue responses have been identified in order to give a better understanding on how the host responds to implants (Dumitriu and Dumitriu, 1994) such as immediate, intense inflammatory reaction, which may be aseptic, produced by rapid rejection of the implants, long term rejection after infiltration by mononucleic cells and macrophages, incomplete fibrous

encapsulation with cellular reaction or completed fibrous encapsulation without cellular reaction. In some cases, slow resorption by infiltration of giant cells or macrophages occurs. Lastly complete bioactivity that can be characterized by development of new functional cells, specific to the tissue in which the implantation took place.

Thus, is crucial that polymers, particularly degradable ones undergo long-term biocompatibility testing to determine if the biological response is adequate to evaluate both the effect of the reaction in the surrounding tissues and in the polymer after implantation.

Apart from that, many of the commercial bone substitute materials that have been developed incorporate calcium phosphates in their system for not just good biocompatibility, but to provide bioactivity, to promote osteoconductivity and at the same time was found to develop osteoinductive ability (Descamps et al., 2008). Osteoinduction can be defined as the "undifferentiated mesemchymal cells were induced to differentiate into the osteogenic lineage, and ultimately to form new bone" occurring away from bone (Friedenstein, 1968; Wilson-Hench, 1987). Osteoconduction referring to process of bone growth on and across a surface. Wilson-Hench (1987) suggested that osteoconductivity is a process by which bone is directed so as to conform to a material's surface.

2.2.1 Degradable Polymers

Biodegradable polymers have been used in surgery for thousands of years, sutures made from gut are thought have been used as early as AD 175 (Parson, 1985). Considering the rapid development in degradable polymeric biomaterial field, it is possible that in future, they may replace biostable biomaterials.

Degradable polymers are normally used in applications where they are no longer required after the defect or fracture has healed. Their applications range from wound closing materials (suture), drug delivery systems, fracture fixation implants and degradable scaffolds. The "biodegradable" term is associated with materials that can be broken down either through hydrolytic mechanism without help of enzymes or with enzymatic mechanism. In the literature, terms have been used to indicate biodegradable such as absorbable, erodible and

resorbable. The shift of interest to this type of material is due to several advantages over non-biodegradable materials. One of the major advantages is there is no need for a second surgical operation to remove the implant once the fracture has healed. Secondly, biodegradable polymers should not display a permanent chronic reaction with the host tissue as the body gradually absorbs them during degradation process and then do not leave permanent residue. Third advantage is they also can trigger tissue regeneration, often achieved by incorporating bioactive fillers with degradable polymer. In addition, as the material degrades gradually, a gradual transfer between the implant and tissue is possible thus preventing from stress shielding from occur.

2.2.1.1 Classes of degradable polymer

Degradable polymer can be grouped into natural and synthetic polymers groups (Table 2.3). Natural polymers are usually derived from renewable resources, such as plant, animal and micro-organism. Synthetic polymers are normally manufactured from petrochemical resources.

Table 2.3 Classes of degradable polymers (adapted from Vert and Guérin, 1991)

Synthetic	Natural
Polypeptides Polydesipeptides Nylon-2/nylon-6-copolyamides Aliphatic polyesters: Poly(glycolic acid) (PGA) and its copolymers Poly(lactic acid)(PLA) and its copolymer and stereocopolymers Poly(alkylene succinates) Poly(alkaline oxalates) Poly(hydroxybutyrate)(PHB) Poly(butylene diglycolate) Poly(ε-caprolactone)(PCL)and its copolymers Poly(dioxannone) and its copolymers Poly(amino trizoles) Poly(dihydropyrans) Poly(phosphazenes) Poly(ortho esters) Poly(cyno acrylates)	Modified polysaccharides (cellulose, starch, chitin etc.) Modified proteins (collagen, fibrin, PHB etc.)

Poly(α-hydroxy acids), such as poly (lactic acid) (PLA), poly(glycolic acid) (PGA) and their copolymers are the most extensively used synthetic polymers, from as early as 1960's. The earliest applications were mostly for wound closure such as sutures. Nowadays, they are used ranges from large implants, to nano size drug delivery devices and porous tissue engineering (Middleton and Tipton, 2000; Vert, 2005; Nair and Laurecin, 2007). PLA can be produced through ring opening polymerization of the cyclic lactide diesters, usually producing polymers with high molecular weight and excellent mechanical properties. The second route is via condensation process of lactic acids (Hyon et al., 1997). PLA exist in three stereoisomers, which is the L and D forms, and racemic mixtures of L/D. Poly (L-lactic acid) (PLLA), is a semi-crystalline polymer with glass transition point usually between 57 and 67°C and melting temperature of 184°C. Poly (L/D-lactic acid)(PLDLA) exists in amorphous phases due to irregularity of the polymer side group and its melting and glass transition temperature vastly depend on the L:D (Rokkanen et al., 2000a; Lu et al., 2003; Gupta et al., 2007). Details of PLA are discussed further in Section 2.2.1.2.

2.2.1.2 Polylactic Acid

Polylactic (PLA) is among the most commonly used synthetic bioabsorbable polymer. PLA is a linear polymer with thermoplastic characteristic and has a pale-coloured appearance (Törmälä et al. 1998). The basic chemical structure of PLA is shown in Figure 2.3.

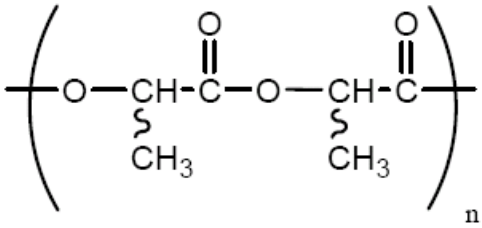

Figure 2.3 Chemical structure of PLA (n= central repeat unit)

(from Garlotta, 2001)

Polylactic acid can be produced using two major processing routes which are by ring opening polymerization and polycondensation of lactic acid. Ring-opening polymerization of lactide cyclic diesters is an efficient method for producing high molecular weight PLA. The second route is solvent based polycondensation

process. Polycondensation process is carried out under high vacuum and high temperature using a solvent to extract the water produced during the polymerisation (Dartee et al., 2000). During this stage, the lactic acid undergoes distillation at reduced pressure for 2 to 3 hours at 130°C, which removes most of the condensation water. A schematic of PLA production is shown in Figure 2.4

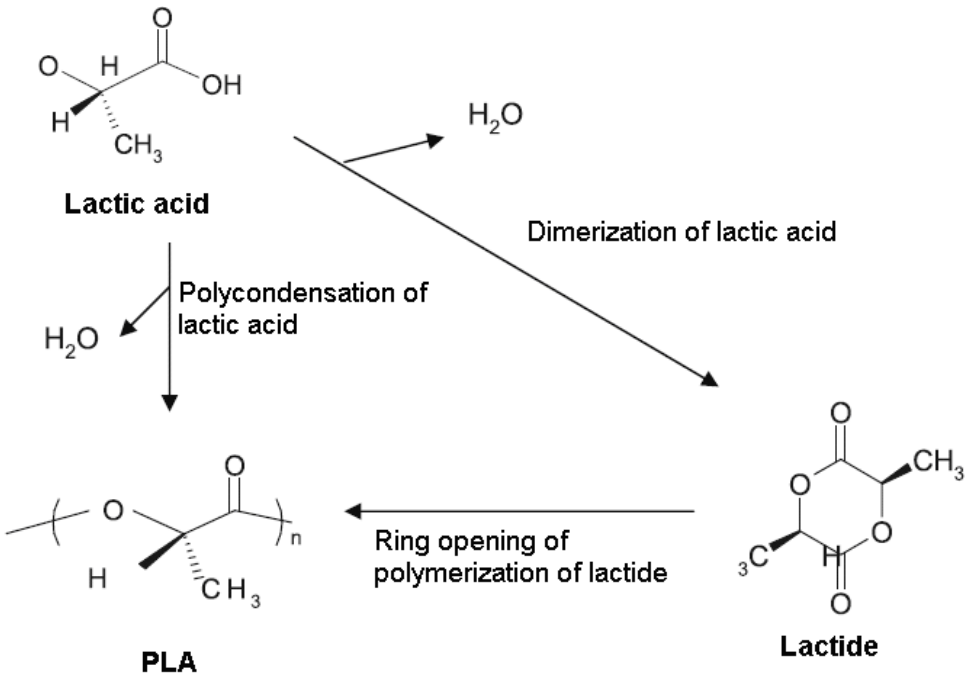

Figure 2.4 Polymerization of PLA

(Jacobsen et al., 1999; Linnemann et al., 2003)

The stereochemistry of PLA is complex as it consists of chiral carbon enabling it to exist in three stereoisomeric forms, L and D and racemic mixture of L/D.

Poly-L-lactides are more commonly used compared to poly-D-lactide for implants because the L-monomer is naturally present in the isomer (Nair and Laurencin, 2007). Poly-L-lactide also considered as an ideal material for load bearing applications in medical field as it has good mechanical properties. PLA is also more hydrophobic in comparison to other aliphatic polyesters such as PGA, due to present of methyl group in their molecular structure. Therefore, their water absorption and degradation rate is slower than PGA (Maurus and Kaeding, 2004; Nair and Laurencin, 2007).

PLA with racemic D/L has random or alternating arrangement of CH_3 and hydrogen (H) groups. This prevents the chains from packing together resulting in

amorphous structure, thus leads to lower strength and faster degradation period normally around 9-12 months (Borden, 2006). This behaviour makes it useful to use in drug delivery applications (Kohn and Langer, 2004; Nair and Laurencin, 2007).

Copolymers of L-lactide with D-lactide or DL-lactide also have been intensively examined. The addition of the D-isomer was observed decreased the crystallinity of the polymer, thus altering the degradation rate of the material. The properties of PLA and it copolymers can be affected by other factors such as molecular weight and polydispersity, degree of chain orientation, polymerization method, porosity, shape and size of the implant etc (Törmälä et al., 1998; Rezwan et al., 2006; Cotton et al., 2008).

2.2.1.3 Degradation of polylactic acid

When implanted in the body, bioabsorbable prostheses usually retain their integrity for certain amount of time, after that they gradually degrade until they are totally absorbed by the body and are excreted. The degradation processes are complex. There are many factors that can influence the process such as chemical structure, molecular weight and distribution of the polymer, presence of residual monomer, crystallinity, pH etc can affect the degradation kinetics (Li, 1999; Rezwan et al., 2006, Avérous, 2008). The predominant mechanism for PLA is hydrolysis (Figure 2.5), it is thought to be because they contained long carbon-oxygen-carbon (C-O-C) chain in their chemical structure. Initially, the samples are homogenous and upon contact water, the C-O-C bond starts to react by absorbing water, causing hydrolysis of the ester bonds (Borden, 2006), and the long molecular chains are broken into shorter ones, resulting in reduction of molecular weight. As the hydrolysis process continues, sufficient molecular chains have been broken to affect the mechanical properties principally mechanical strength, thus allowing mechanical fragmentation which initiates absorption of the implant followed by major mass loss.

The actual mass loss of the polymer is due to release of degradation by-products, and phagocytosis by macrophages and histiocytes. The lactic acid by-product when combined with oxygen, is then transformed into pyruvic acid, which is later excreted from the system through the Kerbs cycle as carbon

dioxide (CO_2) and water and expelled from body through respiration and urine (Ambrose and Clanton, 2004; An et al., 2000; Behravesh et al., 1999; Hughes, 2006; Losken et al., 2008; Middleton and Tipton, 2000, Raikin and Ching, 2005).

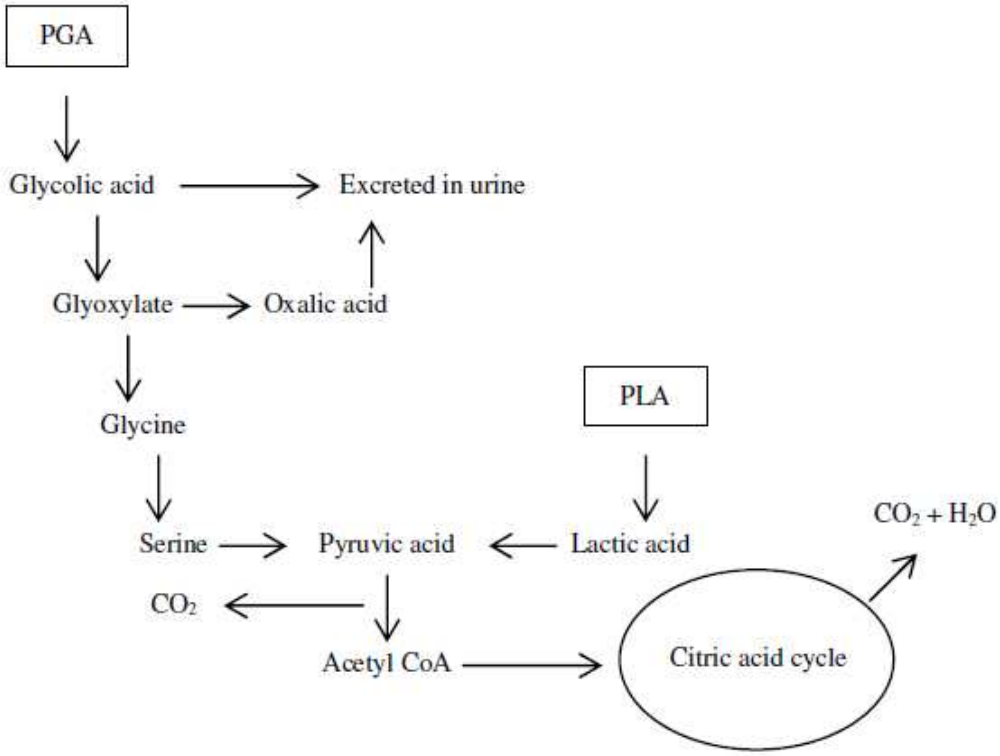

Figure 2.5 The hydrolytic degradation of PLA polymers

(from Suuronen et al., 1993; An et al., 2000)

Semi-crystalline polymer hydrolysis and degradation occurs in two stages. In the first stage, upon contact with water, the amorphous region of the polymer is the first to react by absorbing water which then triggers random hydrolysis cleavage of ester bonds. This reduces the length of the polymer chains. As this only occurs in amorphous regions while crystalline regions are unaffected, the physical appearance of the polymer will remain unchanged. While the structure remains intact, molecular weight of the polymer usually starts to degrade as soon as hydrolysis begins. This follows with the second stage of hydrolytic degradation, normally occurring in the crystalline region. Breakdown of the structure bonds causes reduction in physical properties of the polymer, leading to rapid weight loss of the implants (Li, 1999; Middleton and Tinton, 2000).

An autocatalysis effect is reported to be quite common during the degradation of PLA based material. This phenomenon known as heterogeneous degradation

(Li, 1999; Rezwan et al., 2006, Avérous, 2008). Initially faster degradation is expected to occur at the sample surface due to the diffusion gradient of the water. With time, oligomers are formed throughout the polymer, however those that formed at the surface will easily diffuse away, but oligomers release from the centre of the samples is slow as they need to diffuse through the remaining of the polymer before they can be excreted. This creates high concentration of carboxylic acid end groups in the centre of the samples, which then catalyze degradation and cause a higher rate of degradation inside polymer, compared to on the surface. As degradation progresses, while the component surface thins, the centre of the component becomes extremely viscous until the oligomers are able to penetrate through the surface leading to a burst release. Li et al. (1990a) studied degradation behaviour of PLA_{50} (50:50 of L: D ratio) immersed in saline solution. They reported that there was no reduction in mass or release of soluble product from the sample in the first 7 weeks of the immersion supporting the theory that the oligomers are trapped inside the sample.

Reed and Gilding (1981) observed that reduction in the molecular weight indicated a first sign of degradation as the hydrolysis process splits the chemical bonds of the long chains into shorter chains. The rate was faster at the beginning of the degradation process and slows as hydrolysis ends (Bos et al., 1989a; Matsusue et al., 1992; Furukawa et al., 2000). The degradation of the mechanical properties was observed as occurred earlier than changes in the macroscopic appearance of the implant, followed by major decrease in mass and lastly ingestion of the polymeric debris by phagocytic cells (Pietrzak et al., 1997)

The degradation behaviour of the PLA can be influenced by micro structural, macro structural and environment factors (Törmälä et al., 1998; Rezwan et al., 2006; Cotton et al., 2008). Some of these are shown in Table 2.4 (Vert et al., 1992).

Table 2.4 Factors influencing the degradation of biodegradable polymers (from Vert et al. 1992).

Factors
Chemical structure and composition
Distribution of repeat units in multimers
Presence of ionic groups
Presence of unexpected units or chain defects
Configurational structure
Molecular weight and distribution (polydispersity)
Presence of low molecular weight compounds (monomer, oligomers, solvents, iniators, drugs, etc.)
Processing conditions
Sterilizing process
Morphology (amorphous vs. semicrystalline, presence of microstructures, presence of residual stresses)
Annealing
Storage history
Site of implantation
Adsorbed and absorbed compounds (water, lipids, ions, etc.)
Physiochemical factors (shape and size changes, variations of diffusion coefficients, mechanical stresses, stress and solvent-induced crackings, etc.)
Mechanism of hydrolysis (enzymes vs. water)

Microstructural factors influence the degradation behaviour of polymers through many ways. The first contribution is polymer or copolymer chemical composition/monomer ratio, the second is crystallinity. The degradation usually slows down with increasing crystalline regions in the polymer. The third co-factor is the present of residual monomer or oligomer content. Hydrolytic degradation of the polymer usually increases with increasing content of acidic end groups. The initial molecular weight also can influence the degradation behaviour as it determines the length of the degradation process as higher molecular weight increases the time for total degradation. It has been often observed that filler addition can alter the degradation process, it can be accelerated or retarded depending on the type of filler material. Porosity is also reported to alter the degradation rate, as the pores will either to retard or accelerate the degradation process. Microstructural factors such as size and geometry of the implant may effect the degradation time as larger implants usually degrade slower than small implants as they have lower surface to volume area. Surrounding environmental factors and moisture content may either slow or speed up the degradation, the moisture content may also affect the initiating

of acid end groups formation (Törmälä et al., 1998, Rezwan et al., 2006, Cotton et al., 2008). Properties also vary from batch to batch (Suuronen et al. 1992; Vert et al., 1992; Pistner et al., 1993b; Bergsma et al., 1995c; Aydin et al., 2011).

PLA with stereocopolymers of L-lactide with D- or DL-lactide are less crystalline than 100% PLLA, thus they degrade faster and the rate is dependant on their monomer ratios (Bergsma et al. 1995c, d). Bergsma et al. (1995d) also showed that incorporation 4% D-lactide in PLA96 increased the degradation rate by a factor of two when implanted in rats. Results from in vitro degradation estimated that that degradation of this composite should take 2 to 3 years to complete fully (Pohjonen and Törmälä, 1996). Kallela et al. (1999c) later showed that when 3.5mm SR-PLA (70/30) screws were implanted in sheep, some cracks, clefts and fragmentation was observed after 24 weeks implantation, apart from that, the implants were morphologically unchanged.

2.2.2 Bioactive Calcium Phosphates Ceramic

The mineral component of bone is mainly calcium phosphate. Therefore, for the last twenty years, researchers tried to include calcium phosphate based bioceramics in to produce implants for clinical application. Often different phases are chosen depending on the intended application either to produce a resorbable or permanent implant (Hench 1996, Hench 1998a, LeGeros 2008).

There are two major calcium phosphates that have been used extensively in implants, are hydroxyapatite (HA) and tricalcium phosphate (TCP). HA has a Ca/P ratio of 1.67 with chemical formula of $Ca_{10}(PO_4)_6(OH)_2$. The chemical composition of TCP is $Ca_3(PO_4)_2$ with Ca/P ratio of 1.5 (Kohri et al.1993; Rey et al. 2008). TCP usually present in four different forms such amorphous TCP (am-TCP), apatitic TCP (ap-TCP), α-TCP and ß-tricalcium phosphate which has been used in biomaterials (Table 2.5). Amorphous TCP and apatitic TCP are unstable phases and thermally transform at low temperatures. They are produced through precipitation processes. In contrast, α-TCP and ß-TCP are high temperature stable crystalline phases, thus the use of TCP as biomaterial depends on the stability of the domains. Sintered ceramics can be only obtained from α- and ß-TCP (Rey et al., 2008). α-TCP has aroused same interest in the biomedical field

due to its quick resorption rate, stability in the temperature range 1180-1400°C while ß-TCP is stable below 1180°C (Ryu et al., 2002).

HA is the most stable phase in the physiological environment and it has a low biodegradability, thus preventing bone ingrowth and bone bonding is achieved via chemical bonding at the interface only (Kivrak and Tas, 1998; Jarcho, 1981). At the same time, ß-TCP is a slowly degrading bioresorbable bioceramic, which has been observed to have significant biological affinity and activity (Kalita et al., 2007; Fahami et al., 2012). ß-TCPtcp is more resorbable in vivo and has a higher biodegradation rate than HA thus allowing new bone growth to replace the implanted TCP (Sanosh et al., 2010) and accelerate the formation of the new bone during fracture healing (Choi et al., 2007; Yamauchi et al., 2010). It been reported that the dissolution rate of ß-TCP is 3-12 times faster than of HA (Fang et al., 1992). It has shown that ß-TCP is often favoured for implant materials as it has good tissue compatibility, excellent mechanical strength as well as having the ability to form direct bonding to tissue to regenerate bone without any intermediate connective tissue (Choi et al., 2007).

β-TCP based ceramics have been commercially used for bioresorbable synthetic bone substitutes by orthopaedic surgeons and dentists, in the form of porous ceramic pieces as well as granules. Generally, they are used in the reconstruction of wide range bone defects such as augmentation of alveolar ridge defects after tooth extraction and before implant positioning, sinus reconstruction (Szabo et la., 2005; Zijderveld et al., 2009; Lee et al., 2011), correction of various deformities (Le Huec et al., 1997; Nakagawa et al., 2006), and bone reconstruction following injury or disease (Ogose et al., 2006). Some of the applications of tricalcium phosphate in biomaterials are shown in Table 2.5.

Table 2.5 Tricalcium phosphates as biomaterials (adapted from Rey et al., 2008)

Type of material	Type of tricalcium phosphate involved	Application	Main TCP-related effects
Ceramics	α- and β-TCP	Bone substitute, small bone, replacement, tissue engineering	Biodegradable Dissolution and hydrolysis (for α-TCP)
Ca-P ionic cements	α-TCP, am-TCP, ap-TCP (end product)	Bone substitutes, Dental applications	Active hardening agents Bioresorbable, surface activity
	β-TCP (brushite cements)		Provider of Ca^{2+} and PO_4^{3-} ions
Coatings	am-and ap-TCP, α- and β-TCP	Coating of metallic prostheses	Biodegradable, reactive coating
Mineral-organic composites	am-TCP, α- and β-TCP	Bone replacement and bone substitutes Tissue engineering Dental restorative materials	Mechanical properties, Ca and P release in relation with biological activity

During in vivo studies, it showed that even though calcium phosphate implants degraded and were successfully replaced by normal bone tissue, the mechanical properties of the implants could be severely compromised during the remodelling process. This occurred as the biodegradation rate of TCP was too fast thus significantly weakened the load bearing capacity of the implant-bone system before new tissue could be formed. In order to slow down the rate of biodegradation, biphasic calcium phosphate (BCP) that is a mixture of HA and β-TCP has been used (Daculsi, 1998). The solubility properties of BCP tend to be closer to either β-TCP or HA depending on the weight ratios of ß-TCP/HA in the composite ceramics. Thus, it is possible to exploit their solubility behaviour by varying their composition (and by taking account both impurities and substitutions).

As a general trend, the degradation rate of calcium phosphate is found to reduce in the following order: Tetracalcium phosphate >α-TCP > β-TCP >> HA > Fluoroapatite (FA) (Hench 1996; Hench 1998a; Oonishi and Oomamiuda 1998;

Koerten and van der Meulen, 1999; Huang and Best 2007; LeGeros 2008; Rey et al. 2008).

Since the tricalcium phosphates have higher solubility, it was expected that they could degrade upon implantation and be replaced gradually by the new formed bone tissues. Thus ß-TCP ceramics or HA/ß-TCP composite has been extensively studied to overcome the low resorption of HA (Kivrak et al., 1998) and also been used as starting materials for synthesizing calcium phosphate bone cement (Bohner and Lemaitre, 1996).

2.2.2.1 Degradation of calcium phosphate

It has been generally observed that calcium phosphate resorption or biodegradation behaviour, including tricalcium phosphate is caused by three processes. The first factor is physiochemical dissolution, which largely depend on the pH of the surrounding environment. Secondly, physical disintegration into small particles and lastly biological factors, such as phagocytosis (Hench, 1996; LeGeros, 2008).

During the implantation period in living tissue, TCP interacts with body fluids to form HA as follows (Cao and Hench 1996; Hench 1996; Oonishi and Oomamiuda, 1998):

$$4Ca_3(PO_4)_2\ (solid) + 2H_2O \rightarrow Ca_{10}(PO_4)_6(OH)_2\ (surface) + 2Ca^{2+} + 2HPO_4^{2-}$$

Equation 2.1

TCP implant degradation rate depends on many factors such as TCP dissolution rates, as well as structural and microstructural parameters (crystal size, grain size and porosity of the ceramics) (Varma and Sureshbabu, 2001). Thus tricalcium phosphate powder degrades faster than dense solids. The crystallinity of the compound also alters the degradation behaviour as increases in crystallinity and crystal grain size decrease the degradation rate. Furthermore, the degradation rate of the TCP can be altered by using biphasic calcium phosphates (BCP). The ratios of HA/β-TCP in the BCP bioceramics can be modified. The effective rate of degradation can be altered by reducing the β-

TCP content in the BCP bioceramics compound, as the lower β-TCP content, the slower the dissolution rate(Huang and Best, 2007; LeGeros, 2008).

α-TCP has the structure of a metastable anhydrous phase. While it has same composition, α-TCP has different crystal structure and a higher specific energy than β-TCP. As a result, it has higher solubility rate (Dorozhkin et al., 2002) and is faster resorbed in vivo (Yamada et al., 2007). However, the correlation between dissolution rate and resorption rate do not always following the same trend. In vivo studies showed that sometimes, it possible to have similar degradation rate between the α and ß phases of tricalcium phosphate (Merten et al., 2001; Wiltfang et al., 2002).

Several authors (Wu et al.,1992; Basle et al.,1993) suggested that TCP resorption can be observed through two mechanisms: (i) classical degradation mechanism which is involving the attachment of osteoclast-like cells (TRAP positive) to the ceramic surface, creating resorption pits and (ii) debris disaggregation and phagocytosis caused by multinucleated giant cells (TRAP negative). Thus, this suggests that the degradation of the ceramic heavily depended on its nature and sintering conditions.

The relationship between TCP ceramics and the formation of bone tissue seem to be more complex. Numerous studies have considered the in vivo formation of the bone tissue, degradation and resorption of TCP (Koerten and van der Meulen 1999; Merten et al. 2001; Yuan et al., 2001; Wiltfang et al., 2002; Kondo et al., 2005; Ogose et al., 2006; Walsh et al., 2008) together with the clinical publications on ß-TCP as a potential bone substitute materials (Galois et al. 2002, Ogose et al.2006). Bone formation is generally observed on the contact surface of the degraded α-TCP and β-TCP samples (Kihara et al., 2006), however other observations, such bone formation at a distance from the ceramic surface has also been reported (Neo et al., 1998; Yamauchi et al., 2010).

Osteoconductivity of α-TCP and β-TCP was observed by Yuan and colleagues (2001) in an *in vivo* study in dogs. They reported that with β-TCP samples, osteoconductive activity were present in the soft tissues of the dogs indicating bone formation while it was not seen in α-TCP samples. This probably due higher

dissolution rate of α-TCP, this was resulting in extensive production of Ca^{2+} and PO_4^{3-} ions and eventually leads to changes in the local pH. This acidic environment prevents cells from growing and retards bone formation. However, other authors have reached different conclusions (Wiltfang et al., 2002), using a cancellous bone defect in minipigs, they concluded that α-TCP and β-TCP could be classified as bone rebuilding materials. Later, Kondo et al. (2005) reported that highly purified β-TCP implanted in rat femoral condyles lead to bone conduction followed by bioresorption of the implant. The process continued and eventually the new bone replaced the majority of the β-TCP implants. This observation further suggested that β-TCP not only biocompatible but also a resorbable bioceramic. Koerten and van der Meulen (1999) concluded that while degradation may occur in bioceramics such β-TCP, HA and FA, the rate however depends on what type of the bioceramics used. When comparing *in vitro* and *in vivo* studies, their findings confirmed that β-TCP degrades faster than HA and FA under both conditions.

2.2.3 Composite Biomaterials

The ideal composite material should be acceptable for use in the environment and function requirements of the final device. Composite materials are defined as consisting two or more materials where their physicality can be clearly distinguished at macro levels and are mechanically separable. It is usually produced by mixing two different kinds of materials and their dispersion in one another can be tailored to control to achieve optimum properties. Composite materials usually will have superior and specific properties compare to the original individual components (Hull, 1981).

Composite materials, due to their superior properties have advantages over homogeneous materials. One of their main advantages is that the mechanical, biological and physiological properties can be designed to suit the requirements of the applications better than with the individual materials (Reinhart and Clements, 1987)

The materials requirements for composites for biomedical applications include all the usual mechanical property requirements for general engineering

composites of stiffness, strength, toughness, and so on. However, the most important of all is the material must be biocompatible. Additionally, it is also desirable to be bioactive in order to provide advantageous fixation stability and bone tissue growth (Williams, 1999; Lakes, 2003; Anderson, 2004)

In general, composite materials consist of matrix and reinforcing phases. They can be composed through many ways and the materials can be selected from any established classes of materials such as metals, ceramics and polymers or in many cases from the same type. In composites, the matrix appears in the form of the continuous phase and usually confers the overall form of the composite. The reinforcement phase is usually stiffer than the matrix and can be distinguished in the composite in the in form of a dispersed phase. The area where the matrix and reinforce materials connect is known as the interface (Daniel and Ishai, 1994; de Santis et al., 2009).

Lakes (2003) suggested that classification of composites could be described through shape of the reinforcement such as particles (with no long short dimension), fibres (one long dimension) or the platelet or lamina (with two long dimensions). Apart from that, composite also can be classified according to their matrix based that being used. Thus, composite can be classified as metal matrix composite (MMC), ceramic matrix composite (CMC) and polymer matrix composite (PMC) (Hull and Clyne, 1996). Most biomedical composites are PMC.

As the composite consists of two or more different phases of material, they have different roles to fulfil depending on the type of materials and their intended use. For the low and medium performance applications, the main load-bearing mechanical properties are based on the matrix while the reinforcement only stiffens and strengthens the composite and the geometry of reinforcement materials is often in form of particles or short fibres. However, in the case of high performance structural composites, the main load bearing is typically supported by the reinforcing phase. Normally continuous fibres are used providing the stiffness and strength of the composite parallel to the direction of the fibres used. The matrix contributes by providing support and protection to the fibres and helping in transferring local stresses (Daniel and Ishai, 1994).

As composites are designed with a certain application in mind, their compositions are often tailored to suit this purpose. Therefore, a clear understanding of the relationship between the structure and properties is crucial. In many cases, their relationship is complex thus the prediction of the resultant mechanical properties is often challenging. However, for some structure, the prediction of the properties is relatively simple by using rule of mixtures

$$E_{composite} = E_f V_f + E_m (1 - V_f)$$

Equation 2.2

Where $E_{composite}$ is the modulus of composite, E_f and E_m are the moduli of the reinforcement materials and matrix respectively and V_f is the volume fraction of reinforcing phase (Lakes 2003; Hull and Clyne,1996; Callister, 2000).

The rule of mixtures stated that composite property is a resulted from a weighted mean between the properties of the two components, depending only on the volume fraction of the reinforcing phase (Hull and Clyne, 1996). The rule of mixtures assumes that the stress through the material is constant. The other assumption is the strain is constant and leads to Equation 2.3:

$$\frac{1}{E_C} = \frac{V_f}{E_F} + \frac{(1 - V_f)}{E_m}$$

Equation 2.3

All models fit between these two bounds. In practice, it is not that simple and thus more powerful micromechanics theories are called for, which lead to more complicated mathematical calculations (Daniel and Ishai, 1994; Hull and Clyne, 1996; Lakes, 2003)

In the mean time, improving the matrix-reinforcement interface bond strength could enhance the properties of composite as composite failure tends to occur at the interface. Therefore, should that interfacial bond be strong enough, it should be able to stand higher loads (Hull and Clyne, 1996). In order to increase the interface bonding, the wettability properties between matrix materials with reinforcing phase is crucial. At the same time, the wettability of those two constituents' surfaces depends on hydrophobicity or polarity of the

reinforcement and the type of polar groups of the matrix material. Increasing chemical interactions in the interface will lead to better bonding. The mechanical strength can be further increased with the use of certain coatings or coupling agents or surface treatment such as silane coupling agents which react with both matrix and fibre surface. They are widely used in glass fibre reinforced PMC (Hull and Clyne, 1996). Additionally, interface bonding can also be increase via mechanical interlocking between the matrices and reinforcing phases. However these bonding agents are chemically highly active and their biocompatibility has not been assessed so they are rarely, if ever, used in biomaterial applications (Tanner, 2012).

In the current applications, the major uses of hard tissue implants are as joint replacement to treat problems such as osteoarthritis, fracture fixation, filling of bony defects, such as after a tumour has been removed, and, the newest application, tissue engineering (Williams, 1999; Anderson, 2004, Mustafa and Tanner, 2012). As human bones are very complex composite structures, composites are a clear choice of replacement materials that potentially able to mimic the structure and properties to use in bone repair. Tanner (2010) summarized that the main reasons for using composites is because the mechanical properties of the prosthesis can be tailored to be comparable with bone tissue. The stiffness of the implant needs be similar to that of natural bone, however only few materials have been published to have stiffness close to those of cortical bones. Secondly, the initial strength of the prosthesis needs to be higher than bone. Thirdly, by using composite technology, the biological properties can be tailored according to the applications. Implant materials should allow new bone tissue to grow on the surface thus creating a strong biological attachment between the implant and the bone tissue. The fourth reason is the capability of the composite to biodegrade. As the degradation process occurs gradually while the damaged bone tissue is healing, it allows the gradual transfer of load bearing from the prosthesis to the bone.

As discussed before, bioceramics may have the potential to optimize the bone repair process as some of them reported able to display osteoconductive behaviour and excellent bone bonding properties, they nevertheless are brittle ceramics. Combining bioactive bioceramics with polymers should produce

superior composites, which not only have comparable mechanical properties, but are also able to facilitate bone tissue healing. This idea has encouraged many research groups to study the possibility to composite bioceramics with polymers in order to produce composites that are not only mechanically strong but also have the capability to encourage bone bonding.

One of the earliest clinical applications of composite material was by incorporating carbon-fibre-reinforced epoxy (CFRE) as fracture fixation plates for forearm bone (Hastings, 1978; Bradley et al., 1980; Ali et al., 1990). Carbon-fibre-reinforced epoxy is not only extremely strong, but also lightweight, with modulus close to natural bone and biocompatible to use in human body. The composite is radiolucent, thus inspection of the bone healing under the implant using X-rays is possible (Saringer et al., 2002). Patients were reported able to use their arms earlier when compared to patients treated using metallic prosthesis. The composite was also reported used in bone repair defects in the skull (Al-Shawi et al., 2002). However, while carbon fibre reinforced epoxy shows good compatibility with host tissue; the drawback of this composite that it difficult to bend in the operating theatre thus restricted the applications for fixation in straight bone such as forearm and as preformed shapes in skull applications.

Bonfield and colleagues have taken a different approached in designing new combination of biomaterials by adopting the 'bone-analog' concept, which is to produce replacement materials using similar initial components to bone to produce materials that have similar mechanical and biological properties to the natural bone thus being modulus matched and bioactive. They developed high-density polyethylene (HDPE) reinforced with hydroxyapatite (HA). HA was shown to stiffen PE, and PE to toughen the composite. Additionally, because HA resembles bone mineral, natural bone will grow onto HA. At 40 vol.% HA, the composite stiffness increased from 0.94 to 4.29 GPa (Bonfield et al., 1981; Wang et al., 1994). The first clinical application as orbital floor implants reported good biological responses (Downes et al., 1991; Tanner et al., 1994). Furthermore, HAPEX™, the commercial name for the 40 vol.% HA-HDPE composite, was used as the shaft of middle ear implants. The study reported the implant to have bone-bonding ability thus increasing the long-term stability

especially at the implant-bone interface (Goldenberg and Driver, 2000). However, HA/PE composite is a biostable composite, it does not degrade over time, maintaining constant mechanical properties in physiological solution. In addition, HA/PE composite has been found to provide a favourable environment for human osteoblast-like cell attachment (Huang et al. 1997a).

The encouraging results from the HA filled PE composite has motivated researchers to study other osteoconductive composites using the same basis of bioactive ceramics polymer composites. Other bioactive fillers have been studied such as bioactive glass to get stronger bone-implant bonding. Faster formation of apatite layer formation was observed formed on Bioglass® /PE sample surface compared to HA/PE composite suggesting better bioactivity occurred. However, while the mechanical properties of HA/PE remained constant when immersed in an aqueous environment, the Bioglass/PE composite properties were reduced (Huang et al., 1997b; Wang, 2003).

2.2.3.1 Degradable Polymer- Ceramic Composite

Nowdays, it is common to produce degradable polymer composites by incorporating bioactive materials such as bioactive glasses or calcium phosphates into polylactide matrices.

Bioabsorbable bone implants are especially advantageous as their degradation can be controlled and replaced by host tissue once the bone healed (Laurencin and Lu, 2000). The degradation behaviour of the polymer can be influenced by many factors. Thus, adding a bioceramic phase, among other possibilities, can alter the properties and degradation behaviour of the bioabsorbable polymer matrix.

Li et al. (2005) also reported delayed degradation of the matrix polymer of porous composite scaffolds of polyhydroxybutyrate-polyhydroxyvalerate (PHBV) with sol-gel derived bioactive glass. The porous composites with 0-20 wt.% of bioactive glass were produced using compression moulding, thermal processing and salt particulate leaching techniques. The *in vitro* study revealed that with increasing glass content, water absorption was increased, lead to increases in

weight loss thought to be due to a buffering effect. The molecular weight reduction of the bioactive filled composite was slower than in the unfilled samples. Bioactivity was also observed with the presence of the hydroxyapatite formation on the surface of Bioglass® filled samples. The results further confirm the possibility to modify the degradation rate of the scaffold by incorporation of bioactive glass in polymer.

Zhou et al. (2007, 2009) used a solvent evaporation technique to manufacture 10wt% bioactive glass in poly-L-lactide composite membranes. Degradation testing was performed in phosphate buffer saline (PBS), showing overall degradation in terms of decreased mechanical properties, mass and molecular weight losses. This was thought due to the buffering effect of by the bioactive glass (Zhou et al., 2009). Additionally, it was observed that in the solvent evaporated composite samples, the matrix polymer was covered by the bioactive glass particles thus hindering contact with the PBS solution. It has been widely reported that the addition of bioactive glass or ceramics could delay the degradation process due to neutralization of acidic build up in immersion solution during degradation process (Kikuchi et al. 2002; Maquet et al. 2002; Li and Chang, 2005; Zhou et al. 2009). As bioactive glass degrades, it creates an alkaline environment in response to surrounding fluids thus slowing down the degradation rate.

Contrary to this, Rich et al. (2002) reported the opposite results when adding 40, 60 and 70 wt.% of bioactive glass (S53P4) filler particles (particles size of less than 45μm and 90-135μm) in poly (ε-caprolactone-co-DL-lactide) matrix. They reported that the degradation appeared to be increased in the filled composite compared to the unfilled polymer. Possible explanation for this phenomenon is water absorption usually increased with increase interface surface area/sample volume ratio, thus composite with smaller particles size absorbed more water compared to the larger particles. Apart from that, higher filler content, increased the surface/volume ratio thus the faster formation of Ca-P on the sample surfaces (Jakkola et al., 2004; Rich et al., 2002).

Furukawa et al. (1998, 2000) reported that 40 wt.% HA in PLLA matrix composite had a significantly greater affinity for bone when compared with unfilled PLLA.

Furthermore, when tested after eight weeks implantation *in vivo*, Yusunaga and colleges (1999) reported that the bonding strength between bone and PLLA implants containing 0-50 wt.% HA increased with increasing of HA content. Similar effects have been reported could be achieved by plasma spraying an HA coating onto PLLA (Verheyen et al., 1993). Hydroxyapatite has also been observed to slow down the degradation of the bioabsorbable polymers by forming a hydrolysis barrier (Verheyen et al., 1993, Van der Meer et al., 1996; Guo et al., 1998) or vice versa (Li and Chang, 2005).

Increasing in the calcium phosphate filler content reduced the degradation rate, when 30 and 50 wt.% of bioactive filler (HA) was added into PLLA polymer in comparison to the unfilled polymer (Verheyen et al. 1992). They reported that the mechanical properties of the composite increased with filler and was maximum when 30 wt.% HA was added to the PLLA. They also reported that the mechanical strength in the unfilled composite reduced faster than those of the filled composites. Similar to this finding, Shikinami and Okuno (1999) observed that the degradation rate of a similar composite reduced with increases in HA content. They reported that heterogenous degradation was observed in 20 wt.% HA filled composite. However, when the filler content increased more than 30 wt.%, the composite underwent homogenous degradation due to faster water permeation. Apart from HA, incorporating tricalcium phosphate (TCP), either α-tricalcium phosphate (α-TCP) or ß-tricalcium phosphate (ß-TCP) and in the polymeric degradable matrix was been reported to slow down or to accelerate the degradation rate of the composite.

Heidemann et al. (2001) studied *in vivo* degradation of PLDLA implants filled with TCP or calcium hydrogen phosphate (CHP). They reported that, after 72 weeks implanted in the dorsal muscles of rats, the PLDLA rods totally degraded and showed only mild foreign body reactions. However, in the same study, they observed samples filled TCP or CHP particles of 2.2 µm average size had not been totally absorbed and that inflammation occurred at the implant site. They concluded that the inflammatory response may occurred due to the small size of the calcium phosphate particles used, which had become separated from the surface of the implants.

Kikuchi et al. (2002) investigated the effect of pH on the degradation rate and mechanical properties of ß-TCP in copolymerized poly-L-lactide (CPLA) composite. Their findings indicated that the bioceramic filler further helped the composite in retaining its mechanical strength. The pH of the surrounding solution remained neutral during the entire in vitro immersion. This suggested that the dissolution of the TCP was providing a pH-buffering effect on the solution and thus slowing down the degradation process. Later, Kikuchi et al. (2004) reported that when poly (L-lactide-co-gylycolide-co-ε-caprolactone) (PLGC) was reinforced with ß-TCP, an increased chemical interaction between the TCP surface and C=O bonds was achieved. Thus improved the mechanical strength of the ß-tricalcium phosphate filled composite compared to the unfilled polymer. It was also observed that the degradation of molecular weight of filled samples was slower than the plain composite resulting in longer degradation time, which occurred after 24 weeks in comparison to 8 weeks in the plain polymer.

Bernstein et al. (2010) successfully produced a strong bioresorbable nanocomposite of PCL- filled with 5 or 15 vol.% dense ß-TCP. They reported that the composite not only had excellent compressive strength and ductility but also had good osteoconductive properties, and the dissolution rate was similar that reported by pure cold sintered ß-TCP.

Kobayashi and Sakamoto (2006, 2009) studied 5-14 wt.% ß-tricalcium phosphate (ß-TCP)/poly-L-lactide (PLLA) composites produced by injection moulding followed by a drawing process. Results for bending tests showed that with increasing ß-TCP content, the strength decreased while the modulus increased. They also reported that over the first 8 weeks of immersion, the mechanical properties of the sample remained constant (Kobayashi and Sakamoto, 2006). The effect of pH level (7.4 and 6.4) on the mechanical properties concluded that the degradation rate and mechanical properties of the composite depended on ß-TCP content. Samples with higher ß-TCP content were found to degrade faster and with a lower pH level which thus speed up the degradation rate reducing the mechanical strength of the composite (Kobayashi and Sakamoto, 2009).

Claes et al. (1996) manufactured poly-L/DL-lactide pins for small bone fractures. These implants have initial bending strength of 155-163 MPa, sufficient for use in small bones. The degradation study also reported to match the healing progress of the natural bone tissue. Ignatius et al. (2001) improved the biocompatibility of the composite by adding 10-30 wt.% ß-TCP to increase the biocompatibility of the pins. However, results showed that while biocompatibility was improved at the same time it altered the degradation rate thus compromising the mechanical properties of the composite in vitro. With the addition of ß-TCP, the initial strength was reduced, and the reduction appeared to be faster in the filled composite in comparison to the unfilled samples. They also reported that, in 30 wt.% of ß-TCP, substantially increased water intake was observed, thus affecting the adhesion at the interface, which thought to explain the faster reduction of mechanical properties. They suggested that composite containing 10 wt.% ß-TCP better suited fixation requirements than composite containing higher ß-TCP content.

Although α-TCP has a higher resorption rate than other calcium phosphates, it is still used in bioabsorbable polymers in order to provide better understanding of the effect of degradation process. Ehrenfried et al. (2008) studied PLGA filled with 0-40 wt.% α-TCP and reported that the mechanical properties were increased when α-TCP was added. The composition degradation rate also observed to be significantly slower due to success in pH buffering. However, further investigation using micro-computed tomography (μ-CT) images revealed that all the PLGA samples were actually degrading faster inside the structure, which is normal for this type of polymer (Li et al., 1990b; Li, 1999). A long term in vivo study of α-TCP /PDLLA in a loaded sheep model by Ignatius et al. (2001) showed good results after 12 months implantation. However, after 24 months of implantation, the TCP was almost completely dissolved but there was adverse reaction to remaining PLA to the surrounding host.

Aydin et al. (2011) produced PLLA composite reinforced with HA nanorods for PLLA-based bone plates to mimic the natural apatite shape in bone for load bearing application. They reported that the maximum mechanical strengths were obtained from 50% (w/w) amorphous HA nanoparticles. In vitro bioactivity

tests showed that the plate produced good cellular activity, at the same time the degradation rate was observed to increase with increasing HA content.

2.2.3.2 Mechanical property and manufacturing of PLA based composite

Törmälä et al. (1998) proposed that to ensure survival of the implant during the bone healing, the strength of the devices must exceed the strength of the bone. Traditional fabrication techniques such as extrusion, injection moulding and compression moulding normally produce composites with strengths inferior to those of cortical bone. Thus fibres were used in a polymer matrix composite to enhance the mechanical properties in addition to the particulate reinforcing. However, one of the major limitations of using fibres as a reinforcing element is the weak link of the fibre-matrix interface. Surface treatment can be applied to increase the wettability and interface bonding, however stronger bonding can be achieved if the both of phases are made from the same materials, as increased chemical bonding could form between the two constituents, this idea leads the development of self-reinforced (SR) composite.

Self-reinforced bioabsorbable polymers were successfully produced in the early 1980s. In this composite, highly orientated fibres are embedded in an all polymeric composite. The two phases have the same chemical composition creating an oriented, high strength structure. Self-reinforced structure can be produced in various methods, for example by mechanical deformation such as free drawing, oven drawing, zone annealing, die drawing, rolling, sintering, and fibrillation, often producing a composite with different kinds of microstructure.

The concept of self-reinforced composites was first described by Capiati and Porter (1975). They suggested that the manufacture of self-reinforced composites depends on the differences in fibres and matrix's melting temperature. Although they are same material, the matrix normally has lower molecular weight and crystallinity than the fibres, thus it is possible for the matrix to melt while the fibre just softened. In the same study, they successfully produced self-reinforced polyethylene (PE) by using PE fibres in molten PE matrix. They reported high shear strength was achieved from the composite,

which is in range of glass fibre reinforced polyester when subjected to pull out test. Morphology investigation showed that transcrystalline growth from the melt perpendicular to the fibre direction that might contribute high strength of the composite. Later Lacroix et al. (1998, 1999) manufactured self-reinforced HDPE using solution impregnation and reported nucleation and epitaxial growth around the fibres that contributed to the high strength of the composite, reported to be 1GPa in tensile testing.

Hine et al. (2008) successfully adopted hot compaction and film stacking techniques to produce orientated fibres with and without interleaved film in polyethylene (PE) and polypropylene (PP) based composites (Figure 2.6) over a range of temperatures. They reported that eventhough the optimum compaction temperature was found to be 1°C below the melting temperature of the crystalline phase, the composite lost about 30% of the original orientated phase properties due to bonding structure together.

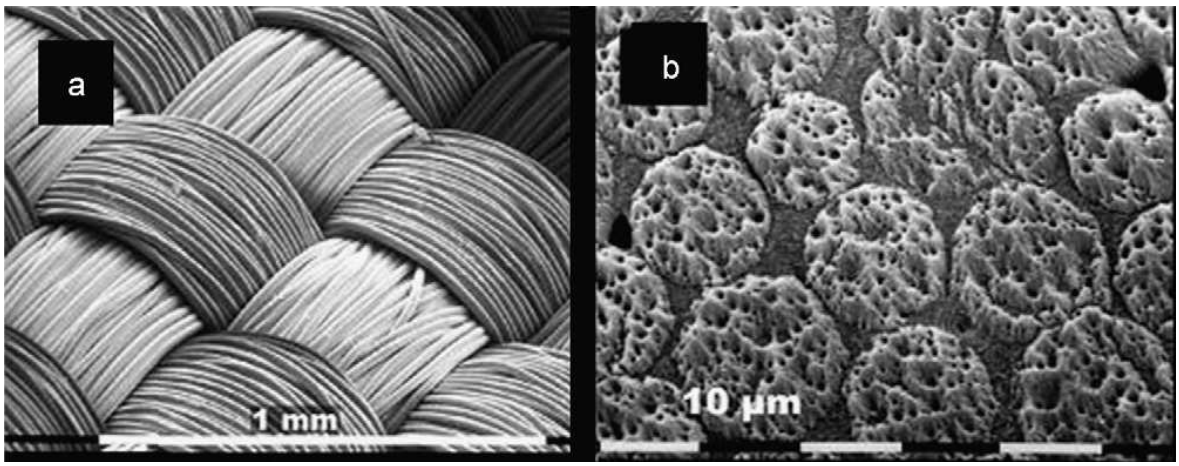

Figure 2.6 Self-reinforced polyethylene based composite a woven cloth made from multifilament bundles; (b) permanganic etched image of compacted woven melt spun (from Hine et al., 2008)

Huang (1998) showed that by using continuous extrusion to produce an orientated self reinforced HDPE composite, the tensile strength was substantially increased by factor of 8.

In the field of degradable polymers, self reinforcing for absorbable composite based on either PLA (SR-PLA) and PGA (SR-PGA) has been intensively adopted and used since 1984 (Törmälä, 1992; Waris et al., 1994). Törmälä et al. (1988)

has successfully developed a self-reinforced PLLA composite with higher strength than earlier non-reinforced degradable polymers for use in osteosynthesis devices (Figure 2.7). The composite was produced by subjected the fibres to a high temperature and pressure (Törmälä, 1992; Törmälä et al., 1998; Rokkanen et al., 2000). The process leads to more melting of other than the inner fibres but still allows the retention of some fibre orientation.

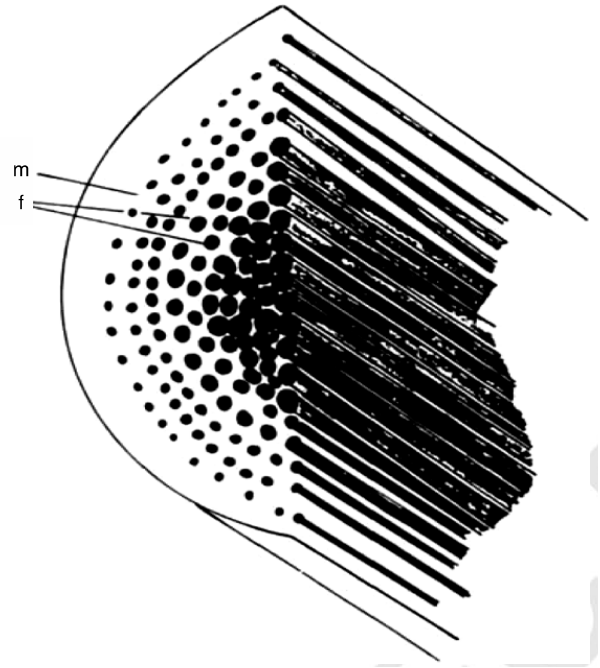

Figure 2.7 Schematic illustration of self-reinforced composite consisting of matrix (m) reinforced with parallel reinforcing elements (f) (Adopted from Törmälä et al., 1991)

Majola et al. (1992) successfully produced self-reinforced PLLA composite using sintering techniques at temperatures of 130-135°C for (PDLLA/PLLA rods) and 162-174°C (PLLA rods). The fibres were initially produced by hot drawing and meltspinning techniques. They reported that the composite had initial bending and shear strengths of 250–271 MPa and 94–98 MPa respectively, which are significantly higher of those non-reinforced PLLA (145 MPa and 53 MPa respectively). In another study, Wright-Charlesworth et al. (2005) using hot compaction technique to produce highly orientated self reinforced PLA filled with HA. They also reported that SR composite has higher initial mechanical properties compare to non-reinforced composite.

The structure also can be prepared by starting from fibres followed by a controlled compression moulding. The heating process in the compression moulding were controlled so that just the surface of the fibres melt, enough to bond with the matrix and attach the fibres together, but not high enough to completely melt the fibres which can destroy the integrity of the fibres. The process parameters such as temperature, pressure and time are very important to maintain the reinforcing effect of the fibres (Hine et al. 1993). Several studies reported successfully produced self-reinforced bioabsorbable polymers using either or both of solid state die-drawing and compression moulding of the fibres (Niiranen and Törmälä, 1999; Kellomäki et al., 2000; Niiranen et al., 2004; Ella et al., 2005; Huttune et al., 2006, Frantzén et al., 2011). Figure 2.8 shows some of commercial bioabsorbable self-reinforced bone fracture fixation pins and screws available in the market. This self-reinforced biodegradable composite reported to have excellent mechanical properties and stiffness comparable to cortical bone (Table 2.6). The superior combination of the composite makes it an excellent starting point in the development of degradable bone fracture implant. Nowadays, bioabsorbable self-reinforced bone fracture fixation devices are in clinical use or in clinical research in more than 20 countries. The surgeon can select materials with tailored *in vivo* strengths retention that suit individual needs in fracture fixation application.

Bleach et al. (2001, 2002) produced self-reinforced PLA composite by using pre-impregnated sheet and compression moulding techniques. Prior to the compression moulding, the pre-impregnated sheet was produced by drawing PLA fibres through a suspension of biphasic calcium phosphate in PLA matrix solution using a pre-pregger machine. The concept of combining bioceramics with self-reinforced composite in order to produce not only high strength and biocompatibility but also bioactivity had been tried earlier by Kellomäki et al. (1997).

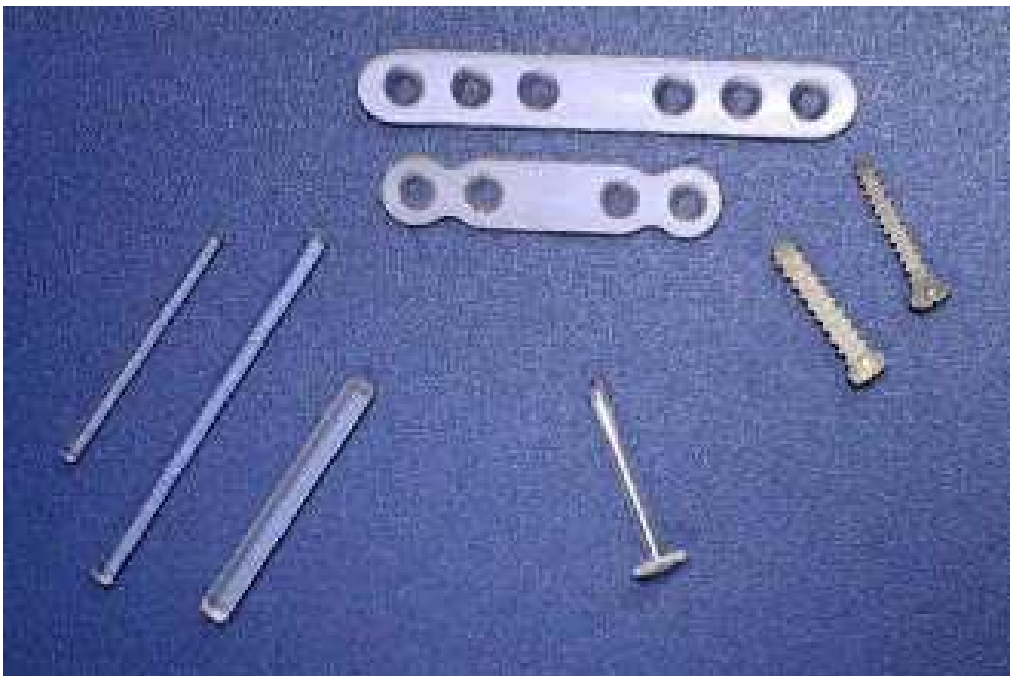

Figure 2.8 Bioabsorbable self-reinforced bone fracture fixation pins and screws (from Waris et al., 2004)

Table 2.6 Mechanical properties of the Self reinforced Polylactic Acid composite

Authors (year)	Materials	Rod diameter (mm)	Tensile strength (MPa)	Bending strength (MPa)	Bending modulus (GPa)	Shear strength (MPa)
Mustafa (2005)	SR-PLLA	4	-	110	4	25
Pohjonen 1997	SR-PLLA	Screw*	789	244	-	147
Manninen and Pohjonen (1993)	SR-PLA85			163-170	5-6	110-116
Törmälä (1992)	SR-PLLA	1.3	-	300	10	220
Suuronen et al.(1992)	SR-PLLA	Screw*	-	200	7	110
Törmälä et al.(1990)	SR-PLLA	1.4	560	360	-	-
Currey, 1998, Hench & Wilson, 1993	Cortical bone		50-150	180-195	7-30	60-90

*** thread diameter (4.5mm) core diameter (3.2mm)**

2.3 FATIGUE OF MATERIALS

2.3.1 Fatigue characterisation

The simplest way to break a material, for example a metal bar is by bending it alternatively to the opposite sides. Fatigue describes changes in the properties resulting from the application of cyclic loads. At the beginning of the industrial era, this phenomenon was investigated extensively due to failure of machine mechanisms after sequences of repeated loads each that were lower than their one time fracture load.

The pioneer study on fatigue fractures of train axles was carried out by W. J. M. Rankine (1843) at the University of Glasgow where he described the finding "It seems likely that fracture begins with the appearance of a small smooth crack of regular shape encircling the axle journal in the course of time, almost joining its ends, and penetrating into the bulk ... Then the area of the inner round core of the undamaged material becomes insufficient to withstand the impacts made upon the axle and it fails"

During 1852-1869, Wöhler conducted a series of fatigue studies using rotating bending fatigue. He proposed the two fundamental laws of fatigue:

1. Iron and steel may fracture under a stress not merely less than the static rupture stress, but also less than the elastic limit, if the application of the stress is repeated a sufficient numbers of times and
2. Rupture will not take place if the range between the maximum and minimum stress levels is less than a certain limiting value regardless the number of cycles is repeated.

In biomaterial applications, polymeric composites have been successfully used for hard tissue repair such as bone fracture fixation, bone plates, intramedullary nails, spine instrumentation, hip replacement and other. Daily activities such as standing, sitting, walking, jogging, stretching and expose the soft and hard tissue to experience repetitive stress that fluctuates with time (Black, 1992).

Fatigue fracture has been recognized as on one of the main causes of implant failure of medical devices (Teoh, 2000), thus provided a serious limitation if such composites are going to use for hard and soft tissue application. It is well known that for many potential clinical applications, the materials will be subjected to cyclic loads. For example, in the acetabulofemoral joint (hip joint), 0.5 to 2 million cycles per annum are applied, varied with the patients's age and activity (Wallbridge and Dowson, 1982), while roughly one million cycles per annum can be estimated for the finger joint (Unsworth et al., 1991).

Wilson et al. (1992) reported that 4.1% of the failures of their cementless hip prostheses were due to fatigue failure after inappropriate heat treatment, while Charnley (1975) recorded that a 0.23% failure rate in 6500 hip replacements prosthesis was caused by fatigue failure.

Figure 2.9 shows a typical fluctuating stress of cyclic loading. A fluctuating stress cycle normally consists of two components, a mean stress (σ_{mean}) and amplitude stress (σ_A). The stress range ($\Delta\sigma$) is the difference between maximum (σ_{max}) and minimum (σ_{min}) stresses in a cycle. The following variables define a given fatigue condition:

Mean stress, $$\sigma_{mean} = \frac{1}{2}(\sigma_{\max} + \sigma_{\min})$$ **Equation 2.4**

Stress amplitude, $$\sigma_A = \frac{1}{2}(\sigma_{\max} - \sigma_{\min})$$ **Equation 2.5**

Stress range, $$\Delta\sigma = (\sigma_{\max} - \sigma_{\min})$$ **Equation 2.6**

The two ratios that normally used in describing fatigue data are the stress ratio (R) and amplitude ratio (A) as follows:

Stress ratio, $$R = \frac{\sigma_{\min}}{\sigma_{\max}}$$ **Equation 2.7**

Amplitude ratio, $$A = \frac{\sigma_{amplitute}}{\sigma_{mean}} = \frac{1-R}{1+R}$$ **Equation 2.8**

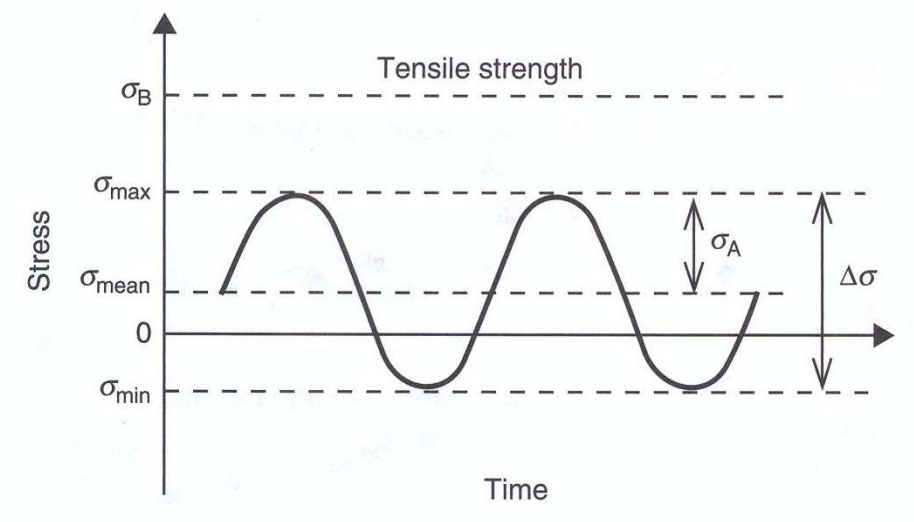

Figure 2.9 Typical fatigue stress cycles (adapted from Dieter, 1988)

2.3.2 The S-N curve

One common way to represent fatigue data is the S-N diagram (or Wöhler diagram), a plot of stress, S against the number of cycles to failure (N) on a logarithmic scale such as those showed in Figure 2.10.

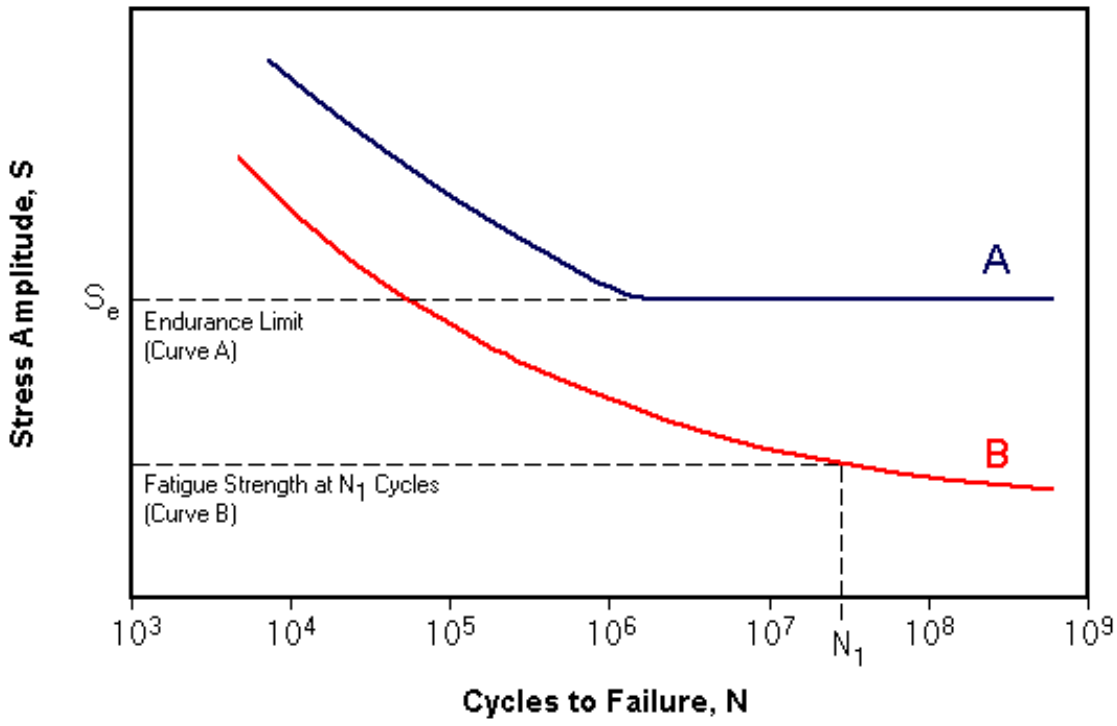

Figure 2.10 Typical stress-strain (S-N) curves showing

(A) a material with an Endurance Limit and (B) a material with no Endurance Limit

The value of stress used is usually the nominal stress either σ_A, σ_{max} or σ_{min}. Reducing the stress normally results in increasing cycles to failure. In some materials, the S-N curve flatten out eventually, the material can endure an infinite number of load cycles without failure. This is known as the endurance limit (σ_e).

Experimental studies have shown that fatigue growth rate can be characterized by cyclic variation in the stress intensity factor (Paris law equation) (Paris, 1962):

$$\frac{da}{dN} = A\Delta K^m$$

Equation 2.9

Where ΔK, is stress intensity factor range during the load cycles, A and m are constants depending on the material, frequency, stress ratio, environmental condition (temperature, humidity) (Hertzberg and Mason, 1980). Figure 2.11 shows a typical Paris plot for short glass filled polypropylene composites with three different short fibre filler contents (Pegoretti and Rico, 2000; 2002).

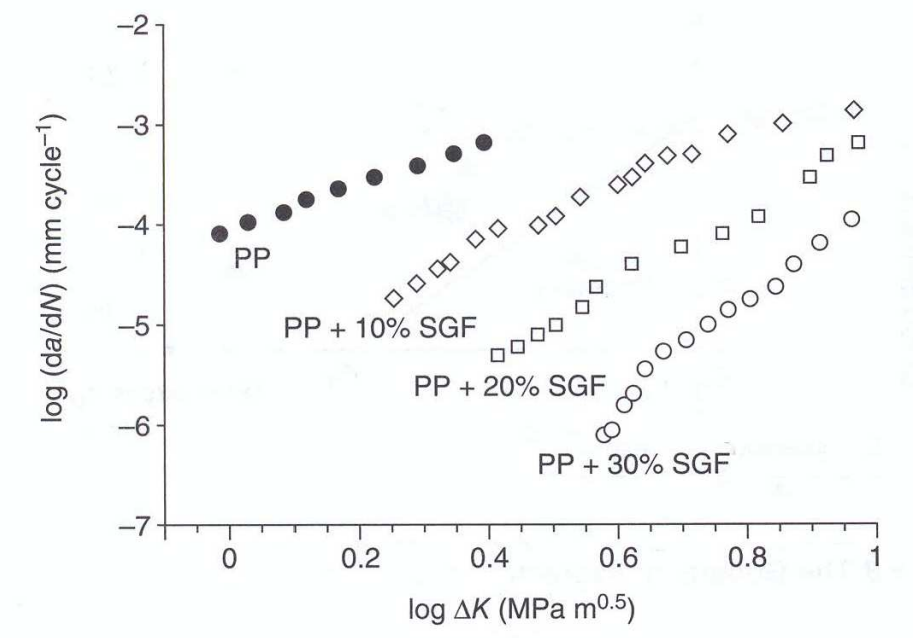

Figure 2.11 Fatigue crack propagation of injected moulded polypropylene composite reinforced with 10, 20 and 30 wt% of short glass fibres (from Pegoretti and Rico, 2000).

2.3.3 Fatigue progress mechanisms

The fatigue progress mechanisms in long fibre composites can be explain by the schematic illustration in Figure 2.12 This progressive mechanism has been supported by Gamstedt (2000) based on his study on the micro mechanisms of fatigue of PEEK and polypropylene fibre reinforced composites. He reported that the fatigue life depended heavily on the matrix and its interface as they control the failure progression. Initially the fibres fail, which then creates cracks, which then propagate into the surrounding matrix. The next phase of crack propagation is in the matrix parallel with the fibre direction, until eventually the individual cracks join leading to final failure.

The effect of different types of matrix on fatigue damage in continuous fibre reinforced composite is illustrated in Figure 2.13. The material that has the stronger interface shows fewer fibre breaks and the crack usually grow across the fibre. In composites with weaker interfaces and prone to debonding propagation, more fibres break resulting to profuse debonding and longitudinal splits that eventually lead to failure.

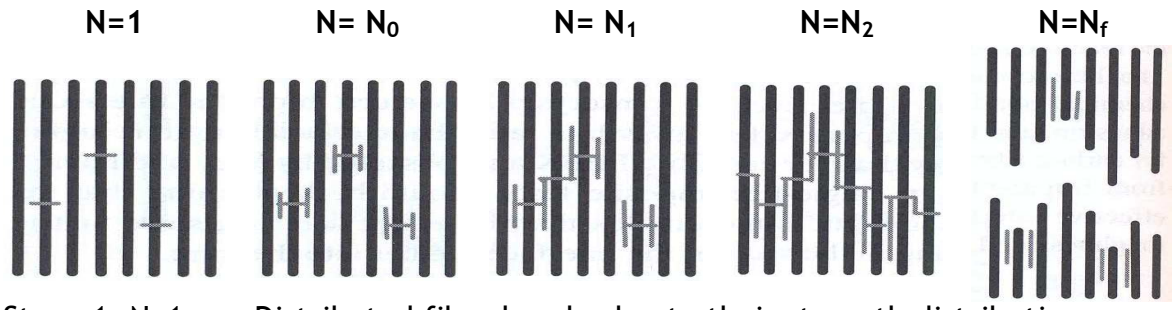

Stage 1: N=1 Distributed fibre breaks due to their strength distribution

Stage 2: N= N_0 Debond growth from the fibre breaks, stress redistribution in load carrying fibre segment

Stage 3: N= N_1 Longitudinal damage grows with further debonding; increase local stress additional breaks of overloaded fibres. This process is controlled by fibre–matrix interface.

Stage 4: N=N_2 Longitudinal cracking continue by progressive debonding and fibre breakage, crack coalescence

Stage 5: N=N_f Failure of specimen by separation

Figure 2.12 Schematic illustration of fatigue damage development until final failure in longitudinal composite, where damage initiates from individual fibre break from which longitudinal cracks or debond propagate (redrawn from Gamstedt, 2000)

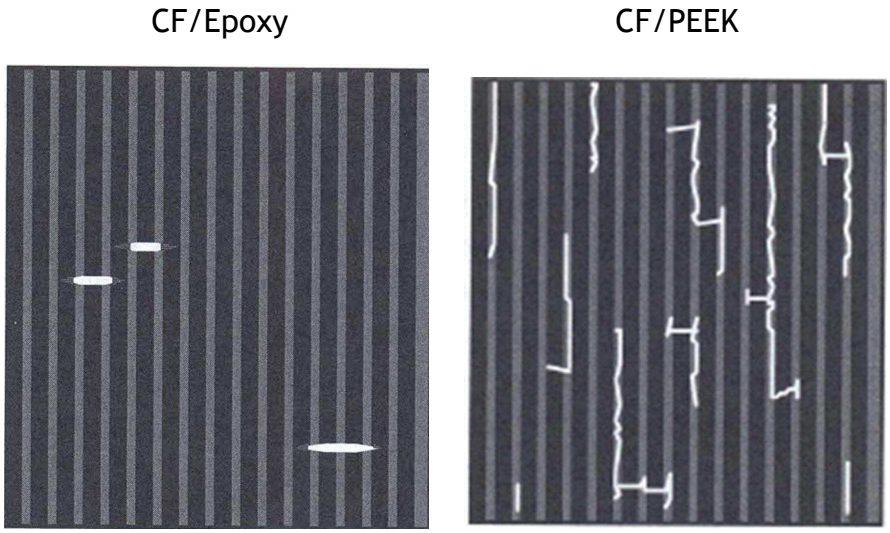

Figure 2.13 Schematic illustrations of fatigue damage states of unidirectional longitudinal carbon fibre reinforced plastics.

Carbon fibre/epoxy show fewer fibres fractures from which matrix cracks have propagated in the transverse directions, CF/PEEK demonstrate more fibre fractures and abundant longitudinal cracking (redrawn from Gamstedt, 2000)

Microscopy observation by Schadler et al. (1992) on the fatigue failure of a single carbon fibre in polycarbonate microcomposites reported that fibre strength dominated the early damage behaviour but after fibre failure, the damage growth was dependent on the matrix.

In practice, the failure of structures is more common in compressive loaded regions compare to tensile regions. Hsiao et al. (1995) argue that precise compressive testing often difficult due to global buckling and the near grip zone failure shadowed the compressive failure of the composite itself. The mechanics of compressive failure has been review by various authors (Fleck, 1997; Pruitt and Suresh, 1992).

In compressive loading, while the stiffness of the fibre remains the same, with increased compressive loading, Poisson's ratio effect generates transverse strains across the fibres that may initiate fibre kinking and buckling of the fibre. Kink band formation and propagation has been established as the primary failure compressive mechanism in limiting the strength of unidirectional fibre reinforced composites (Jelf and Fleck, 1992; Soutis and Fleck, 1990 and Budiansky, 1983).

In general, the initiation of kink bands is controlled by the o fibre-matrix interface. Madhukar and Drzal (1992) investigated experimentally the link between fibre/matrix adhesion and the failure mode of unidirectional carbon fibre epoxy composite. They showed that the integrity of the matrix/fibre interfaces would determine how composites would fail in compression. They reported that while compressive modulus was affected only slightly by fibre surface treatment, the compressive strength and maximum strain however were highly sensitive. The obvious observation was the failure mode changed with increases in interfacial strength. The composite failed in delamination and global delamination buckling at the lowest interfacial strength (Figure 2.14a), at the same time induced Euler buckling thus reducing the compressive strength. In the intermediate interfacial strength composite, delamination was observed only at the specimen edges while reducing the end tab debonding. As load increased, local microbuckling of the fibre column occurred and propagated into the neighbouring columns, thus lead to final failure (Figure 2.14b). With increases in the interfacial strength, the composite failure mode changed to shear failure. While for the highest values of the interfacial shear, the specimen failed in yield, with stepped fracture surfaces, which indicated the compressive failure of the fibres in planes, perpendicular to the fibre axis (Figure 2.14c). This phenomenon occurred because the fibres can be compressively loaded to the maximum as a strong interface able to provide strong lateral support to the fibres without buckling thus further increasing the compressive strength.

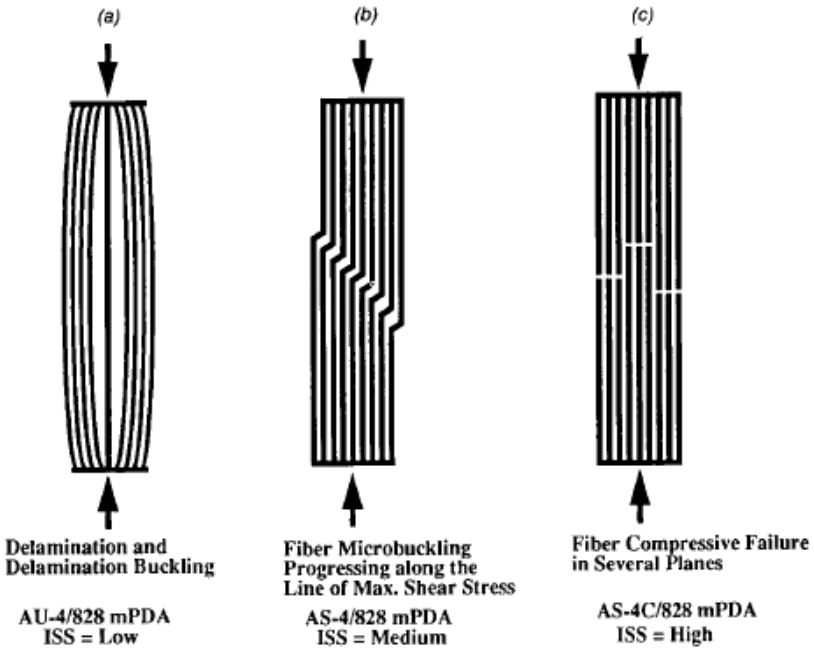

Figure 2.14 Schematic of the major failure modes detected for the three types of graphite/epoxy composites with different strength fibre-matrix interface

These failure modes are: (a) global delamination buckling (poor matrix-fibres interface), (b) local fibre microbuckling (intermediate fibre-matrix interfaces) and (c) fibre compressive failure (highest fibre-matrix interfaces) (from Madhukar and Drzal (1992)

The failure mechanisms in cyclic loading are similar to those for tests to failure but at lower speed due to nature of the fatigue test. During compression loading, failure initiated once the fibres buckled, acted as initiation site for fatigue damage growth, which later caused the neighbouring fibres to buckle in successive manner to create kink bands during cyclic loading. A micrograph of the fatigue crack in a carbon fibre reinforced epoxy is shown in Figure 2.15. This finding were supported by Tai et al. (1995) who found similar wrinkled patterns on broken buckled fibres in compressive fatigue of carbon fibre/PEEK composite. The fracture surfaces showed two distinct regions of a tensile side and compression side, showing that the fibres had buckled.

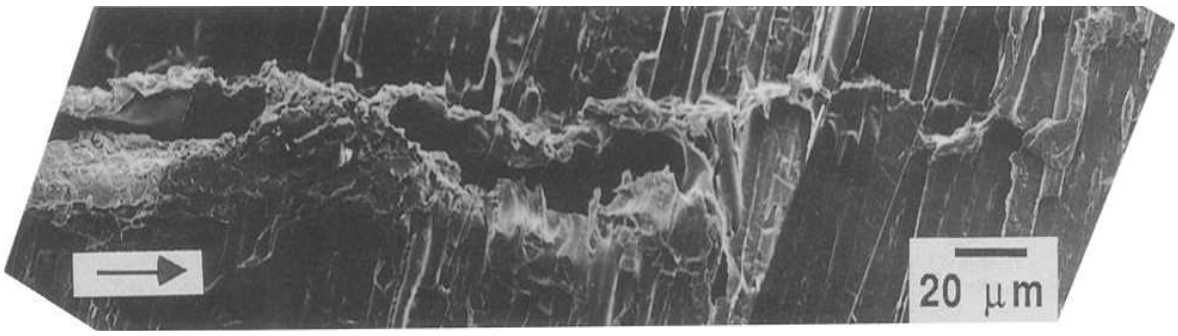

Figure 2.15 Micrograph of a compressive fatigue crack in a unidirectional 0°carbon-fibre reinforced plastic after 6000 cycles (from Pruitt and Suresh, 1992) showing the crack propagating across the fibres in the direction indicated by the arrow.

2.3.4 Factors influencing fatigue behaviour

When subjected to fatigue conditions, composite materials generally suffer from 'fatigue damage' consisting of cycle-dependent reduction in internal integrity (Reifsnider, 1990). In composite materials, the fatigue behaviour mostly comes from matrix degradation rather than filler fracture, which is usually observed by the present of crack propagation in the matrix resulting in failure.

Polymers are viscoelastic materials that are influenced by varying testing conditions. Some of the major factors that influence fatigue behaviour of the polymeric composites are discussed below:

2.3.4.1 Test frequency

Strain rate or load frequency is closely related to dissipation and heat generation in cyclic loading of thermoplastic composite. The energy dissipation per second (Ė) is given by:

$$\dot{E} = \pi f J''(f,T)\sigma^2$$

Equation 2.10

where f is the applied frequency and T is absolute temperature, σ is peak stress and J'' is loss compliance, (Ferry, 1970). Ferry (1970) defines loss of compliance as 'the strain 90° out of phase with the stress divided by the stresses'. It is a measurement of energy dissipated or lost as heat per cycle of sinusoidal often used to compare different system at the same stress level.

As most of the energy is dissipated in the form of heat, therefore, any increases in test frequency, will increase the temperature, stress amplitude and internal friction. As the temperature rises, it will reduce the modulus and is often observed to lead to an increase of energy dissipated due to poor conductivity and high damping of the plastic material, which later can lead to thermal fatigue.

Moore (1993) conducted a study to measure the effect of load frequency on fatigue lives for a quasi-isotropic carbon fibre/PEEK laminate loaded in cyclic tension at 0.5 and 5Hz. The results confirmed the suggestion that composites subjected to higher frequency loading have shorter fatigue lives when compared with lower frequency tests at the same applied stress. Moore also reported that the sample heated and matrix yielded at lower stresses when tested at higher frequency, this lead to the suggestion that in high stress regions, the temperature that accumulated might even exceed the material's glass transition temperature.

Another study on effect of loading frequency in fatigue live of carbon fibre/PEEK laminated was reported Xiao and Al-Hmouz (1998). The tests were carried out at 1, 5 and 10 Hz at various stress levels (Figure 2.16) and compared the changes in hysteresis loss and temperature. They reported that at higher frequency, the fatigue lives were reduced considerably. Although, there were no particular relationship between the frequency and the mechanical loss (measured by area of the hysteresis loops), the temperature increased rapidly at higher frequency loading suggesting that heat generated from the test did not have sufficient time to dissipate at higher frequencies.

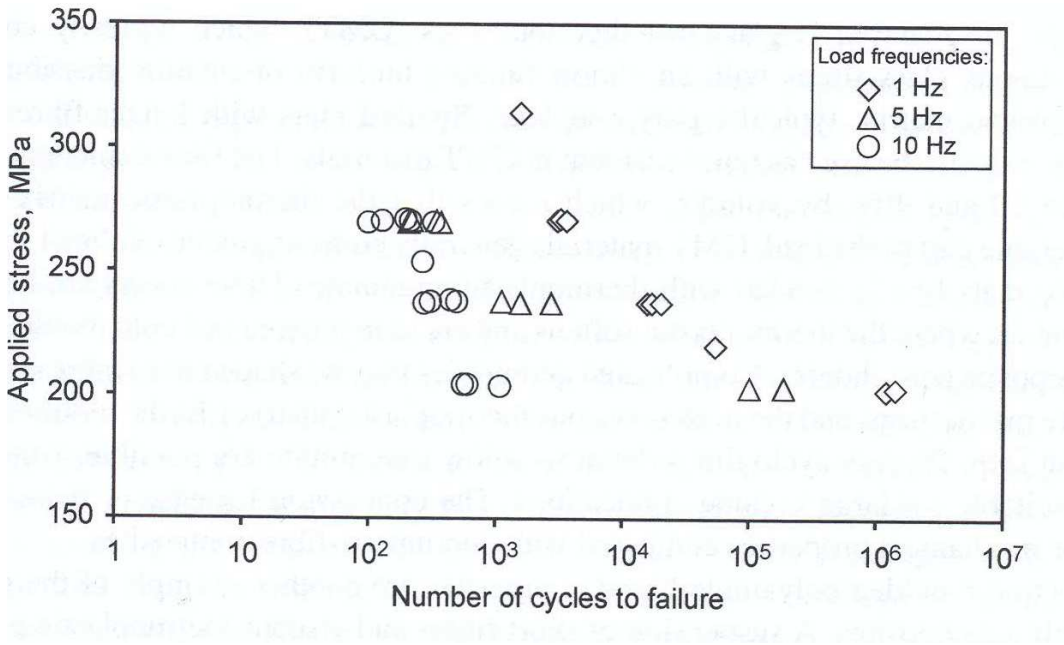

Figure 2.16 Stress-life data for laminated carbon fibre reinforced PEEK in tensile fatigue at various frequencies (from Xiao and Al-Hmouz, 1998)

However Lewis et al. (2003) reported different finding when comparing the influence of load frequency on the fatigue lives of acrylic bone cement tested at 1 and 10 Hz. The fatigue lives increased with increasing of frequency thought to be because of viscoelastic structure of bone cement. As the frequency increased, the strain at initiating pores decreased, thus preventing or slowing down the crack initiation, which leads to increased of fatigue life.

2.3.4.2 Effect of Crystallinity

In general, crystalline polymers are more fatigue resistant than amorphous polymers because of their structure due to:

- rigid crystalline phase that imbedded in amorphous phase acts as animpedance to crack propagation
- fracture energy can be absorbed by crystallite deformation hence increasing the fatigue resistant properties.

The crack propagation rates in amorphous polymers differ. Polystyrene (PS) and poly(methylmethacrylate) PMMA for example, craze in preference to shear yielding, giving higher fatigue crack propagation rates. On the other hand, polymers such poly(vinyl chloride) (PVC) and polycarbonate (PC) tend to fail by

shear yielding, necking and crazing, thus have slower crack propagation rates (Hertzberg et al., 1975). This difference in behaviour is thought to be due to increase chain flexibility, which aids more uniform stressing of the macromolecules under cyclic loading conditions.

In another fatigue study of carbon fibre/PEEK composite, Folks et al. (1993) compared the hysteresis loss during cyclic loading with a dynamic mechanical thermal analyzer, in both slowing cooled and quenched samples reporting that the loss angles were higher for the later. Rapidly cooled samples had larger hysteresis loops, which would suggest that this material is more likely to experience adiabatic heating if the mechanical generated energy cannot transfer out. Heat and damage accumulation can accelerate failure progresses in fatigue testing. They also concluded that samples that undergo rapid cooling have a weaker interface as confirmed by clean protruding fibres pull-out on the tensile fracture surface. On the other hand, slowly cooled composites are thought to have better interfacial bond as shown by their characteristic failure of more even and planar fracture surface with the fibres covered with more polymer residue.

Curtis et al. (1991) reported that although rapidly cooled unidirectional longitudinal carbon fibre/PEEK laminates have shorter compression fatigue lives than those that had been cooled slowly from the processing temperature, there is no difference on fatigue performance in tensile loading of carbon fibre/PEEK angle-ply laminates for samples that undergo rapid or slow cooling from the processing temperature.

Bureau et al. (2002) suggested that transcrystalline zone around the fibres are crucial to provide better resistant to the fatigue crack propagation. If the transition between transcrystalline regions to amorphous phase is distinct, then it is more likely that the crack will propagate along those interfaces. They discovered that the crack propagation rate is higher in unidirectional glass-fibre reinforced polypropylene samples that have distinct different morphological phases compared to smoother transitions between transcrystalline and amorphous phases (Figure 2.17).

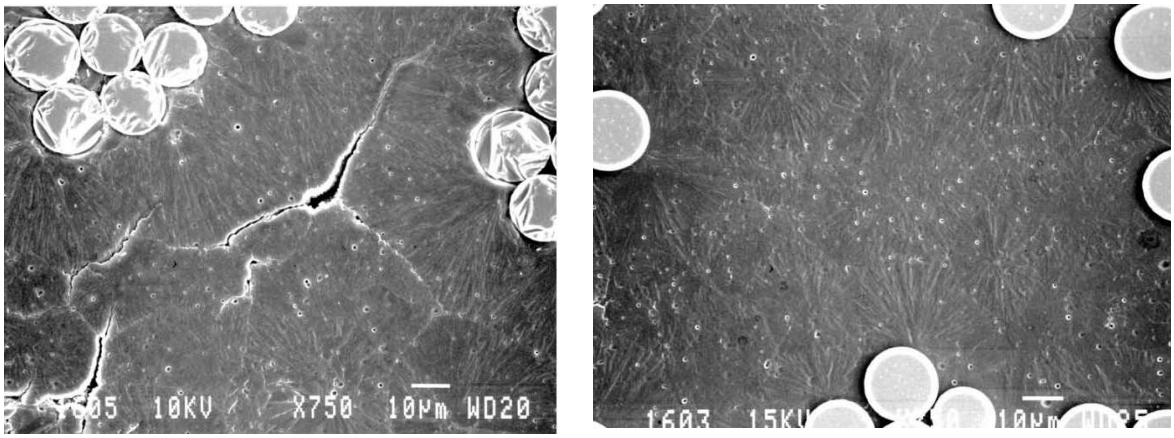

(a) (b)

Figure 2.17 Micrograph of glass-fibre reinforced polypropylene:

a) distinct interfaces between transcrystalline and amorphous zones resulted in rapid fatigue crack propagation, whereas (b) composite with a smoother phase transition gave higher resistance to fatigue crack propagation (Bureau et al. 2002)

2.3.4.3 Temperature

Test temperature can alter the fatigue life of polymeric composites. Andrews and Walker (1971) investigated the effect of the temperature on fatigue fracture of polyethylene at various temperatures ranging from 20 to 50°C and reported that the fatigue life of the polymer decreased approximately 20-25% for every 10°C increase in test temperature.

The decrease in fatigue properties probably due to changes of the materials viscoelastic state at the same time effecting their fracture toughness properties and chemical stability. Sauer and Richardson (1980) reported higher crack propagation rates due to lower stress values was observed in PMMA and polystyrene (PS) polymers when tested at higher temperatures. This finding is similar to a previous study of PS, when tested at series of temperature from 5°C to 75°C. It was reported that even with increasing the temperature, the S-N still maintained it general shape, the stress levels decreased and so were the fatigue lives of the material (Weaver and Beatty, 1978). This finding were further confirmed by Johnson et al. (1989) whom reported that the fatigue lives of bone cement was further reduced when testing at 37°C in comparison to room temperature at 24°C.

Tang et al. (2000) studied effect of temperature on tension-compression fatigue study of vinyl ester/E-glass unidirectional fibre composite at 4, 30 and 60°C in salt water environment. They reported that while there is no significant difference between the fatigue life when tested at 30 and 60°C, the fatigue life of composite tested at 4 °C was significantly longer than that tested at 30°C.

2.3.4.4 Liquid environment

Implants once implanted in the body are subjected to degradation as they operate in a wet environment consisting of saline solution and at body temperature of 37°C. Hence, the long term properties of the polymeric implant can be affected by the degree of the degradation. Johnson et al. (1989), as mentioned previously, investigated the effect of the liquid environment on the fatigue behaviour of acrylic cement in saline. Their result showed that while maintaining the same temperature (24°C), the fatigue life of the bone cement increased in saline compared to in humid laboratory air. It was thought to be due to viscoelastic structure of the polymer and plasticizing effect of saline, which decreases the initiating crack strain and slows down the crack rate thus increasing the fatigue properties.

Similar behaviour was reported by Nguyen et al. (1997) in their study on fatigue fracture of PMMA bone cement in Ringer's solution. They found that PMMA had higher fatigue and increased fatigue resistance properties in Ringer's solution compared to testing in air.

2.3.4.5 Reinforcing Phases

In polymeric composites, reinforcement is used to develop stiff and strong composites with enhanced mechanical properties and more often to reduce cost of the product. The most common reinforcements include rubber particles, glass spheres, ceramic fillers and fibres. Lang et al. (1984) discussed that toughening mechanisms in composites can be achieved through crack bridging, fibre pull-out, kink-banding and shielding mechanisms. Ritchie (1988) proposed a model of the role of crack tip shielding mechanism on the crack growth rate regime. This finding showed that a process-zone shielding mechanism should able to change the slope, m in the Paris regime, but should not alter the crack growth

behaviour at near-threshold regime. Some of the zones shielding mechanisms are shown in Figure 2.18.

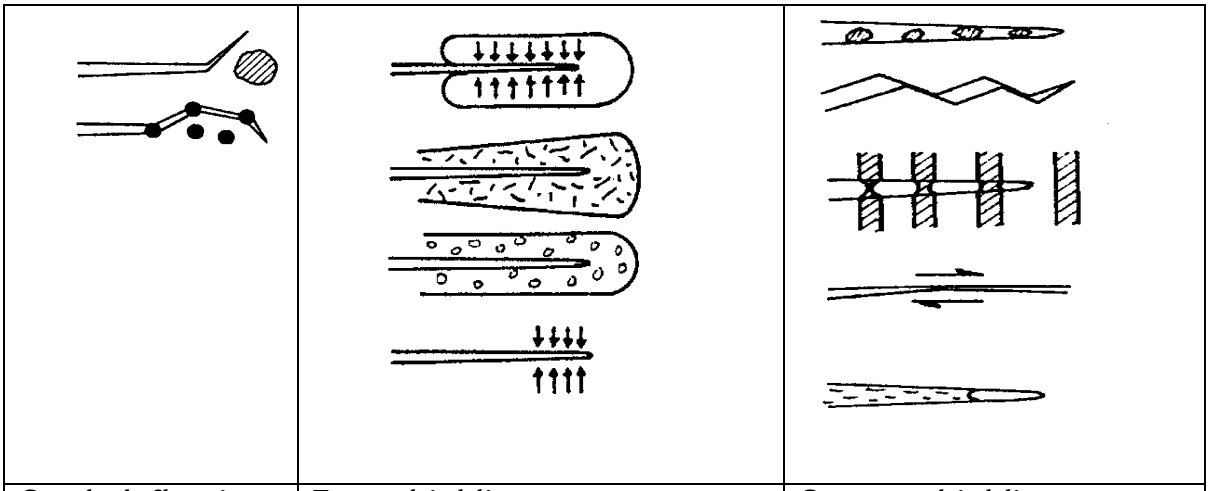

Crack deflection	**Zone shielding:** transformation toughening, microcrack toughening, crack wake plasticity , crack field void formation, residual stress fields	**Contact shielding:** wedging, bridging, sliding, combination of wedging and sliding

Figure 2.18 Schematic illustration of the mechanism of crack tip shielding: crack deflection, zone shielding and contact shielding (from Ritchie, 1988).

This model was later confirmed experimentally by Azimi et al. (1996), who reported that addition of rubber particles decreases the slope, *m*, and retarded crack growth at high crack growth rates. At low values of stress intensity range (ΔK), the crack growth was similar to those of non-reinforced blank resin. They argued that at low ΔK levels, the process zone shielding is small as the rubber was not highly stressed thus the crack growth is minimal. In contrast to this, at high ΔK levels, the process zone was observed to be larger than the size of the fillers, thus the rubber additions within this region are highly stressed. The rubber particle cavitations caused significant matrix plasticity thus reducing the crack propagation rate. At the same time, they also shown that addition of glass particles in the rubber-toughened blends enhanced the fatigue crack growth resistance obtained from interaction between the glass fillers at the crack tip and the plastic zone triggered by the rubber particles.

Friedrich and Karsch (1981) observed that in the fatigue crack growth of glass filled polyamide 6.6, the cracks were prone to grow along the filler-matrix interface. The fracture surface showed adhesive failure indicating that better

interfacial efficiency would lead to reduction crack propagation in particulate composites. Further improvements in the fatigue and fracture toughness were achieved by incorporating short glass fibres or carbon fibres into PEEK injection moulding compound (Friedrich et al., 1986). In fibrous composites, crack propagation mechanisms are usually initiated by fibre pull-out. There is an optimum pull-out energy closely related to fibre length and interfacial adhesion (Kelly, 1970). Nevertheless, interfacial adhesion has a crucial effect on fatigue crack growth resistance in short fibre composites.

Caprino (2003) reported that the fatigue damage in chopped-strand-reinforced thermosetting matrices is analogous to that of continuous fibre laminates. Damage starts in the form of interface cracking, which normally increases as the cycles progress, which leads to reduction in the residual mechanical properties and finally fatigue failure. Damage commonly results from matrix cracking and/or debonding of the fibre-matrix. In short fibre reinforced thermoplastics produced by injection moulding, there are various fatigue damage mechanisms, which can be observed depending on the matrices and the composite microstructure characteristic. For ductile matrices, matrix yielding or fibre-matrix debonding may occur. For brittle matrices, damage normally arises from micro cracks or crazing, commonly occur around transversely oriented fibres.

Karger-Kocsis and Friedrich (1988) investigated the influence of fibre length in short-fibre reinforced polyamide 6.6. They reported that a low crack growth rate was observed in long glass fibre, moderate in short fibre composites and fastest in unfilled matrix. The slower growth rate probably due to more constraint deformation experienced by the matrix in longer glass fibre composite, with evidence of larger damage zone in front of the crack tip in compact tension specimens compare to the shorter reinforcement and the unreinforced matrix.

Harris (2003) states that it is relatively rare to compare directly the effect of continuous and short fibre of same type in identical composite, due to differences of manufacturing parameters. However, Harris et al. (1990) were able to minimize the production difference by producing composite with same volume fraction of 0.35 for both short and long continuous carbon fibres in epoxy composite. The continuous fibre reinforcing composites were produced using a

conventional pre-pregging method while the chopped short fibre composite was produced by a glycerol-alignment method. As shown in Figure 2.19, although the quasi-static strength of the short fibre composite is much lower than that of the long-fibre laminate, its fatigue response is increased as a percentage of the UTS.

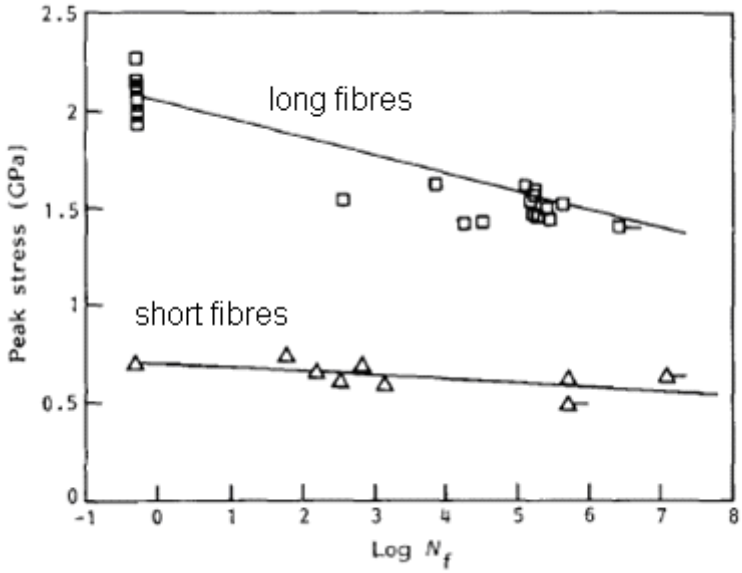

Figure 2.19 S-N diagrams for unidirectional carbon/epoxy laminates reinforced with continuous and discontinuous fibres (from Harris et al., 1990)

Harmia (1996) reported that the resistance to fatigue crack propagation of fibre-reinforced polypropylene was increased when surface modification agent used to improve the interfacial adhesion of the composite.

2.3.4.6 Loading conditions

Commonly, when the test condition is not simply uniaxial tensile aligned with the fibre direction, it may cause more stress to be placed on the matrix and reduce the fatigue resistance properties. This can be observed in flexural fatigue and tension–compression loading testing of unidirectional composite. More often, it also occurs in fatigue testing of laminated materials.

Ramani and Williams (1976) studied fatigue behaviour of 18-ply (0°±30°) carbon/epoxy laminates in various combinations under axial tension-compression loading. They reported that the fatigue resistance reduced as the compressive stress increased, due the extensive shear damage caused by weak interfaces bonding between the matrix and fibres. Kunz and Beaumont (1975) and Berg and

Salama (1972) reported that during pure compressive fatigue testing, fatigue cracks propagated in CRFP through the spreading of fibre buckling failure zones. Compressive buckling failure is the dominant failure mode in many kinds of fibre-reinforced composites and normally is initiated by shear failure in the matrix, possibly due to debonding activities.

Fernando et al. (1988) showed that compression and shear stress were more likely to effect the composite containing Aramid fibres (Kevlar, K) than carbon or glass fibres as lower fatigue lives were observed in ±45° KFRP laminates than in CFRP or GFRP. Microscopic examination revealed that KFRP samples showed kinking and splitting of the fibres resulting from interfibrillar weakness (Figure 2.20). Similarly, when tested in torsional mode, which is the weak part of the composite where the failure was normally dominated by shear, the composite had low resistance to shear fatigue (Philips and Scots, 1976).

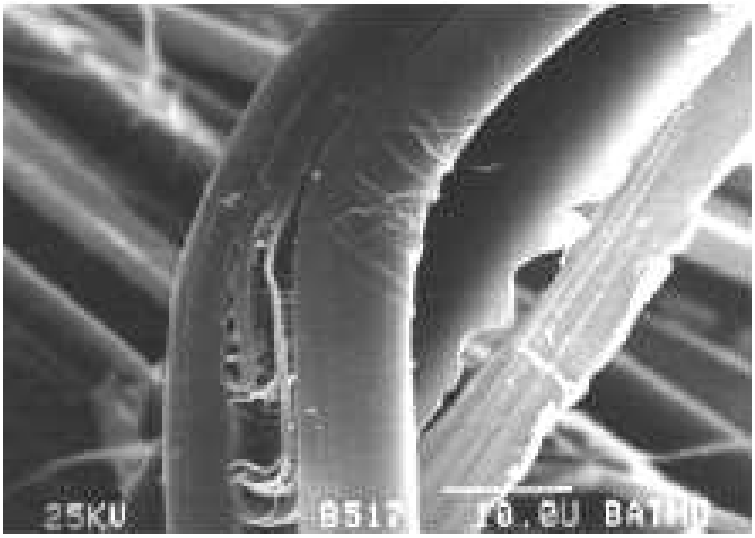

Figure 2.20 Splitting and kinking damage in Kevlar-49 fibres after fatigue cycling (Fernando et al., 1988)

The deleterious effect of compression loading in tension-compression fatigue behaviour of unidirectional carbon fibre reinforced epoxy resin composite was reported by Morris (1974). The specimens were tested in zero-tension, zero-compression and fully reversed tension-compression. The fully reversed fatigue testing showed similar results with zero-compression loading indicating compression induced effects such as fibre buckling and delamination, matrix

shear are dominant in unidirectional continuous fibre composite thus leading to reductions in fatigue resistant (Figure 2.21).

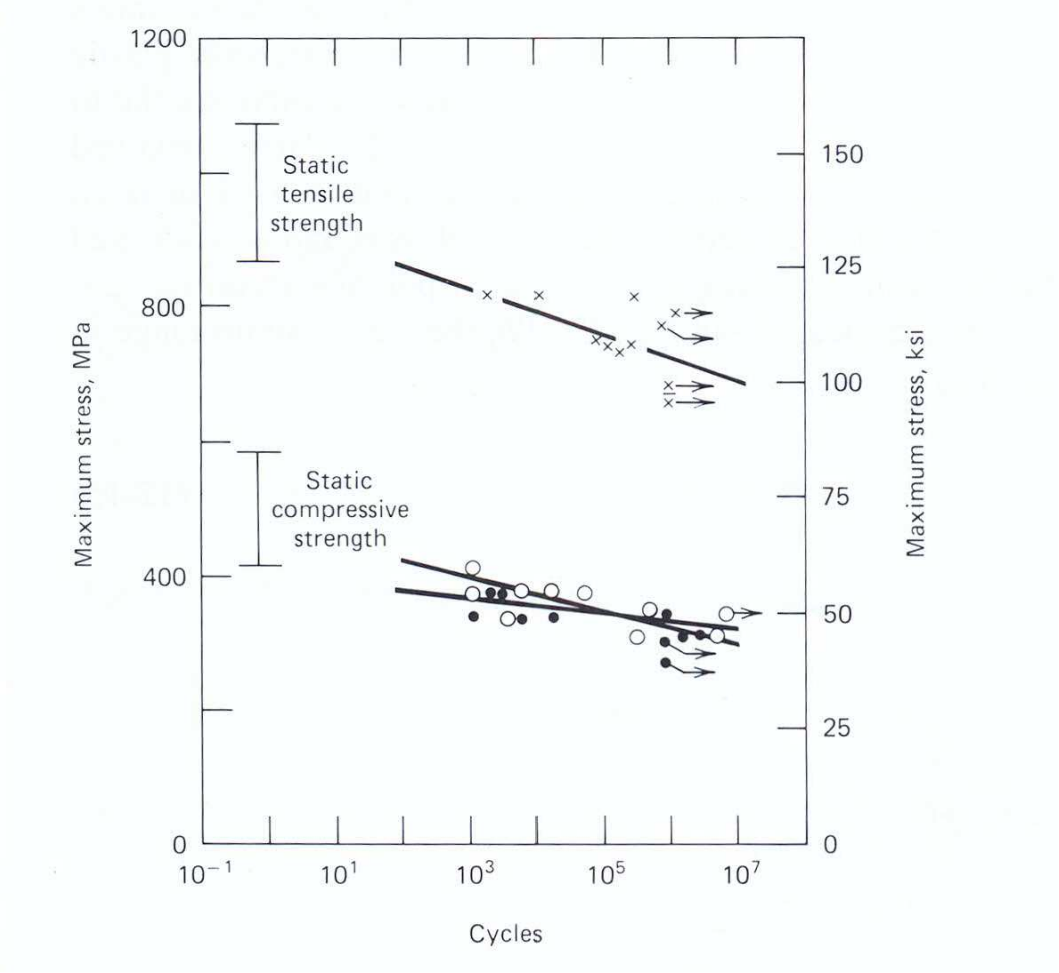

Figure 2.21 Effect of the compressive stress on the axial load fatigue behaviour of unidirectional carbon fibre-reinforced epoxy resin for zero- tensile (x),compression-zero (•) and tensile-compression (o) (Morris, 1974)

This finding was further confirmed by Gamstedt and Sjögren (1999) who compared tension-tension (T-T) and tension-compression (T-C) loading modes for cross-play glass/epoxy and single fibre model composite with the fibres perpendicular to the loading direction. They reported that composite laminate degraded more rapidly in tension-compression loading compare to tension-tension loading. This reduction may attributed to higher debond growth around transverse fibres in the T-C loading as result from the faster crack tip opening under the compression loading for sufficiently large debond. This caused early transverse crack initiation which resulting in premature appearance of transverse cracking that lead to early fatigue failure (Figure 2.22).

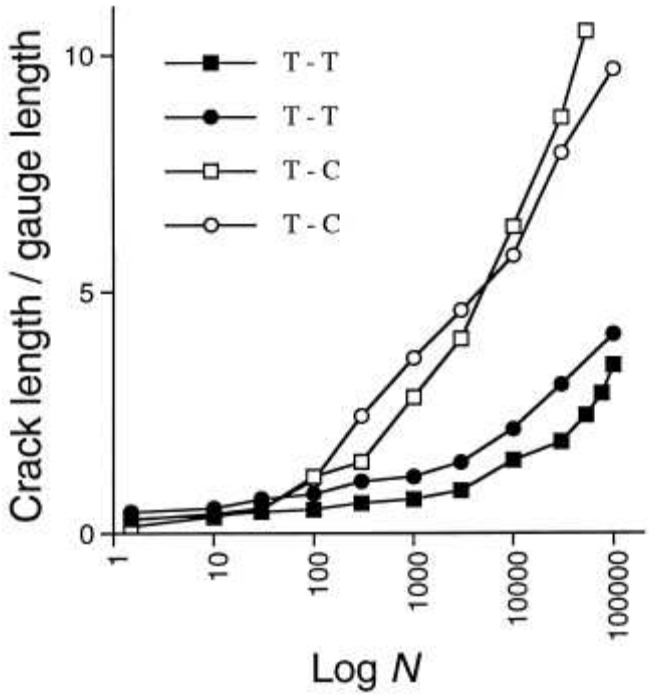

Figure 2.22 Progression of transverse crack length in fatigue

in tension-tension (T-T) and tension compression (T-C) loading with respect to number of load cycles for both 0°/90°crossply composite and individual fibre in resin samples. The paper doesn't differentiate between the symbols for these two sample types (from Gamstedt and Sjögren, 1999)

2.3.5 Biaxial fatigue theories

Over the years there has been a significant number of fatigue tests performed, however huge data of the fatigue analysis are on lightweight structure, while on the materials level, the majority of research is in uniaxial cyclic loading and the development of associated degradation rules (Harris et al., 1997; Peterman, 2004). However, most of engineering components, including medical implants operate under complex multiaxial stress conditions, therefore it only makes sense to test the materials under multiaxial loading in order to provide better understanding of the degradation of the material properties. The fatigue behaviour of fibre reinforced composites in multiaxial cyclic loadings has been analyzed only in a handful of experimental investigations (Perevozchikov et al., 1988; Limonov, 1988; Andersons et al., 1994; Ellyin and Martens, 2001; Shokrieh and Lessard, 2003). One of possible reason there were only a handful of experimental work were carried out is due to difficulties to set up the experimental and complexity of the test as well as viabilities of test parameters and data.

In general, biaxial fatigue testing is achieved by applying axial (σ) and shear/torsional (τ) stress using the same frequency to a specimen, which can be in-phase (proportional) or out of phase (when a phase shift between axial and torsional cycles is present) as shown in Figure 2.23.

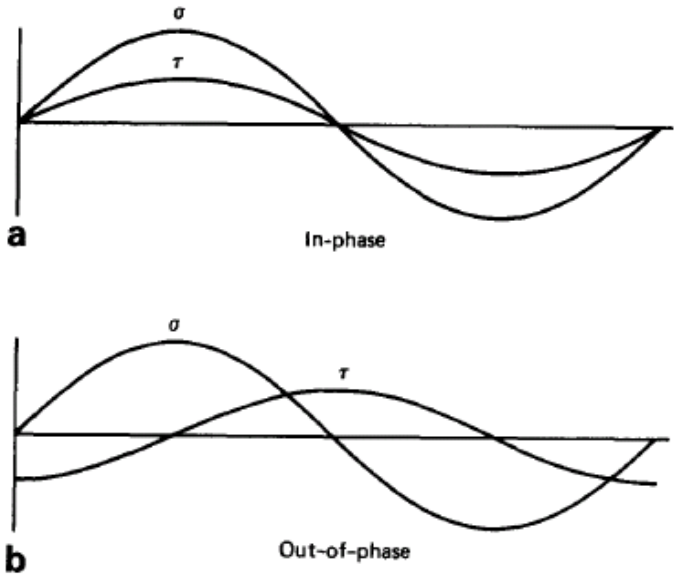

Figure 2.23 Biaxial fatigue cycles:
(a) in-phase, (b) 90° out-of-phase(from Jayaraman & Ditmars, 1989)

Testing out-of-phase often presents more problems compared to in-phase testing. One of the major problems is in determining the representative stress or strains since the magnitude and direction of the principal stresses change through the loading cycle. This influences the fatigue properties of the materials. Numerous multiaxial life prediction models have been proposed. Parameters, such as stress, strain and energy absorption, have been used to explain the fatigue behaviour, but are still insufficient to universally correlate the data for a wide variety of materials and testing conditions, as other factors may be present during the experimental work such as:

- the fatigue failure could occurring in any phase, either in-phase (resulting from maximum alternating stresses of strains having fixed principal axes directions) or in out-of-phase (principal axes rotate and the ratio of the principal stresses varies continuously)

- crack initiation and propagation directions were discovered can be affected by the type of materials and environmental effects, including corrosion, fretting, and low/high temperature (creep/fatigue interactions)
- existence of stress or strain concentration and the mean stress.

Materials parameters such as heat treatment, chemical composition, microstructure, impurity, crystallography and anisotropy also play important roles.

2.3.5.1 Multiaxial fatigue theories

Since the early 1900s, many multiaxial fatigue theories has been developed in order to provide better understanding of fatigue failure as well as prediction of the fatigue life. However, most of these studies are limited to the in-phase field. Due to increasing concern over multiaxial failure of components that are subjected to out-of-phase loading, mainly in the automotive industry such as crankshafts and drive shaft, some studies on out-of-phase fatigue have been performed but they are still limited.

Much of the research in multiaxial fatigue is in metals. It was generally accepted that cyclic loading produced cyclic plasticity, which in turn nucleates fatigue crack and growth propagation. Kanazawa et al. (1997) showed the present of slip bands in fatigue fracture failure on crystallographic planes closely aligned with the maximum shear plane. This lead to the conclusion that plastic strain is controlled by maximum shear strain alone, thus most of the later biaxial studies are conducted in strain based control.

An early study on the influence of phase angle in biaxial fatigue was carried out by Nishihara and Kawamoto (1945) in high cycle torsion/bending fatigue tests on various metals. Their data was further analysed by Little (1969) who reported that the fatigue limit decreases with increases in phase angle. Several other authors also reported similar finding (Kanazawa et al., 1977; Ellyin et al., 1991). Ellyin and co-workers suggested that such effects are possibly caused by formation of the circular path created when the principal stress and strain rotated during cyclic loading, allowing dislocation to move along all possible slip planes. This created extra cyclic hardening in the material to resist the motion,

thus leading to more damage accumulation in out-of-phase loading compare to in-phase loading. However, they observed that this assumption is only applicable to low cycle fatigue case, as when the plastic strain decreases, so does the effect of out-of-phase loading.

Kanazawa et al. (1977) tested an isotropic batch of 1% Cr-Mo-V steel under out-of-phase loading in tension-torsion fatigue testing at various biaxiality ratios and phase angles. They showed that out-of-phase is more damaging in low cycle fatigue. Contrary to this finding, Sonsino and Grubisic (1985, 2001) observed that if biaxial testing were performed under load control, out-of-phase conditions would increase the fatigue life.

Therefore the effect of loading path on the biaxial fatigue should be examined. In fatigue testing, the loading condition that often use is shown in Figure 2.24. In uniaxial testing, the biaxiality ratio ($\lambda = \tau/\sigma$) for tension-compression and torsion conditions are zero and infinity respectively. In the in-phase case, the loading path can be represented by straight line, while for out-of-phase condition, the loading path is ellipsoidal and the shape of the ellipse is controlled by the magnitude of λ, which again is controlled by the difference in the phase angle.

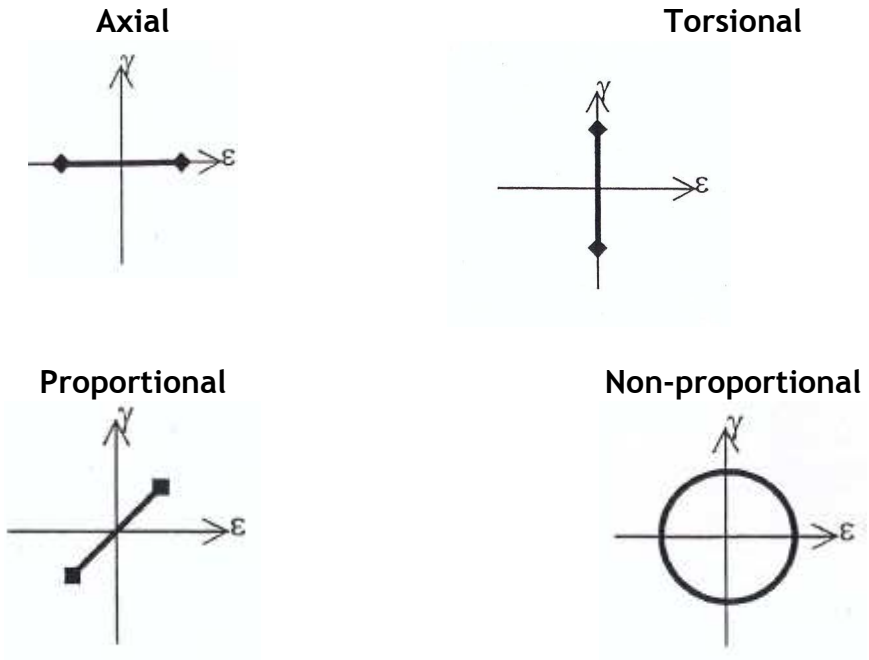

Figure 2.24 Loading histories of in-phase (proportional) and out-of-phase (non-proportional) (from Socie, 1987)

Figure 2.25 shows the strain histories for both proportional and non-proportional loading. The strains are given by intersections of the loading line with axial strain (x-axis) and shear strain (y-axis). In order to obtain the same strain range in proportional and non-proportional loadings, the applied axial strain (tension) and shear strain (torsion) for non-proportional loading (ε_N and γ_N) must be increased relative to the proportional loading condition (ε_p and γ_p). If the comparison is based on the applied strain, out-of-phase testing is expected to be less deleterious because the maximum strain is smaller. However, if the comparison is carried out on the basis on maximum strain, then the out-of-phase loading will be equal or more damaging than in-phase as it undergoes higher strains. The increase in additional strains is arising from formation of additional cyclic hardening occurring due to non-proportional loading. In strain-controlled test, this will increase the stress amplitude and consequently reduce the fatigue life of the specimen. However, it was observed that at small plastic strain levels, the strain hardening is insignificant, thus does not affect the fatigue life of the materials. However if larger plastic strains occur, the hardening factor can increase as much as 2 (stainless steel), thus can significantly reduce the fatigue life of the specimens (Socie, 1987).

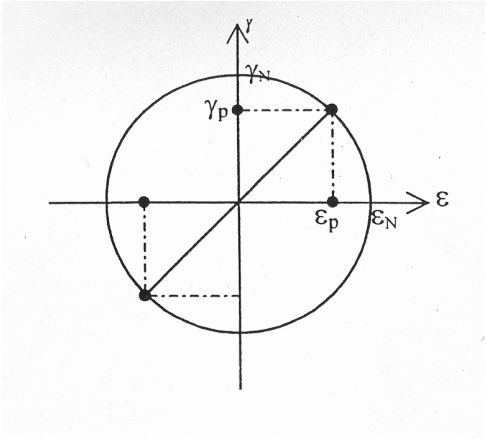

Figure 2.25 Strain histories for proportional and non proportional loading (from Socie, 1993)

While fatigue characterization and failure progression for polymeric fibre composites has been well documented for uniaxial loading, only a limited number of studies consider the fatigue behaviour under multiaxial loading.

Smith and Pascoe (1989) studied biaxial fatigue behaviour of glass/epoxy in flat cruciform specimens under multiaxial state of stress in both monotonic and fatigue loading environment. They summarized three main and irreversible damage mechanisms, which are rectilinear cracking (combined resin cracking and fibre/matrix debonding), delamination and shear degradation of fibre-matrix interface. At the same time they also reported that under general loading conditions, the failure mechanism is combination of the main mechanisms described above.

Chen and Matthews (1994) studied carbon/epoxy plates under different stress combinations of biaxial flexural fatigue. They reported that matrix cracks and delamination were the major damage mechanism of the composite and used reduction in the secant stiffness to quantify the fatigue damage.

Tanaka et al. (1996) studied the biaxial tension-torsion fatigue of woven glass-fabric composite, particularly the stress-strain relationship and the progressive damage of the composite with respect to the loading path. They reported that both damage accumulation and its sequence significantly depends on the loading path. Damage was dominated by tensile stress even at low biaxial stress ratios.

Ton That et al. (2000b) studied the effect of loading path as well as the combination of loading levels on HDPE reinforced with particulate HA composite in fully reversed tension compression and torsional fatigue testing. They reported that the superposition of torque on axial loading reduces the fatigue life significantly. A similar observation was reported with respect to the loading path. Out-of-phase loading was reported to be less damaging in comparison to the in-phase loading during biaxial testing.

Fujii and co-workers (1995, 1996, and 2000) studied the damage progression and stiffness degradation in plain-woven glass polyester laminated tubular specimen under tension-torsion biaxial fatigue. They reported that the modulus degradation in tension and shear is suitable to monitor the fatigue life at any biaxiality ratio.

Adden and Horst (2006) tested non-crimp fabric glass/epoxy tubes under tension/torsion fatigue of tubular samples. They reported that the crack density

in the specimen was affected by the different biaxial loading conditions. Interestingly, the crack density for pure shear fatigue is higher than in biaxial loading.

In unidirectional continuous fibre composite, failure is normally observed in compression phase through buckling mode. Often misalignment of the fibre has been seen to initiate the microbuckling failure. Several studies had been carried out to study the effect of fibre waviness and misalignment (Hsiao and Daniel, 1996; Potter et al. 2008). However, the effect of these parameters on biaxial fatigue behaviour has not been thoroughly investigated until recently, Schmidt et al. (2012) conducted a study on the effect of local fibre waviness on biaxial fatigue damage mechanisms of glass fibre reinforced polymer. The test was carried out at various biaxial ratios of tension-compression and torsional in-phase. They reported that while fibre waviness did significantly affect the increase in crack density and modulus degradation, early initiation of delamination occurred due to fibre waviness, and considerably reduced the fatigue strength of the composite.

2.3.5.2 Biaxial fatigue models

Biaxial fatigue has been approached via three distinct methodologies: high cycle fatigue using stress-based theories, low cycle fatigue using strain-based theories and crack growth (Brown and Miller, 1982; Toor, 1975; Elyin, 1988). This part of the literature will only briefly touch on the stress-based criteria. Stress-based criteria are usually more suitable to use in predicting long life fatigue failure of materials (more than 10^5 cycles). The majority of data usually exists in the high cycle region as the finite life approach is used to establish S-N curves. At the same time, it provides simpler testing than strain-based low cycle fatigue region since the user does not need to make adjustment or differentiation between loads (stress) and displacement (strain control). Ellyin (1988) summarized that plastic shear deformation plays a major role in crack nucleation and early growth, thus all multiaxial fatigue approaches usually include stress and strain theories.

Stress based criteria are summarized in Table 2.7. Literature showed that three most popular stress-based criteria, often referred to as the classical failure

criteria, which include the maximum principal stress criterion (Rankine), the maximum principal shear stress criterion (Tresca) and the octahendral shear stress criterion (von Mises). The model is based on extensions of static yield criteria to fatigue. Previous studies showed that Rankine criterion results provide good correlations to represent failure in brittle materials, while Tresca and von Mises give good correlation for ductile materials at long fatigue lives (Brown and Miller, 1973; Fatemi and Kurath, 1988). For anisotropic materials, the Tsai–Wu criterion is often used due to its ability to treat interactions terms as independent components and take into account the difference in strengths due to positive and negative stresses, it can also be specialized to account for different material symmetries and multiaxial stresses. The Tsai-Wu criterion has been used by various authors (Carter, 1977; Hayes and Wright, 1977; Cezayirlioglu et al., 1985) for compact bones. Several authors also reported good correlation to estimate failure in continuous fibre polymeric composites (Amijima et al., 1991; Tanaka et al., 1998).

Table 2.7 Some representative of biaxial fatigue model of stress -based criteria (adapted from Ellyin, 1988)

Criterion	Relationship	Notes
Maximum principle stress (MPS)	$\sigma_1 = \sigma_F$	$\sigma_1 > \sigma_2 > \sigma_3$
Maximum Shear Stress (Tresca)	$\tau_{\max} = \frac{1}{2}\max[(\sigma_1 - \sigma_2),(\sigma_2 - \sigma_3),(\sigma_3 - \sigma_1)] = \frac{1}{2}\sigma_F$	Hydrostatic stress insensitive
Strain energy density (SED)	$\sigma_1^2 + \sigma_2^2 + \sigma_3^2 - (\sigma_1\sigma_2 + \sigma_1\sigma_3 + \sigma_2\sigma_3) = \sigma_F$	
Distortion Strain Energy Density (von Mises)	$(\sigma_1 - \sigma_2)^2 + (\sigma_2 - \sigma_3)^2 + (\sigma_3 - \sigma_1)^2 = 2\sigma_F^2$	Hydrostatic stress insensitive

Note: σ_1, σ_2, σ_3 are principle stresses.

2.4 FATIGUE OF BONE AND BONE REPLACEMENT MATERIALS

2.4.1 Fatigue of Bone

Within the last few decades, there been increasing numbers of studies focused on understanding the fatigue behaviour of bone. At the same time, due to increases in the lifespan of both women and man, with individuals seeking to maintain an active life, better understanding of the progressive degradation of bone properties through fatigue seem relevant.

Bone has the ability of self-repairing, therefore, normally fatigue fracture occurs when the remodelling process is out-paced by the fatigue process. On the other hand, the damage from the cyclic loading is greater than the remodelling needed to prevent failure. Sudden increase in individual physical activity can cause fatigue fractures, clinically known as 'stress fractures', prone to occur in lower limbs bone including the metatarsal, tibia, femur and pelvis, varied with activities of the individuals. For example, fatigue fractures are more common in the tibia among athletes (Matheson et al., 1987) while metatarsal fatigue fractures normally observed among military recruits and ballet dancers (Poulles et al., 1989; Kadel et al., 1992).

Evans and co-workers (Evans and Lebow, 1957; King and Evans, 1967) were among the first to establish the S-N curve for human bone in fatigue life. The specimens were tested in fully reversed flexural loading in vitro. Carter and Hayes (1977) reported that when tested in vitro, the S-N curve for human bone may not be asymptotic, i.e. there is no fatigue limit. Microscopic analysis showed that cyclic tension resulted in failure at the cement lines and promoted osteon pull out, thus may created micro fractures in the bone leading to fatigue failure which becomes more severe when the load or deformation approaching yield. Further tests by Carter et al. (1981) in uniaxial tensile and compression suggested that fatigue behaviour of bone can be significantly correlated using strain range and degradation of the modulus models. Figure 2.26 shows a comparison of different S-N curves for bone obtained from various studies.

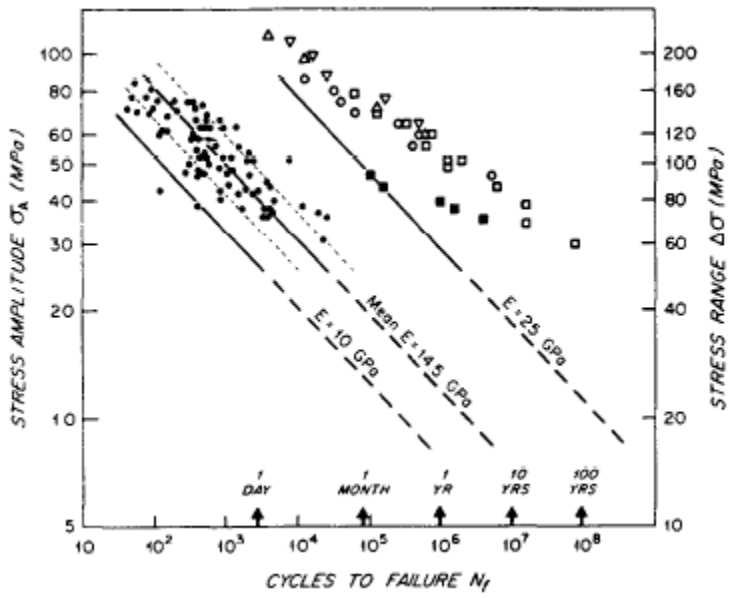

Figure 2.26 Comparison of stress amplitude versus cycles to failure of various fatigue studies of bone (from Carter et al., 1981)

Note: Filled circles (Carter et al. (1981); closed squares (Gray and Korbacher (1974); open circles (Swanson et al. (1971); upward triangles (Lafferty and Raju (1979); downward triangles (Carter et al. (1976); open squares (King and Evans, 1967).

It was reported in the literature that the failure estimation was improved by using a stress-based model, in comparison to number of cycles to failure (Caler and Carter, 1989; Zioupos et al., 2001). An early study by Caler and Carter (1985) also showed that the time to failure of bone is a combination of cumulative fatigue and creep. Results showed that creep dominated the damage when the stress range exceeding 60 MPa, while at lower stress, the bone life is primarily a function of fatigue damage. Caler and co-workers (Carter and Caler, 1985; Caler and Carter, 1989) suggested that fatigue degradation of the bone is also depending on the stress ratio. For example, in tension cyclic loading, bone showed significant time dependent degradation (creep) while in cyclic compression loading, the damage was dominated by cycle-dependent damage. Pattin et al. (1996) described the mechanical degradation of the bone during axial load controlled fatigue loading by recording the changes in secant modulus and cyclic dissipated energy that were produced. The result showed that modulus degradation and energy dissipation increased considerably at loading levels above critical damage strain thresholds of 2500 and 4000 με in tensile and compressive fatigue respectively.

Work on the fatigue of human cortical bone did not include the effect of torsional load until Vashishth et al. (1997) carried out multiaxial fully reversed biaxial fatigue of bone using torsion and tension/compression. Superposition of torsional on axial loading leads to dramatic reductions in fatigue life (Vashishth et al., 2001). A further study revealed that increasing the phase angle caused significant reductions in fatigue life of bone (George and Vashishth, 2005). During in-phase testing, the damage that produced was equally influenced by the magnitude of mixed mode crack initiation and propagation (tension, compression, torsional). For out-of-phase loading, only the torsional mode was significantly affected, thus reducing the contribution of the mix-mode behaviour load that extends the fracture path. The second factor is the magnitude of the principal plane rotation. Damage normally takes place on principal planes that become the main site for damage localization. During the test, out-of phase loading creates principal plane rotation, so the damage is diffused over a larger volume, while in-phase the damage is concentrated on a small volume, which leads to faster failure fracture. Figure 2.27 showed the influence of phase angle on the fracture surface damage.

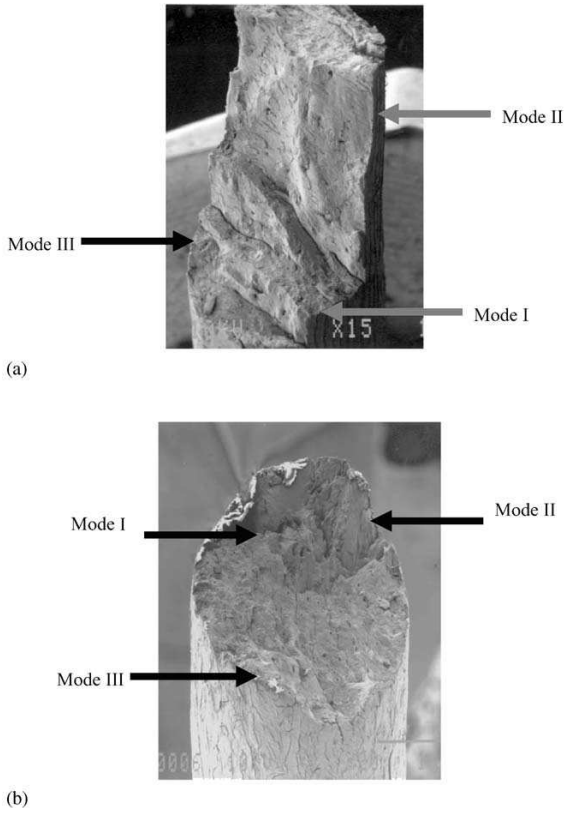

Figure 2.27 Influence of phase angle at reversed axial loading (±50A) and torsional loading (±30T) superimposed (a) out-of-phase, (b) in-phase in bovine bone (from George and Vashishth et al., 2005)

2.4.2 Fatigue of Polymeric Biomedical Composites

Bone fracture can be treated by internal or external fixation devices. In internal fixation, bone fragments are held in alignment by various implants such as screw, plates, wires, pins and intramedullary nails. Polymer composites have been investigated successfully for this type of application.

There have been a limited number of experiments on the fatigue properties of biomedical thermoplastic composites reinforced with continuous fibres. Curtis (1991) investigated carbon fibre (CF) poly (ether ether ketone) (PEEK) and compared it to carbon fibre epoxy composite. The unidirectional laminated composites were subjected to tensile only fatigue and the PEEK matrix composite showed inferior fatigue properties with fewer cycles to failure when compared with CF epoxy. Microscopic examination revealed that longitudinal splits grew faster in the PEEK matrix compared to the tougher epoxy matrix. The split appeared to originate from fibre fractures caused by stress concentrations that initiated interfacial debonding and then grew with the help of the local shear stress, along the fibre to form macroscopic splits. This caused further damage to the material that resulting in 'brush manner' failure when it was no longer able to redistribute load effectively. Pannkoke and Wagner (1991) compared the fatigue behaviour of unidirectional carbon fibre composite with epoxy, PEEK, poly(aryl ether ketone)(PAEK) and polycarbonate matrices under cyclic tensile loading at low temperature (77K). They reported that the three thermoplastic based composites have lower fatigue limits compare to those based on the epoxy matrix. They also observed that the fracture surface of thermoplastic-based composite showed a brushed like fracture with strangling fibre bundles, compared to the planar and brittle crack surface seen in the epoxy-based composite. The difference in the fracture surface indicated not only weaker interface in thermoplastic-based composite, but also an increased tendency for debond-prone growth during fatigue as shown in Figure 2.28.

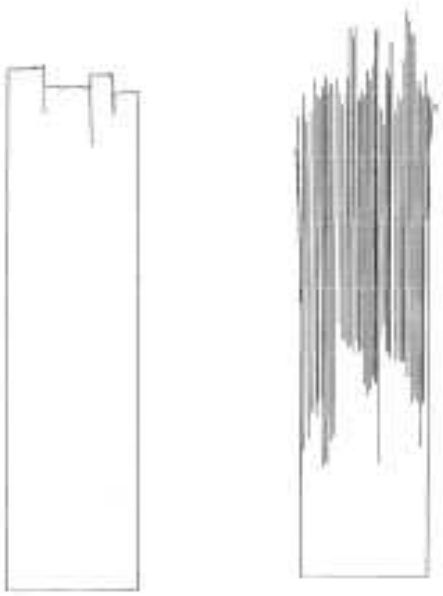

(a) Brittle failure (b) 'Brush failure'

Figure 2.28 Appearance of failed coupon (a) brittle failure mode common for static loading and strong interfaces, and (b) 'brush' type rupture indicative of fatigue failure and weak interfaces (redrawn from Gamstedt et al., 1999).

The incorporation of laminated composite structures using long carbon fibres introduces further complexity into the structural response under dynamic loading conditions, as the fatigue strength depends upon the length as well as the orientation of the fibres relative to the loading direction (Buggy and Carew, 1994)

Fujihara et al. (2007) investigated the fatigue bending properties of braided carbon/epoxy laminated composites with the target of a compression bone plate to repair diaphyseal fractures. Interestingly enough, they reached the conclusion that for an optimal braiding angle of 20° the fracture resistance under fatigue loading was maximized. Braided carbon fibres were also used to reinforce PEEK bone plates (Schambron et al., 2008). Preliminary fatigue experiment indicated that CF/PEEK bone plate was likely to perform well under physiological loads and when subject to a saline environment. In fact at 75% of the static strength, failure was not reached even after more than 300,000 load cycles, and the devices performed better than those made of A316L stainless steel.

Fatigue properties of screws made of biostable polysulfone (PSU) or bioresorbable poly-l-lactide-co-glycolide (PLGA) polymers reinforced with short

carbon fibres has been investigated by Jan and Grzegorz (2005). CF/PSU had better fatigue properties than CF/PLGA composites.

In contrast, for mechanical properties of particulate reinforced composites, the effect of biphasic loading is strongly depending on the interface between the particles and the matrix. Friedrich and Karsch (1981) considered the micromechanism of general damage in particulate composites in detail (Figure 2.29):

- Stage I: When the applied force reaches a certain value, the polymer matrix detaches from the filler particles, creating series of voids on both sides. Just a small amount of plastic strain is needed to initiate damage
- Stage II: voids grow in the stress direction, creating more plastic strain. Dimple-like holes form around the particles with width corresponding to particle diameter (D_P). Crack length, L will stabilize when the local stress around the particles reduces. As the tensile test progress, shear stress is produced on the plane at 45° to the tensile axis and the material the start to fail
- Stage III: shear stress caused further strain on matrix until holes coalesce and lead to composite failure

Usually, increases in filler content, reduces the strain in steps I and II, which changes the ductile fracture of the matrix to brittle fracture of the composite. This is because, with increasing of filler content, the maximum strain in the composite is reduced and the matrix is unable to develop full resistance to crack growth.

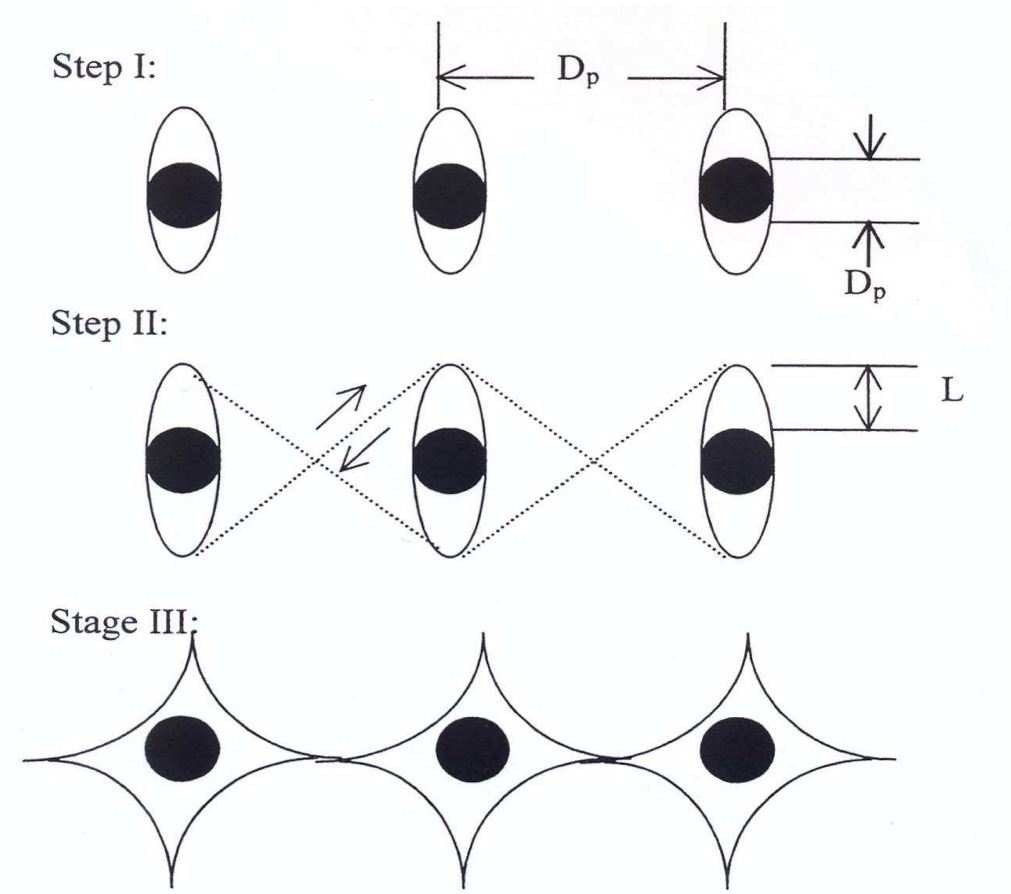

Figure 2.29 Schematic illustration of interfacial separation of filler particles and matrix (redrawn from Friedrich and Karsch, 1981)

Harper (1995) reported that addition of HA particles (up to 40 wt.%) in PEMA based bone cement PEMA/nBMA (polyethylmethacrylate/n-butylmethacrylate) produced minimum changes in the tensile strength, however there were large increases in Young' modulus and decreases in strain at maximum strength. They also reported that the fatigue resistant was also reduced and this was thought to be caused by poor interfacial bonding between the HA particles and polymeric matrix. In contrast, Matsuda et al. (2004) reported that introducing HA fibres, significantly reduced the crack propagation rate and resulting in better fatigue resistance.

Local fracture and crack growth of polybutadiene rubber embedded with hard particles was investigated by Liu and Rav-Chandar (1996). They reported that voids in the matrix opened up while in tension. Increases in stress created large voids with main crack tip, which then triggered crack propagation leading to failure at the process zone tip. At the same, it was reported that a toughening

mechanism via crack tip blunting was also observed, taking place before and after crack growth. As particulate composites are heterogeneous materials, the degree of crack tip blunting often differs with the position of the advancing crack tip.

The fatigue behaviour of HAPEX™ at 37°C in saline was determined under uniaxial (fully reversed axial tension-compression and fully reversed torsional loads) and biaxial (various combinations of fully reversed axial and torsional loads) loading conditions (Ton That et al., 2000a and 2000b). S-N curves under uniaxial loading indicated fatigue limits at between 37 and 25% of the ultimate strength of the materials. Superposition of torque on axial loading reduces considerable the fatigue limits of HAPEX™.

McGregor et al. (2000) investigated hydrostatically extruded HAPEX™ and suggested that due to the molecular alignment produced by the hydrostatic extrusion that anisotropic mechanical properties were produced and significantly increased flexural strength and fatigue life compare with conventional isotropic HAPEX™.HDPE reinforced with HA whiskers exhibited a four to five fold increase in fatigue life compare with equiaxed particles at either 20 and 40 vol.% filler content (Kane et al., 2008). These results confirm the observation of Joseph and Tanner (2005) who found a marked dependency of the fatigue behaviour on the surface behaviour of HA-filled HDPE composites.

Research on the fatigue behaviour of biomaterials have been mainly conducted on the non-degraded polymeric materials (Curtis, 1991; Harper, 1995; Matsuda et al., 2004; Fujihara et al., 2007; Schambron et al., 2008) with a very limited number of studies focus on the continuous fibre reinforcement composite. Most of the studies on self-reinforcement PLA composite are also in the area of static loading, thus creating a gap on in the field of cyclic behaviour. In the field of the fatigue testing itself, due to complexity of nature of the fatigue test, only handful of the experiments were conducted in biaxial loading with none of these carried out on the degraded specimen. The present study therefore trying to address the lack of information on the fatigue behaviour of the degradable biomaterials by following the aim and objective as stated in Chapter 1.

CHAPTER 3 - MATERIALS AND METHODS

3.1 MATERIALS

The materials used in this study are Polylactic acid (PLA), a degradable polymer that is commonly used in biomaterials applications and reviewed in detail in Chapter 2. Calcium phosphate, used as the filler is a bioactive material and also widely used to promote bone formation. In this study, the materials are in form of a three phase composite originally developed by Kellomäki (1997) and optimised by Bleach et al. (2002). The composite consisted of drawn PLA fibres in a PLA-calcium phosphate composite matrix.

3.1.1 Polymers

The matrix polymer was polylactide (PLA_{70}) (Purac Biochem, Holland), in form of fine white granules with inherent viscosity of 6.1 $dl.g^{-1}$. It has L:D,L ratio of 70:30 that is 70% PLLA and 30% a racemic mixture of PLLA and PDLA. Polylactide fibres with an L: D ratio of 96:4 of 96% PLLA and 4% PDLA, (PLA_{96}) with an average diameter of 27μm bundled together in 30 filaments was used as the reinforcing phase. The fibres were supplied by Degradable Solutions, Switzerland with individual fibre strength of 5.6N. The reported density of PLA is 1.26 Mgm^{-3}.

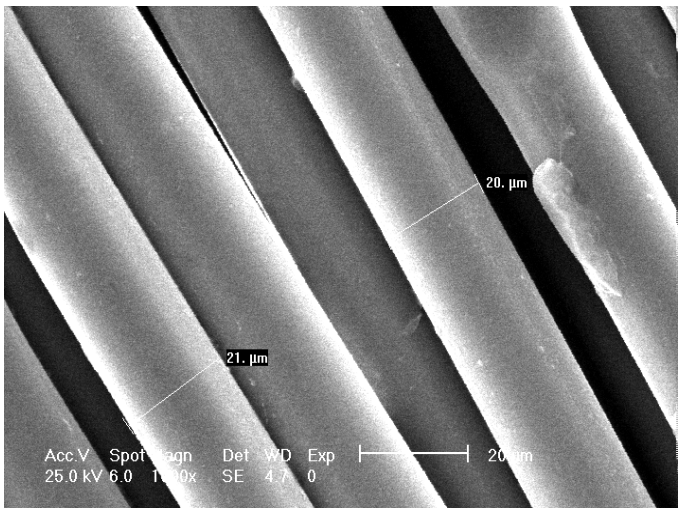

Figure 3.1 SEM image of PLA_{96} fibre (from Dr Wojciech Chrzanowski)

3.1.2 Calcium Phosphates

Tricalcium phosphate (TCP) (Plasma Biotal Ltd, Tisdeswell, UK) with Ca:P ratio (1.5) was used as particulate filler material. It was a fine white powder, with mean particle size of $d_{0.5}$= 3.03μm ($d_{0.1}$=1.89μm, $d_{0.9}$=4.51μm) and has a specific surface area of 2.30 m^2g^{-1}. The theoretical density of TCP is 1.70 gcm^{-3}.

3.1.3 Saline solution

Degradation studies and fatigue testing were carried out in saline solution at 37°C. Phosphate buffered saline (Sigma-Aldrich Company Ltd, Dorset, UK) in tablet form was dissolved in distilled water to produce a degradation solution with pH range of 7.20 -7.60.

3.2 METHODS - SAMPLE PREPARATION

3.2.1 Pre-Pregging

Prior to the pre-pegging process, the matrix solution was prepared by adding 20g PLA_{70} to 500ml acetone in a large spherical flask. The mixture was then stirred using magnetic stirrer plate for approximately 4 hours at room temperatures. Once the polymer had dissolved, 40.47g tricalcium phosphate was added and stirring was continued for at least 12 hours at room temperature to ensure a homogenous mix. This gave 60 vol.% of TCP filler in the matrix as determined by calculation, after acetone evaporation.

Pre-pregging was performed using a purpose built pre-pregger (Research Tool Corporation, USA). The PLA_{96} fibres were pulled through the matrix bath using the pre-pregger. Prior to the drawing process, two spools of PLA_{96} fibres were put on the spindles. Each spool contained 30 fibres and was approximately 500m in length. The pre-preg was attached with 2.8mm die and guide wheels. The fibres were threaded through the guide wheels, through the matrix bath and die then wound onto a rotating drum to produce a continuous sheet of pre-pregged composite. The fibre speed used was 5 m. min^{-1}. As the matrix bath had no cover the acetone was able to evaporate, therefore more acetone was added periodically to retain an even consistency. Any excess matrix on the fibre bundle

was removed by a wiper system, which was fitted at the exit of the matrix bath (Figure 3.2).

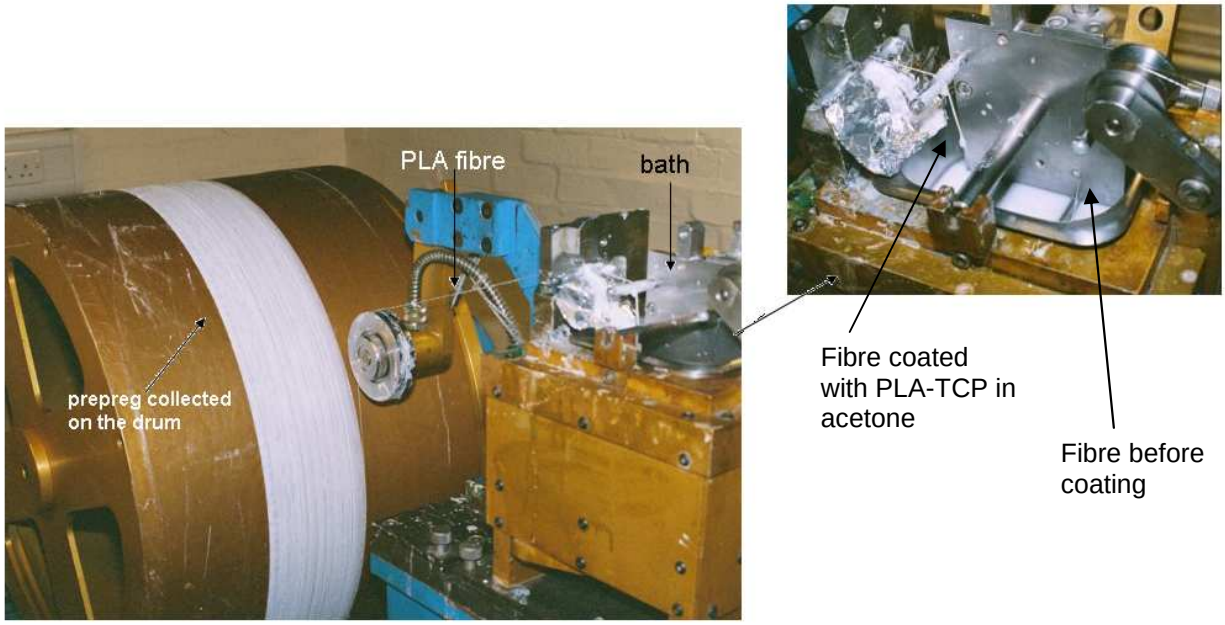

Figure 3.2 Pre-preg fabrication process showing PLA fibre being drawn through matrix bath contains PLA-TCP solution (photographs from Prof K.E.Tanner)

The collecting drum was covered with silicone paper in order to prevent the fibre from sticking to the surface of the drum. Its transverse movement was adjusted to 2.8mm per rotation so that fibre bundles would be laid down next to each other. The process was stopped after a fully covered drum with one layer of pre-preg was manufactured. Masking tape was taped at the cutting line and the pre-preg was cut off the drum and left to dry overnight. Later, it was cut into shorter lengths for ease of handling and pressed under a weight for another 24 hours. After that it was dried in a vacuum oven for further 24 hours. Lastly, the pre-preg was kept in sealed plastic bags with silica gel to prevent moisture absorption and thus the initiation of degradation.

The final content of Ca-P in the prepreg was 12.82 wt.% as determined by ashing method described in section 3.2.5

3.2.2 Differential Scanning Calorimetry

DSC-7 (Perkin Elmer, Connecticut, USA) was used to determine thermal properties of the polymer. Liquid nitrogen was used to enable the measurement

to be made below ambient temperature. The heat sink temperature was set at 20ºC below the lowest temperature required and left for an hour to stabilise. Approximately 5.5mg of the sample was sealed in aluminium pan and placed in DSC chamber with an empty aluminium pan as reference. The heating/cooling regime used was as follows:

1. First the sample was held at 25ºC for 3 minutes
2. The sample was heated from 25ºC to 220ºC at heating rate of 20ºC min^{-1}
3. The samples was held at maximum temperature of 220ºC for 1 minute
4. It was cooled down to 25ºC at cooling rate of 20ºC min^{-1}
5. The sample was held at the minimum temperature of 25ºC for 3 minutes
6. Second heating from 25 ºC to 220 ºC at heating rate of 20ºC min^{-1}

3.2.3 Moulding Procedure

The composites were compressed into a cylindrical mould (100 x 7 mm in length and diameter) at 140 ºC or 150 ºC using a hydraulic press (Bradley & Turton Ltd, England) after preliminary trials to optimise sample preparation. 5.2g of the pre-pregs were measured for each rod. The pre-preg was carefully hand placed in the mould with care to ensure the fibres were aligned with the mould direction. The mould was firstly held at 5 MPa while it was heated to the desired temperature. The time taken to reach the desired moulding temperature was 20 to 25 minutes. Once the compression moulding temperature was reached, the pressure was increased to 10 MPa and applied for 5 minutes. Then the mould was left to cool in the press under pressure of 5 MPa. The cooling was aided by water circulating in the press. The rods were machined into cylindrical dumbbell specimens according to ASTM standard E466 (Figure 3.3). The specimen surface was polished with fine SiC paper to remove any machining marks. The early studies of quasi-static tension, compression and torsion and at 25% UTS fully reversed tension-compression fatigue test for specimen moulded at 140°C (T140) were performed with 20 mm gauge length. However due to problems with buckling, the gauge length was reduced to 13 mm for the rest of the test.

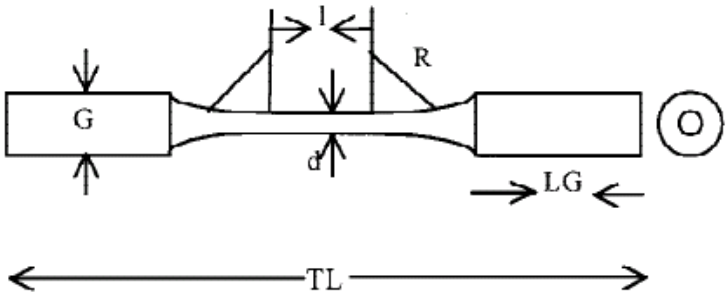

Symbol	Description	Dimension(mm)
L	Gauge length	13, 20
D	Gauge diameter	3.5
LG	Grip length	34.5
G	Grip diameter	7
R	Radius of curvature	28
TL	Total length	100

Figure 3.3 The dimensions of tangentially blended dumbbell specimens of self-reinforcement composite

3.2.4 Density measurement

The density of the composite was measuring using the Archimedes' principle, a body submerged under a liquid will experience an up thrust equal to the weight of the liquid displaced, in this case distilled water. This method involving weighing the specimen in air on the balance, (M_a) and measuring the specimen buoyancy (M_b). The density of the composite (ρ_c) is calculated by

$$\rho_c = \frac{M_a}{M_b} \times \rho_w$$

Equation 3.1

Where $\rho_w$the density of distilled water at the room temperature (21°C), is 0.998 Mgm^{-3}

3.2.5 Ash Weight Measurement

The weight percentage of TCP in the composite was determined after burning off PLA at 600ºC. The porcelain crucible weight was recorded as W_0. The TCP/PLA composite sample was placed in the porcelain crucible and the weight was recorded as W_s. The crucible with the sample was placed in the centre of a

furnace, which had been stabilised at 600°C and left for 60 minutes then allowed to cool. The residue in the crucible was measured as W_R, and the TCP content (wt.%) was calculated by

$$wt.\% = \frac{W_R - W_0}{W_S - W_0} \times 100$$

Equation 3.2

3.2.6 Degradation Protocol

The samples were randomly allocated into 4 groups (weeks 8, 12, 16 and 20) each group containing five samples to investigate the effect of the degradation on the quasi static and fatigue strengths. The mass of each sample was recorded prior to degradation (m_o). 500ml polypropylene bottles were rinsed with saline solution; all five samples for each period were placed in one bottle and then were filled with phosphate-buffered saline (PBS). $V_{solution}/V_{sample} > 20$ was used (Niemelä et al., 2008). The bottles were incubated at 37 °C in an incubator (Sanyo, Japan) and the PBS was changed every three weeks, at which time its pH was measured using a Hanna pH meter (Hanna Instruments Ltd, UK). At each degradation period, the samples were removed from the bottles and surface water was blotted off with a tissue and the wet weight (m_w) measured to determine the water absorption (WA). After weighing, the samples were rinsed with deionised water and ethanol to remove the residual salts. The samples were then dried in a vacuum oven at room temperature until there was no further weight loss and the dry mass (m_d) recorded (approximately 5 days). The weight measurements were carried out using a Ohaous analytical balance (Ohaous Analytical, USA). Quasi-static testing, fatigue testing and SEM were carried out on dry degraded samples.

$$Mass\ loss = \frac{m_d - m_o}{m_o} \times 100\%$$

Equation 3.3

$$Water\ absorption\ (WA) = \frac{(m_w - m_d)}{m_d} \times 100\%$$

Equation 3.4

3.3 METHODS - FATIGUE TESTING

3.3.1 Test preparation

The quasi and fatigue tests were carried out using a MTS Bionix 858™ servohydraulic (Minneapolis, USA) machine. It has with axial and torsional actuators in series that allow tension-compression and torsion to be applied simultaneously, in or out-of-phase (Figure 3.4). The machine is fitted with a load cell of 2.5 kN axial and 25 Nm torsional capacity. The actuator has a range of 100mm linear and 140° rotational maximum motions with integral displacement transducers, controlled by MTS Testware® software. Data of force, displacement, angle, torque, number of segment and test time were collected and stored in a computer (Dell, UK) during the test.

In order to ensure there is no additional stress on the test sample, the specimen axis needs to coincide perfectly with the actuator axis. Any misalignments will produced additional bending stress or shear stress to the calculated axial and torsional loads on the specimen, which is not included in stress calculation. The alignment rod that was used to align the grips had a major diameter equal to the diameter of the grip section of the specimen that is 7mm. During the alignment, the alignment rod was held by upper grip then gradually lowered into the bottom grip. The rod then aligned to ensure no additional bending and the lower grip positioned so that when the sample was placed in the grips it was correctly aligned.

Figure 3.4 MTS Bionix Test System with computer control terminal

The dimensions and density of each specimen were measured before the testing was carried out. In order to ensure the temperature equilibration, the specimen was then soaked for at least half an hour in saline solution at 37ºC prior to testing. The test was performed in an environment chamber with the specimens sprayed with saline at 37ºC. As the tests were carried out in wet environment (Figure 3.5), it was not possible to use an extensometer to measure the displacement. Therefore, the deformation of the axial and torsion were recorded from actuator movement, which then converted into true strain by taking into account correction factor calculated from the specimen dimensions and geometry (Appendix A1).

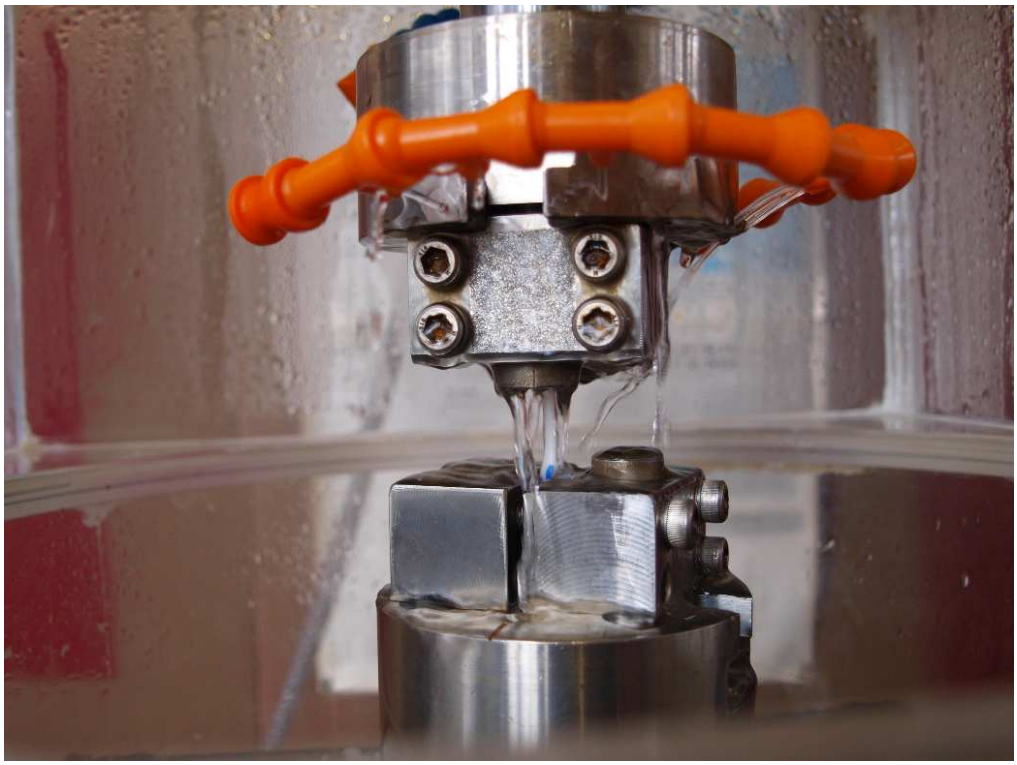

Figure 3.5 Test set up with sample covered in flowing saline solution performed in environment chamber (at 37°C)

3.3.2 Monotonic testing

Quasi-static tests in tension, compression and torsion to failure were performed to establish the ultimate tensile strength (UTS), ultimate compressive strength (UCS) and ultimate shear strength (USS) of the material. Tensile and compressive monotonic test were carried out at a crosshead speed of 5 mm min^{-1}, giving a strain rate of 0.0055s^{-1}. For the same strain rate, the rotation rate was calculated to be 2.5° min^{-1}. The yield point of the materials was taken at 0.2% strain offset on the stress versus strain curves (Reilly and Burstein, 1975).

From the force-displacement data, the stress and strain were calculated using Equations 3.5 and 3.6.

The axial stress, $\sigma = \frac{F}{A}$ **Equation 3.5**

Where F= axial force and A= πr^2 which is cross sectional area of the gauge section of radius r,

And

$$\text{axial strain } \varepsilon = \frac{\delta}{l}$$

Equation 3.6

Where δ = axial deformation and l = gauge length

From the torque-angle data, the shear stress and shear strain can be calculated using Equations 3.7 and 3.8.

$$\text{shear stress, } \tau = \frac{2T}{\pi r^3}$$

Equation 3.7

$$\text{shear strain } \gamma = \frac{r\theta}{l}$$

Equation 3.8

Where θ = angle of twist (rad), polar second moment of area J = $\pi r^4/2$ for a cylinder

The modulus can be calculated using Equations 3.9 and 3.10 below:

$$\text{Young's modulus, E} = \frac{\sigma}{\varepsilon}$$

Equation 3.9

And

$$\text{Shear modulus, } G = \frac{\tau}{\gamma}$$

Equation 3.10

The monotonic test moduli were calculated over the stress range 2.5 to 5.0 MPa.

3.3.3 Fatigue Testing

Fatigue testing was carried out in a physiological environment using sinusoidal loading at a frequency of 2Hz under load control. The data was collected at every 0.05s, giving 100 data points per load cycle. Tests involved fully reversed cyclic uniaxial fatigue at 25%, 50% and 75% of the UTS or USS respectively. For

the uniaxial torsional loading, a biaxial template was used with axial load set to zero. This template was used to ensure that no additional axial stresses were developed as result of the changes in specimen length produced by creep.

The force and torque load ranges were calculated individually for each sample by taking into account the sample diameter in order to ensure the stress ranges were constant.

Fatigue testing was carried out using different combinations of axial and torsional loading as shown in Table 3.1. The procedure was repeated with out-of-phase loading at various phase angles: 0, 30, 60 and 90º

Table 3.1 Uniaxial and biaxial fatigue test categories

Load level	0% UTS	±25% UTS (25A)				±50%UTS (50A)	±75% UTS (75A)
0% USS	none	/#				/	/
±25% USS (25T)	/#	0°	30°	60°	90°	0°	none
±50% USS (50T)	/	0°	none			0°,90°	none
±75% USS (25T)	/	none				none	none

'/' test performed; '#' plus test on degraded specimens

In order to study the role of tension stress in fully reversed tension-compression fatigue, uniaxial tension only (+50A) fatigue was performed.

To investigate the long term properties of the materials, selected tests were performed on soaked specimens: 8,12,16 and 20 weeks soaked specimens were subjected to monotonic tension and torsion and uniaxial fatigue (±25% UTS and ±25% USS).

Five repeat tests were performed at each stress level. Failure was defined as either fracture of the specimens into two parts (only those which failed inside gauge section were considered valid in case of tensile), failed at fractured strain (which 6mm in compressive and 40° in torsional displacements), or in case of non failure, run outs were defined after 1.5 x10^6 cycles. Analysis of cycles to failure was the based on 30% reduction (N_E=70%) in the modulus, as recommended by ASTM D671-87. The unbroken specimens were subjected to

monotonic tension to failure to investigate the fatigue damage that has been produced.

3.3.4 Statistical Analysis

The statistical analysis was done using Wilcoxon-Mann-Whitney test for two unrelated designs, for example test for strength and modulus of the T140 and T150 specimens. The Kruskal-Wallis test was used for results for tests performed under three or more conditions, for example to test the statistical difference in the number of cycles to failure between 0°, 30°, 60° and 90° out-of-phase in a combined loading fatigue. Due to relatively small sample size in this study, $p<0.05$ was used. All data analysis was performed using Kaleidagraph software.

3.3.5 Microscopic Characterisation

Macroscopic observation was carried out using optical microscope NORMANSKI Nikon Eclipse ME600 (Nikon, Japan).

Microscopic examinations were carried out using a Carl Zeiss Sigma scanning electron microscope (SEM) (Carl Zeiss, Germany), with accelerating voltage of 5-10 keV. For fractures surface, samples were mounted onto stubs using carbon cement. For internal structure observation, the specimens were moulded in epoxy resin (MetPrep Ltd, UK) and left overnight to set. The specimen then polished with progressively finer silicon carbide papers (300-1200 grades) and further polishing using finer diamond paste from 15 to 1μm and then cleaned in an ultrasonic bath. All samples were coated with carbon prior to the SEM examination.

3.3.6 Hysteresis Loop

In order to quantify the actual damage accumulated by material caused by fatigue loading, the damage must be characterized and quantified. Damage can be defined as the gradual degradation in mechanical properties, such as modulus, as well as amount of energy absorbed by the materials.

The energy absorbed, or hysteresis, H, is the difference between the energy density integral at the beginning and end of a cycle and represents the energy,

which was not returned by the specimen during the load cycle (Figure 3.6). In this study, it was calculated using Kaleidagraph software. The secant modulus is defined as the ratio of the stress range to the strain range, which in this study was calculated over the maximum applied load. Fatigue damage accumulation within the material was characterised by the decrease in secant modulus and the increase in dissipated energy with number of cycles.

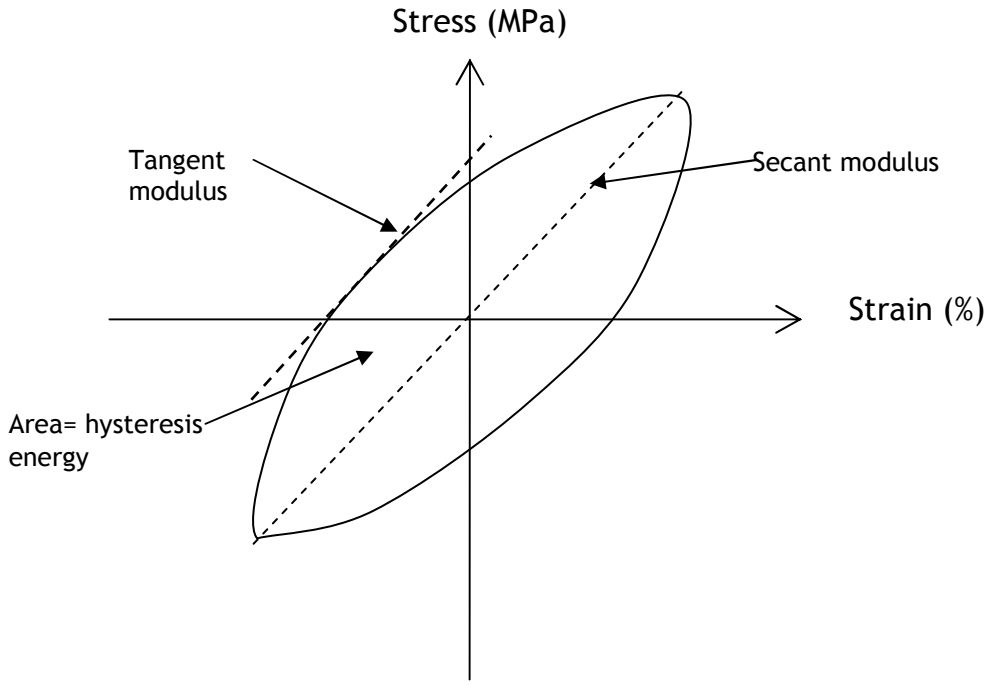

Figure 3.6 Calculation of material response (hysteresis loop)and secant modulus under fully reversed cyclic loading (tension-compression)

3.3.7 Calculation of Principal Stress and Maximum Shear Stress

The principal stress criterion is used when the principal stress axes coincide with the principal material axes and the maximum shear stress criterion is used when failure are dominated by shear stress.

The general expression of the axial stress (σ_x) and shear stress (τ_{xx}) under sinusoidal loading can be given as:

$$\sigma_{x(t)} = \sigma_{x(0)} \sin\left(2\omega\pi t\right)$$

Equation 3.11

and

$$\tau_{xy(t)} = \tau_{xy(0)} \sin(2\omega\pi t - \phi)$$

Equation 3.12

Where $\sigma_{x(0)} = \frac{4P_{max}}{\pi d^2}, \tau_{xy(0)} = \frac{16T_{max}}{\pi d^3}, \phi$ is the phase angle between the axial and shear stresses and P_{max} and T_{max} are the maximum axial and torsional loads.

The principal stresses, ($\sigma_{1,2}$) and maximum shear stress (τ_{max}) can be calculated by:

$$\sigma_{1,2} = \frac{\sigma_{x(t)}}{2} \pm \left[\left(\frac{\sigma_{x(t)}}{2} \right)^2 + \left(\tau_{xy(t)} \right)^2 \right]^{0.5}$$

Equation 3.13

$$\tau_{max} = \left[\left(\frac{\sigma_{x(t)}}{2} \right)^2 + \left(\tau_{xy(t)} \right)^2 \right]^{0.5}$$

Equation 3.14

Thus,

$$\sigma_{1,2} = \frac{4P}{\pi d^2} (\sin 2\pi\omega t) \pm \left[\left(\frac{4P}{\pi d^2} \right)^2 \sin^2 (2\pi\omega t) + \left(\frac{16T}{\pi d^3} \right)^2 \sin^2 (2\pi\omega t - \phi) \right]^{0.5}$$

Equation 3.15

And

$$\tau_{max} = \left[\left(\frac{4P}{\pi d^2} \right)^2 \sin^2 (2\pi\omega t) + \left(\frac{16T}{\pi d^3} \right)^2 \sin (2\pi\omega t - \phi) \right]^{0.5}$$

Equation 3.16

The variations in the axial and shear stresses over one cycle are shown in Appendix A3 under the various combinations of axial stress, shear stress and phase angle shown in Table 3.1

3.3.8 Tsai-Wu Parameter

The Tsai-Wu criterion requires three constants and accounts for differences in tensile and compressive strengths. Tsai-Wu criterion's basic assumption is that there exists a scalar failure surface, I_F in the stress-space (Tsai and Wu, 1971) where:

$$I_F = F_i\sigma_i + F_{ij}\sigma_i\sigma_j = 1$$

Equation 3.17

Where F_i and F_{ij} are strength tensors of the second and fourth rank, respectively and the usual contracted stress notation is used ($\sigma_4 = \tau_{23}$, $\sigma_5 = \tau_{31}$ and $\sigma_6 = \tau_{12}$). For anisotropic materials, the equation 3.17 reduced to:

$$F_1\sigma_1 + F_2\sigma_2 + F_6\sigma_6 + F_{11}\sigma_1^2 + F_{22}\sigma_2^2 + F_{66}\sigma_6^2 + 2F_{12}\sigma_1\sigma_2 = 1$$

Equation 3.18

As the shear strength in principal material coordinates is independent of shear stress sign, thus $F_6 = 0$, and test condition used in this study give σ_1 as axial stress, σ_6 as shear stress, while $\sigma_2 = 0$, so the equation 3.18 reduces to:

$$F_1\sigma_1 + F_{11}\sigma_1^2 + F_{66}\sigma_6^2 = 1$$

Equation 3.19

Where I_F IS Tsai-Wu constant (I_F=1 for failure) and F_1, F_{11} and F_{66} have the following values,

$$F_1 = 1/X_t - 1/X_c$$ **Equation 3.20**

$$F_{11} = 1/(X_t X_c)$$ **Equation 3.21**

$$F_{66} = 1/S^2$$ **Equation 3.22**

Where X_t is ultimate tensile strength, X_c is ultimate compressive strength, S is ultimate shear strength.

CHAPTER 4 - UNIAXIAL FATIGUE

4.1 INTRODUCTION

The first section of the experimental work focussed on optimising the fabrication so that specimens suitable for the fatigue studies could be produced. Previous work had established the fabrication parameters (Bleach et al. 2000, Kellomaki, 1997) but it soon become apparent that many variables affected this process and work was required to standardise the procedure. One important factor to consider when compression moulding pre-preg is moulding temperature. Logic indicated that this temperature should be above the melting temperature of the matrix (PLA_{70}) in order to ensure it can flow fill in the voids between the fibres, yet at the same time lower than melting temperature of the fibres (PLA_{96}) to ensure that structural integrity of the fibres was not compromised. DSC (Section 3.2.2) was used to establish the melting ranges of the matrix and fibres and help choosing the compression moulding temperatures. SEM was also used to assess the impregnation of the matrix around the fibres after compression moulding.

From the DSC results, moulding temperatures of 140°C and 150°C were chosen to study the effect of the moulding temperature on the uniaxial fatigue behaviour. All specimens were tested to failure in tensile, compression and torsion to determine their initial mechanical properties such as yield, ultimate stresses, moduli and strain to failure. Uniaxial fatigue tests were carried out in fully reversed tension-compression and torsion. In order to investigate the effect of the compressive loading to the fatigue lives, tension only fatigue tests were also carried out and compared with fully reversed uniaxial fatigue. SEM was used to study the fracture surfaces.

4.2 METHODS

The specimens used for uniaxial fatigue studies were compression moulded at 140 (T140) and 150°C (T150) using the methods described in Section 3.2.3. Prior to the testing, the density of each specimen was measured as describe in Section 3.2.4 followed by quasi-static testing as described in Section 3.3.2, in order to obtain mechanical properties such as yield and ultimate stresses, moduli, strain at yield, strain at ultimate strengths and strain at failures in tension,

compression and torsion. Uniaxial fatigue testing was then carried out at ±25% (25A, 25T), ±50% (50A, 50T) and ±75% (75A, 75T) of UTS (A) or USS (T) and at 50% of UTS for tension only testing. All tests were carried out at the approximately percentage of their individual ultimate strength. Fatigue damage analysis was then carried as described in Section 3.3.6 for fatigue life, reduction in secant modulus and increase in energy absorbed and fracture surface. Fracture surfaces were observed using optical and scanning electron microscopy as described in Section 3.3.5.

4.3 RESULTS- MATERIALS CHARACTERISATION

4.3.1 Compression Moulding Temperatures

The range of glass transition and melting temperature for the PLA_{70} matrix and PLA_{96} are shown in Table 4.1. T_m onset is the temperature when the melting peak starts, while T_m end is the temperature at which the melting peak ends. T_m peak represent the temperature at maximum exotherm. The DSC results indicated that the melting range of the matrix was between 90 and 130°C and the melting range of the fibres was between 139°C and 178°C. These temperatures were used to choose the compression moulding temperature where the matrix would melt but not the fibres.

Table 4.1 Glass transition and melting temperature range for the PLA_{70} matrix and PLA_{96} fibres

Material	Sample	Tg/ °C	Tm onset/°C	Tm end/°C	Tm peak/°C
PLA_{70}	1	62.9	88.3	130.2	124.5
Matrix	2	61.5	85.8	128.7	120.3
	3	62.3	97.7	132.9	125.2
	average	62.2 ± 0.7	90.6 ± 6.3	130.6± 2.1	123.3 ± 2.7
PLA_{96}	1	62.3	143.2	188.8	180.1
Fibres	2	64.0	132.6	177.3	178.9
	3	64.8	142.8	183.3	177.3
	average	63.7± 0.6	139.5± 5.2	183.1± 3.4	178.8± 0.9

4.3.2 Density Measurement

Table 4.2 shows the densities of the composite moulded at 140°C (T140) and 150°C (T150). Compression moulding temperature has no significant effect on the density of the samples.

Table 4.2 Density of self reinforced PLA filled TCP

Materials Conditions	Mean Density ± S.D /Mgm^{-3}
Compression moulded unidirectional fibre at 140°C	1.295 ± 0.009
Compression moulded unidirectional fibre at 150°C	1.297 ± 0.016

4.4 RESULTS-MONOTONIC TEST

4.4.1 Mechanical Properties

Under tension, the specimens fractured slowly, all failures occurred at the end of the shoulder or in the gauge length, the main failure mode was fibre pull out indicating the strength of the individual fibres. This fracture surface is expected in tensile fracture of continuous fibres reinforcement composite. In compression, the specimens gradually bent and buckled; they collapsed, but did not fracture into separate parts. In torsion, white spiral marks (crazing) were observed around the surface of the gauge length, the specimens had not fractured at 140º rotation when the machine reached its maximum total rotation. However after being freed from the testing grips, it was noticed that the specimens were slightly bent, probably due to release of plastic strain.

Figure 4.1 shows typical stress-strain curves for T140 and T150 loaded in tensile, compressive and torsional tests in saline solution at 37ºC. The ultimate mechanical properties are shown in Tables 4.3 and 4.4. Under tension, the materials displayed ductile behaviour and fractured with substantial amounts of yield. During the regions after the yield, the fibres were gradually pulling out from the two grip sections. When moulded at 140 ºC, the material had a long region of approximately constant stress while the strain reached 50%. On the other hand, when moulded at 150 ºC, after the initial yield point, the sample

continued to support an increasing strain up to 45% strain and then again failed gradually.

In compression, the elastic behaviour was similar to that seen in tension. The ultimate compressive strength was reached and material started to fail until it finally fractured by buckling and collapsing increasing the compressive displacement. The compression curves had similar shape for T140 and T150 specimens.

For torsional testing, USS was reached at shear strain of about 3%. Thereafter, once the material started to yield, the shear stress decreased, but with the specimen size and shape used, the rotation needs to be more than 140º to give 16% strain, the total rotation that available with the mechanical testing machine used. As shown in compression testing, the shapes for stress-strain curves in torsional testing are also similar for both T140 and T150 specimens.

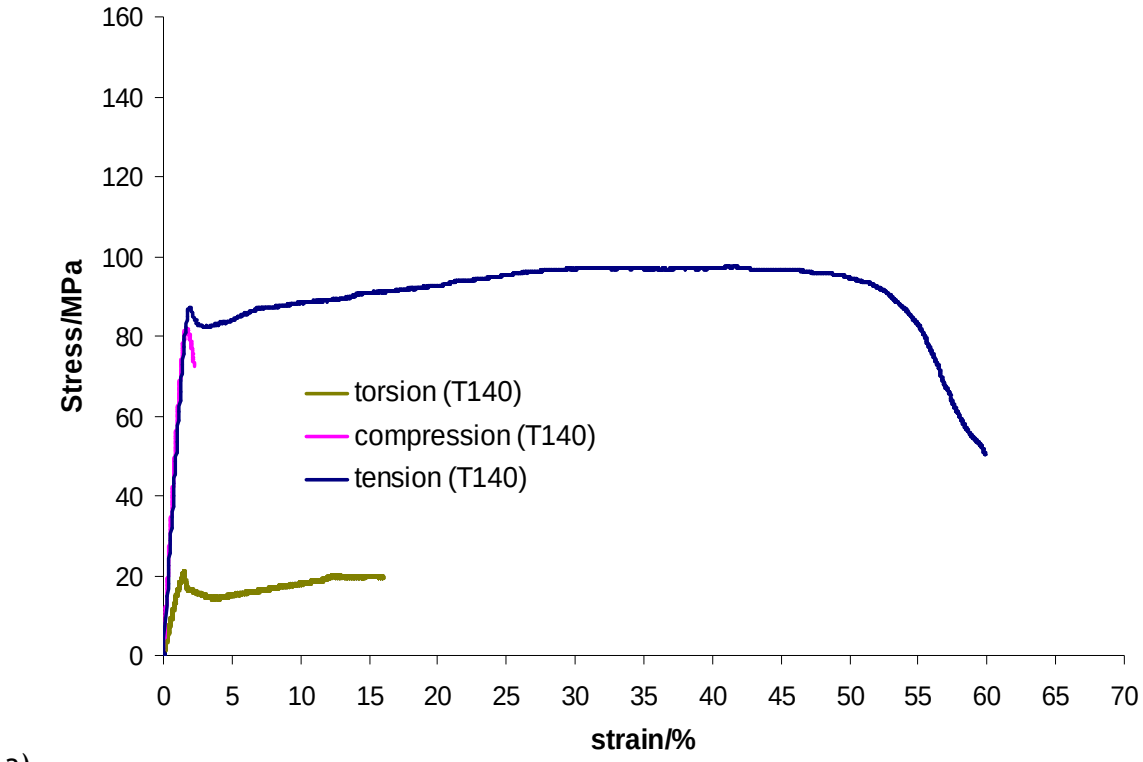

a)

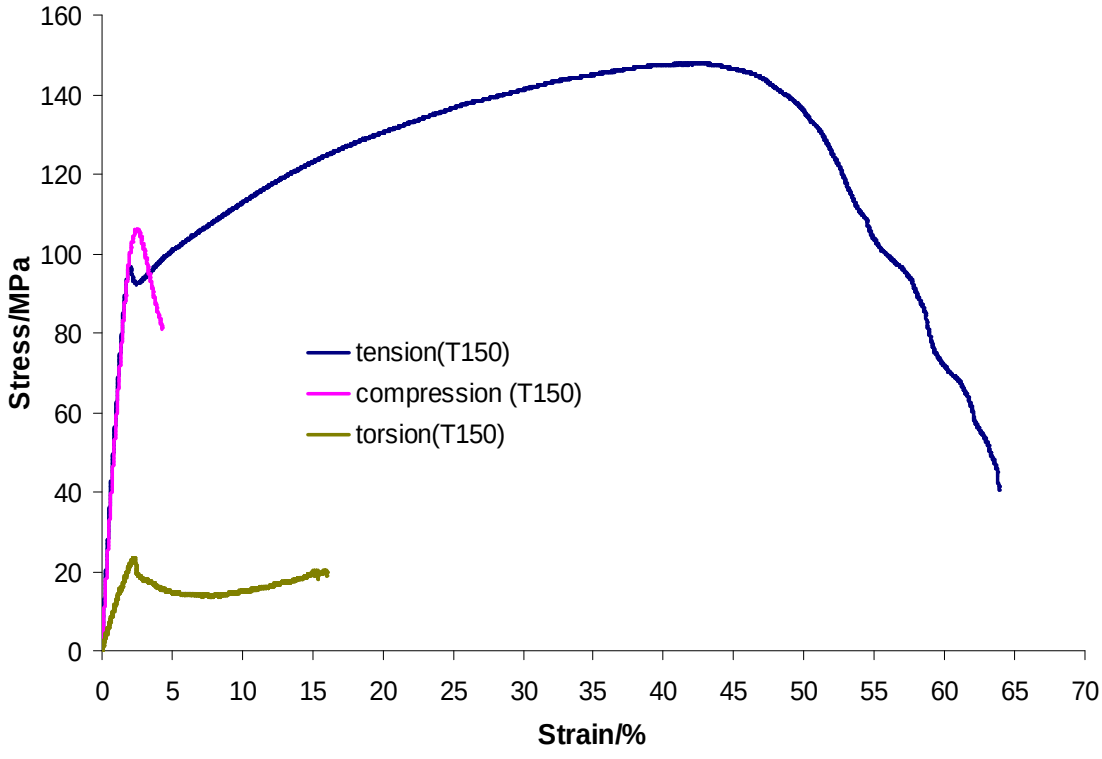

b)

Figure 4.1 Stress strain curve of PLA-PLA-TCP tested at 37°C in saline

a) moulded at 140°C b) moulded at 150°C

Table 4.3 Quasi-static results of 140°C moulding temperature

Test mode	Initial Max Stress (MPa)	Ultimate Stress (MPa)	Modulus (GPa)	Strain at Yield (%)	Strain at Ultimate Stress (%)	Strain at failure (%)
Tension	81.90 (±3.14)	100.61 (±4.97)	5.33 (±0.02)	2.02 (±0.10)	33.36 (±6.36)	56.34 (±8.72)
Compression	81.67 (±2.06)	81.67 (±2.06)	5.96 (±0.52)	1.67 (±5.4)	1.67 (±5.4)	2.34 (±0.5)
Torsion	26.10 (±5.61)	26.10 (±5.61)	1.43 (±0.05)	1.99 (±0.46)	1.99 (±0.46)	>16

Table 4.4 Quasi-static results for 150°C moulding temperature

Test mode	Initial Max Stress (MPa)	Ultimate Stress (MPa)	Modulus (GPa)	Strain at Yield (%)	Strain at Ultimate Stress (%)	Strain at failure (%)
Tension	97.93 (±6.56)	139.77 (±11.58)	6.36 (±0.11)	3.04 (±0.81)	43.62 (±4.33)	66.34 (±6.75)
Compression	108.11 (±3.44)	108.11 (±3.44)	6.03 (±0.19)	2.23 (±0.19)	2.23 (±0.19)	4.01 (±0.42)
Torsion	26.49 (±4.32)	26.49 (±4.32)	1.20 (±0.12)	3.47 (±1.85)	3.47 (±1.85)	>16

Changes in mechanical properties of the composite due to effect of the moulding temperature can be considered by comparing the results in Tables 4.3 and 4.4. At the higher moulding temperature of 150°C, the material is stronger in both tension ($p<0.05$) and compression ($p<0.05$). The moduli in tension and compression are also increased but the difference was not statistically significant. The T150 composite also more ductile with higher strain at failure under both tensile and compressive loads ($p<0.05$). In torsional loading, the material was also slightly stronger with increased of moulding temperature but no significant differences were observed in the shear moduli. The higher properties in specimens moulded at 150°C are thought to be due to better fibre/matrix adhesion as at the higher moulding temperature which allows better impregnation of the fibres bundles by the matrix. SEM examination confirmed that for specimens moulded at 140°C and 150°C, better consolidation and fewer gaps between the fibres were seen in the materials moulded at 150°C (Figure 4.2).

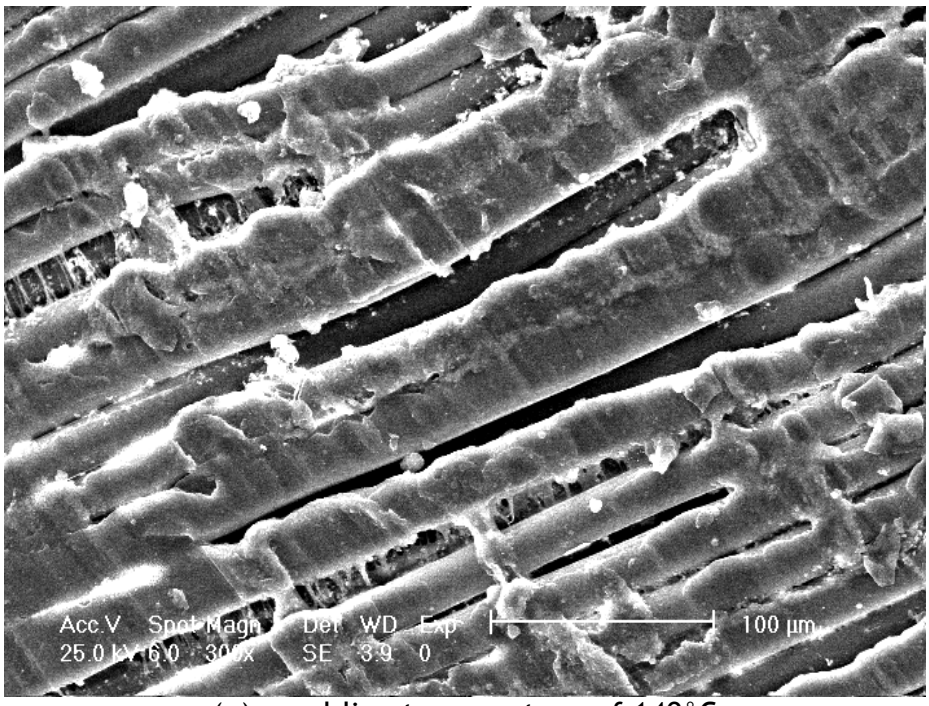

(a) moulding temperature of 140˚C

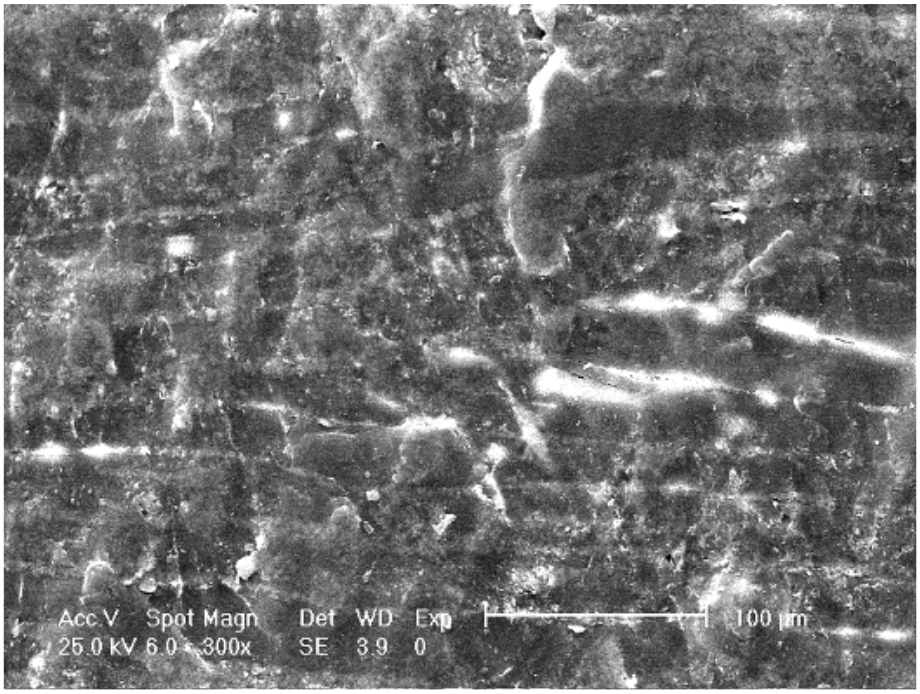

(b) moulding temperature of 150˚C

Figure 4.2 SEM image of pre-pregs moulded at a) 140˚C and a) 150˚C moulding temperatures showing better consolidation of the fibre/matrix at higher moulding temperature (Scale bar= 100µm) (SEM images from Dr Wojciech Chrzanowski)

Based on the results obtained in investigation the effect of the compression moulding temperature on the initial mechanicals properties, a moulding temperature of 150°C was used to study the fatigue behaviour of composite in both uniaxial and biaxial loading and effect of degradation on the fatigue behaviour. For the comparison study the effect of moulding temperature on the fatigue behaviour of composite, moulding temperatures of 140°C and 150°C were used and the specimens were tested in uniaxial tension–compression and tension only loading.

4.4.2 Fractography

Tensile failure

Initial optical microscopic observation on the fracture surface of the tensile quasi-static tests showed that the samples failed in a similar manner, therefore only samples moulded at 150°C (T150) were examined under SEM. Both specimens showed a similar fracture surface with fibre pull-out, indicating a ductile failure consistent with the high tensile strain to failure of the material (Figure 4.3). The fibre failure has occurred at various levels with extensive pull-out of the fibres from the PLA_{70} matrix. Figures 4.3b and 4.3c show extensive fibre drawing indicating ductile fracture, which is a typical fracture mode in long fibre composites. Figure 4.3d shows that surface of the fibres were covered in matrix with exposed of TCP particles indicating interfacial failure. Figure 4.3e displays the broken fibre with distinct fracture point, v-notch opening and progressing to the unstable fracture orthogonal to the fibre axis. The roughness of the surface indicates intensive plastic deformation of the drawn PLA chains and suggests that the final fracture has occurred due to the failure of the polymer network.

(a)

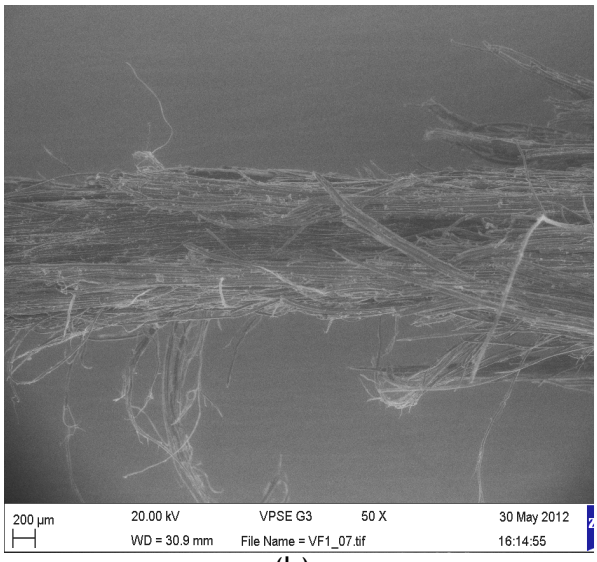

(b)

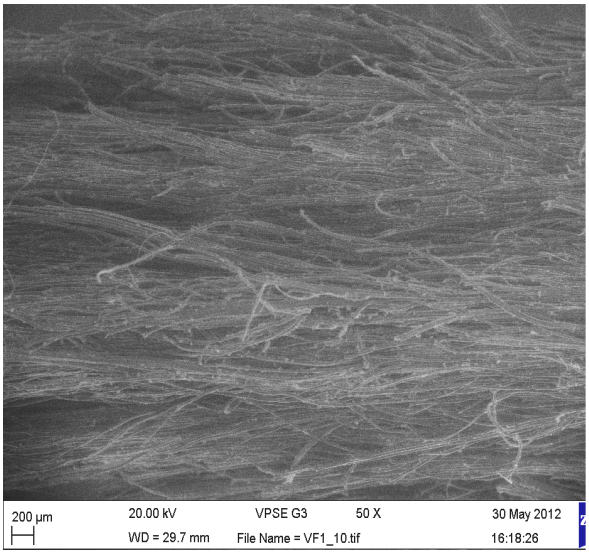

(c)

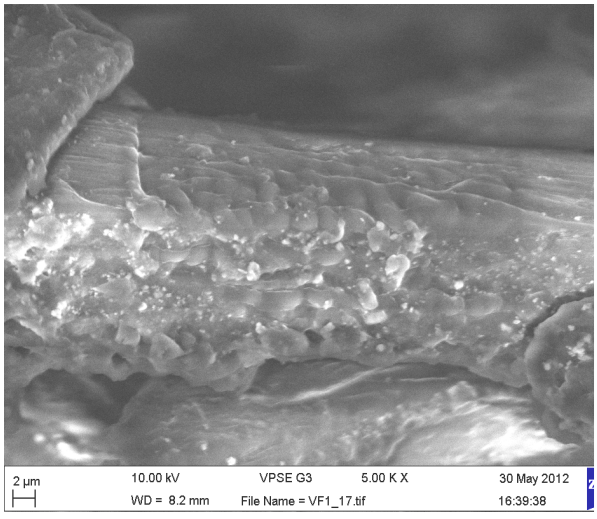

(d)

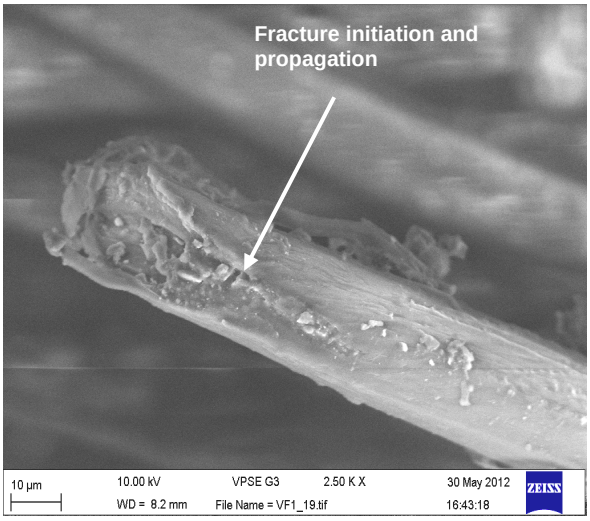

(e)

Figure 4.3 Fracture surface of tension tested PLA-PLA-TCP composite moulded at 150˚C

(a) general view (b)-(c) closer view of the drawn fibres; (d) exposed TCP particles at the bottom of fibres; (e) sharp fracture surface of the individual fibre with exposed TCP particles in the matrix. (Scale bars (a) 5mm); (b)-(c) 200 µm; (d) 2 µm) (e) 10 µm)

Compressive Failure

As the compressive force gradually increased, the specimen buckled, putting one side into compression and the opposite side into tension. The Euler buckling loads were calculated to be approximately 656N and 965N, corresponding to uniform compressive stress of about 70MPa and 100MPa, for specimens moulded at 140°C and 150°C (Appendix A2). The samples failed as the result of buckling without fracture indicating the ductile characteristic of the materials. The general view of the fracture morphology is show in Figure 4.4a. Despite increases in strength and strain in samples moulded at higher moulding temperature, both specimens showed similar failure.

Figures 4.4d and 4.4e show higher magnification views of the fracture surfaces with plastic buckling in both samples. Failure was initiated due to intrafibrillar failure, leading to kink band formation in the matrix. The fibre kinking occurs at multiple locations throughout the matrix (Figures 4.4b and 4.4d). The accumulation of the kink bands created the transverse tensile stresses that caused the longitudinal splitting of the sample, which can be observed in Figures 4.4c and 4.4e.

Figures 4.5 shows the cross sections of the non-tested specimen, while Figure 4.6 shows cross sections of the composite after subjected to the compression loading. Figure 4.5a shows the cross section of the composite across the fibre direction while Figures 4.5b and 4.5c show the cross section parallel to the fibres direction. Upon subjected to the compression loading, the fibres buckled thus triggered formation of the kink band across specimen, lead to crack propagation in the transverse direction to the fibre and final failure due to failure of the matrix-fibre interface (Figure 4.6)

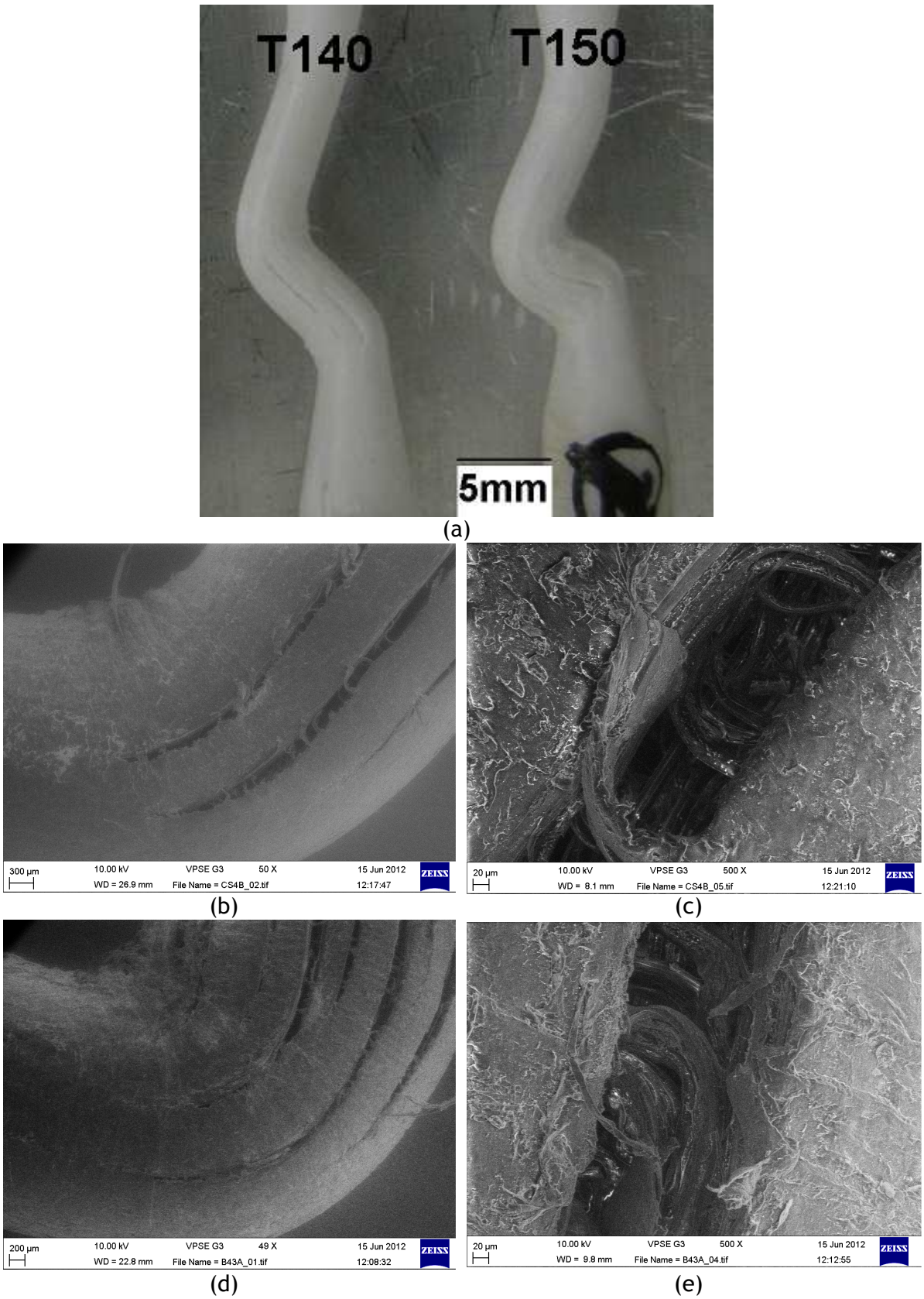

Figure 4.4 Surface of compression tested PLA-PLA-TCP composite (tested at 37˚C in saline)

(a) general view of compression fracture of samples moulded at 140˚C (T140) and 150˚C; (b)-(c) closer view of fracture surface of samples moulded at 140˚C; (d)-(e) closer view of fracture surface of samples moulded at 150˚C. (Scale bars (a) 5mm; (b) 300 µm; (c) 20 µm; (d) 200 µm; (e) 20 µm)

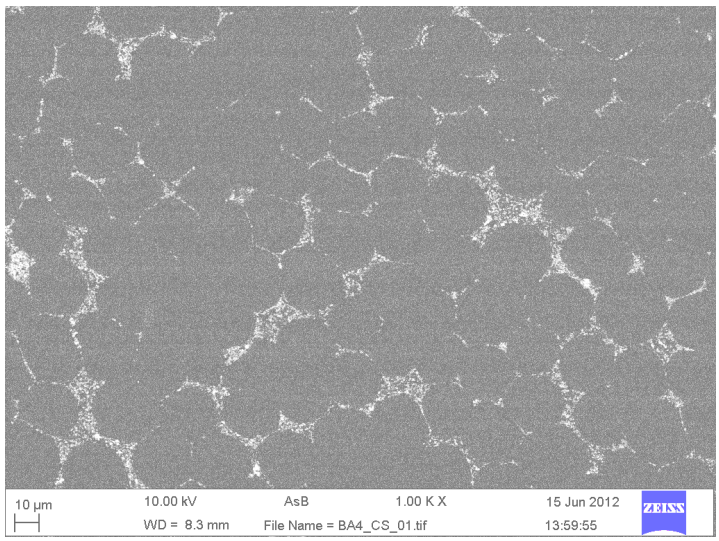

(a)

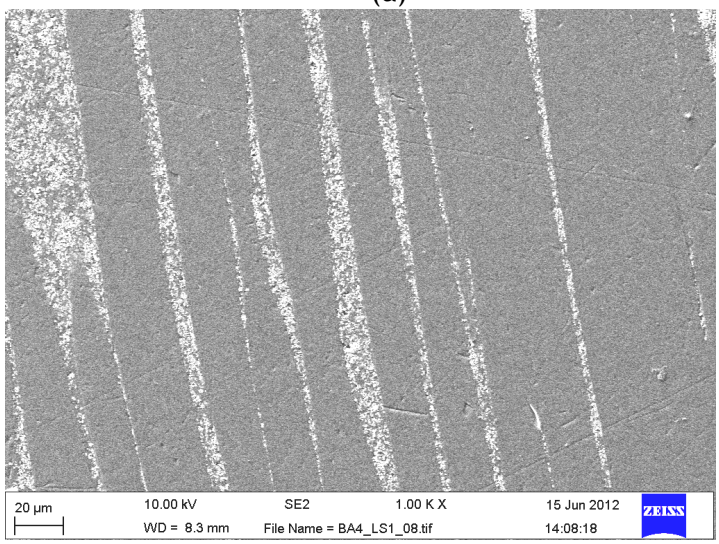

(b)

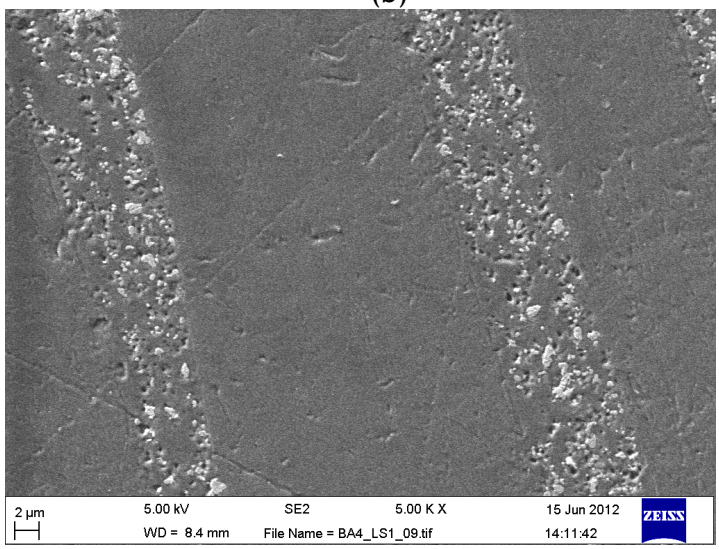

(c)

Figure 4.5 SEM of cross section of untested composite moulded at 150°C.

(a) cross section view of fibres (dark) surrounded by matrix (lighter); (b) longitudinal (c) fibre/interface showing the distribution of the fibres in matrix and the uniform dispersion of the TCP particles in the matrix. (Scale bars (a) 100 µm; (b) 20 µm; (c) 2 µm)

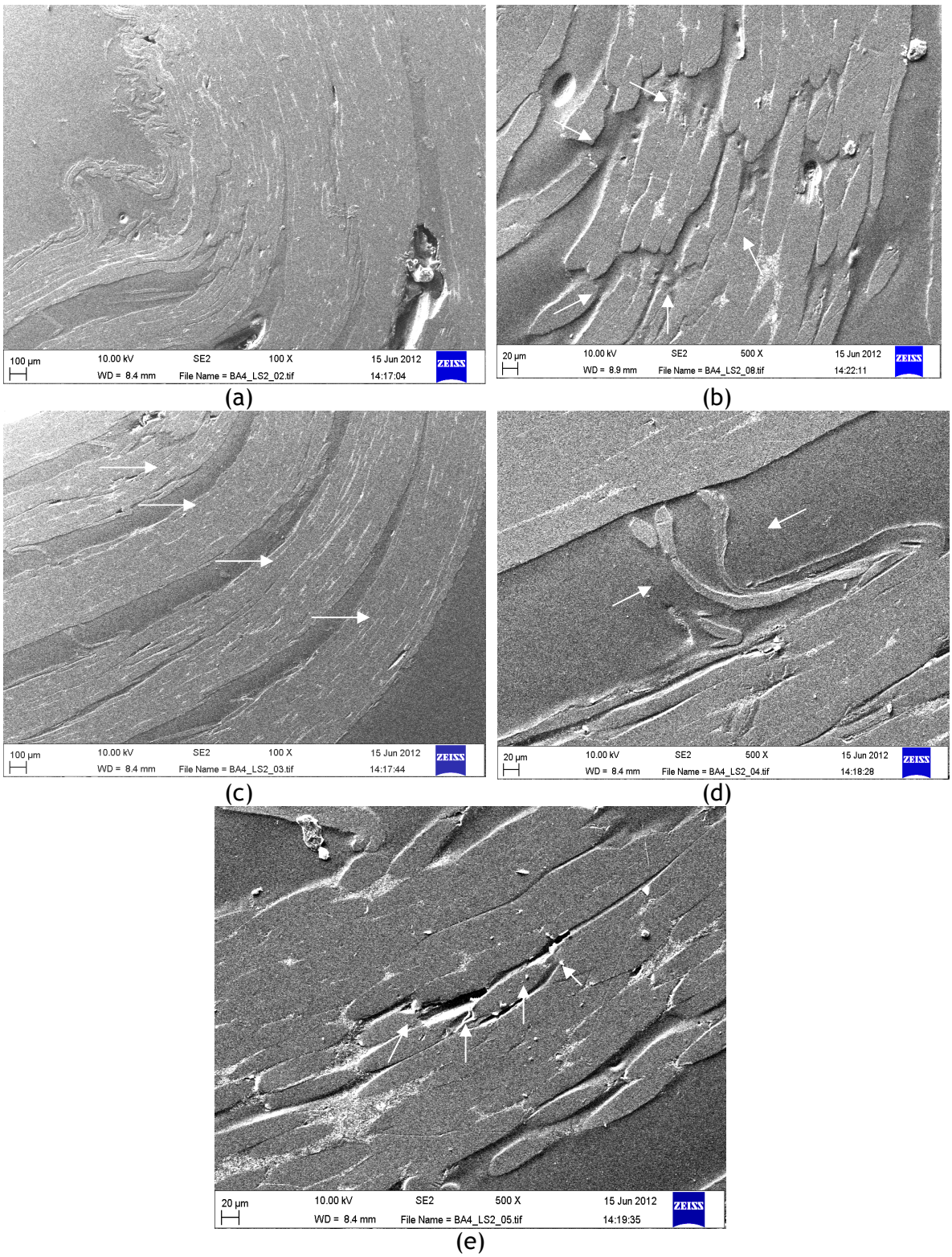

Figure 4.6 Cross sections of compressive loading fracture regions

(a) general view of the concave side; (b) crack propagation across the fibre in transverse direction; (c) internal kink band formation; (d) fibre kink bridging the internal split between the bundled fibres (e) vertical crack propagation. (Scale bars (a) 100 µm; (b) 20 µm; (c) 100 µm; (d) and (e) 20 µm)

Torsion

Figure 4.7 shows a surface of a specimen moulded at 150°C that underwent monotonic torsion testing. As the moulding temperature moulding did not produce significant differences in torsion properties, only a sample moulded at 150°C was observed under SEM. Even though the sample did not fracture into separate parts after 140º rotation, a significant number of crazes (white spirals) running around the specimen parallel with the fibre direction are visible, the whitening is due to drawing of the PLA–TCP matrix. Part of the fibre breakage also visible under microscopy as shown in Figure 4.7a. A closer view of a craze is shown as a spiral crack, formed by drawing of the PLA –TCP matrix, run around the specimen in the direction of shearing in the form of twisted lines (Figures 4.7b and 4.7c).

A clear damage at microscopic level is displayed in Figure 4.7d, where the separation between the fibres and the matrix has occurred due to shear fracture. Figure 4.7e shows more severe form of damage where a spiral crack, formed by drawing of the PLA fibres that eventually lead to fracture of the fibres, runs around the specimen in the direction of shearing.

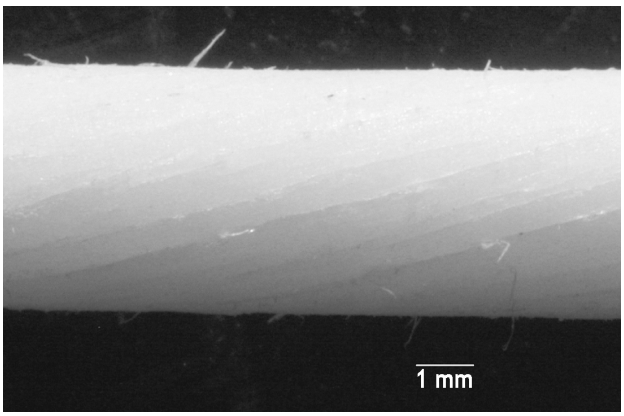

(a)

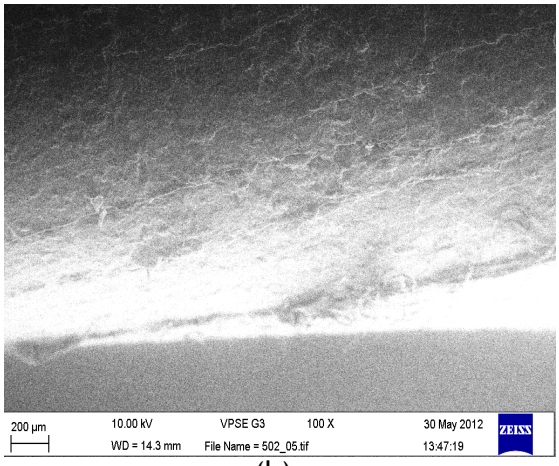

(b)

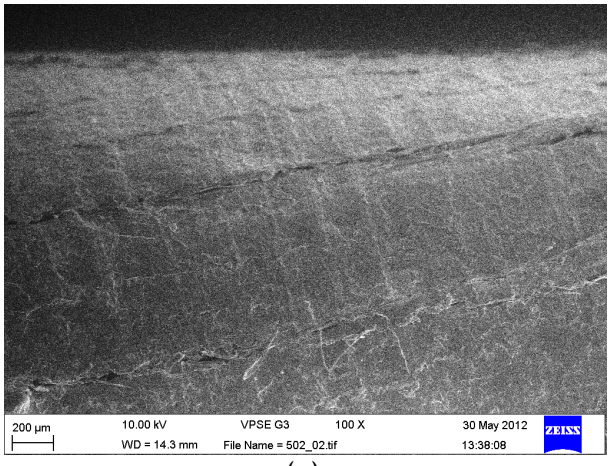

(c)

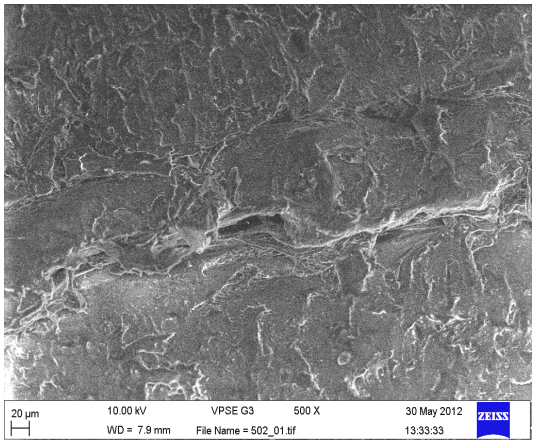

(d)

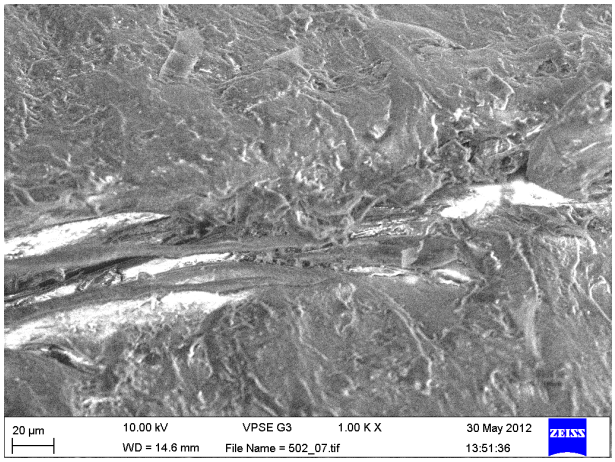

(e)

Figure 4.7 Surface of a torsion tested PLA-PLA-TCP composite (tested at 37°C in saline)

(a) twisted crack line; (b)-(c) closer view of the craze marks; (d) spiral longitudinal damages due to twisting and (e) fibres drawing due to shear failure (scale bar (a) 1 mm; (b)-(c) 200 µm; (d)-(e) 20 µm)

4.5 RESULTS - UNIAXIAL FATIGUE TESTING

4.5.1 Analysis of Effect of Moulding Temperature on Uniaxial Damage

The data shown in Tables 4.3 and 4.4 were used to calculate 25%, 50% and 75% of UTS and USS for both T140 and T150. These are shown in Table 4.5.

Table 4.5 The stress levels of PLA-PLA-TCP composite with different moulding temperatures

	% UTS (MPa)			% USS (MPa)		
	25%	**50%**	**75%**	**25%**	**50%**	**75%**
140°C (T140)	25.15	50.30	75.46	6.52	13.05	19.57
150°C (T150)	39.94	69.88	104.82	6.62	13.24	19.86

The S-N curve for axial and torsional fatigue of composite moulded at different temperatures as a percentage of the ultimate strength in that direction is shown in Figure 4.8 while the results in terms of stress are shown in Figure 4.9. Despite the differences in the ultimate strengths for tension and torsion, the S-N curves for the two loading directions appear to be similar. In axial fatigue, as expected, specimens moulded at higher moulding temperature have increased fatigue life. This is consistent with the findings of the quasi-static tests. However, no significant effect of the moulding temperature on the fatigue life in torsional was observed. For material moulded at both temperatures, torsional loading lead to earlier failure than tension-compression loading even when considered as a percentage of the ultimate strength. When the actual stress levels are considered, the T150 specimens have slightly increased fatigue life compared to T140, but there is no obvious effect on the torsional fatigue life. The increase in axial fatigue life would be expected from the increased axial strengths at 150°C moulding temperature compared to 140°C (Tables 4.4 and 4.5). The torsional strength was not affected and the torsional fatigue lives were also not affected.

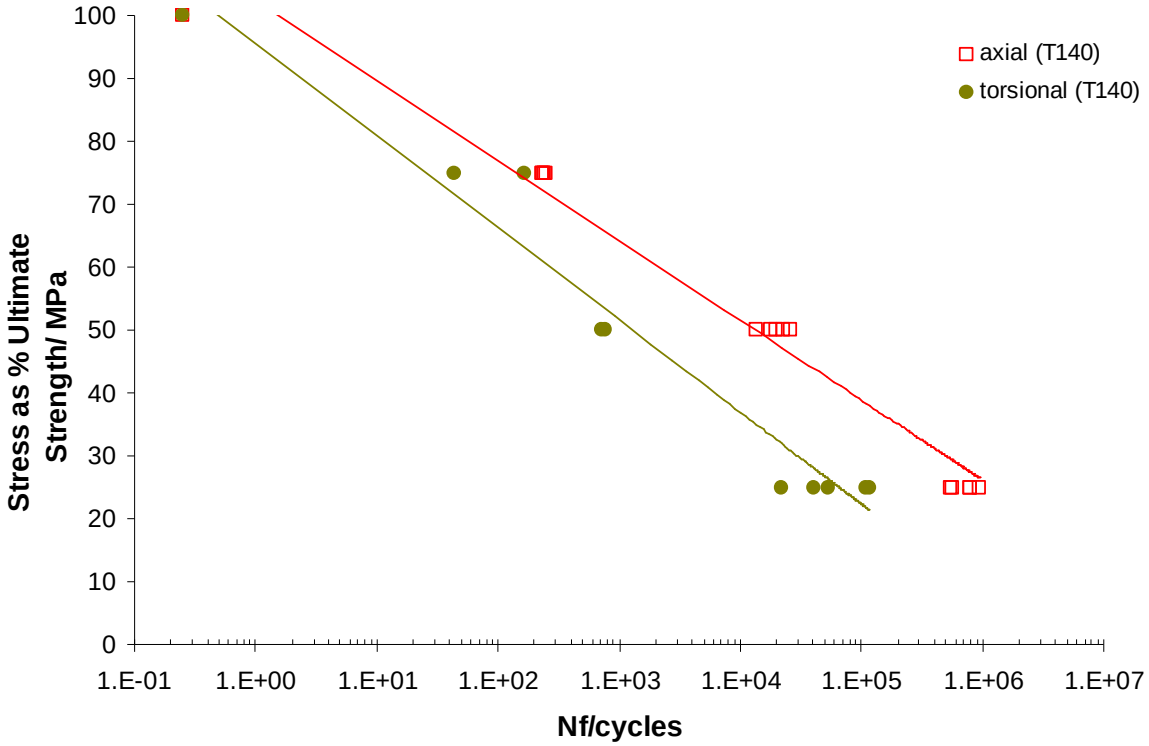

a)

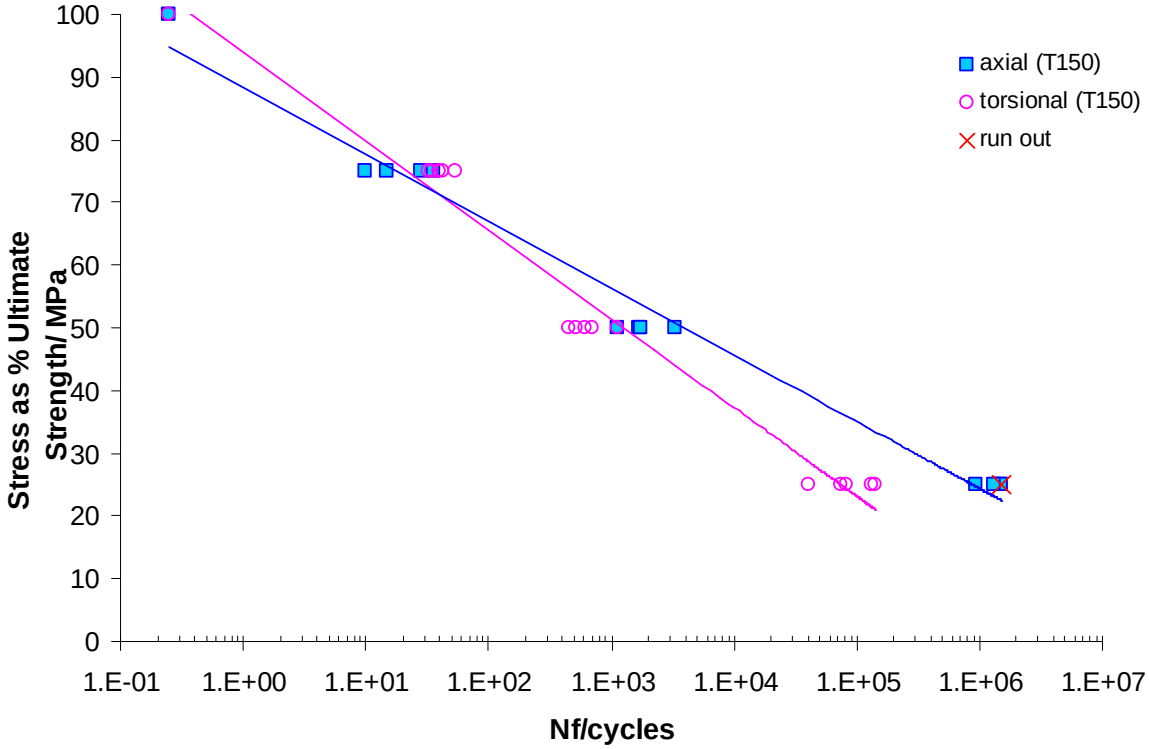

b)

Figure 4.8 S-N curves for fully reversed axial and torsional fatigues plotted in terms of percentage of ultimate strength for (a) 140°C moulding temperature (b) for 150°C moulding temperature

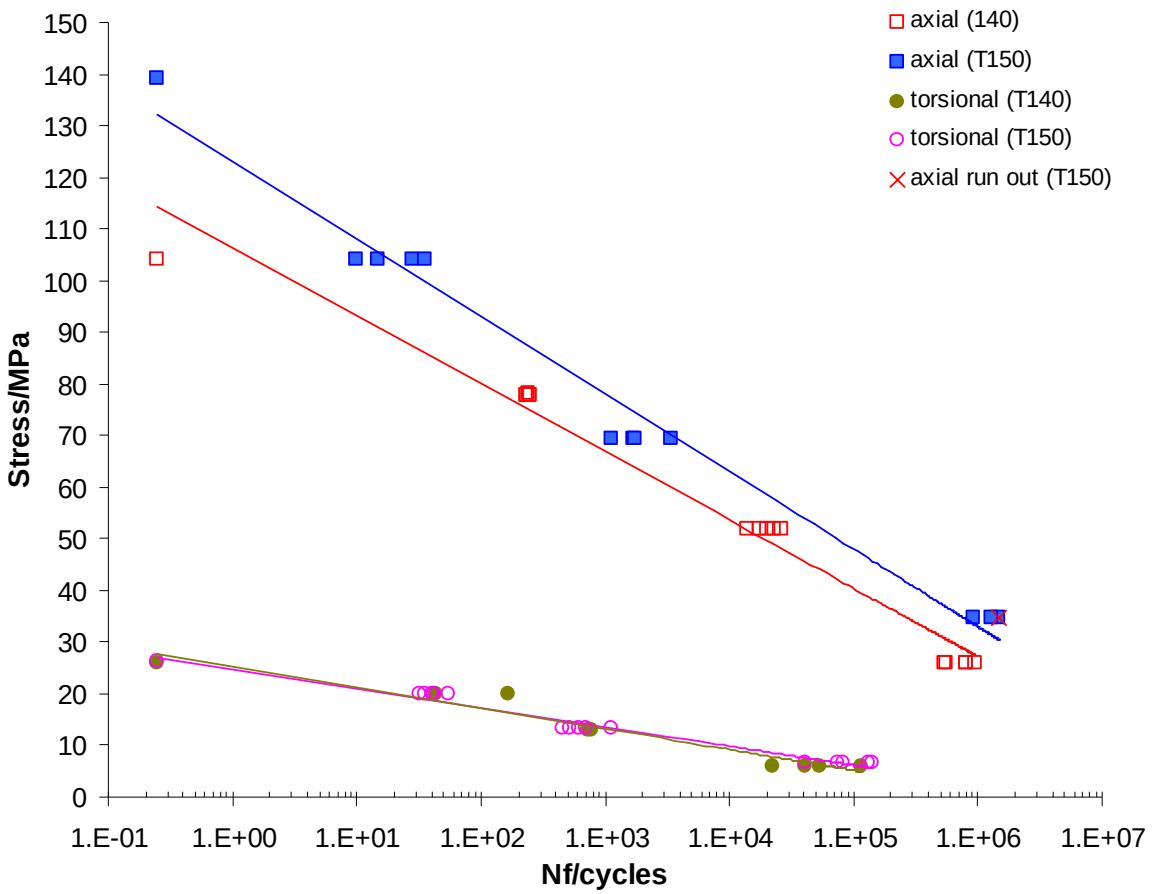

Figure 4.9 S-N curves for axial and torsional fatigue plotted in terms of stress for 140°C and 150°C moulding temperature

Figures 4.10 and 4.11 show the axial and torsional hysteresis loops respectively after various numbers of cycles for composite moulded at 140°C (T140). The hysteresis loops were regular and symmetrical at the start of loading for all load levels and in both loading directions. At ±25% UTS, the loops start to open up after 500,000 cycles, and at ±50% UTS from 10,000 cycles. The loops become non-symmetrical as the modulus reduces, the effect is greater in the compressive phase than tensile phase, which is indicative of the different mechanical response to tension and compression. As the number of cycles increases, the material becomes more damaged and this is reflected by the increasing amount of hysteresis seen by the increasing area inside the loop (energy absorbed), in addition to the modulus decreasing. In comparison to axial fatigue, the torsional hysteresis loops were smaller and more inclined at equivalent stress levels, the loops are less open at the start of testing than the axial loops.

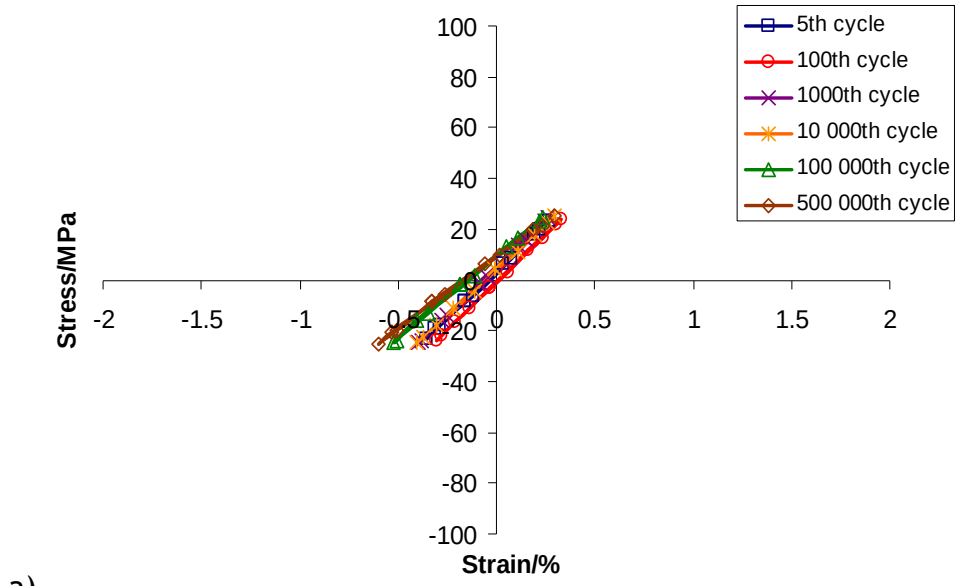

a)

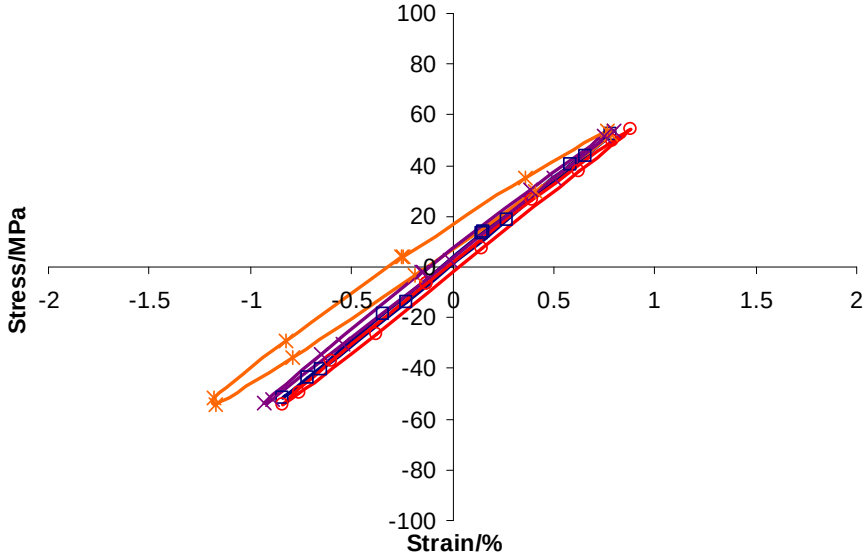

b)

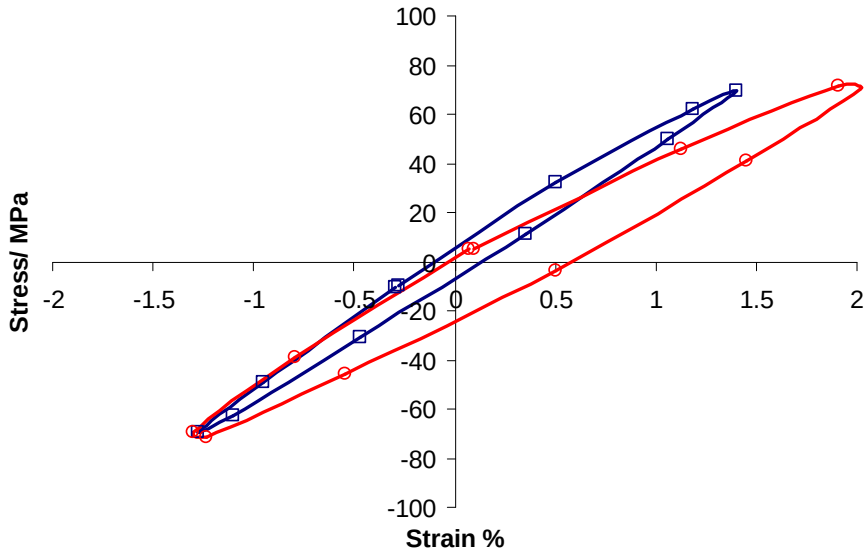

c)

Figure 4.10 Hysteresis loops for axial tension-compression fatigue (at 140˚C moulding temperature)

(a) ±25%UTS (b) ±50%UTS (c) ±75%UTS

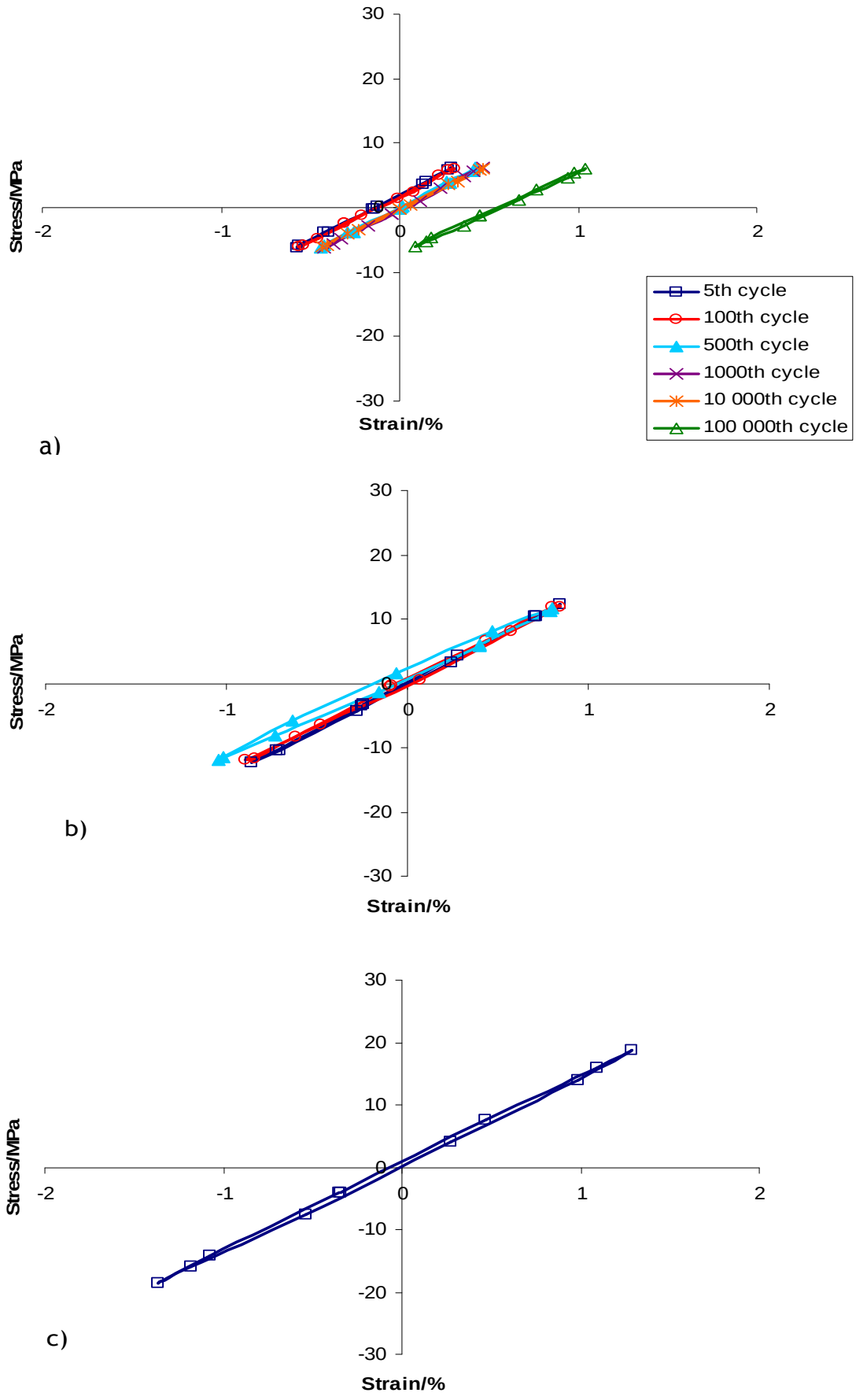

Figure 4.11 Hysteresis loops for torsional fatigue (at 140˚C moulding temperature) ±25%USS (b) ±50%USS (c) ±75%USS

From these graphs, the energy absorbed per load cycles and secant moduli for axial and torsional fatigue were calculated and are shown in Figures 4.12 and 4.13 respectively. As the applied stress increases, the secant modulus is reduced due to the larger strain range and the hysteresis loops also increase in area indicating increased absorbed energy. With the increasing number of cycles, the materials become more damaged, as shown by increasing energy absorbed and decreasing modulus. At ±25% UTS, the modulus start to drop at 10^4 cycles however the energy absorbed remain fairly constant. At ±50% UTS, the moduli was retained up to 10^3 cycles and the damage became apparent thereafter. At ±75% UTS, the damage become apparent as early as first 10 cycles observed with the increase in the energy absorption and degradation in modulus. In general the energy absorbed per load cycle increases before the secant modulus start to decrease.

In torsional fatigue, at ±25% USS, the modulus starts to drop after 10^4 cycles, but the energy absorbed remains constant up to $2x10^5$ cycles and then shows a slight increase. For ±50% USS, the modulus and energy absorbed remain constant up to 10^2 cycles before damage accumulation become apparent. For ±75% USS, damage accumulation starts as early as from 10 cycles. The energy absorbed increased at approximately the same point where the modulus starts to drop.

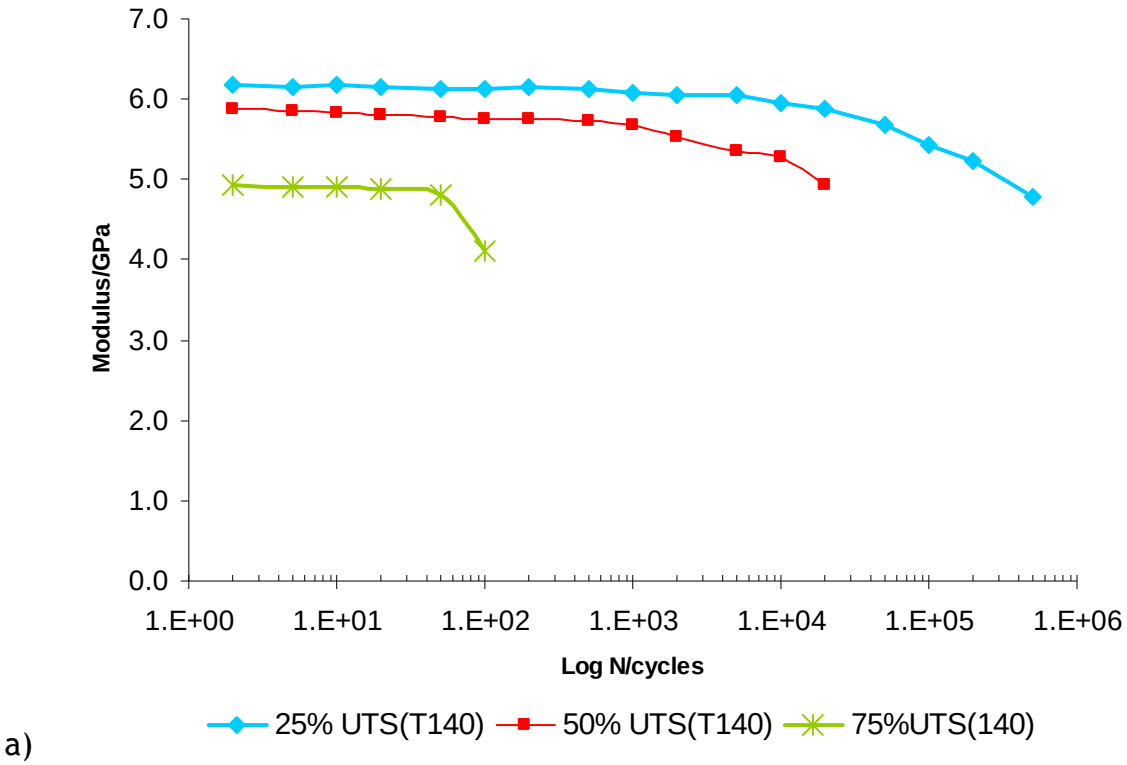

a)

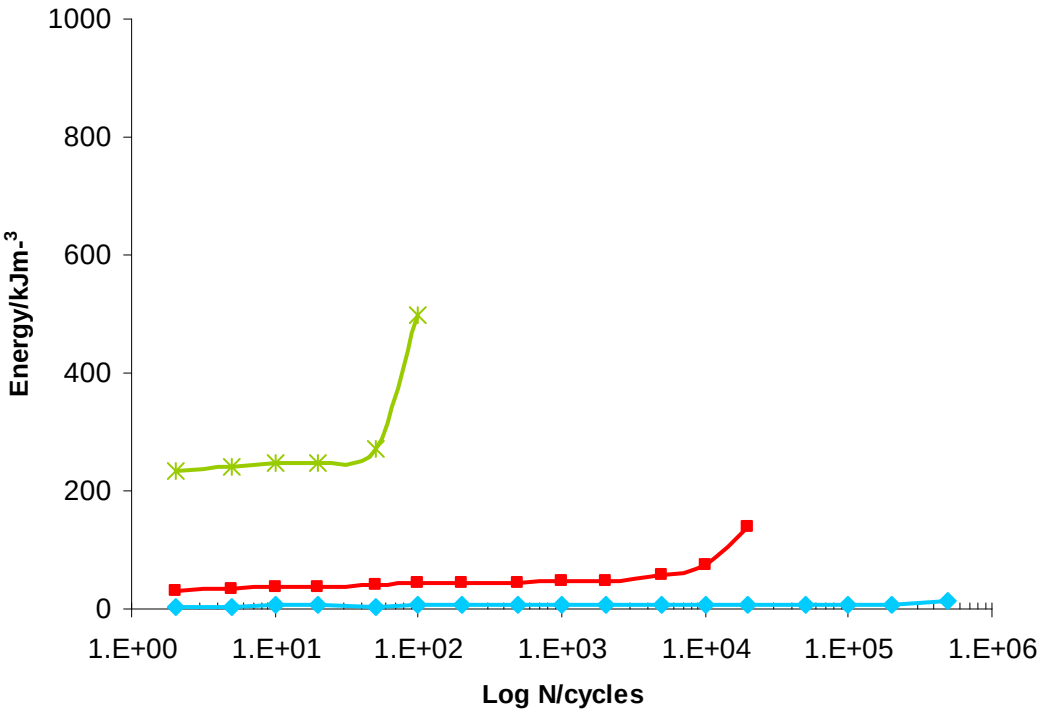

b)

Figure 4.12 Variations in a) secant modulus b) energy absorbed for axial fatigue with number of load cycles (at 140°C moulding temperature)

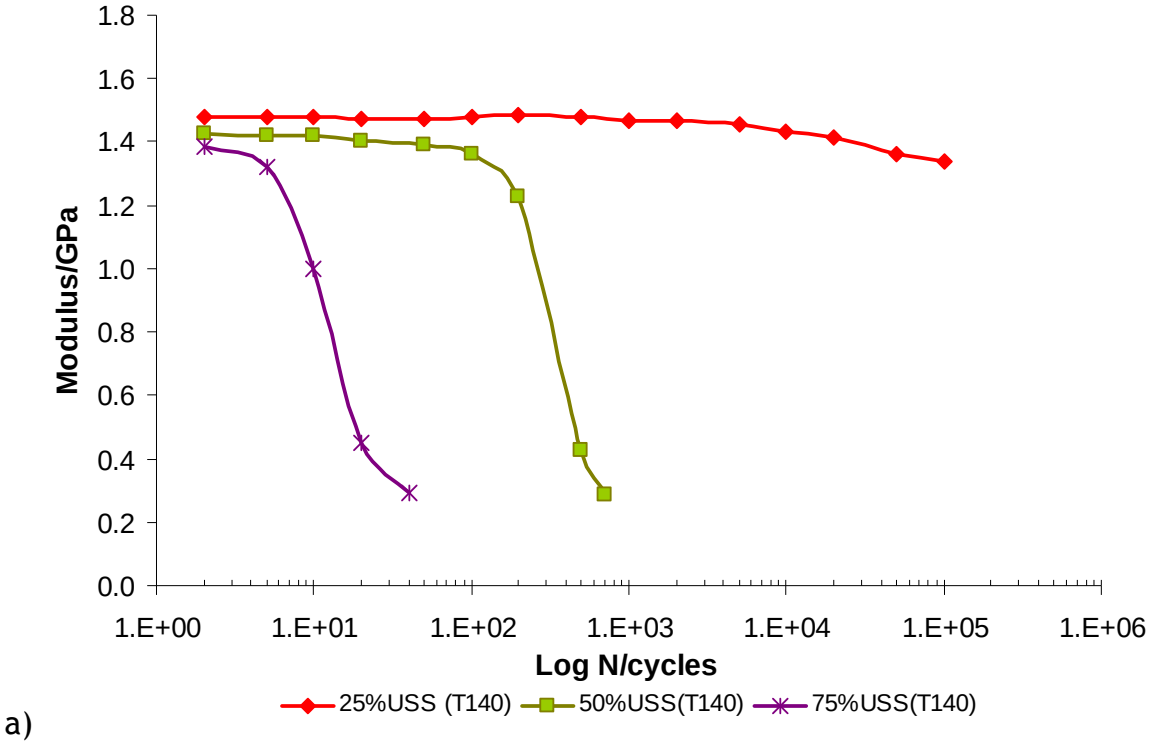

a)

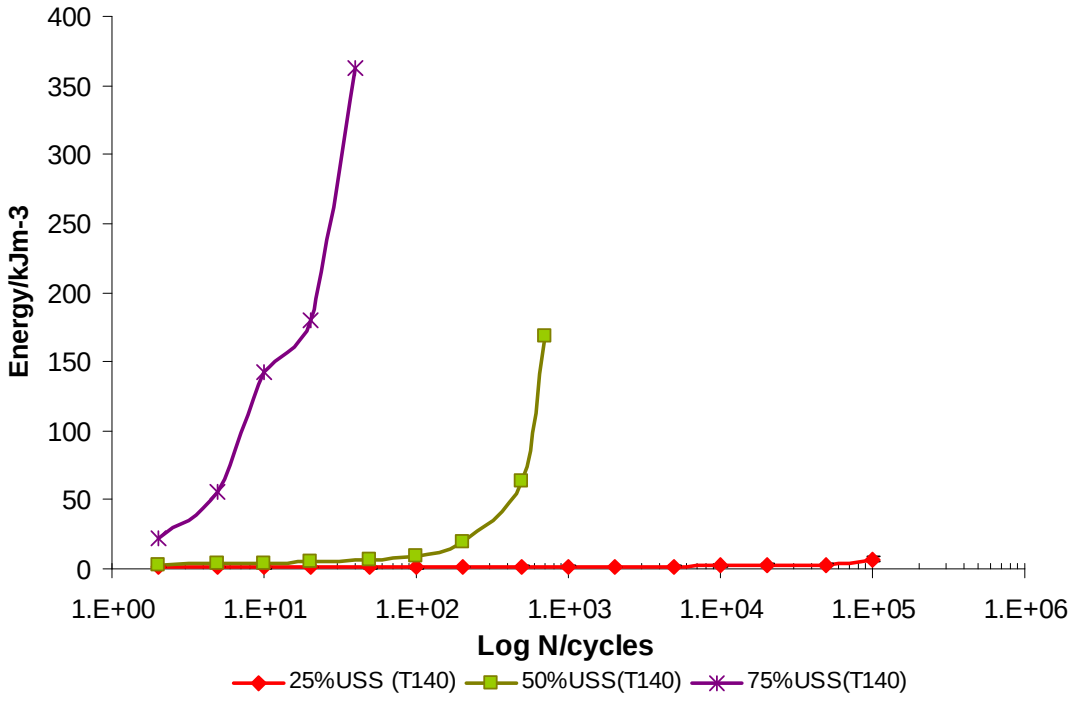

b)

Figure 4.13 Variations in a) secant modulus b) energy absorbed for torsional fatigue (at 140°C moulding temperature)

Figures 4.14 and 4.15 show the axial and torsional hysteresis loops respectively after various numbers of cycles for composite moulded at 150°C (T150). Again the hysteresis loops were regular and symmetrical at the start of the loading at all load levels and in both loading directions. At ±25% UTS axial loading, the axial loop are regular in the beginning, however they started to open up after 500 000 cycles, while at ±50% UTS this occurred as early as 1000 cycles. Similar to T140 specimens, the modulus reduces more in the compressive phase than the tensile phase, which is indicative of the different mechanical response in tension and compression. As the number of cycles increases, the materials become more damaged and this is reflected by the increasing of area inside the hysteresis loops, which is energy dissipated, in addition to the decreases in the modulus. The torsional hysteresis loops were similar to those for T140 specimen, where it was smaller and more inclined at equivalent stress levels in comparison to axial hysteresis loop, and even at start of cycling.

It can also be seen from Figures 4.14 and 4.15 that the hysteresis loops gradually shift along the x-axis, indicating dynamic creep in the material. Due to the fully reversed nature of the fatigue applied, each load cycle resulted in a tensile and a compressive strain. In the case of axial tension-compression fatigue, final fracture is determined by the maximum compression strain. The strain range is relatively constant at the beginning of cycling. For axial loading, strain increased in the compression direction, which is the weaker direction in monotonic testing. In torsion, the stress and strain regime should be totally symmetrical, but some creep occurred during testing. However, the loops remained symmetrical throughout torsional fatigue. From the observation, the direction of creep depended on the gripping of the specimens prior to testing. The creep is thought to be from any slight misalignment of specimens around the longitudinal direction of the grips at start of the test, despite the efforts made to ensure that the samples were aligned with the test machines axis. It is difficult to ensure samples are absolutely aligned given that the grip alignment and sample gripping are done by hand.

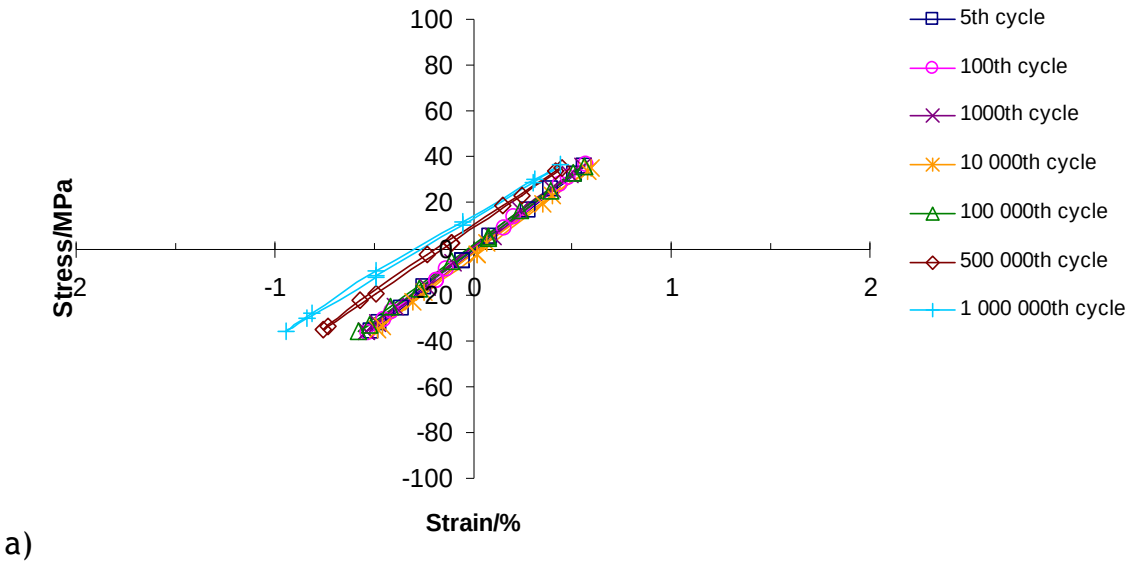

a)

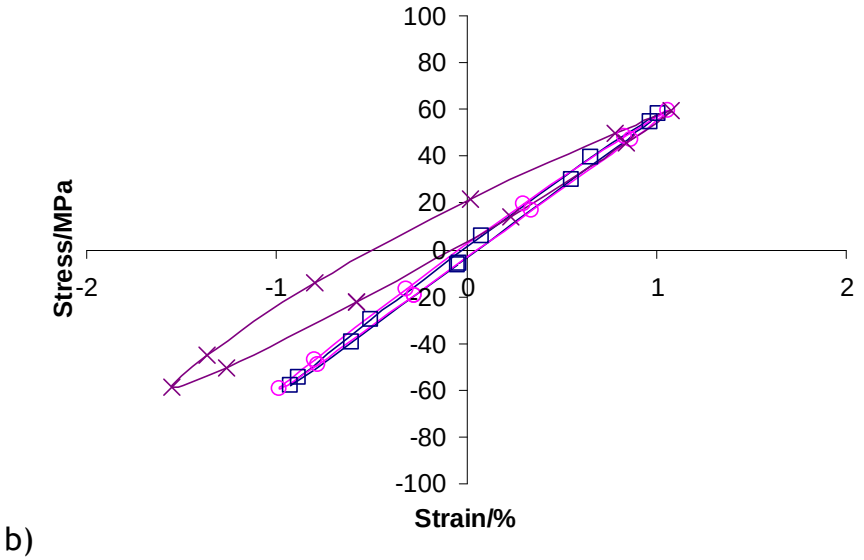

b)

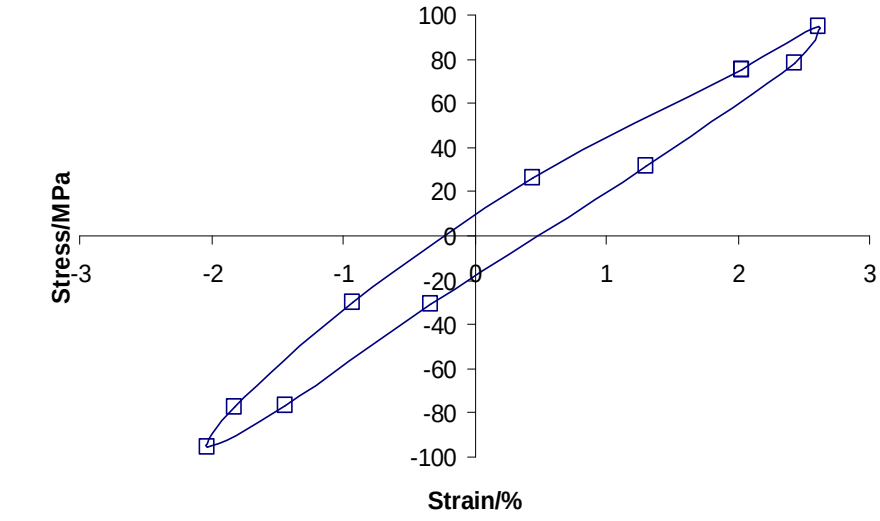

c)

Figure 4.14 Hysteresis loops for axial tension-compression fatigue (at 150˚C moulding temperature)

(a) ±25%UTS; (b) ±50%UTS; (c) ±75%UTS

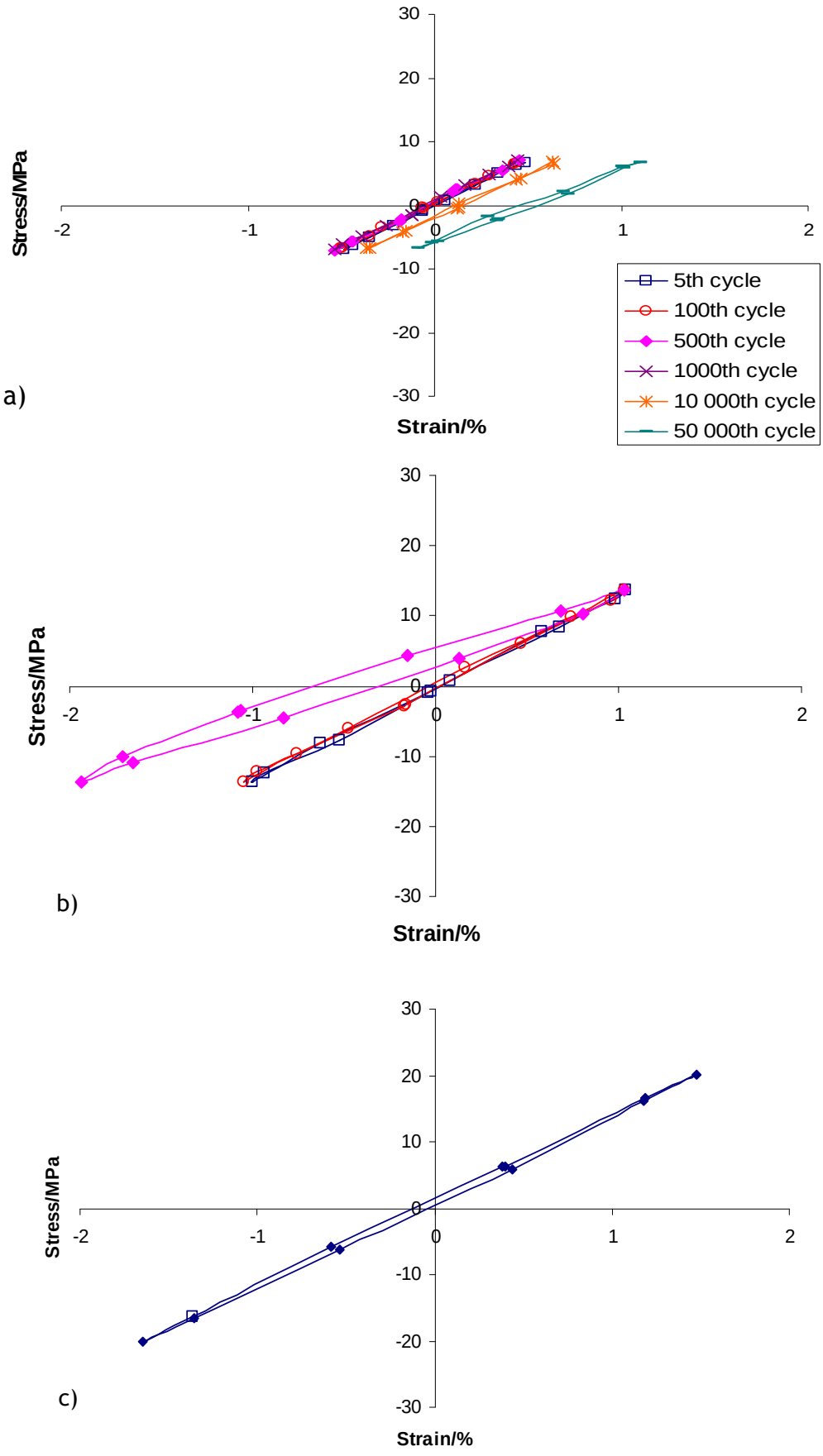

Figure 4.15 Hysteresis loops for torsional fatigue (at 150˚C moulding temperature) ±25%USS (b) ±50%USS (c) ±75%USS

The variations of energy dissipated and secant modulus for specimens moulded at 150°C (T150) are calculated and shown in Figures 4.16 and 4.17 respectively. As the applied stress increased, the secant modulus reduced due to the larger strain range and hysteresis loops are also become larger indicating increased absorbed energy. As the number of cycles increased, the materials become more damaged, as shown by the increasing energy absorbed and the modulus decrease. For ±25% UTS and ±25% USS, the modulus start to drop after 100,000 and 50,000 cycles, but the energy absorbed remain fairly constant. For ±50% UTS and ±50% USS, the modulus and energy absorbed remain constant up to 100 cycles, but damage accumulation become apparent from then on. For ±75% UTS and ±75% USS, damage accumulation starts as early as 10 cycles.

Closer comparison of the effect of the temperature moulding on the energy absorption and degradation of modulus of the composite after ±25% USS fatigue test is shown in Figure 4.18. As number of cycles to failure progress, similar trends were observed in both T140 and T150 specimens in term of degradation of the modulus. However, T150 showed less and slower energy absorption in comparison to T140. Similar behaviour was also observed at ±50% USS and ±75% USS.

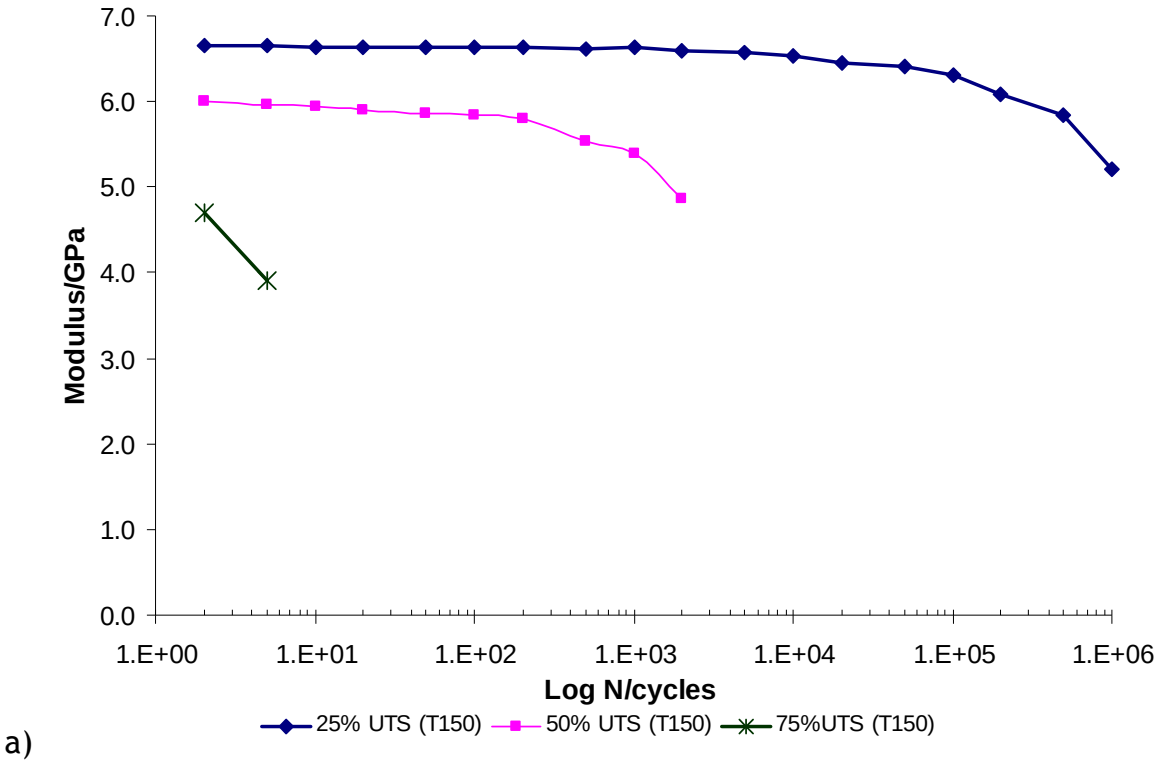

a)

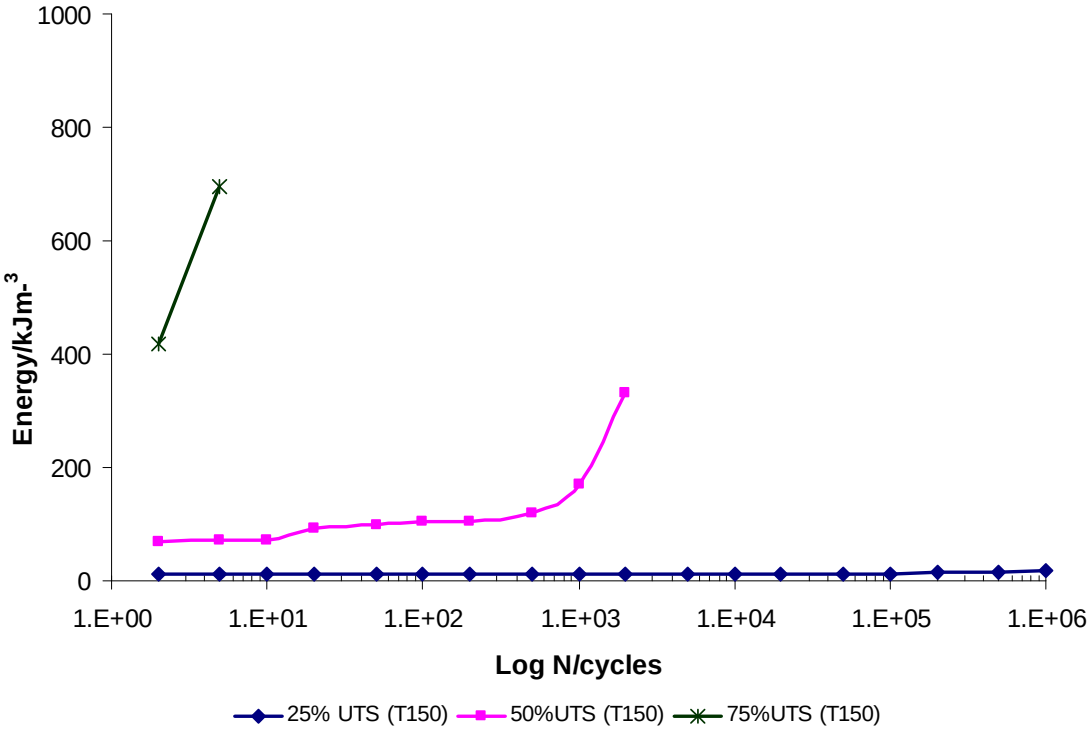

b)

Figure 4.16 Variations in a) secant modulus b) energy absorbed for tension-compression fatigue (at 150˚C moulding temperature)

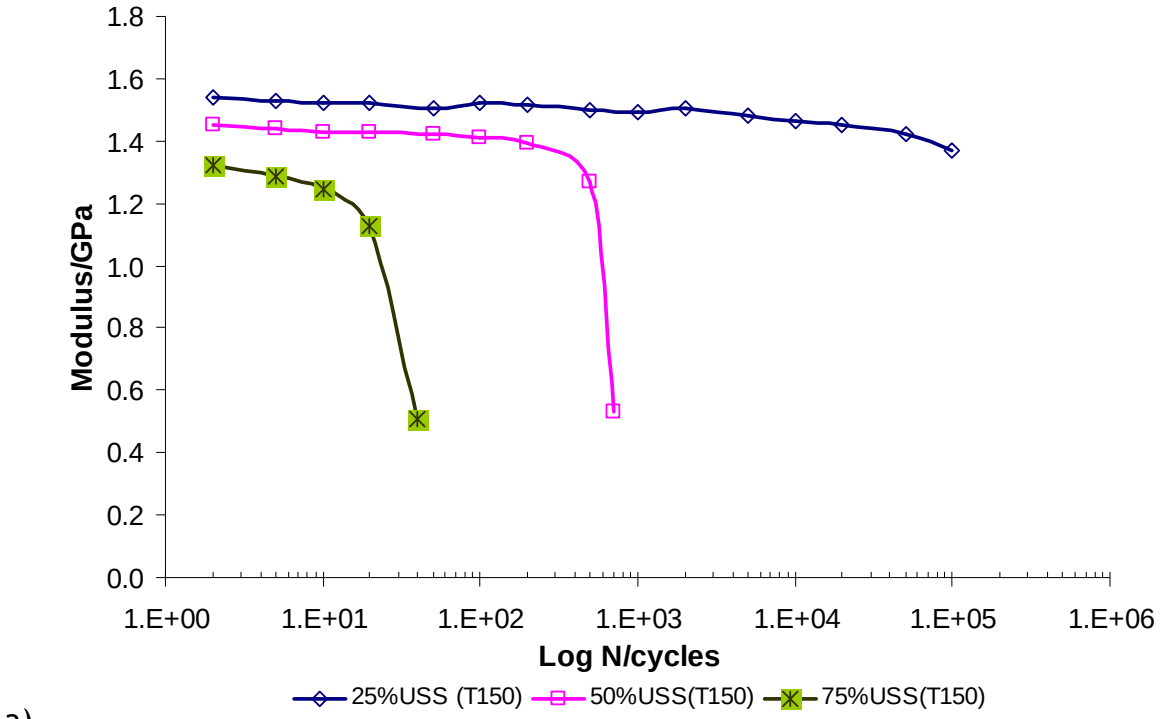

a)

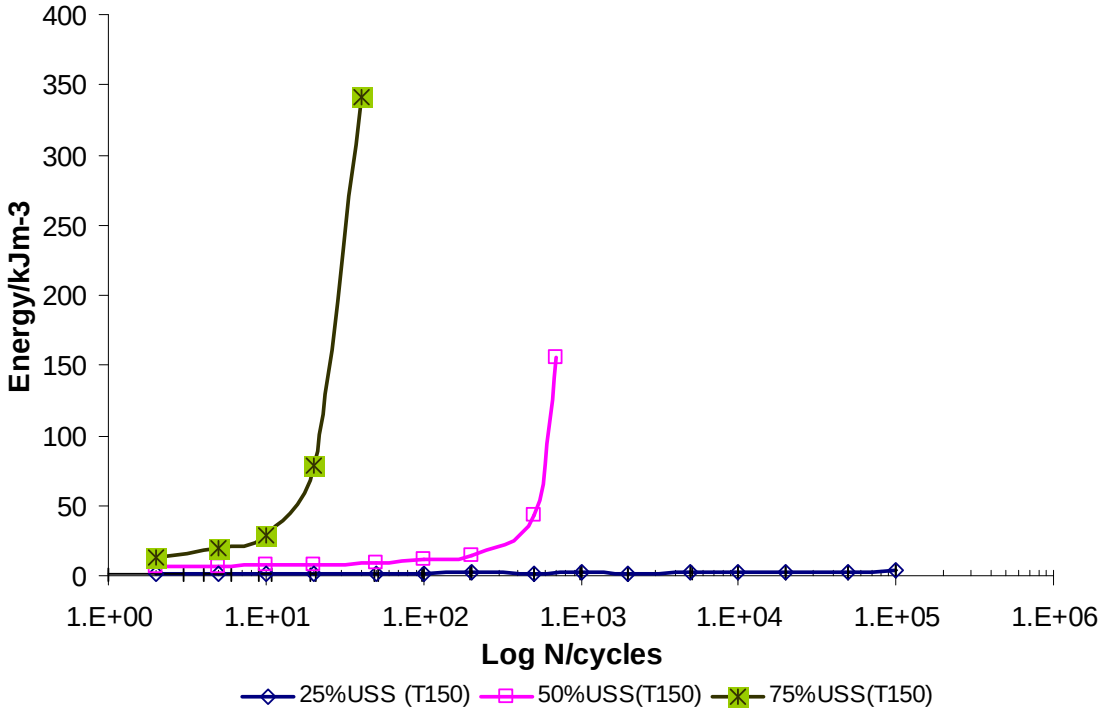

b)

Figure 4.17 Variations in a) secant modulus b) energy absorbed for torsional fatigue (at 150°C moulding temperature)

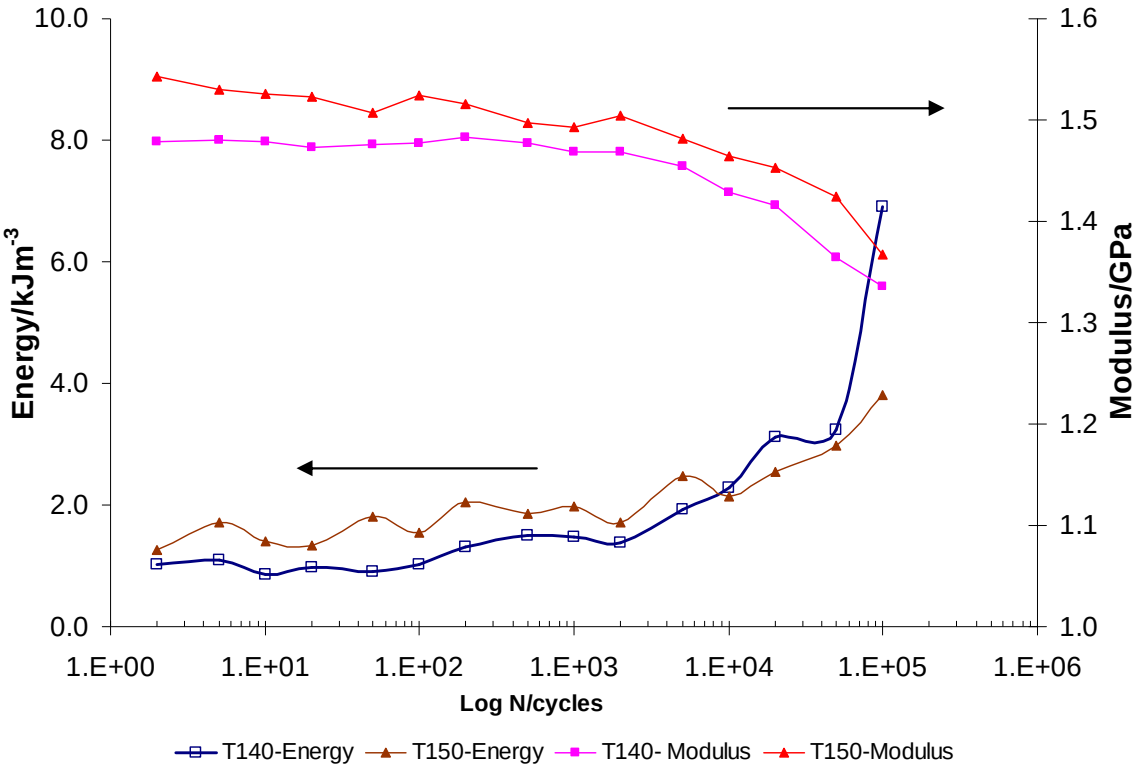

Figure 4.18 Variations in energy absorbed and secant modulus with moulding temperature of self reinforced PLA filled TCP composite tested at ±25% UTS

4.5.2 Analysis of Effect of Loading Mode on Axial Fatigue Damage

Figure 4.19 compares the fatigue lives of composites that have been moulded at different temperatures loaded in tension only with fully reversed tension-compression. It should be noted that the testing was carried out at different stress level, which were 50% of the relevant UTS values, which is 50 MPa for T140 and 69.5 MPa for T150 respectively. Thus, the testing for 140°C samples were either 0 to 50 MPa or ±50 MPa, while for specimens moulded at 150°C, the stresses were 0 to 69.5 MPa or ±69.5 MPa.

For composite compressed moulded at 140°C, the addition of compression loading significantly reduced the fatigue life by approximately 89.7% ($p<0.05$), from 197,461 (±94,216) to 20,188 (±4,792) cycles to failure. A similar finding was observed when tested the composite at moulded at higher temperature of 150°C, the effect of compression loading reduced the cycles to failure by 95.19%, from 35,031 (±32,261) to 1,800 (±1,166).

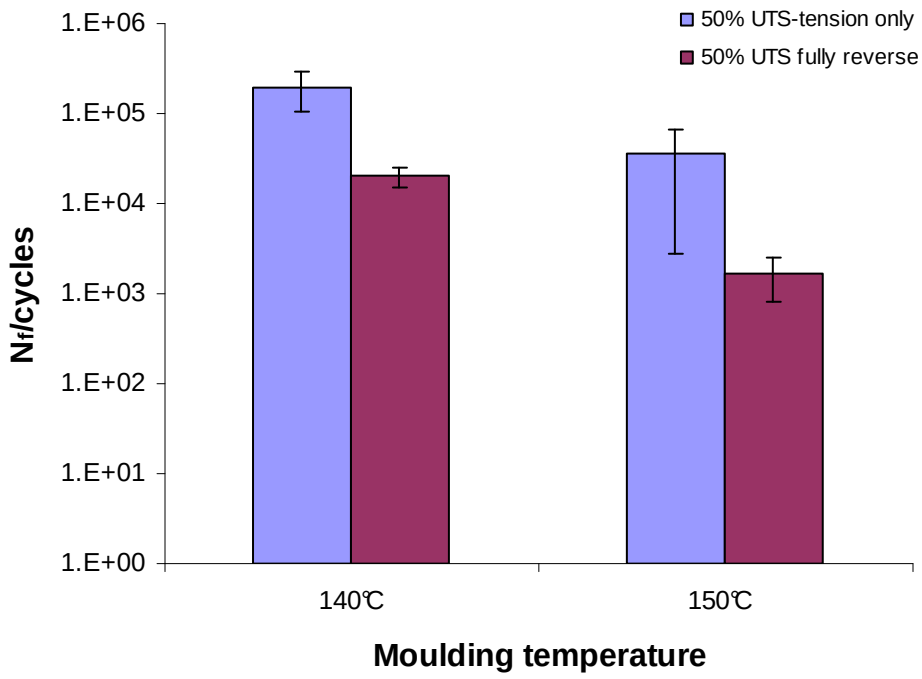

Figure 4.19 Effect of loading mode on fatigue lives of composite moulding at 140°C (T140) and 150°C (T150)

Figure 4.20a shows the hysteresis loops for tension only fatigue for T140. When compared to the fully reversed testing shown in Figure 4.10b, the loops for T140 in tension only were open from the start of loading however they remain fairly constant up to 10,000 cycles, thereafter the area inside the loops starts to increase in combination with a decrease in the modulus.

For T150, when comparing the hysteresis loops in Figures 4.14b and 4.20b, the loops for the first 100 cycles were smaller in tensile only fatigue test compared to tension-compression fatigue. While the loops for tension-compression loading started to open up after 100 cycles, tension only fatigue loops remain constant till approximately 10,000 cycles before the damage become more apparent. The hysteresis loops for both T140 and T150 tensile only fatigue shifted along the strain axis as testing progresses indicated tensile creep occurred during the test.

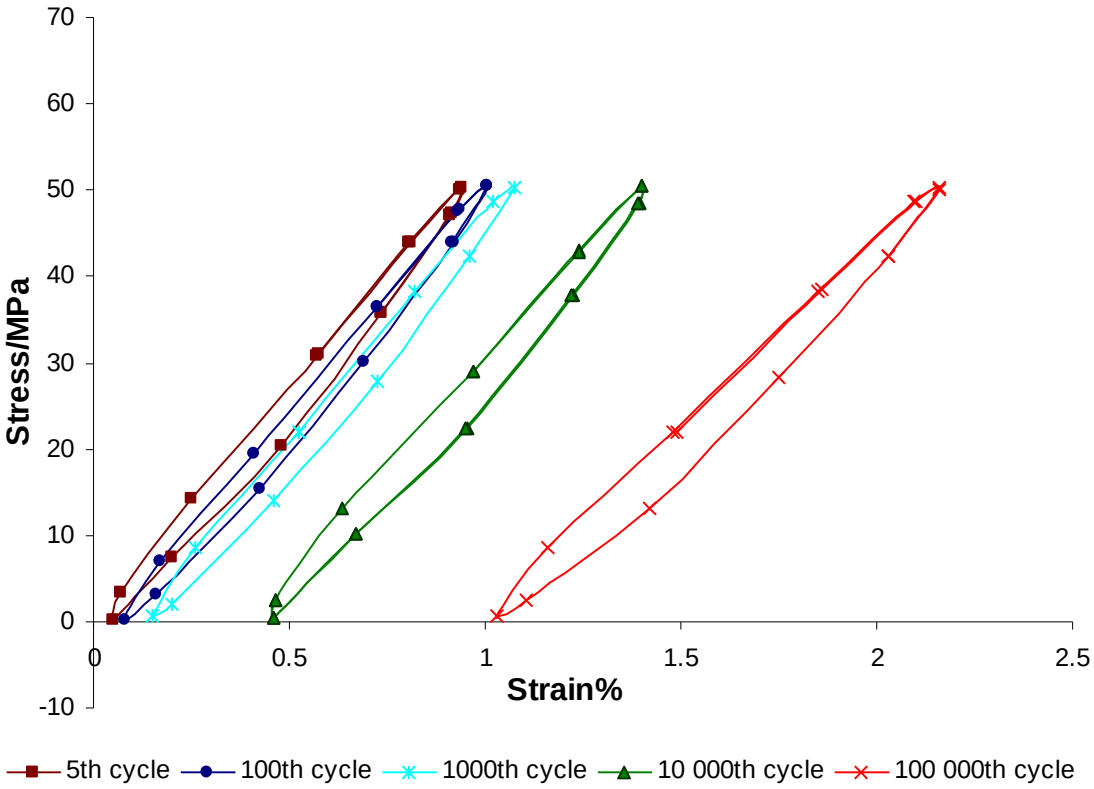

a)

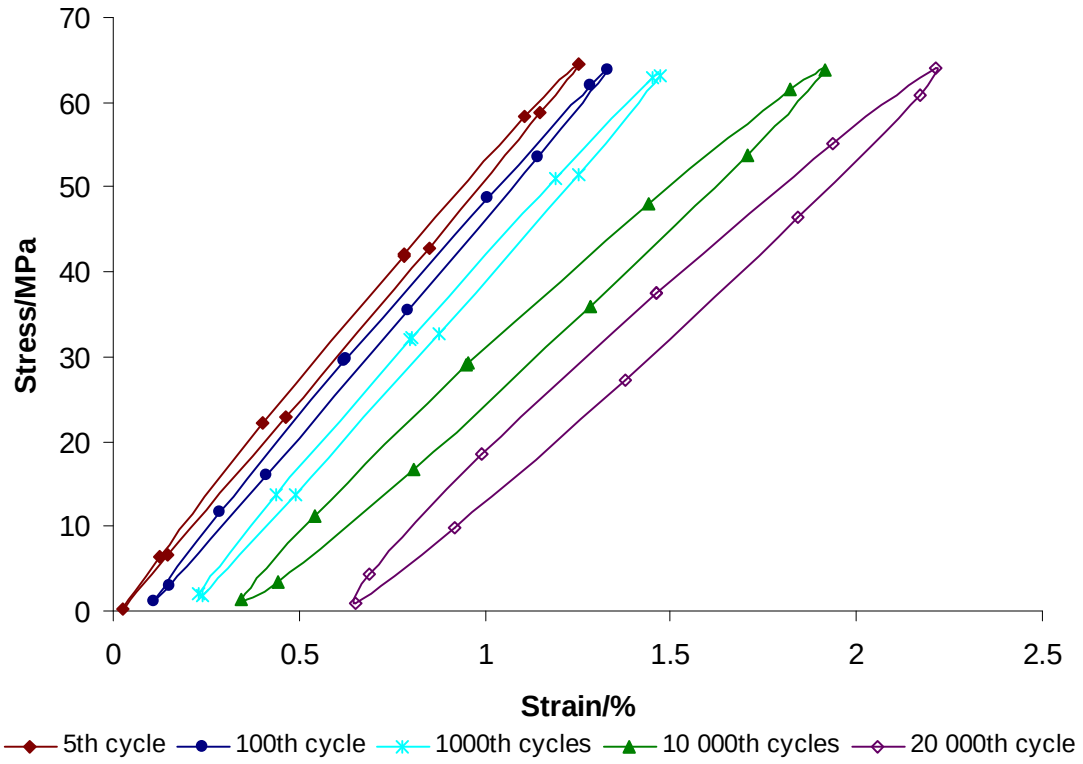

b)

Figure 4.20 Hysteresis loops for uniaxial tension only fatigue with different moulding temperature (a) +50% UTS 140˚C (b) +50% UTS at 150˚C

Figure 4.21 shows the variations in the secant modulus and energy absorbed for both materials moulded at 140°C and 150°C in tensile only fatigue test in comparison to fully reversed tension-compression fatigue both at 50% UTS. For T140 specimens, the modulus in tension only fatigue is constant till 500 cycles, after which the reductions become apparent. However the modulus reduces prior to increase of the energy absorbed indicating that failure was initiated by fibre breakage. Subsequent load cycles lead to crack propagation in the matrix, which can be observed with increases in the energy absorbed per load cycle. From 3,000 cycles to 10,000, the energy absorbed was constant while the modulus continued to decrease. This probably due to slowing of the crack propagation caused by a crack blunting mechanism. Inefficient crack arrest mechanisms led to further crack propagation in the matrix which can be observed by steady reductions in the modulus and increases in the energy absorption. In comparison with addition of the compression loading, the secant modulus drops from as early as the first 10 cycles indicating that the damage has already started. The increase in energy absorbed becomes more apparent after 100 cycles in comparison to 2000 cycles for the tensile only fatigue. As loading continued, the energy dissipation increased dramatically after 1,000 cycles, while at the same time, a reduction in the modulus was observed. This indicates that the compression damage was dominant at this stage, which caused rapid crack propagation as observed as increasing energy absorbed.

Figure 4.21b shows similar behaviour for T150 specimens. The energy absorbed in the first 10 cycles of tension-compression and tension fatigue is fairly constant while a slight reduction in the modulus was observed. However, it is noteworthy that up to this number of cycles, both secant modulus and energy absorbed for tension-compression and tension only are similar, indicating that the damage produced by the compressive stress has not yet become apparent. In comparison to the tensile only loading, energy absorbed in tensile-compression loading increases rapidly after 10 cycles indicating at this stage the compression damage has started to dominate the fatigue behaviour of the composite. However, the energy absorbed for the tension-compression increased prior to reduction in the modulus indicating that the composite was still able to retain stiffness despite increasing damage. The deleterious effect of the compression mode becomes apparent after 200 cycles as the secant modulus starts to reduce but not

statistically significantly, while energy absorbed increased significantly ($p<0.01$) in comparison to the testing in tension only indicated severe degradation of composite strength from this point leading to failure.

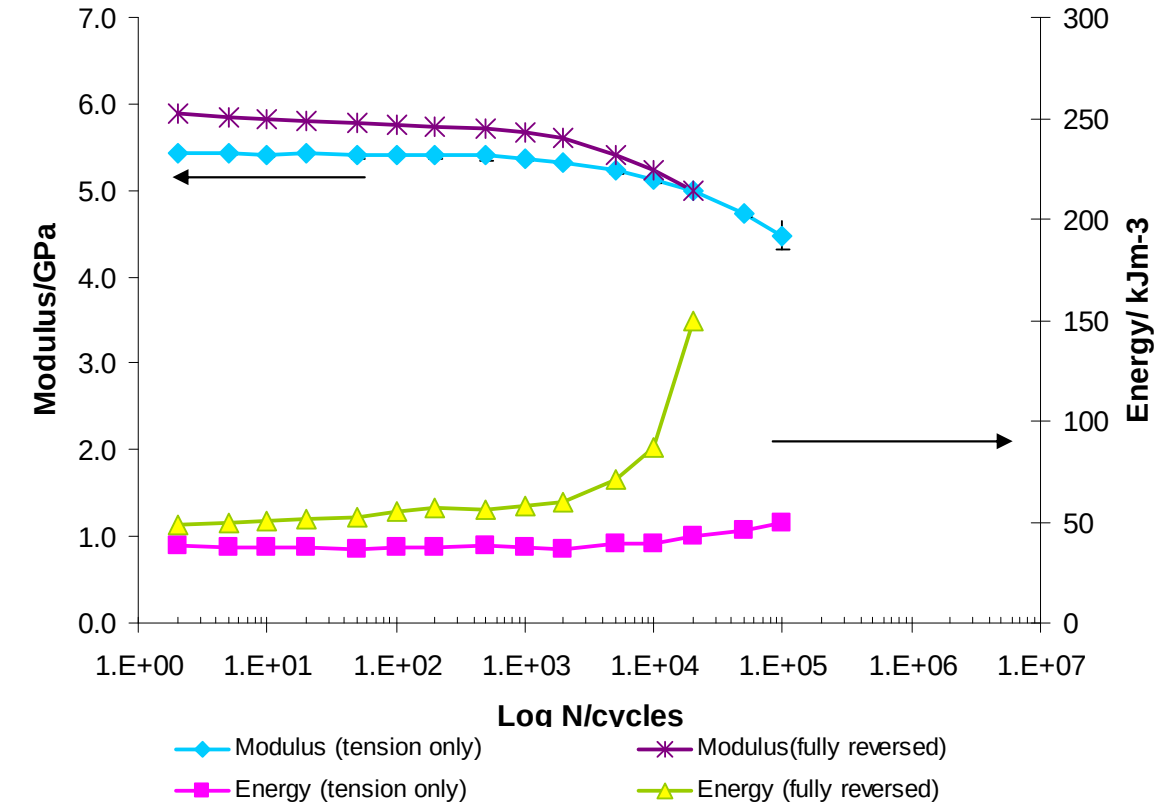

a)

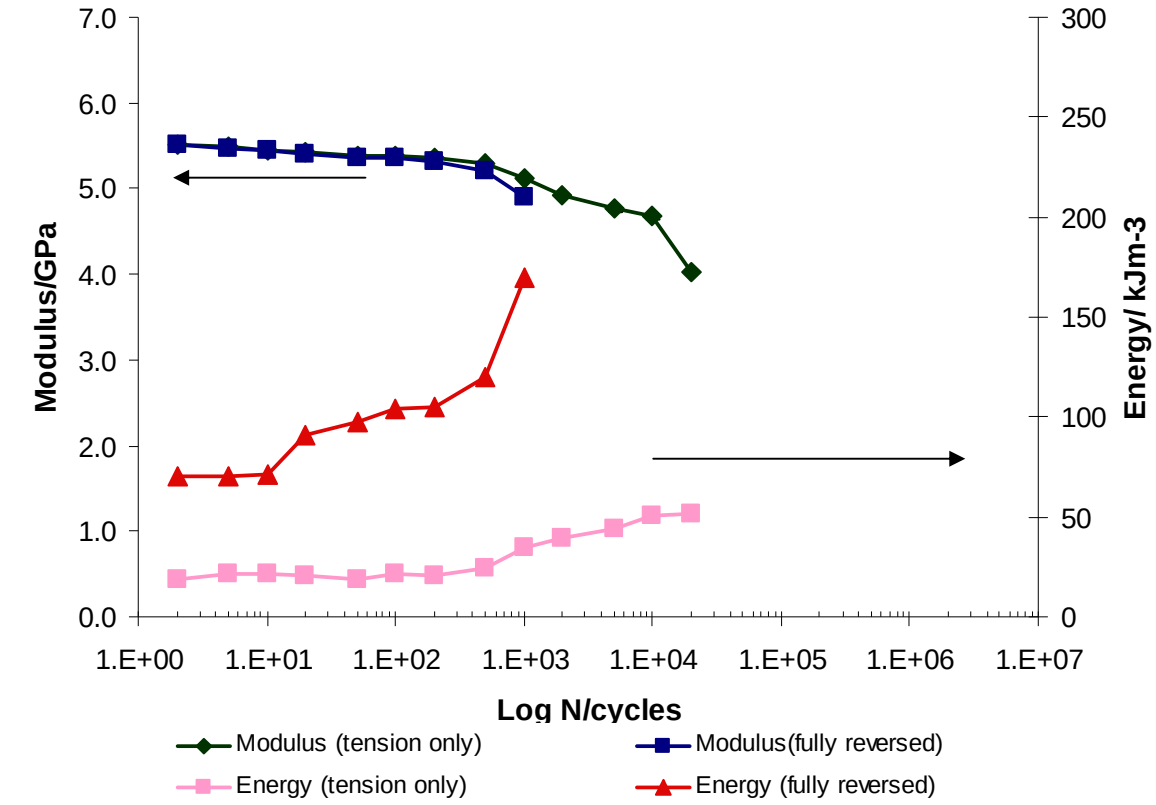

b)

Figure 4.21 Variations in secant modulus and energy absorbed at 50%UTS uniaxial tension only and ±50% fully reverse tension compression fatigue for moulding temperature of (a) 140˚C and (b) 150˚C

4.5.3 Fractography

Figures 4.22 and 4.23 show the fracture surfaces of specimens moulded at 140°C that failed under ±25%UTS and ±50% UTS respectively. At ±25% UTS, the crack propagation started at the weakest side of the specimen which resulting sharp fracture surfaces of the broken fibres, some bundled together (Figures 4.22b and 4.22d). Figure 4.22f reveals the smooth surfaces of the ends of fractured fibres, which are still quite well bonded to the matrix. The TCP particles are also visible on the matrix surface, some shown by pits left behind in the matrix. Figure 4.22c shows some fibre kink bands evident of plastic buckling of the specimen. Accumulation of the kink bands in the samples also produced sufficient transverse stresses to lead to longitudinal splitting of the matrix as observed in Figure 4.22g.

When tested at the higher stress, the specimen fractured in a different manner as shown in Figure 4.23a. Instead of the failure initiating at the weakest side of the specimen surface seen in Figure 4.22a, the failure mechanism appeared to start from the centre, due to axial delamination that caused the fibres to open up and lead to plastic buckling failure. Cross section examinations show that the stress caused the fibres to split apart in the centre, initiating kink bands in multiple directions, propagating along the axis of the specimen and causing the fibres to separate from each other in a brush like manner (Figures 4.23b and 4.23c). This axisymmetic failure mode indicated that specimen moulded at 140°C has poor interfacial bond between the fibres as expected. Also the lower moulding temperature may have produced less melting and thus poorer bonds in the centre of the sample compare to the surface as the matrix phase may have not reach melt temperature. Figure 4.23d shows the internal compression failure that split the fibres bundles in the middle of the specimen. During tension-compression fatigue testing, transverse tensile stresses were generated when the specimen in the compressive phase. This caused failure between the fibres either at fibre-matrix interfaces or longitudinally at the matrix-TCP interfaces. This failure was confirmed by higher magnification view of cross section of the fractured specimen (Figure 4.23e). It can be observed that the crack propagates thorough the interfaces between the fibres and travels along the axis of the specimen causing the fibres to split apart. Figures 4.23f and 4.23g show higher

magnification examination and reveal gaps between the fibres suggesting poor attachment between the fibres and the matrix.

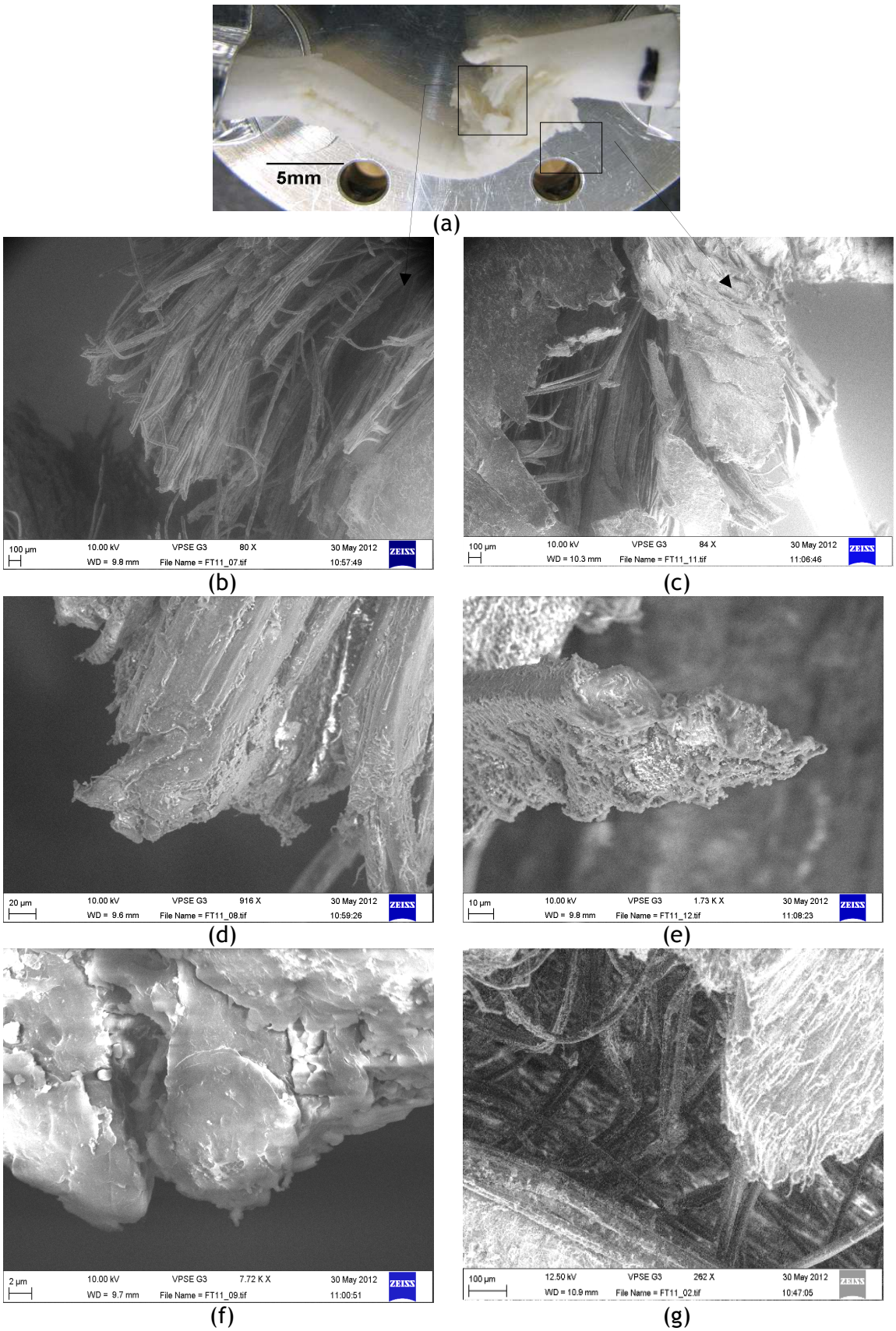

Figure 4.22 Fracture surface damage by tension-compression ±25% UTS fatigue for a sample moulded at 140°C

(a) general view of sample fracture; (b) fibre bundle fracture; (c) kink bands in fracture fibres (d)-(e) fibre fracture at crack start and end path of crack propagation path; (f) end of fibre fracture and (g) fibre kinks inside longitudinal split of matrix (scale bars = (a) 5 mm; (b),(c) &(g) 100µm; (d) 20µm; (e) 10µm; (f) 2µm)

(a)

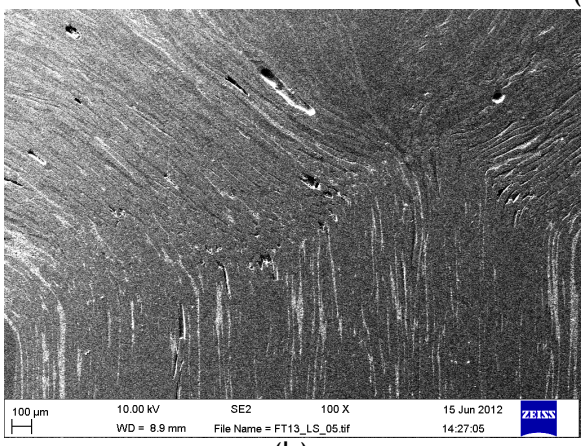

(b)

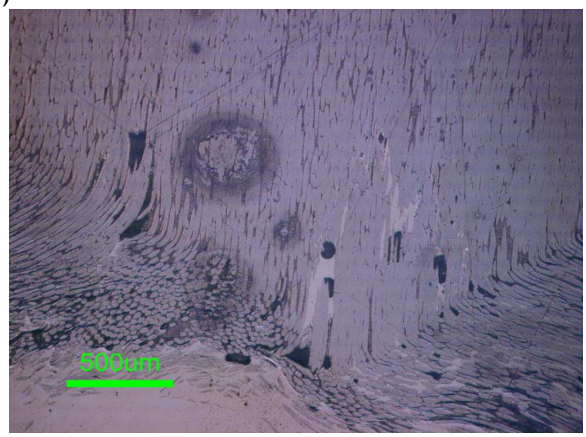

(c)

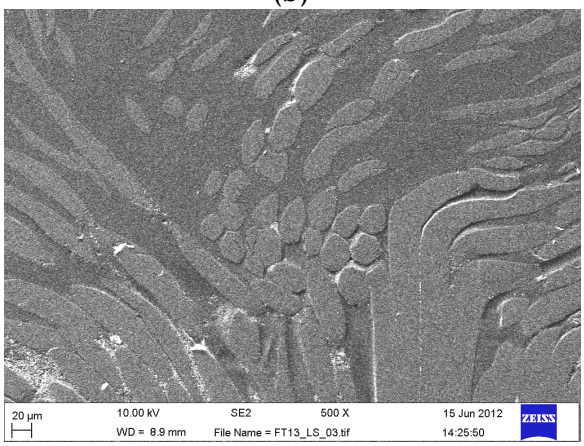

(d)

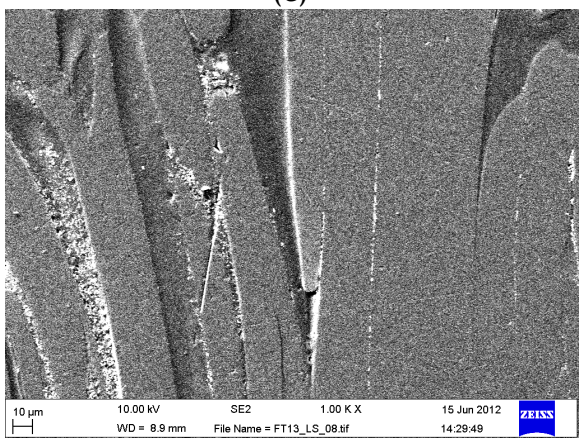

(e)

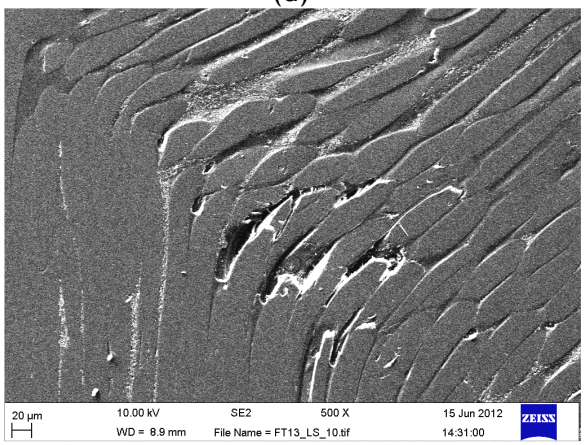

(f)

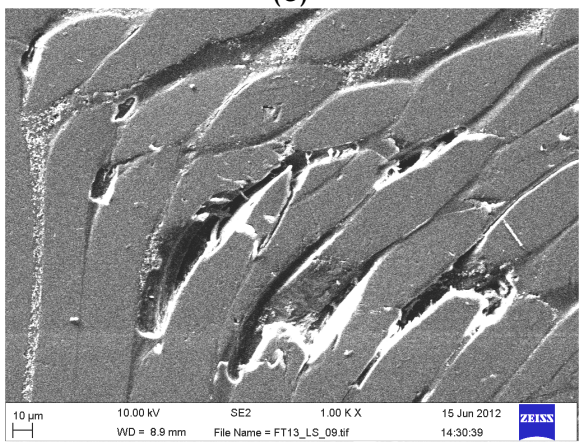

(g)

Figure 4.23 Fracture surface damage by ±50% UTS fatigue for a sample moulded at 140°C

(a) general optical view of sample fracture; (b) -(c) SEM micrographs showed kink band formations on lower and upper side of the specimen; (d) fibre split at the centre of specimen; (e) closer view of crack travelling path (f)-(g) gap between the fibres at the fibre buckled line (scale bars = (a) 2mm; (b) 100µm; (c) 500µm; (d) 20µm; (e) 10µm; (f) 20µm and (g) 10µm)

Figures 4.24 and 4.25 show the fracture surfaces of specimens moulded at 150°C that failed under ±25% UTS and ±50% UTS fatigue loading respectively. Figure 4.24a shows the general view of the fatigue specimen at the lower stress level, indicating that the fracture started at one side and progressed slowly toward the centre of the specimen where the final fracture took place. At the same time, longitudinal splitting can be seen on the specimen surface suggesting the failure resulted from multiple kink bands created by internal stresses inside the specimen during the testing. Figures 4.24b and 4.24c show the fibres were drawn out during the process resulting in a staggered fracture surface indicating slow crack propagation as more energy was used to draw the fibres out. Higher magnification revealed that the fibres have rough fracture surfaces consistence with ductile failure. The rough fractured surface also covered with matrix indicated good interface bonding had been achieved during moulding process and the presence of the TCP on the fibres surface indicated failure occurred at matrix-fibre interface. As the specimen did not break into two separate pieces, the crack path was assumed to have started from weakest side indicated by the broken fibres propagated toward unbroken, but buckled, side as shown in Figure 4.24d in shear failure manner. A closer view of the interval fracture (Figure 4.24e) revealed a fracture propagation path halted in front of unbroken fibre, evident of crack arrest by a fibre bridging mechanism.

At higher stress, the specimen showed similar failure mode to the specimens tested at ±25% UTS. Figure 4.25a shows the general view of the surface damage. With increased stress, rapid development of kink bands occurred which resulted in more severe damage of the fibre at fewer cycles. Figure 4.25b and Figure 4.25c show the crack path in the specimen. Internal fibre bridging was observed between the horizontal split of the specimen, most likely caused by transverse stress initiated by kink band formation (Figure 4.25d). Figure 4.25e shows transverse crack formation between the fibres indicating failure due to interfacial cracking.

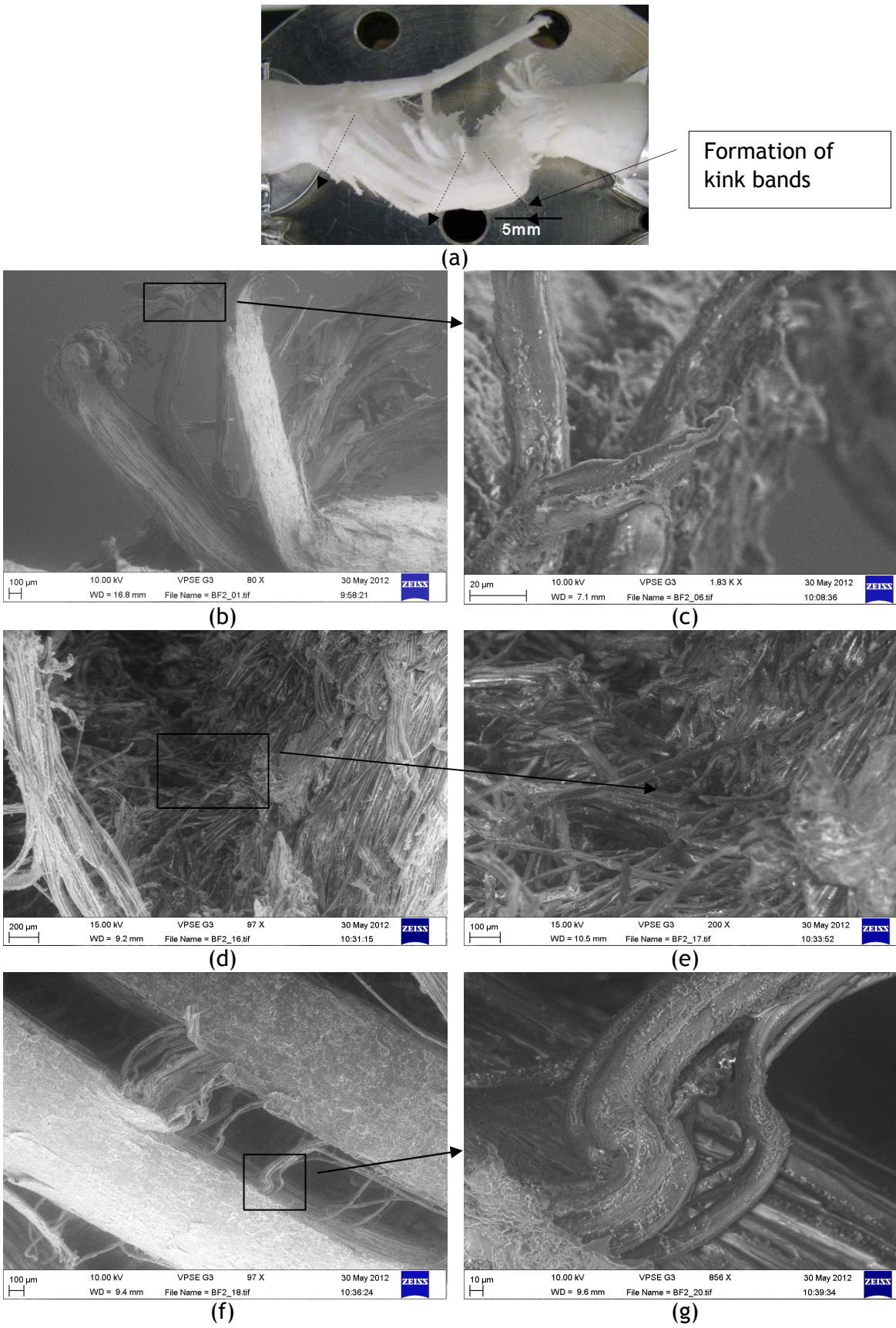

Figure 4.24 Fracture surface damage by tension-compression ±25% UTS fatigue for a sample moulded at 150°C

(a) general view of sample fracture ; (b)-(c) drawn fibres with staggered fracture surfaces; (d)-(e) internal fracture surface indicating crack propagation path; (f)-(g) longitudinal splitting with fibres bridging. (Scale bars (a) 5mm, (b)100µm; (c) 20 µm; (d) 200µm; (e) 100µm; (f) 100µm; (g) 10µm)

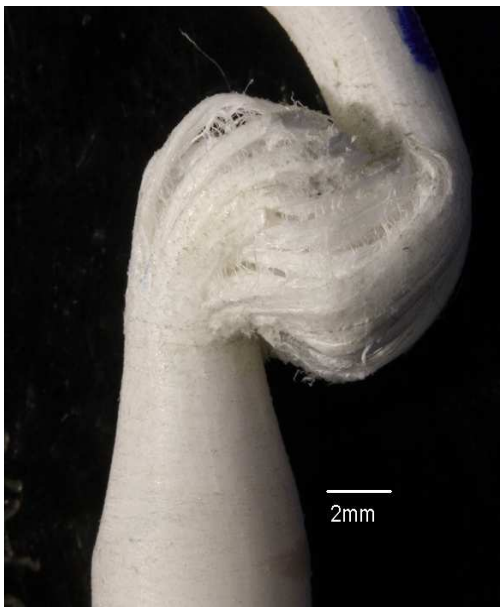

(a)

(b)

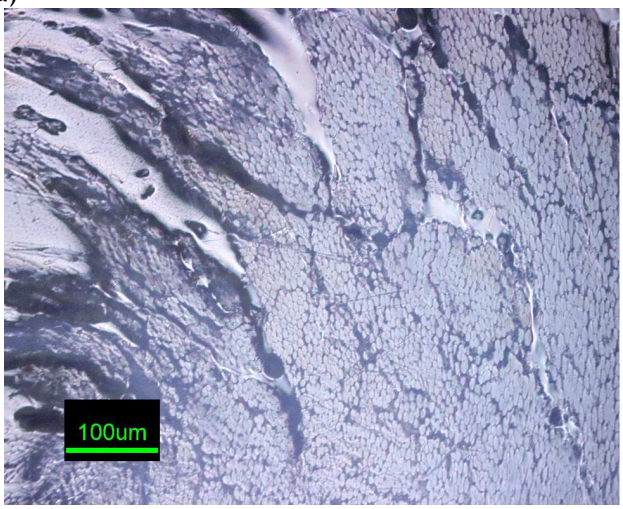

(c)

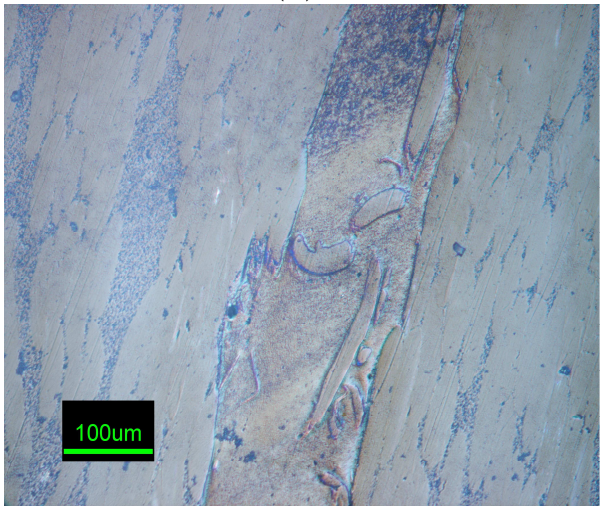

(d)

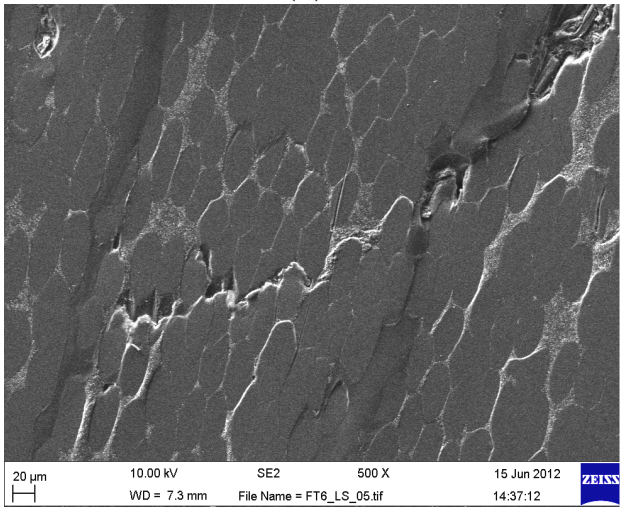

(e)

Figure 4.25 Cross section of fracture surface damage by tension-compression ±50% UTS fatigue for a sample moulded at 150°C

(a) general view of sample fracture; (b) -(c) crack propagation in the matrix ; (d) fibre bridge in the f fracture line; (e) transverse crack propagation. (Scale bars (a) =2 mm, (b)500 µm, (c)-(d) 100 µm and (e) 20 µm)

Figure 4.26 shows the fatigue damage observed at ±50% USS. The materials did not fracture into two separate pieces, again indicating the ductile nature of the fibres. The failure mechanism of the torsional fatigue is similar to the quasi-static torsional testing, with longitudinal splits parallel to the fibres. At high magnification (Figure 4.26c and 4.26d) extensive damage with fibre breakage and exposure of the TCP particles is seen which suggests that TCP particles were detached from the drawn PLA fibre and final fracture occurred due failure of the fibre-matrix interface.

When tested in tension only, the specimens failed with brush-like rupture with multiple layers of fibrils indicated the fatigue failure influenced by weak interface and finally drawing and failure of PLA fibres (Figure 4.27a). At higher magnification defibrillation and decohesion mechanism of the reinforcing agent from the PLA_{70} matrix are clearly observed indicating ductile tensile failure behaviour (Figure 4.27b). At the same time, SEM examination revealed that there were a series of spiral crack on the specimen gauge normal loading axial which probably cause by effect of tensile stress on the matrix (Figure 4.27c).

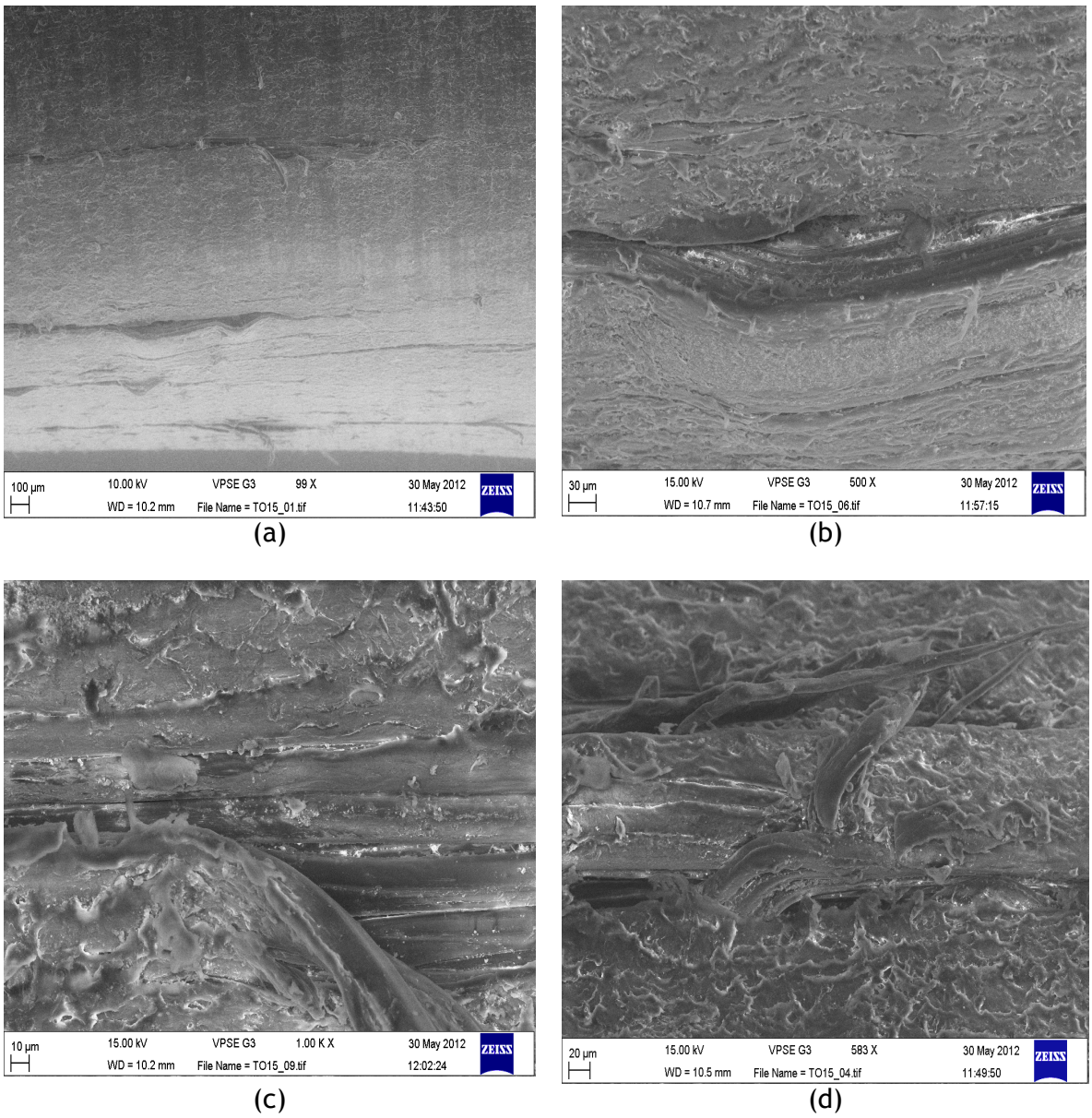

Figure 4.26 SEM of fracture surface damage by torsional ±50% USS of a T150 moulded sample

(a) general view; (b) matrix crack parallel to main axial fibre orientation (c) exposed TCP particles and (d) fibre fracture. (Scale bars (a) 100 µm; (b) 30 µm; (c) 10 µm; (d) 20 µm)

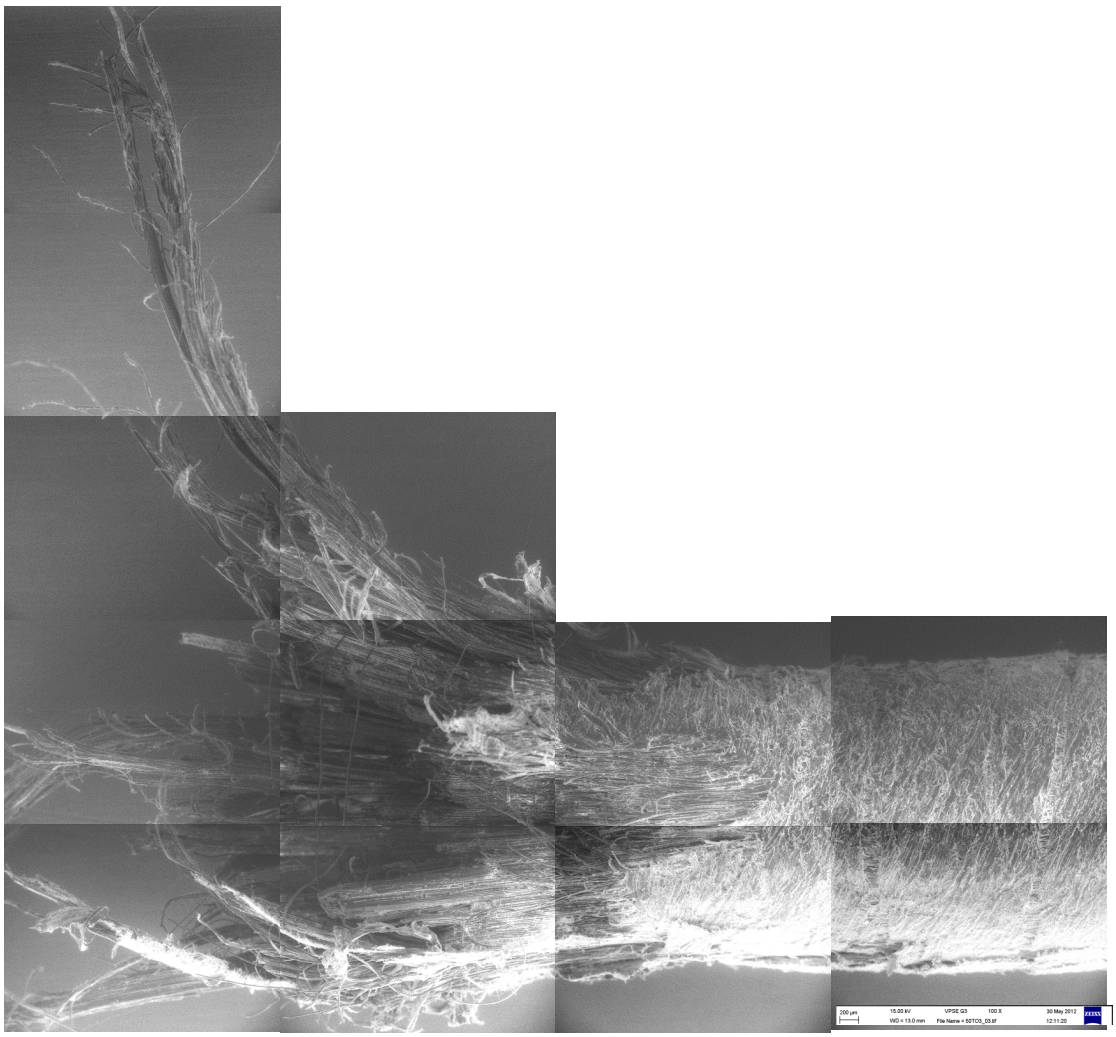

(a)

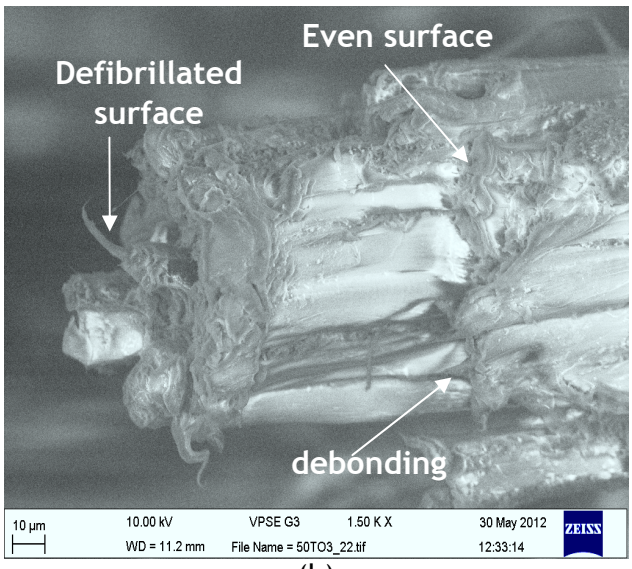

(b)

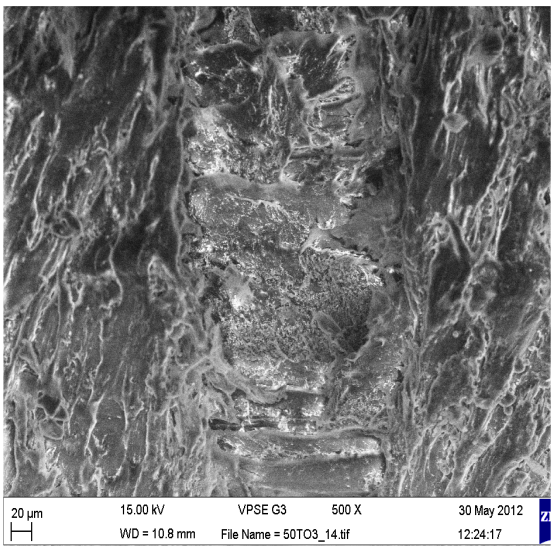

(c)

Figure 4.27 Fracture surface damage by tension only fatigue at (+150% UTS) of a T150 moulded sample

(a) optical general view of fracture surface; SEM (b) fibres fracture covered in matrix and defibrillation along the fibre axis and (c) debonding between matrix and fibres. (Scale bars (a) 200µm; (b) 10µm and (c) 20µm)

4.6 RESULTS - TENSILE TESTING OF UNIAXIAL FATIGUED SPECIMENS

The tensile stress-strain curves of samples that had been fatigued to 1.5 million load cycles but had not failed together with non-fatigued specimens are illustrated in Figure 4.28. It can be seen that the fatigued specimens display similar characteristics to the non-fatigued, however the stresses have reduced. The mechanical properties are showed in Table 4.6. Compared to the non-fatigued, the fully reversed ± 25% UTS axial fatigue tested samples showed significantly ($p<0.05$) reduced ultimate strength, but the reduction in modulus was not statistically significant. In term of failure strains, fatigued specimens were not significantly affected. These effects show the limited damage to the materials presumably occurring mainly in the composite matrix, rather than the fibres.

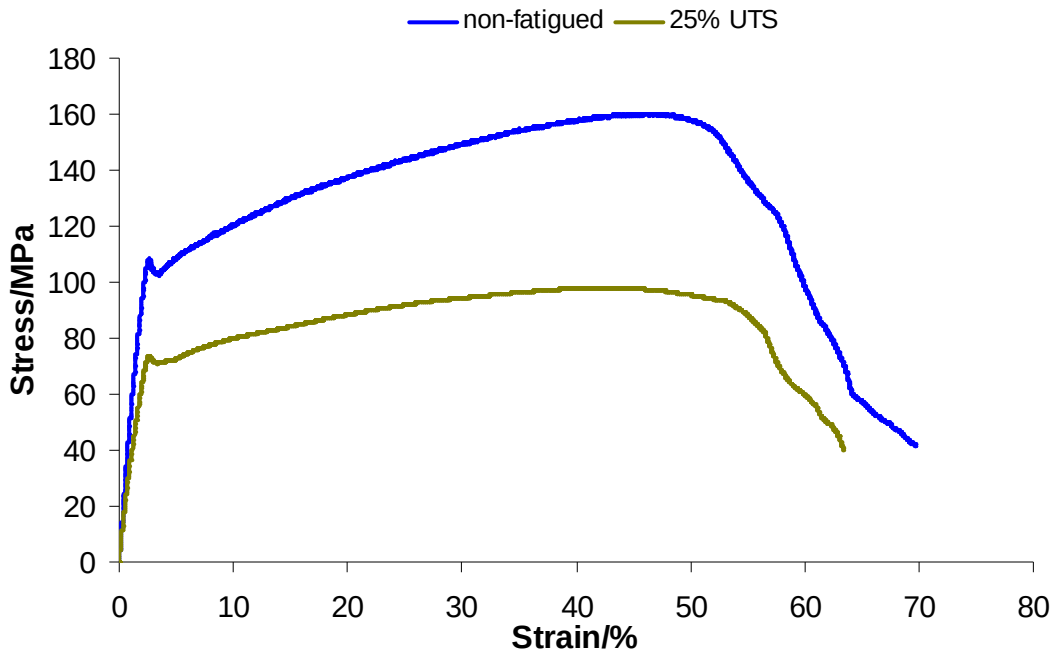

Figure 4.28 Tensile stress-strain curve of a non-fatigued and a ±25% UTS fatigued specimen loaded for 1.5 million load cycles (tested at 37°C in saline)

Table 4.6 Monotonic tensile testing results for uniaxial fatigue specimens (at 37˚C in saline)

Fatigue Mode	No of specimens	Modulus /GPa	Ultimate Stress/MPa	Failure Strain/%
Non-fatigued	5	6.36 ±0.11	139.77 ±11.58	66.34 ±1.75
±25% UTS	2	5.24 ±1.36	107.85 ±13.72	64.17 ±1.48

4.7 DISCUSSION

4.7.1 Effect of compression moulding temperature

There are many factors in the compression moulding process that may influence the properties of the composite such as pre-preg lay–up, compression moulding temperature and pressure (Garmendia et al., 1995). Hou et al. (1996) reported that the number of voids and their size largely depended on the processing conditions. At higher moulding temperatures, the matrix was found to be less viscous as the viscosity of a thermoplastic is normally inversely proportional to temperature. Thus higher temperatures allow better impregnation of fibre bundles, resulting in increased consolidation. Voids in composites prevent efficient load transfer between fibres and matrix. Therefore, increases in moulding temperature, reduced the voids formation the composite, thus increase the mechanical properties.

The compression moulding temperature is particularly important when moulding PLA-PLA-TCP pre-pregs since it should be high enough to ensure that PLA_{70} matrix completely melts, but low enough to prevent the PLA_{96} fibre from losing properties. Hine et al. (1993) reported that hot compaction of the polyethylene fibres can be achieved by melting the surface of the fibres to allow them to coalesce. This approach allowed optimum properties of the composite to be maintained as the temperature used is high enough to melt to surface of fibres but low enough to avoid excessive melting of the fibres and loss of strength. A similar approach was taken by Bleach et al. (2001) in order to produce similar composite used PLA_{96} fibres in PLA_{70}-calcium phosphate matrix.

A different approach was taken by Tormälä et al. (1991) who produced fibre reinforced composite by compression moulding PLA fibres with no matrix but by

applying sufficient heat and pressure, they melted the outside layer of the fibres to give a matrix. Their specimens with reducing amounts of matrix from the outside to the centre of the composite as can be seen in Figure 2.7 in Chapter 2.

Based on this finding, the compression moulding of the composite ideally should be above the start of the melting range of the fibres, but below the peak of melting temperature that is between 139°C and 178°C.

4.7.2 Monotonic Testing

The results showed that the composite is stronger in tension than in compression and torsion. The tensile and torsion loading directions are more ductile than the compressive which is typical in long continuous fibre reinforced composites (Shinozaki and Groves, 1973). Tensile modulus and the ultimate stress generally increased as the moulding temperature was increased with significant differences only between the values of ultimate tensile stress. The compression properties also showed a similar trend. However, there is no significant difference in the compressive modulus with these two moulding temperatures.

The increases in mechanical properties are thought to be a result of better interaction between fibre and the matrix when the specimens were moulded at higher temperature. This conclusion is confirmed by SEM examination. Figure 4.2a shows that at a compression moulding temperature of 140°C, the pre-preg layers were still distinguishable and there were gaps between the fibres. Figure 4.2b shows that better interaction, closer compaction and fewer gaps between the fibres and matrix were observed in specimens moulded at 150°C. The may cause voids in the composite that may contribute to the lower mechanical properties. With the increase in moulding temperature, the matrix viscosity reduced thus allowing better flow between the fibres. Figure 4.5 shows cross section of T150 where nearly all the fibres surrounded by a thin layer of matrix, which would account for the increased mechanical properties. This finding was supported by Bleach et al. (2001) who produced similar composites. Their results showed similar trend in mechanical properties when moulded at higher temperature (150°C) compared to compression moulding at 130°C and 140°C. Capiati and Porter (1975) investigated the interfacial strength of polyethylene fibre-polyethylene matrix composites. They reported that the interfacial

strength originated from the epitaxial growth of the matrix from the melt onto fibres. However Lacroix et al. (1998) reported the opposite effect of the moulding temperature. The results of the mechanical properties of self-reinforced polyethylene that being produced using pre-preg methods degraded with increased moulding temperature from 120°C to 140°C. However the melting temperature of the PE was in range of 120 to 130°C. It was thought that the degradation in mechanical properties degradation was due to thermal damage of the fibres at higher temperature because of loss of molecular and crystalline orientation. Based on DSC results in this study, compression moulding at120°C or 160°C was not investigated, as these were below or above the fibre melt temperature.

In general, the tensile fracture of continuous fibre composites is caused by fibre failure. Since the fibres have a distribution of strains to failure, some of the fibres will fail at sooner than others upon application of load. This fibre break will serve as initiation points for further damage. Longitudinal damage normally grows by debonding, matrix cracking or yielding, all of which are influenced by the fibre/matrix adhesion. Then, the nearby overloaded fibres fail leading to further damage till a complete composite failure occurred. Therefore, in composites with strong interfaces, the crack normally grows across the fibre, which resulted in separation of specimen with smother fracture surface. However, composites with weaker interfaces, the crack prone to travel along the fibre matrix interface via longitudinal cracking resulting in more fibre break and brush like surfaces (Gamstedt, 2003). On other hand, tensile failure of the particulate filled polymer composites such as the matrix in this composite is caused by the brittle failure mode of cavitation formation and crazing. This is normally dominated by the filler/matrix interfacial failure, as discussed by Fredrich and Karsh (1981). In this study, the material is a triphasic composite, consisting continuous fibres with particulate filler embedded in the matrix, therefore all factors may contribute to the failure mechanism. As tensile load is applied, the fibres pulled away from matrix and broke. The debond grows from the fibre fractures that lead to longitudinal damage with further debonding. With weak interfaces, the debonding will propagate along the matrix-fibre interfaces. SEM examination revealed abundant fibre fracture due to fibre drawing (Figures 4.3b and 4.3c) with some of the fibre fracture with distinct

fracture point, v-notch opening and progressing to unstable fracture orthogonal to fibre axis (Figure 4.3e) indicating ductile fracture. The interfacial strength between the PLA matrix and TCP, which embedded in the matrix is solely due to the mechanical interlock between the two phases. It was produced by the act of shrinkage between the matrix tricalcium phosphate particles during the cooling from the moulding temperature. Bleach et al. (2001) showed matrix and fibres have similar shrinkage during cooling as they are from similar materials, TCP however has lower shrinkage thus generating a tensile strength around it upon cooling. The PLA fibres and matrix bonding on other hand are resulted from weak hydrogen bonds formed during the compression process. Some limited damage is also expected during pre-pregging as the fibres are slightly soluble in the acetone used, but this may be beneficial in promoting a bond between the fibres and matrix. Figures 4.3d and 4.3e show the fracturing and drawing of fibres with the surface covered in matrix with exposed TCP particles indicate interfacial failure at the matrix and fibres. Schadler et al. (1992) observed the fracture of single carbon fibre in polycarbonate micro composites and showed that fibre strength may dominate the early damage behaviour but after fibre failure, the damage growth was dependent on the matrix.

It is noteworthy that the values of quasi-static properties of tensile test of T150 composite are higher than T140. This may be expected for the composite strength as it is largely depended on the fibre/matrix adhesion. While for the strain to failure, Gamstedt (1999) noted that the strains to failure of unidirectional composite are governed by strain to failure of the fibres. Since the same PLA_{96} fibres was used in specimens at moulding temperatures of 140 and 150°C, the differences cannot be caused by batch to batch variations properties of the PLA_{96} fibres.

Microscopic examination of compressive failure occurred by buckling, with Euler buckling loads found to be 80-90% of the ultimate compressive strengths for specimen moulded at 140°C and 150°C. The initial yield stress for T140 and T150 were 80MPa and 97MPa respectively. Thus in compression, the failure could be initiated from tensile stresses produced by Poisson's ratio effects in the matrix. The critical load calculated for the both of the specimens were within the range of the initial failure of the fibres. The specimen shape used in this study may not

be ideal for monotonic compressive testing as it has slender gauge. However, Ton That (2000) reported that the values obtained using the same standard were within reasonable agreement when compared to ASTM D695-85 standard specimens used by Saunders (1998).

Lankford (1995) found that the most common failure mode in long fibre composite in compression failure was via shear crippling, which occurs at sufficiently large strains to cause the matrix to deform in a non-linear manner known as plastic microbuckling. This is normally associated with fibre kinking and buckling. Both compression specimens (T140 and T150) failed under same mode (Figure 4.4a). SEM examination showed that the fracture initiated at the weakest side due to fibre fracture, leading to formation of fibre kinks that cause interfacial debonding between the matrix and fibres (Figures 4.4b and 4.4d).

Cross section examination revealed the crack initiated on the tensile side of the flexed fibres creating kink bands with further debonding toward the centre of the specimen where final failure occurred by plastic buckling (Figures 4.6a and 4.6b). Longitudinal splitting was also observed on the specimen surface with visible fibre bridging at cracks which caused by transverse stress created in the matrix during the test (Figures 4.4c and 4.4e). While fibre/matrix adhesion does not affect the modulus results, the strength and strain to failure were sensitive to the interfacial strength as they both increased significantly with the increase of the moulding temperature. A similar finding was reported by Madzukar and Dzal (1992).

Shinozaki and Groves (1973) studied the mechanical properties of highly orientated continuous fibre PP composites. They found that the low compressive yield stress is due to local buckling that may be caused by intermolecular or interfibrillar shear, where the compressive stress acts in the molecular direction that led to formation of kink bands. This finding was supported by Alcock et al. (2006) who studied high volume fraction highly oriented PP (>90%) composite. They showed that the failure of the composite in compression was caused by micro buckling, which occurred along shear planes in the unidirectional composite. The importance of the fibre-matrix interface adhesion in influencing

the tensile and shear behaviour in polymeric composite is well known in the literature and will be discussed further in the fatigue section.

The material is reasonably ductile in torsion. Microscopic examinations in Figure 4.7a shows damage developed in the spiral direction. At higher magnification it can be seen that the damage mechanism was caused by splitting of the matrix parallel to the fibre direction (Figure 4.7e). A similar observation has been reported by Jelf and Fleck (1994) when studied the torsional behaviour of unidirectional carbon-fibre epoxy laminates.

4.7.3 Effect of moulding temperature on uniaxial fatigue

The S-N curve for fully reversed axial and torsional loading for both moulding temperatures show that the torsional fatigue life is less than the axial fatigue life at similar percentages of the appropriate ultimate strength, therefore, if the axial and torsional strains are plotted against the number of cycles, the shear strain is expected to be larger than the axial strain at a similar number of cycles. As the average cycles to failure for the lowest load level used in this experiment exceeded run out limit, therefore it was unable to identify a definite fatigue limit for the unidirectional self-reinforcement PLA –TCP composite. However, as two specimens moulded at 150°C (T150) showing a run out when tested at low level stress, the fatigue endurance limit may exist below 34.9 MPa for samples moulded at 150°C, although more tests at lower stress levels are needed to prove this. Therefore when designing an implant which is to be cyclically loaded, a lower maximum stress is applicable than for static loading.

As this is a tri-phase composite, there are two factors involved in the fracture toughness of the specimen, which are the influence of the filler and shape of both reinforcing materials, which in this composite is the long continuous fibre. All specimens (T140 and T150) failed in compression when tested in the tension-compression fatigue loading. This finding is expected as quasi–static test results revealed that the composite has superior mechanical properties in tension compare to compression.

It is noteworthy that the stress levels of the fatigue tests were carried out based on their individual properties from quasi-static tests as shown in Figure 4.9. In

general, T150 showed superior fatigue resistance to T140, which is as expected since with higher moulding temperature, provided better interfacial bonding between the matrix and fibres. This finding is concomitant with quasi-static results and expected from the literatures.

At closer inspection revealed that at low stress level for T140, the mean fatigue lives is 732,404 cycles. It was expected that at 25% of UTS, T140 should also have non-fracture results as shown by T150. The lack of non-failure results obtained at the low stress level of 25% UTS for T140 are probably due to differences to the stress per volume in the specimens as these specimens had slightly longer, 20mm gauge length than the other samples. This testing was performed during optimisation of sample shape and lead to the reduction in the gauge length. Fracture strength of materials is influenced by pre-existing defects either microstructural in origin or introduced during the fabrication process. Parker (1957) studied the role of pre-existent cracks in failure of the bridge structures and summarised that the failure was influenced by the cracks that were present in the structure prior to use. Therefore in the light of this finding, it is reasonable to assume that specimens will fail as a consequence of the pre-existing defects. It is also reasonable to assume that the probability of the failure is highly influence by the sample size, as higher volume or overall surface area of materials may contain more pre-existent defects. However this is not a new conclusion, Leonardo da Vinci showed over 500 years ago in his simple wire testing apparatus that longer wires are weaker compared to shorter sections (Parsons, 1939). This finding led to the conclusion that larger pieces of material will contain more critical defects than smaller ones that might influence the wire strength. Weibull analysis (1951) revealed that a certain component's strength variability and its chances of survival is the function of its volume and the applied stress. Therefore low stress level fatigue of T140 showed that increasing stress/volume of the specimen decreased the fatigue lives of the composite as the probability of the component survival is reduced. However, if such result are been taking into account in the plotting S-N graph, the trend will still be similar and T150 still have superior fatigue resistant in comparison to T140.

Interface strength in composites has a significant effect determining the outcome of the fatigue resistant properties of the materials. Harmia (1996) summarized that poor adhesion between the reinforcement and the matrix increased the fatigue sensitivity in glass Nylon 66 fatigue testing. This may due to faster crack growth at weak interfaces than in a continuous composite and causes easier debonding of the filler from matrix. He also reported that by improving the adhesion between the filler and the matrix, the fatigue resistance of the composite improved and debonding of the filler occurred closer to the crack tip. This finding was further reconfirmed by Liang et al. (1999) in their study of fatigue behaviour of glass bead reinforced polymer composites. They suggested that for poorly bonded material, interfacial debonding took place between the filler and the matrix thus encouraging the development of cavities under tensile stresses. Therefore, enhancing the bonding between the filler and matrix improved the stress distribution and in resulted in increased strength and fatigue properties. Deng et al. (1998) showed that the failure modes of the composites are strongly influenced by the fibre/matrix adhesion. They noticed matrix cracks were present in the composite with stronger bonding between fibre and matrix, which was not present in composite with weaker fibre/matrix adhesion. This may also contribute to increased mechanical properties of the composite. A similar result was shown in this study, increasing the moulding temperature, increased the bonding between the matrix and the reinforcement, resulting in increased strength and fatigue resistant as showed from both quasi-static and fatigue tests.

Analogous to testing to failure, fatigue also has a crack front progressing through the material. However, in fatigue testing, the propagation rate is orders of magnitude smaller than in quasi-static testing. Nevertheless, the crack will grow to a critical length, which is determined by various factors including applied load, frequency and specimen geometry. In this study, the fractures are most likely controlled by the moulding temperature during fabrication and the applied load. As the cycles progress, the crack growth rate increases and the material eventually fails. Therefore, based on this observation, it is reasonable to assume that the mechanism that operates in monotonic testing would also operate in fatigue. Gadaree and Salee (1983) proposed that filler in the matrix can act as crack arrest mechanism to slow down the crack propagation rate by pinning

down the crack front, this agrees with the ideas of Suresh (1998). He suggested that crack tip interaction with the dispersed filler particles in the matrix will have a strong influence on geometry of the crack front and the crack growth rate. The tricalcium phosphate particles used in this study, especially any agglomerates present, could provide a pinning barrier to the crack propagation. However due the weak interfaces, the crack by passes the obstacles by going around the particles and travels through the matrix. The surfaces in Figures 4.22f and 4.24c showed exposed tricalcium phosphate particles and longitudinal debonding of the fibre as evident of tricalcium phosphate particles left behind during crack propagation, suggesting that due the weak interface between the tricalcium phosphate and the matrix, the crack by passed the obstacles by going around the particles and travelled through the matrix and leaving the particles behind. In torsional loading on the other hand, the present of the TCP particles was expected to provide crack pinning, as the direction of the crack is parallel to the direction of twisting. However, in continuous fibre reinforcement where the composite is weaker in shear, repeated torsion presumably debond the tricalcium phosphate the particles, thus final failure is by shearing and fracture of the PLA fibrils, this can be observed in Figure 4.26.

Both T140 and T150 specimens failed in the compression phase, which is typical for a continuous unidirectional fibre reinforced composite (Jelf and Fleck, 1992) as such composites are normally weaker in compression than in tension. With subsequently cycling, the materials start to fail becoming weaker and less stiff; this is illustrated by extension and kinking of the PLA fibrils and separation of the composite interfaces, which in turn relates to the creep response of the materials. Judging from the variation of strain over the whole process of tension-compression fatigue, it can be said that the material is weakening. This is approached asymptotically towards the end of the cycling, until the specimen buckled and fractured in compression, as the material is weaker in compression than in tension. The maximum strain to fracture of T150 for ±50% UTS is about 5.3%, which is higher than that obtained by monotonic compression due to repeated nature of fatigue testing and concurrent creep. At the higher applied loads of ±75% UTS, the composite behaved in a similar manner but with more rapid fracture and lower strain to fracture. Thus, it can be concluded, even in the presence of tensile loading, the failure of unidirectional fibre reinforced

composite is dominated by its compressive properties. Further discussion on the effects of the loading condition will be considered in Section 4.7.4.

Previous investigators have shown individual effects on the failure mechanisms of compression and tension in fully reversed fatigue test. McEvily et al. (1964) discovered that some polymers including polyethylene and polycarbonate behaved in similar fashion to metallic component when subjected to fatigue tests. Later, Nisitani and Takao (1977) studied the fatigue behaviour of carbon steel and reported that the crack tip closed under compression and opened up while in tension in fully reverse fatigue loading. Pattin et al. (1996) showed that for bone there was far less degradation in tangent modulus and energy dissipated with compressive fatigue than tensile fatigue, as bone is stronger in compressive than it is in tension.

However, in this tri-phasic unidirectional fibre reinforced composite, the crack may be initiated by the fibre fracture during the compression loading, however crack propagation is controlled by different mechanism in tensile and compression loading. In tensile loading, the transverse strains compress the PLA fibre-matrix interface, crack propagation now depends on the interfacial strength between the TCP filler and matrix interface as proposed by Friedrich and Karsch (1981). In the compressive loading, while the stiffness of the fibre is remained the same, the Poisson's ratio effect generates transverse strains across the fibres that may initiate fibre kink and buckling of the fibres. Kink band formation and propagation has been established as the primary failure compressive mechanism in limiting the strength of the unidirectional fibre reinforced composites (Jelf and Fleck, 1992; Soutis and Fleck, 1990 and Budiansky, 1983). Argon (1972) suggested that the initial stage of kink band formation was initiated by fibre misalignment and shear yield strength of the matrix. Similar findings were observed by other authors such as Fleck et al (1995), Vogler and Kyriakides (2001) and more recently by Lemanski and Sutcliffe (2012). Contrary to this, Martinez et al. (1997) showed that variations in the initial fibre misalignment might not be the only factor that contributes to further reduction in compressive strength of the fibre-reinforced composite. This leads to the assumption that even thought kinking maybe the dominant mechanism, a competing mode of failure may be contribute to the reduction in

compressive strength during the failure (Garland et al., 2001). Creighton and Clyne (2000) studied the compressive response of carbon-fibre/epoxy composites produced by pultrusion where the fibre misalignment was estimated to be below 1°. They reported that while the failure was due to kink band formation, the strength was substantially influenced by the present of pores in the matrix material, which lead to the conclusion that fibre misalignment may not be the main cause of the compressive failure that initiated kink formation. Kozey (1993) also observed splitting cracks triggered the final kinking failure of carbon fibre polymer composite. In this study, as the fibres were hand lay-up, misalignment would be expected fabrication, which might contribute to the formation of kink bands and buckling failure, as were observed during testing.

Elber (1970) argued that compressive loading could produce undesirable results. The problem lies in the cyclic creep, which is now compressive and cycle-dependent, softening gradually thus reduces the tangent modulus and the compressive load encouraging buckling. Sandor (1972) proposed another theory for crack growth in compression loading, each subsequent cycle creates a monetary tensile stress at the hole and later at the crack tip. Dillon and Buggy (1995) studied flexural fatigue behaviour of carbon fibre/PEEK and carbon fibre/epoxy and reported that compressive fatigue is more deleterious for thermoplastic composites. Mishnaevsky and Brøndsted (2009) through a statistical modelling study of cyclic compressive loading showed that repeated compressive loading increased the variability of the misalignment of the fibres. Thus it logical to assume that it will influence the compressive fatigue failure of the composite.

SEM examination (Figure 4.3e) shows that the non-fatigued T150 specimen failed in tension with a distinct fracture point, v-notch opening and progressing to an unstable fracture orthogonal to fibre axis. In contrast to non-fatigued specimens, Figure 4.24c showed the fibre failure of the ±25% UTS tension-compression for T150 at a start of the crack propagation path. The fracture surface showed clear drawing and defibrillation of the fibre indicating ductile failure and the fibre defibrillation surface with a similar v-notch on the fracture surface. This shows that under compression loading, shear deformation nucleated on the inner (compression) side then induced tensile microcracks on

the tensile side of the fibres during the buckling of fibres in the early progress of the failure as discussed by Lankford (1995) and Dobb and Robson (1990), but with more extensive drawing than non-fatigued specimens indicating slow fracture damage due to fatigue. Tai et al. (1995) showed similar findings in the compressive fatigue of carbon fibre/PEEK composite. They observed that the fracture surface of broken and buckled fibres led to distinct regions, with a tensile side and a compression side, which showed buckling failure and local bending of the fibres. The fracture surface for T140 also had a similar fracture trend, but with sharper and flatter fracture surface indicated faster crack propagation than in T150 samples.

The effect of the fibre/matrix adhesion strength becomes more apparent at higher stress levels. Fractography analysis of T150 at ±50% UTS and ±75% UTS revealed that the fracture mode is due to shear failure driven by micro buckling of the fibres in a similar manner to those at ±25% UTS but occurring faster. However, at the lower moulding temperature, the fractured surface of T140 showed distinct differences to T150 (Figure 4.23) when tested at ±50% UTS and ± 75% UTS fatigue stress. The fibres were separated from each other in a brush like manner and failed under axial delamination buckling. This observation indicates that specimens moulded at the higher moulding temperature, 150°C, have better fibre/matrix interfacial strength than those at 140°C. This finding is in agreement with others reported in the literature. Madhukar and Drzal (1992) investigated experimentally the link between fibre/matrix adhesion and the failure mode of unidirectional carbon fibre epoxy composite. They found that while compressive modulus was affected slightly by fibre surface treatment, the compressive strength and maximum strain however were highly sensitive, to fibre treatment, both strength and strain improved with increasing of interfacial shear strength. The failure mode of the composite was also changed. They observed that in specimens with poor interfacial strength, the failure occurs by delamination and global delamination buckling. With increases in the interfacial strength, the composite failure mode changed to shear failure, while for the highest values of the interfacial shear, the specimen failed in yield with stepped fracture surfaces, which indicated the compressive failure of the fibres in various planes are perpendicular to the fibre axis.

The fracture surfaces for torsional fatigue for ±50% USS for both T140 and T150 are similar, with fatigue striations, in the form of incremental crack advancement between the fibres, observed over the outer half of the specimen surface. This finding is agrees with Found et al. (1985) who reported that in torsional loading, the crack propagates along the surface while for compression the crack normally grows through the thickness of the specimen. Higher magnifications revealed breakage of fibres due to drawing and exposure of the TCP particles in the well of the crack. This suggested that weak interfacial bonding allowed the TCP to separate from the polymer matrix and that the final fracture was due to shearing of the PLA chain network along the twisting direction. Torsional loads (±75% USS) resulted in fewer cycles to failure at the same strain limit indicating at higher load the crack propagation rate was faster and the failure mode was more brittle.

In summary, optical microscopy and SEM confirmed the break down of the composite due to formation of kink bands that lead to failure by buckling. The disentanglement and cumulative rupture of the PLA fibre with TCP particles on the surface indicating inefficient crack propagation by both fibre bridging and filler reinforcing mechanisms. The final fracture mechanism was fracture and buckling of the fibres as described by Fleck (1997) indicating the dominant influence of compression loading in unidirectional continuous fibre composite properties. The crack path is normal to the loading direction in axial fatigue, while in torsional fatigue, surface cracks as observed in Figure 4.26, run along the spiral direction of specimens, and are relatively large in comparison to the gauge length. Socie et al. (1985) reported similar observation from fractography analysis for steel alloy specimens damaged by fatigue. The tensile fatigued specimens failed with individual slip bands observed on the fracture surface. However, torsional fatigue fracture surfaces had been burnished generated from rubbing of the two crack surfaces during testing.

The reductions in modulus and increases in energy absorbed were used monitor the degradation in mechanical properties of the composite caused by the fatigue. Burr et al. (1985) and Pattin et al. (1996) in their studies of the uniaxial fatigue of bone argued that the differences in the response to increasing energy absorbed (area in the loop) is linked to the microcrack formation within the

composite volume during damage accumulation. Based on the axial modulus, the numbers of cycles at which damage started to accumulate is dependent on the loading condition. It is about 1000 cycles for T140 and after 100 cycles for T150 at ±50% of their individual ultimate strength. Furthermore, at higher loads damage starts within the first 100 cycles or 10 cycles for T140 and T150, respectively. For torsional fatigue, although results from the quasi-static tests suggested that the composite was more ductile in torsion than in tension and compression; torsional fatigue is more damaging than axial tension-compression fatigue as reflected by lower modulus. This observation was coherent with the finding that torsional fatigue lives are lower than axial fatigue lives. Based on the torsional modulus, the number of cycles at which damage starts to accumulate was noticeably load dependent, similar to the axial fatigue. For T140, at low stress level of ±25% USS, the damage becomes apparent after 1,000 cycles and accelerates faster than T150 to failure. While for ±50% USS, the damage started in about 100 cycles and within the first 10 cycles for ± 75% USS. These levels of threshold are only of the order of thousands of cycles or less, hence considerably lower than the fatigue lives for ±25% UTS and ±25% USS, which suggests that crack nucleation occurs within a relatively short time and that the most of the fatigue life of the materials is spent in growing and propagating the crack. Similar torsional fatigue behaviour was observed for specimens moulded at 150°C.

It should be mentioned that, unlike axial properties, torsional properties from the testing to failure results are not statistically significantly affected by the moulding temperatures. It is widely discussed in literature that the strength of the fibre composite is highly influenced by the interface strength between the reinforcement and the matrix. Recently, Felfel et al. (2011) suggested that the interface strength is often dependant on the direction of the load being applied during the test with respect to the direction of the fibres or interfaces. In tension and compression, the applied load is parallel to the fibre direction, thus the interfaces have significant impact. This confirms with quasi-static results that by increasing the moulding temperature and thus reducing voids between the fibres, increases the matrix-fibre interfaces and significantly increases the tensile and compressive strengths. However in torsion, shear stresses will be generated in the PLA-PLA-TCP interfibre matrix. Thus, the PLA-TCP interface

strength is significant in torsion as the load applied is perpendicular to the fibre directions. Nevertheless, the torsional fatigue lives of T150 increased but slightly. However, when compared to the fatigue damage progress in terms of energy absorbed and reduction in secant modulus, better interaction between the matrix and fibres was achieved with higher moulding temperature at 150°C, benefiting the fatigue resistance of the material considerably as shown by lower energy absorbed and reduced modulus degradation and less plastic deformation at similar fatigue stress levels in T150 specimens in comparison to the T140 (Figure 4.18).

For ±25% UTS loading on samples that were moulded at 150°C, two out of five samples did not fracture after 1.5 million cycles, and were considered have run-out. Although the fractures were not observed in the run-out specimens, they still underwent damage and these were reflected by decreases in secant modulus, and increases in dissipated energy and creep. Rao and Drzal (1991) showed that the axial modulus and the interfacial shear strength in the composite are linked to each other because the stress transfer is a function of the matrix. Hence, it is logical to assume that a decrease in modulus will lead to corresponding decrease in interfacial shear strength and vice versa. Therefore, when compared to the mechanical properties of the non-fatigued specimens in this study, for the unbroken fatigued specimens, the reduction in modulus and strength produced by fatigue is of the order of 20%. Furthermore, the strain to failure has reduced because in addition to interface debonding, some plastic deformation has occurred during fatigue.

4.7.4 Effect of Loading Mode on the Axial Fatigue

The effect of the inclusion of compression loading on the fatigue lives of the continuous unidirectional fibre reinforced PLA-PLA-TCP composite is shown in Figure 4.19. However, as both of T140 and T150 were tested at different stress levels, it is not possible to compare directly the fatigue resistance based on the fatigue lives with effect of the moulding temperature. However, this section will discuss the additional damage produced on composite structure of fully reverse tension-compression in comparison to tension loading only.

The fatigue failure mechanism of the continuous unidirectional fibres in tension only loading is distinctly different to the fully reversed failure mechanism. Therefore, in order to provide better comparison of the fatigue behaviour of these materials, the underlying mechanism should be examined. Generally, the failure mechanism in tensile fatigue originates from fibre fracture. Fibre breakage occurred on the first application of the maximum stress, exceeding the strength of the weakest fibre. The fracture sites are scattered randomly thought out the composite. With additional load cycles practice of fibres located adjacent to the broken fibre occurs due to stress concentration. As loading progress, more fibres break (Talreja, 1981) the broken fibres cause shear stress concentrations around the tip of the broken fibre. With cyclic loading, the interface may then fail leading to debonding of the fibre from the surrounding matrix. The debonding will then serve as a stress concentration site for the matrix for the longitudinal tensile stress, crack propagation will depend on the type of matrix used in the composite.

Gamstedt and Talreja (1999) reported an interesting phenomenon in the failure of unidirectional fibre composites with different matrices in response to tensile only fatigue. A composite with a brittle matrix showed higher fatigue resistance compare to a ductile thermoplastic, possibility due to the sharper micro cracks present in brittle matrix, compared to many broken fibres in a ductile matrix composite during fatigue.

The differences mechanism of the crack propagation in two types of matrices, epoxy (thermoset) and PEEK (thermoplastic) has been well investigated by Hartwig and Hubner (1995) and Gamstedt et al. (1999). In both composites, the damage originated from fibre breaks, however the epoxy matrix showed more brittle behaviour, formed transverse crack propagated in the matrix across the fibres direction, forming fibres bridging with adjacent fibres. In contrast, PEEK matrix showed tougher behaviour thus provided higher resistant to the matrix crack growth, thus the crack tend to form in longitudinal, along the fibre direction in order to reduce shear stress between the fibres.

As both of T140 and T150 show similar fatigue fracture surfaces, thus only T150 was observed under SEM (Figure 4.27a). The specimen has a brush like fracture

surface indicating that the final failure was due to interfacial failure. This finding is consistent with results reported in the literature for continuous unidirectional fibre composite. Fractography shows fibre fractures in T150 are still covered with residual polymeric matrix, which is a good indication of strong interfacial bonding between the fibres and matrix (Figures 4.3e and 4.27b). The SEM of fibres at the fracture surface of failed T150 is shown in Figure 4.27a. When compared to the non-fatigued T150 specimens, which failed by tensile testing (Figure 4.3e), the non-fatigued T150 specimen failed with distinct fracture point, v-notch opening and progressing to an unstable fracture orthogonal to the fibre axis. In contrast to non-fatigued specimens, defibrillation and debonding of PLA_{96} fibres from the PLA_{70} matrix in fatigue specimen are clearly observed in Figure 4.27b indicating slow failure propagation caused by fatigue.

Furthermore, the damage surface of the composite under tensile fatigue appeared more brush-like and rougher in appearance (with drawn and straggling fibres) than specimens failed under quasi-static loading (Figures 4.3a to 4.3c). However a closer view (Figure 4.27b) showed that some of the fibres failed in bundles, which are relatively flat, which suggests localized small-scale damage. In the literature, composites with efficient load transfer between the fibres tend to fracture with more brittle appearance, similar to that shown in Figure 2.28a while in composites with weaker interface tend to fracture in brittle manner similar to Figure 2.28b. Even though T150 did not fully resemble this extreme case, the fracture appeared to combination of the brush manner and the flat even surface of brittle fashion indicating competing crack blunting mechanisms were present during the progression region. The finding is also agreed with fatigue fracture surfaces of continuous fibre composites reported by Katogi et al. (2012).

In continuous fibre reinforcement composite, crack tip blunting can be achieved via crack bridging and debonding along the fibre interface. Advancing the matrix crack, strong interfacial bonding between matrix and fibre leads to fibre bridging. Figure 4.27b shows that crack tip blunting via fibre bridging was ineffective leading to further fibre bridging cracks. Gamstedt (1999) reported that the transition between the crack propagation and crack arrest is controlled

by the predominance of these two mechanisms, which precluded other mechanism. Once the debonding set in, the crack will slow down the progressive growth of crack bridging, which will be suppressed to prevent catastrophic failure. Figure 4.27b showed the evident of the fibre bridging and debonding along the matrix interface. However, both of the specimens failed under tensile fatigue, indicating that ineffective crack tip blunting mechanism occurred during the test.

Studies by Morris (1970) and Gamstedt and Sjögren (1999) showed compression loading have a major influence fatigue fracture behaviour of continuous unidirectional fibre composite. They compared the fatigue lives in zero-tension and zero-compression to the fully reversed tension-compression loading and found that the dominant failure mode lies in the compression loading.

The same effect has been seen in the current study. Figure 4.19 shows that the addition of compressive loading reduces the fatigue lives of both T140 and T150, from 10^5 to 10^4 and 10^4 to 10^3 respectively. The addition of the compressive stress in the axial fatigue damage in the compression phase become more dominant as early as from 100 cycles and 10 cycles to failure in T140 and T150 respectively leading toward the final failure in compression loading (Figures 4.21a and 4.21b). Correa et al. (2007) showed that tension-compression fatigue is more damaging than tension-tension loading as tension-compression cycles open up the near tip contact zone and caused increments in damage. Recently, Vaughan and McCarthy (2011) showed that more damage was sustained by the composite and caused fibre-matrix debonding in compressive loading compare to tensile loading and was large enough to trigger ultimate failure.

4.8 CONCLUSIONS

Composite moulded at higher temperature (150°C) T150 has increased mechanical properties in terms of higher yield and ultimate tensile and compression stresses and modulus in comparison to the lower moulding temperature (140°C) T140 due to better interaction at matrix-fibre interfaces and matrix-filler interfaces.

Similar superior fatigue property was also achieved by T150 in comparison to the T140 as shown in the S-N curves. Both of the composites failed in the compression phase indicating that the specimens have lower compression properties in comparison to tension. The failure mechanism was initiated by formation of kink bands from the misalignment of the fibres in the specimen and led to microbuckling failure. The effect of loading mode on the axial fatigue properties showed that the fatigue resistance was significantly reduced when tested in fully reversed tension-compression loading in comparison to tension only, indicating the deleterious effect of the compressive phase on the fatigue lives.

In contrary to the axial properties, mechanical properties in torsional testing in both quasi-static and fatigue testing showed non-significant differences with respect to increasing the moulding temperature. However, as better interaction was achieved between the interfaces in the composite phase promote better fatigue resistance as less damage was observed in T150 in term of lower energy absorbed and reduction in secant modulus in comparison to the T140. In the summary, composite moulded at 150°C has better fatigue properties compared to 140°C moulding temperature.

CHAPTER 5 - BIAXIAL FATIGUE

5.1 INTRODUCTION

The fatigue failure of fibre-reinforced composites under biaxial loading is more complex than under uniaxial loading. Due to the anisotropy of the fibre composite, the fatigue degradation can be accelerated due to the stress coupling effect on the material damage where axial stress, which acts along the fibres and shear stress across the fibre matrix interface, are combined. Therefore, biaxial cyclic evaluation for fibre composites is crucial. In this study, biaxial fatigue was studied in saline solution at various loading conditions and phase angles in order to investigate the stress coupling effect on the fatigue behaviour of the composite.

5.2 METHODS

The pre-preg materials were prepared as described in Sections 3.1 and 3.2 and compressed moulded at 150°C as described in Section 3.2.3. The fatigue testing was performed in saline solution at 37°C as described in Section 3.3.3 using parameters shown in Table 3.1 which are at 25A25T, 25A50T, 50A25T and 50A50T at 0° phase angle. To investigate the effect of phase angle, 25A25T loading regime was also tested with 30°, 60° and 90° phase angle and 50A50T at 90° phase angle. The fracture surfaces were investigated using optical and SEM microscopy on selected specimens as described in Section 3.3.5. Fatigue analysis was calculated in terms of reduction in secant modulus and energy absorbed as described in section 3.3.6. S-N or Wöhler curves were plotted based on principal stress, maximum shear stress and Tsai-Wu calculations as described in Sections 3.3.7 and 3.3.8.

5.3 RESULTS

5.3.1 Analysis of Biaxial Fatigue

The fatigue lives analysis for in-phase biaxial fatigue at various stress loading are shown in Figure 5.1. Full statistical analysis is shown in Table 5.1. Statistical analysis (Kruskal-Wallis) showed there is significant difference ($p<0.05$) between the numbers of cycles for each of the in-phase load cases. When compared to the uniaxial fatigue live results (Figure 4.8b in Chapter 4), the axial fatigue lives of specimen moulded at 150°C were significantly reduced when tested in combination with torsion loading. This indicated the fatigue resistance of PLA-PLA-TCP composite was greatly influenced by shear stresses. The addition of 25% of torque (25T) on 25A significantly ($p<0.01$) reduced the fatigue life from 1,307,972 (±270,005) to 31,912 (± 9,689) cycles. A further significant reduction ($p<0.05$) was observed with the addition of 25T, to give 25A50T, reducing the fatigue life further to 2,483 (±1,744) cycles. Similar results were observed at the higher level of axial loading (50A). Superposition of torque reduced the number of cycles from 1,974 (±958) cycles at 50A to 597 (±220) cycles obtained at 50A25T. The reduction however was not statistically significant. Further additional of 25T to give 50A50T reduced the number of cycles to 442 (±18).

When considering the effects of adding axial stress (25A or 50A) to shear stress of either 25T or 50T. Adding 25A to 25T to give 25A25T significantly ($p<0.05$) reduced the fatigue lives and adding another 25A to give 50A25T, the increase in axial stress significantly ($p<0.05$) reduced the number of cycles to failure from 31,912 ± 9,689 cycles in 25A25T to 597 ± 220 cycles in 50A25T. For 50% USS level, adding 25A on 50T (to give 25A50T) increased the average fatigue lives but not statistically different from 980 ±474 cycles in 50T cycles to 2,483 ±1,744 cycles in 25A50T, adding another 25A to make 50A50T reduced the fatigue lives but not statistically significant to 442 ±18 cycles.

It can be summarized that for the fatigue lives, the alteration in the fatigue lives of the specimen was dominated by the higher stress loading either by 50A (50A25T) or 50T (25A50T). Minimal changes were observed in the specimen fatigue lives with the addition of 25T on 50A (to give 50A25T), similarly 50T for when combined with 25A (to give 25A50T). However a significant reduction was

observed when comparing 50A with 50A50T, while virtually no difference was seen between 50T and 50A50T, indicated that at equal loading conditions, the failure was dominated by shear failure.

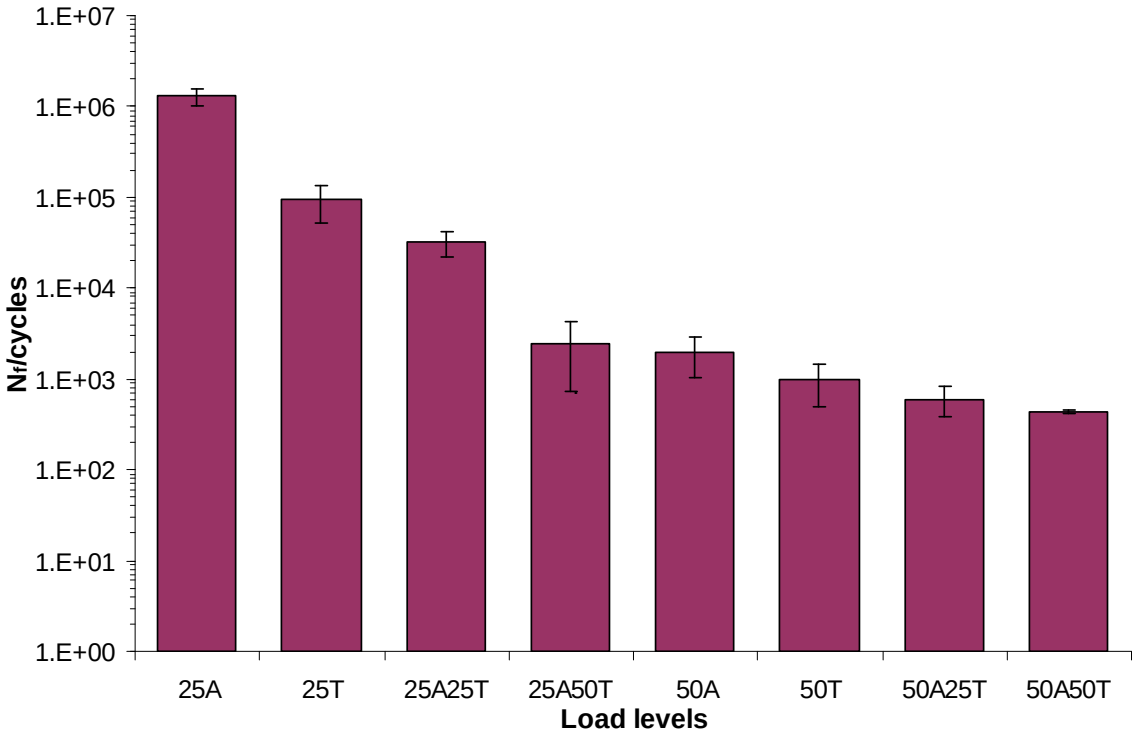

Figure 5.1 Fatigue lives of in-phase biaxial fatigues compare to uniaxial fatigue

25A represent ±25%UTS, 50A represent ±50% UTS, 25T represent ± 25%USS, 50T represent ±50% USS (error bars indicate standard deviation, n=3-5)

Table 5.1 Levels of significance for in-phase biaxial fatigue (Mann-Whitney test) at various loading regime. P<0.05 indicated by single underline and p<0.01 indicated by double underlines

Load cases	25T	25A	50T	50A	25A25T	25A50T	50A25T	50A50T
25T								
25A	0.0025							
50T	0.0075	0.0023						
50A	0.0079	0.0023	0.0705					
25A25T	0.0283	0.0023	0.0130	0.0142				
25A50T	0.0080	0.0023	0.0838	0.5772	0.0155			
50A25T	0.0075	0.0022	0.5411	0.0624	0.0129	0.0763		
50A50T	0.0075	0.0022	0.1197	0.0486	0.0127	0.0637	0.1083	

The effect of phase angle on the biaxial fatigue at 25A25T is shown in Figure 5.2. Kruskal–Wallis analysis showed that there was no statistical difference for 25A25T when comparing the 4 differences phase angles (0°, 30°, 60° and 90°). However when individual group comparison was performed using Mann-Whitney, increasing the phase differences from 0° to 90°, the number of cycles to failure increase significantly ($p<0.05$) from 31,912 ±9,689 to 82,905 ±11,134 cycles while the rest of the group showed increases in the numbers of cycles to failure but the effect was not statistically significant. Similar observation was shown at 50A50T (Figure 5.3) for phase angles of 0°and 90°. An increase in phase angle, increased the fatigue live of specimens significantly ($p<0.05$) from 442 ±82 at 0° to 1,395 ±451 at 90°. These results indicate the beneficial role of out-of-phase loading on the fatigue damage of the specimens.

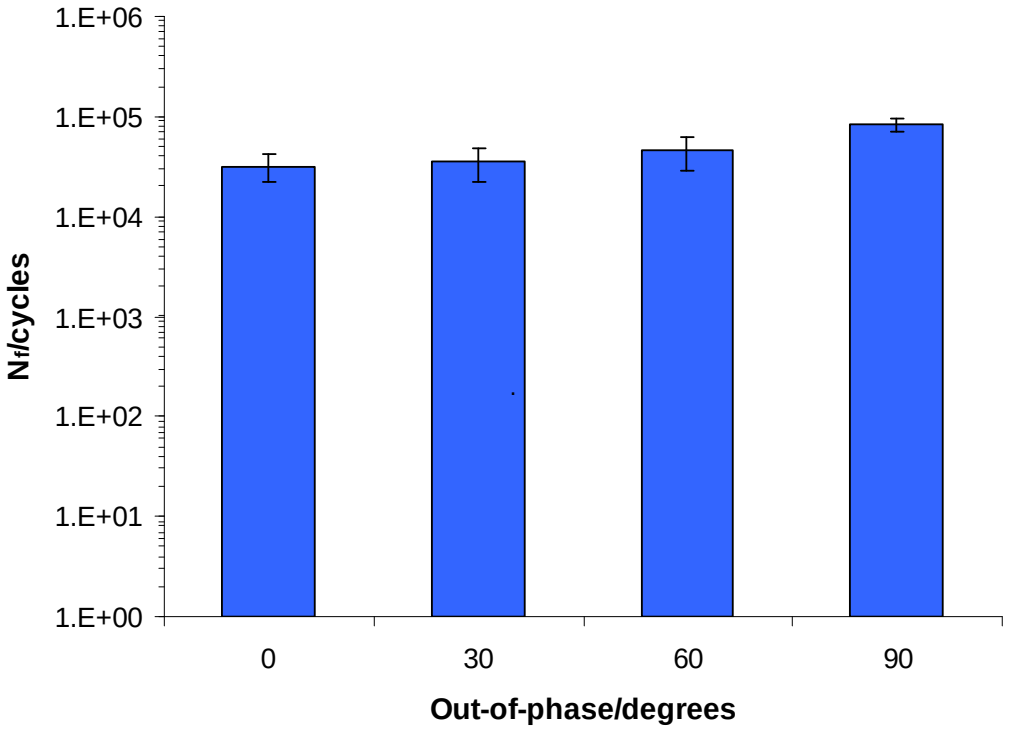

Figure 5.2 Number of cycles to failure for in-phase (0˚) and out-of phase (30˚, 60˚, 90˚) biaxial fatigue 25A25T (error bars indicate standard deviation, n=3-5)

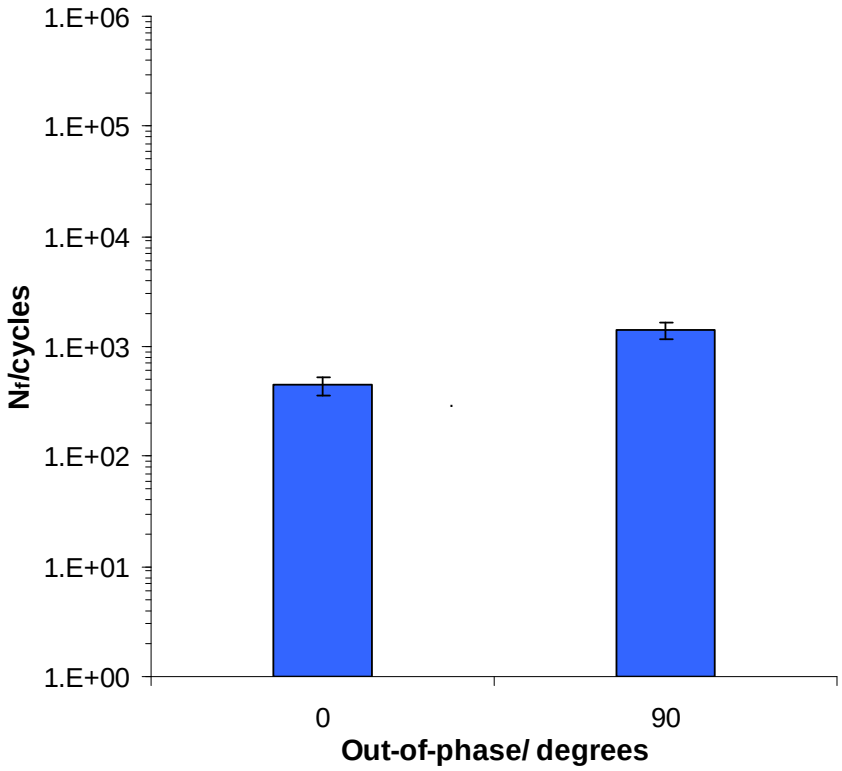

Figure 5.3 Number of cycles to failure for in-phase (0˚) and out-of phase (90˚) biaxial fatigue 50A50T (error bars indicate standard deviation values, n=3-5)

Each of the biaxial fatigue test has two hysteresis loops, one for axial and one for torsional loading. The individual loops are similar to those obtained in uniaxial fatigue test (Chapter 4), therefore, each analysis of the biaxial test can be presented in a similar manner to the result for uniaxial fatigue. Figure 5.4 show the general hysteresis loops for combined axial and torsional loading, in-phase and 90º out-of-phase 25A25T loading. Generally, the in-phase and out-of phase hysteresis loop are similar and symmetrical. However, the loops for in-phase testing are closer to the origin while the out-of-phase were displaced along the horizontal axis, showed a non-zero mean strain resulted from Poisson's ratio effects.

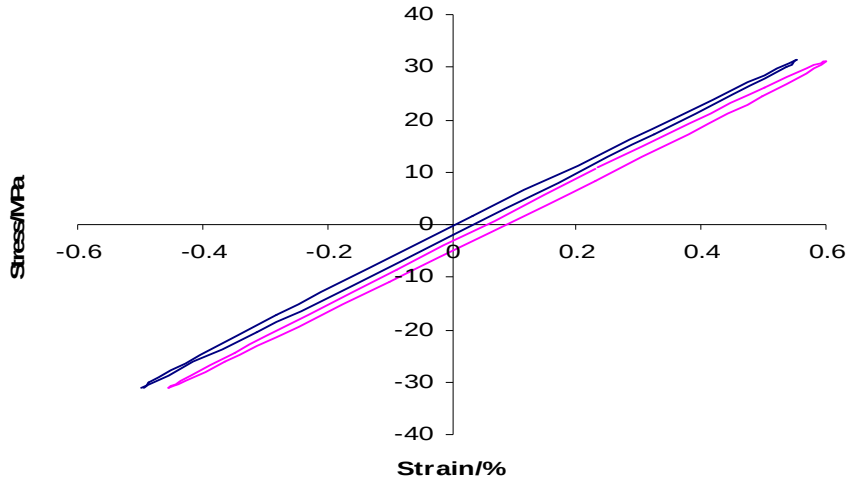

(a)

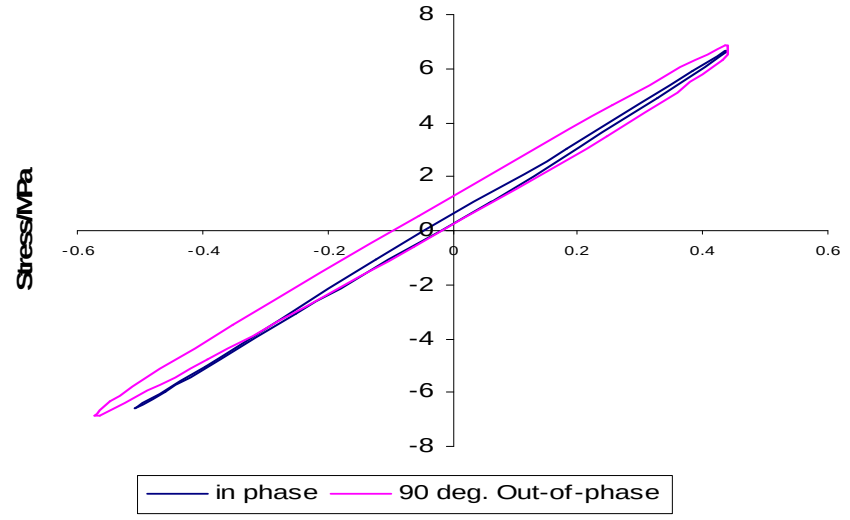

(b)

Figure 5.4 Typical initial fatigue hysteresis loops for biaxial fatigue 25A25T

(a) axial loop; (b) torsional loop, both in-phase and 90°out-of-phase

Further analysis of the hysteresis loops shows a gradual reduction in secant modulus with cycling (Figure 5.5), a similar trend to that observed in uniaxial fatigue. Overall, the initial values of axial secant modulus are similar. More variation was observed for the initial values of torsional secant modulus loading. The axial modulus is higher than the torsional modulus, which is in agreement with the findings from the uniaxial fatigue tests.

At low stress level, 25A25T, the changes in axial energy absorbed increased gradually from the beginning of the cycles until failure. However increasing stress by 25T (to give 25A50T), caused the axial energy absorbed to increase at approximately 2,000 cycles while the axial secant modulus dropped at the same point. In torsional loading, addition of 25T on 25A25T caused the shear energy absorbed to increase and the shear secant modulus reduced, at the same point, about 200 cycles.

At 50A loading, addition of 25T on 50A25T resulting in earlier increases in axial energy absorbed from 200 cycles in 50A25T to 100 cycles in 50A50T, while the axial secant modulus in both loadings reduced after increasing the energy absorbed. In torsional loading, adding 25T on 50A25T caused the shear energy absorbed to increase as early as 50 cycles in 50A50T in comparison to 200 cycles in 50A25T. Shear secant modulus reduced after the energy absorbed increased at about 500 cycles (50A25T) and 50 cycles (50A50T) respectively. At the same time, it was observed that 50A50T has the lowest secant modulus and highest energy absorbed in axial and torsional direction compare to the other groups indicated maximum damage to the composite was due to superimposition of biaxial loading.

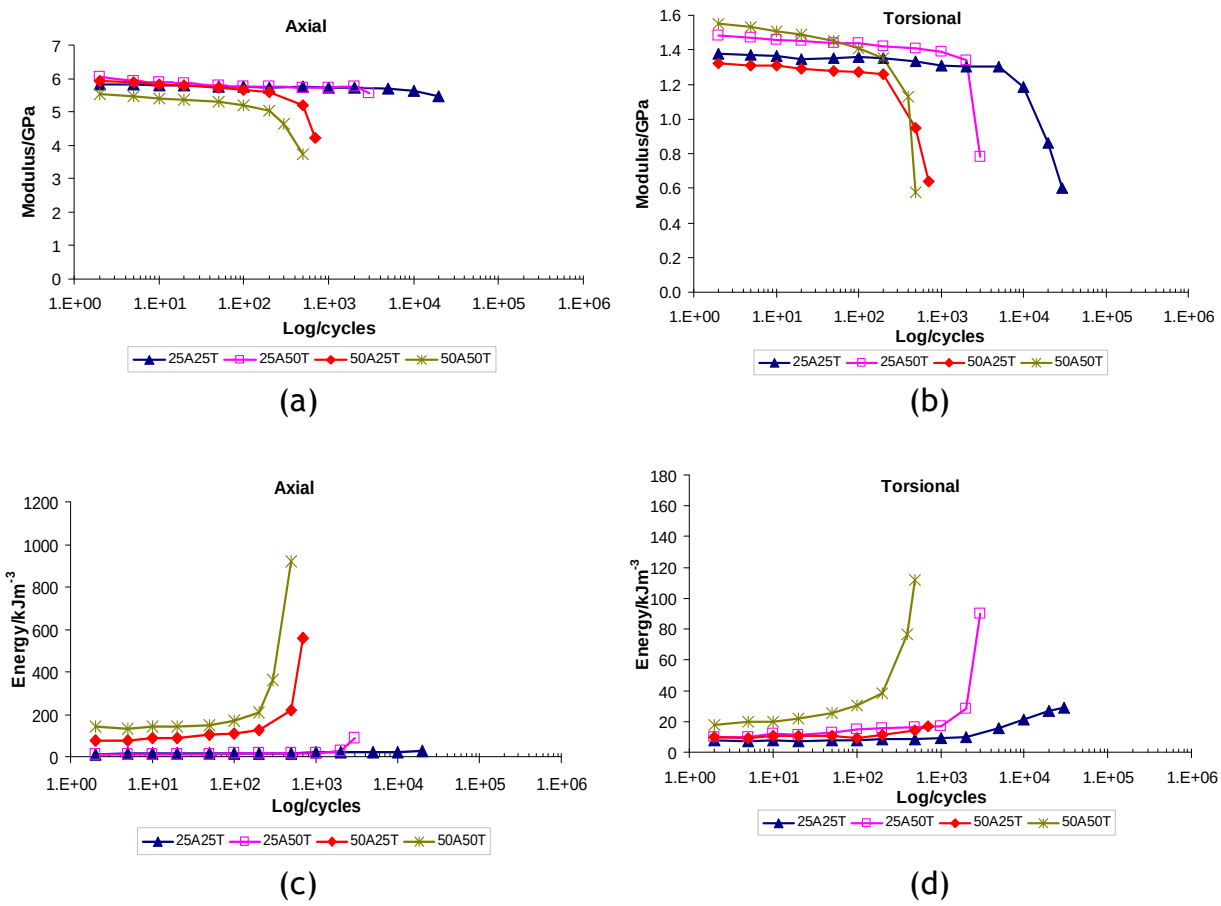

Figure 5.5 Variations in secant modulus and energy absorbed for in-phase biaxial fatigue at various stress level

(a) axial secant modulus; (b) torsional secant modulus; (c) axial energy absorbed; (d) torsional energy absorbed

The fatigue damage in-phase and out-of-phase for each biaxial fatigue case for 25A25T are shown in Figure 5.6. As the number of cycles increased, gradual reductions in secant modulus were observed. Overall the initial values of the moduli are similar to those obtained for the individual loading. The axial modulus is higher than torsional modulus as expected.

In torsional loading, the energy absorbed is similar to that for axial loading even though the applied shear stress is smaller compared to applied axial stress, suggesting that composite failure is affected by the superimposed loading and that shear failure dominated the failure mechanism. At the same time, it can be seen that for 25A25T in-phase, the axial and torsional moduli drop, at about same point around 10,000 cycles, while the energy absorbed increased around 500 cycles in axial and 2000 cycles in torsional before become more apparent in

response to the apparent reduction of the moduli. On the other hand, 90° out-of-phase has higher axial modulus, lower absorbed axial and torsional energy compared to other cases, which is consistent with its relatively low fatigue damage characteristics. However, 25A25T at 30°out-of-phase showed the lowest secant torsional modulus compared to the other cases. Since it also has lowest initial secant values, this variation is assumed to be due to variation of fibre placement in the specimens. This assumption is in agreement with values of energy absorbed, which indicated that damage occurs in the out-of-phase specimens similar to that show by the in-phase specimens (Figure 5.6d).

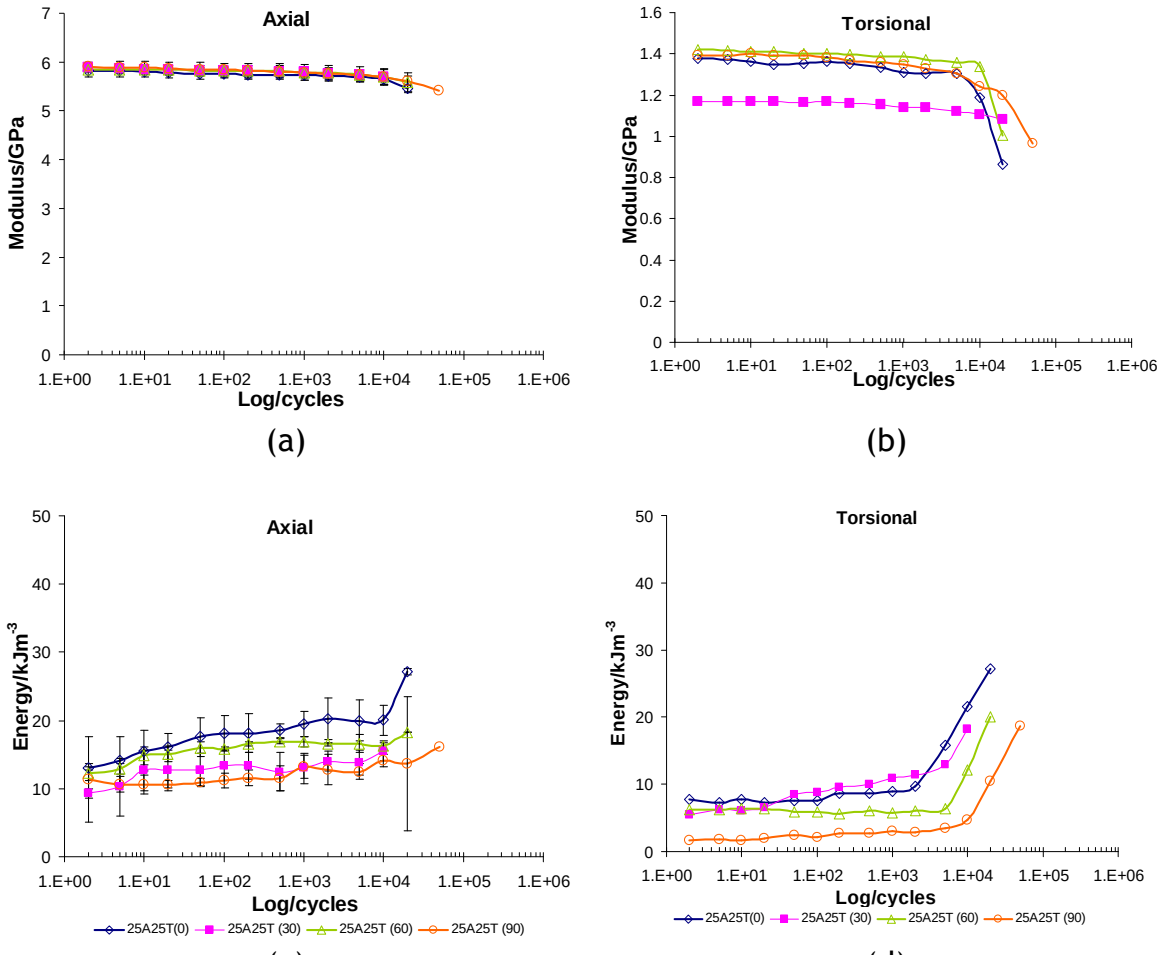

Figure 5.6 Variations in secant modulus and energy absorbed for 25A25T in and out-of-phase biaxial fatigue (0°, 30°, 60, 90°)

(a) axial secant modulus; (b) torsional secant modulus ; (c) axial energy absorbed; (d) torsional energy absorbed

Finally, for the high biaxial stress loading of 50A50T, 90°out-of-phase again shows features of lower fatigue damage accumulation compared to in-phase fatigue (Figure 5.7). The changes for 50A50T in-phase in absorbed axial energy seem to start at about 50 cycles, followed by a reduction in secant axial modulus after approximately 100 cycles. 90°out-of-phase showed these changes starting much later. It can be seen that the modulus drops while energy absorbed increased at the same point, about 500 cycles in axial loading. Interestingly, the energy absorbed increased gradually in comparison to in-phase. For torsional loading, the in-phase initial secant modulus is slightly higher than out-of-phase, however, the in-phase modulus reduced gradually from the start of the testing before sinking further below the out-of-phase at about 200 cycles, while the energy absorbed increased in parallel with decreasing modulus and the behaviour become apparent at the same point. The out-of phase variation showed that the energy absorbed increased before the modulus reduced. The modulus drop become apparent at about 500 cycles while the increase of energy absorbed started earlier at about 100 cycles. It also can be seen that in-phase has higher energy absorbed and lower secant modulus in axial and torsional, indicating the effect of superimposed loading on the composite structure. This finding is similar to observations at the lower stress level of 25A25T. In general, it can be observed that the phase angle affects the axial and torsional behaviour, the lower the phase angle between stress directions, the sooner the moduli drop and the energy increases.

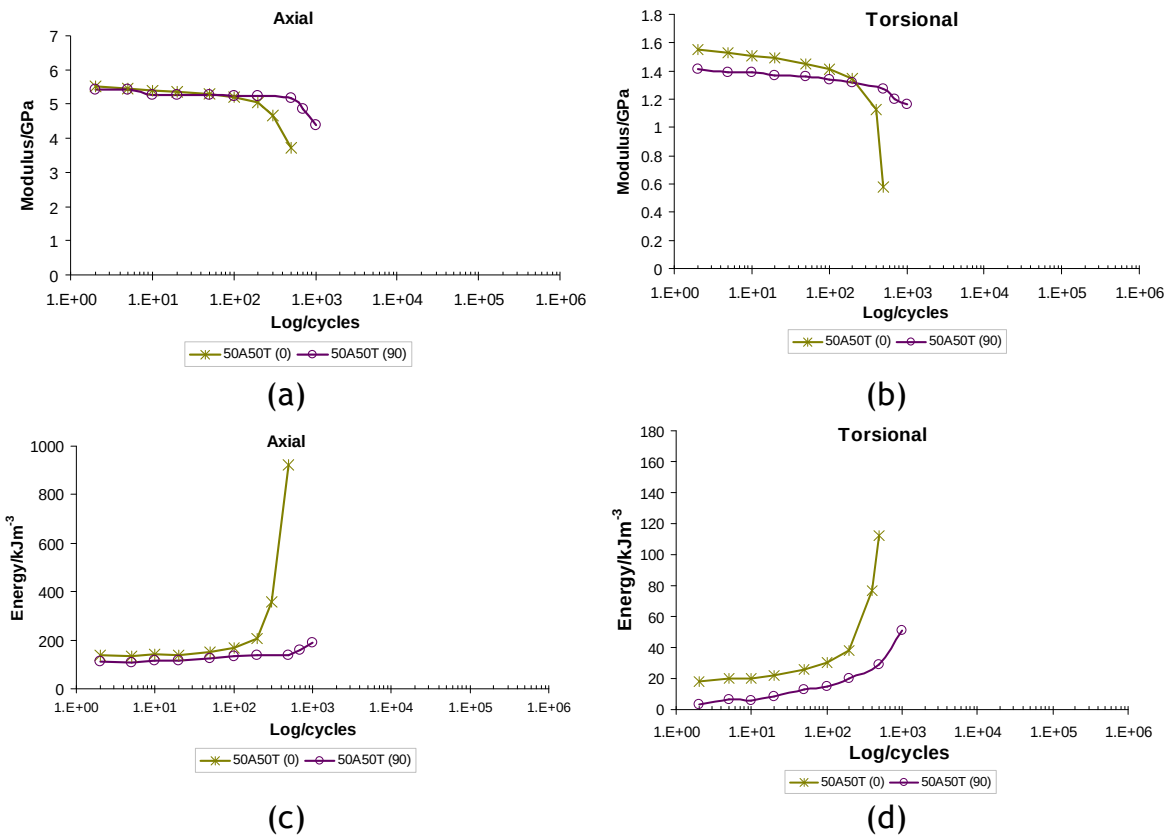

Figure 5.7 Variations in secant modulus and energy absorbed for 50A50T in and out-of-phase biaxial fatigue (0, 90)

(a) axial secant modulus; (b) torsional secant modulus ; (c) axial energy absorbed; (d) torsional energy absorbed

In summary, the damage produced from fatigue study of the composite in all biaxial cases is strongly dependent on the level of the applied axial and torsional stresses. The dominant effect of the torsional compared to the axial properties can be seen. The torsional and axial properties are shown to be interlinked, as an increase in one leads to slight changes in the damage characteristics in both axial and torsional conditions, which combine to produce the final failure. Increasing phase differences resulted in slightly increased fatigue properties with lower degree of fatigue damage accumulations. This finding is similar to those reported in literature, as increasing the phase angle of biaxial loading increases the number of cycles to failure (Ton That, 2000; George and Vashishth, 2001; George and Vashishth, 2005).

5.3.2 Determination of S-N Curves

The values of three combined stress parameters, maximum principal stress (σ_{1max}), maximum shear stress ($\tau_{12\ max}$) and Tsai-Wu parameter (I_{Fmax}), were calculated for each load angle combination (Table 3.1) and are shown in Appendix A4. These values are then plotted against the number of cycles to failure and shown as S-N curves in Figure 5.8 to 5.10. The linear regression lines are plotted using four different loading conditions. The all conditions line is used for all data point given by uniaxial and biaxial at all loading levels and phase angles. All biaxial loading conditions represent only biaxial loading, at various loading levels and phase angles. In order to study the correlation loading levels effect at 0° phase angle, in-phase condition is plotted. Out-of-phase conditions consists data tested at equal stress level, 25A25T and 50A50T at different phase angles, 0°, 30°, 60° and 90°. All equations with their correlation coefficients (R^2) are given in the graphs.

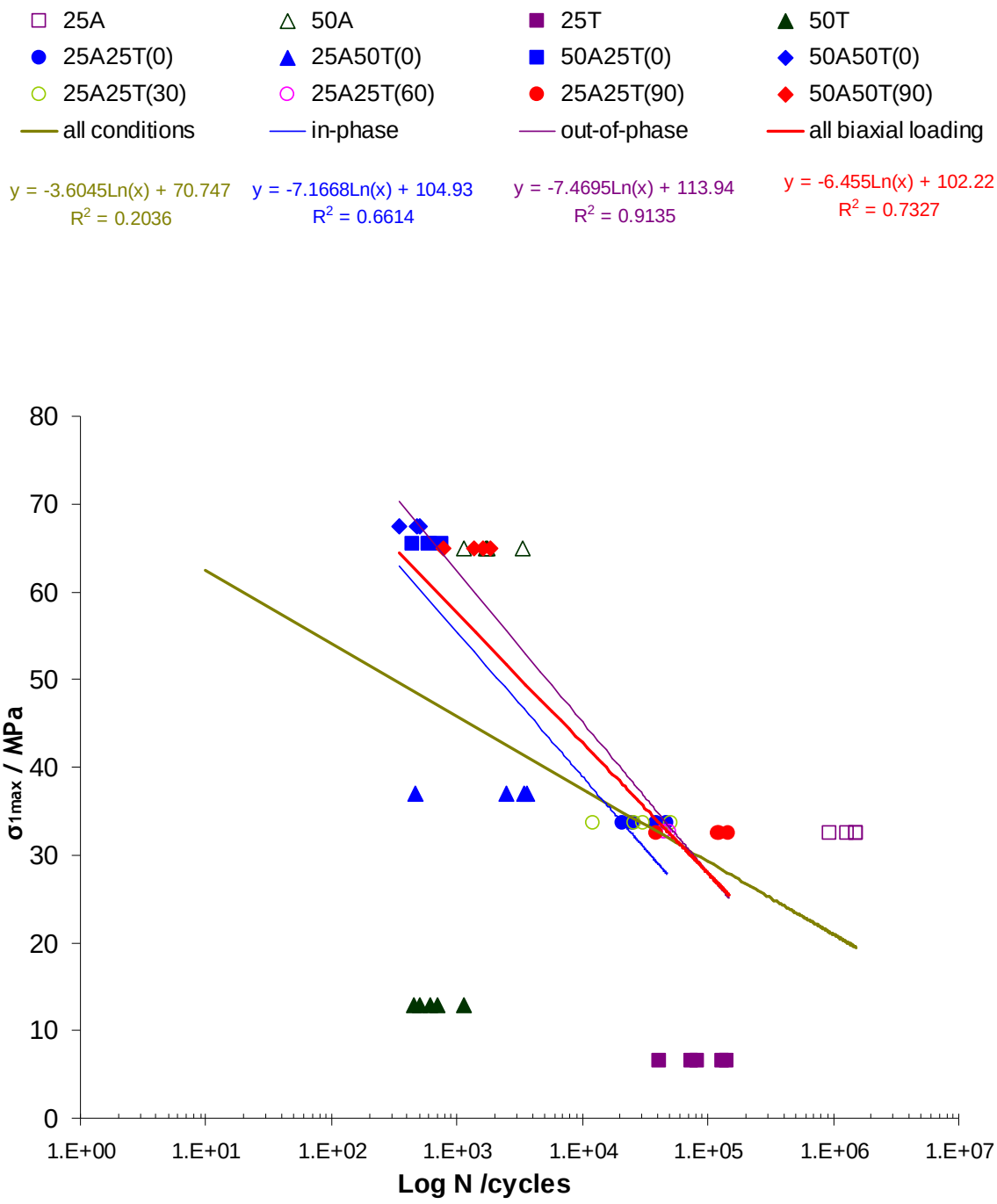

Figure 5.8 S-N curve for maximum value of principal stress (σ_{1max}) versus cycle to failure. With least squares fits for all data (—), in-phase (—), out-of-phase (—) and all biaxial loading (—)

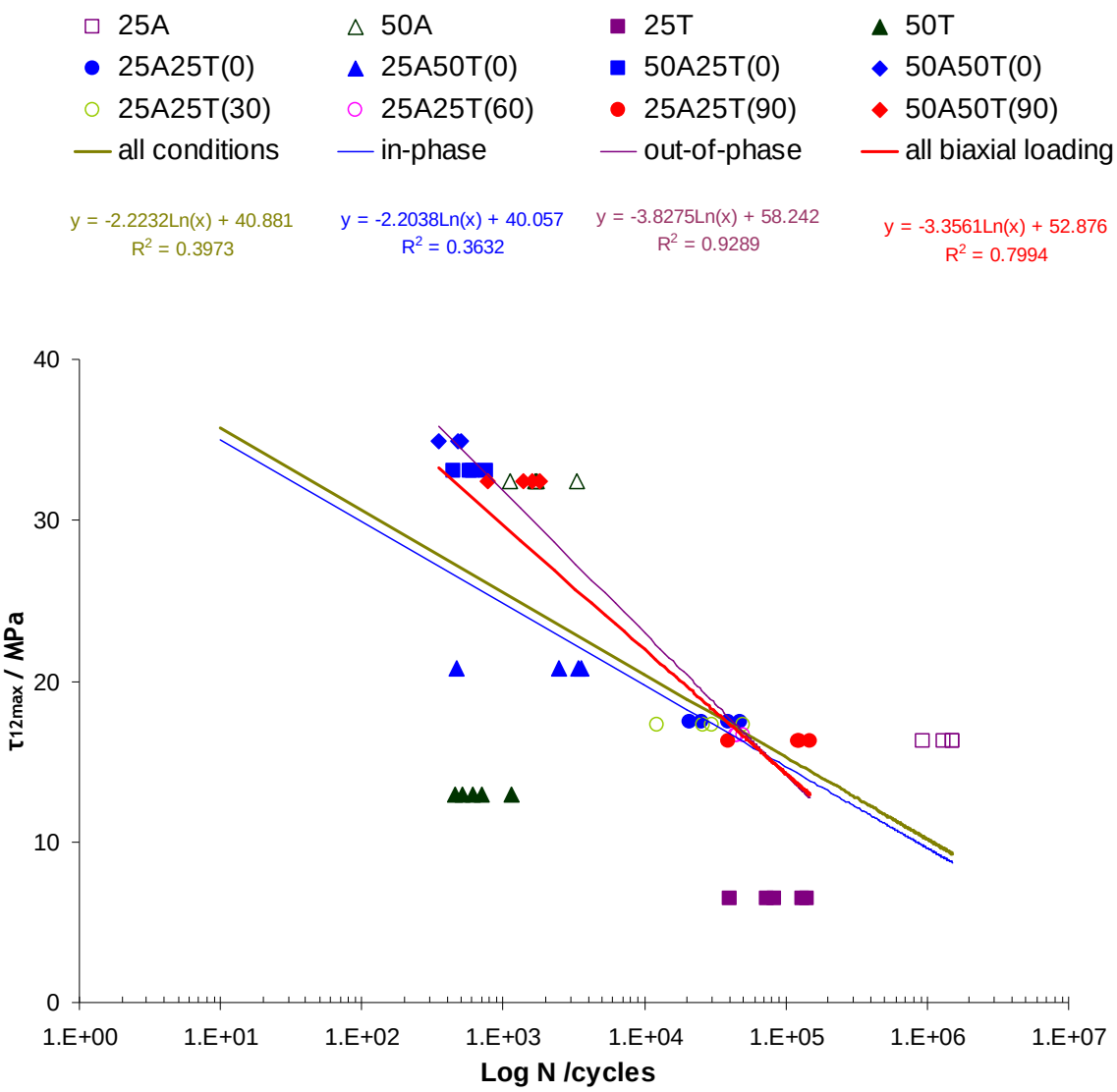

Figure 5.9 S-N curve for maximum value of maximum shear stress (τ_{12max}) versus cycle to failure

With least squares fits for all data (—), in-phase (—), out-of-phase (—) and all biaxial loading (—)

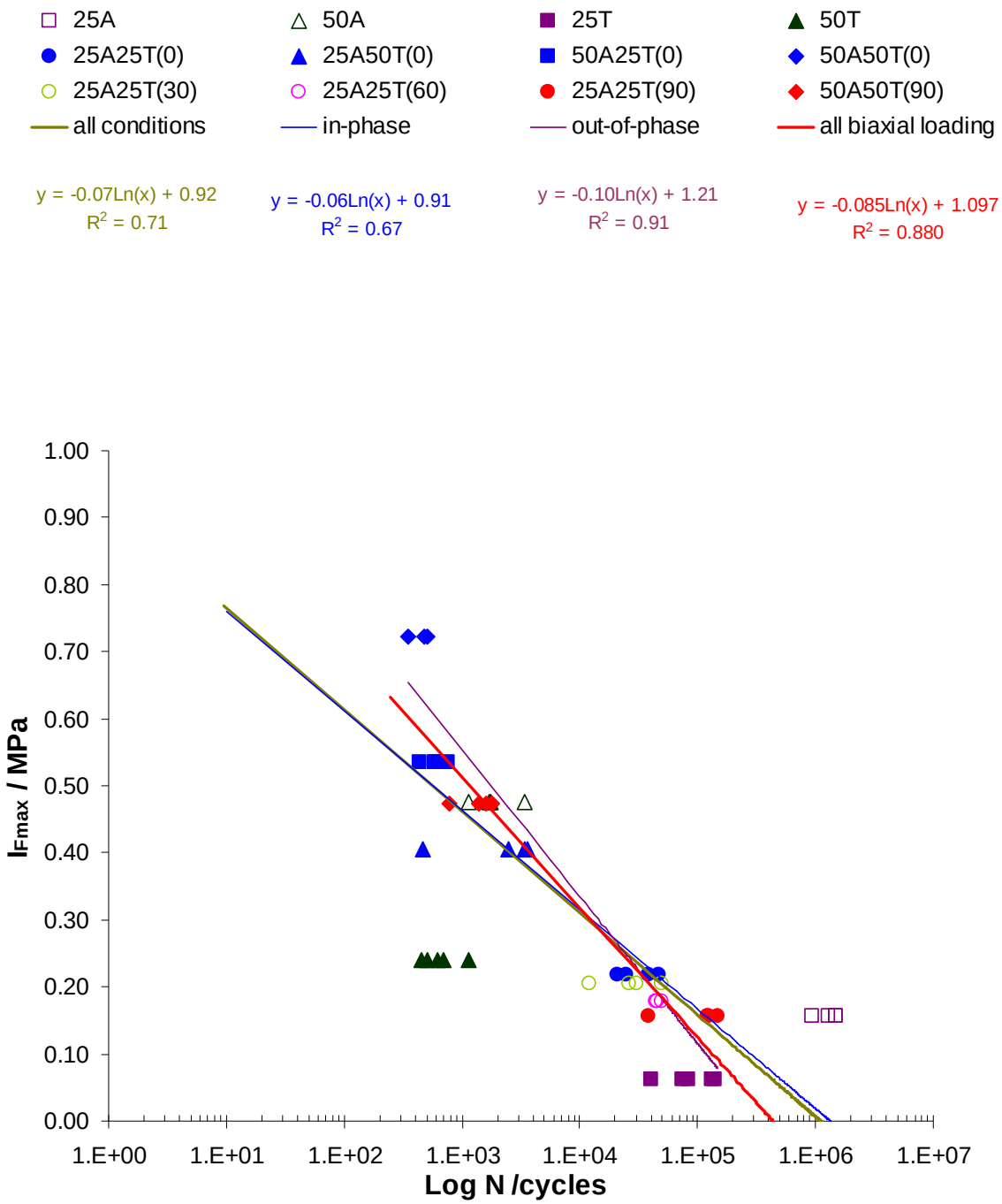

Figure 5.10 Maximum value of Tsai-Wu parameter (I_{Fmax}) versus cycle to failure

With least squares fits for all data (—), in-phase (—), out-of-phase (—) and all biaxial loading (—)

It can be seen from these figures that principal stress, maximum shear stress and Tsai-Wu parameter all showed different levels of fit for all failed PLA-PLA-TCP specimens. Thus, the correlation coefficient for the least square fit (R^2) was calculated and is shown in Table 5.2 for all loading conditions. The R^2 value is highest for I_{Fmax} and lowest for $\sigma_{1max,}$ indicating that Tsai-Wu parameter is the best prediction of number to cycles to failure for combination of axial and torsional load condition and phase angle. However for the Tsai-Wu parameter R^2= 0.71 so still quite low. However this value includes the uniaxial fatigue. Tensile-compression failure criterion is best described using the principal stress rather than Tsai-Wu (Amijima et al., 1991), thus another condition is used, for biaxial loading only, increase the R value to 0.88. The result was similar with all loading condition while for effect of the phase angle, the maximum shear stress line giving the best prediction indicator.

Table 5.2 Results of linear regression for σ_{1max}, τ_{12max} and I_{Fmax} versus log N

Variable	Slope	Intercept	R^2
Condition: All conditions (uniaxial and biaxial)			
σ_{1max}	-3.6	70.74	0.20
τ_{12max}	-2.22	40.88	0.40
I_{Fmax}	-0.06	0.92	0.71
Condition: biaxial condition only (in-phase and out-of-phase)			
σ_{1max}	-6.45	102.22	0.73
τ_{12max}	-3.35	52.87	0.79
I_{Fmax}	-0.08	1.09	0.88
Condition: effect all load levels (in-phase, uniaxial and biaxial)			
σ_{1max}	-7.17	104.92	0.20
τ_{12max}	-2.2	40.05	0.36
I_{Fmax}	-0.06	0.91	0.67
Condition: effect of phase angle			
σ_{1max}	-7.47	113.94	0.91
τ_{12max}	-3.82	58.24	0.92
I_{Fmax}	-0.09	1.21	0.91

In summary, it can be seen that maximum shear stress is best for predicting cycles to failure when the specimen was loaded at constant load levels but different phase angles, but when combining all stresses and stress level and phase angle, the Tsai-Wu criteria is the best predictor. Thus for the prediction of the fatigue life of non-tested combinations of axial and torsional loads and phase angle, the Tsai-Wu criterion should be calculated.

5.3.3 Fractography of Biaxial Fatigue

Fractography analysis was carried out for specimens tested at 25A25T in-phase and out-of-phase to study the effect of the phase loading in biaxial fatigue testing in the specimen structure.

The fracture surface of 25A25T in-phase is shown in Figure 5.11 and it was compared with fracture surfaces after 25A and 50T fatigue testing showed in Figures 4.24 and 4.26 respectively. Optical and SEM examination showed that the fracture surfaces of 25A25T does not resemble axial failure but have more torsional failure characteristics, contained longitudinal cracks with interfibre splitting which is indicating the failure is dominated by shear failure. At the same time, more severe fibre breaks on the matrix surface in the shear direction (Figure 5.11e) can be observed which are not seen in uniaxial torsional fracture surfaces, indicating the influence of axial stress on the specimen failure mechanism. At high magnification (Figures 5.11d and 5.11e) extensive damage with fibre breakage and exposure of the TCP particles can be seen, suggesting that TCP particles were detached from the PLA_{70} matrix. As the specimen failed due to splitting of the fibres parallel to the fibres direction shows that final failure of biaxial 25A25Tspecimens is due fibre-matrix interface, and is dominated by torsional shear.

Figure 5.12 shows the fracture surface of specimens tested at 25A25T out-of-phase. It can be seen that the fracture surfaces have similar longitudinal cracks and splitting of the fibres (Figures 5.12b to 5.12c) as observed in in-phase specimen, but that the damage was reduced. This correlates with fatigue damage observed through alteration in the mechanical properties as discussed in Section 5.3.1.

When tested at the higher torsional loading of 25A50T in-phase (Figure 5.13), the surface fracture showed higher torsional damage with more longitudinal cracks observed as compared to uniaxial ±50% USS (Figure 4.26) and biaxial 25A25T in-phase (Figure 5.11) indicating that higher damage occurs with increases in loading. Surface fracture cracks with exposed fibres suggest failure of the fibre-matrix interface, and that the failure is dominated by torsional shear causing the final failure.

All specimens tested at 50A25T and 50A50T at 0° phase angle failed under axial loading in compression with surface fractures similar to ±50% UTS as discussed in Chapter 4, while the 50A50T at 90°out-of-phase specimens failed under shear, but the fracture surface of the specimens' fracture surface was altered when the actuator of MTS testing machine dropped and crushed the samples at the end of testing, thus the SEM analysis was not carried out for these specimens.

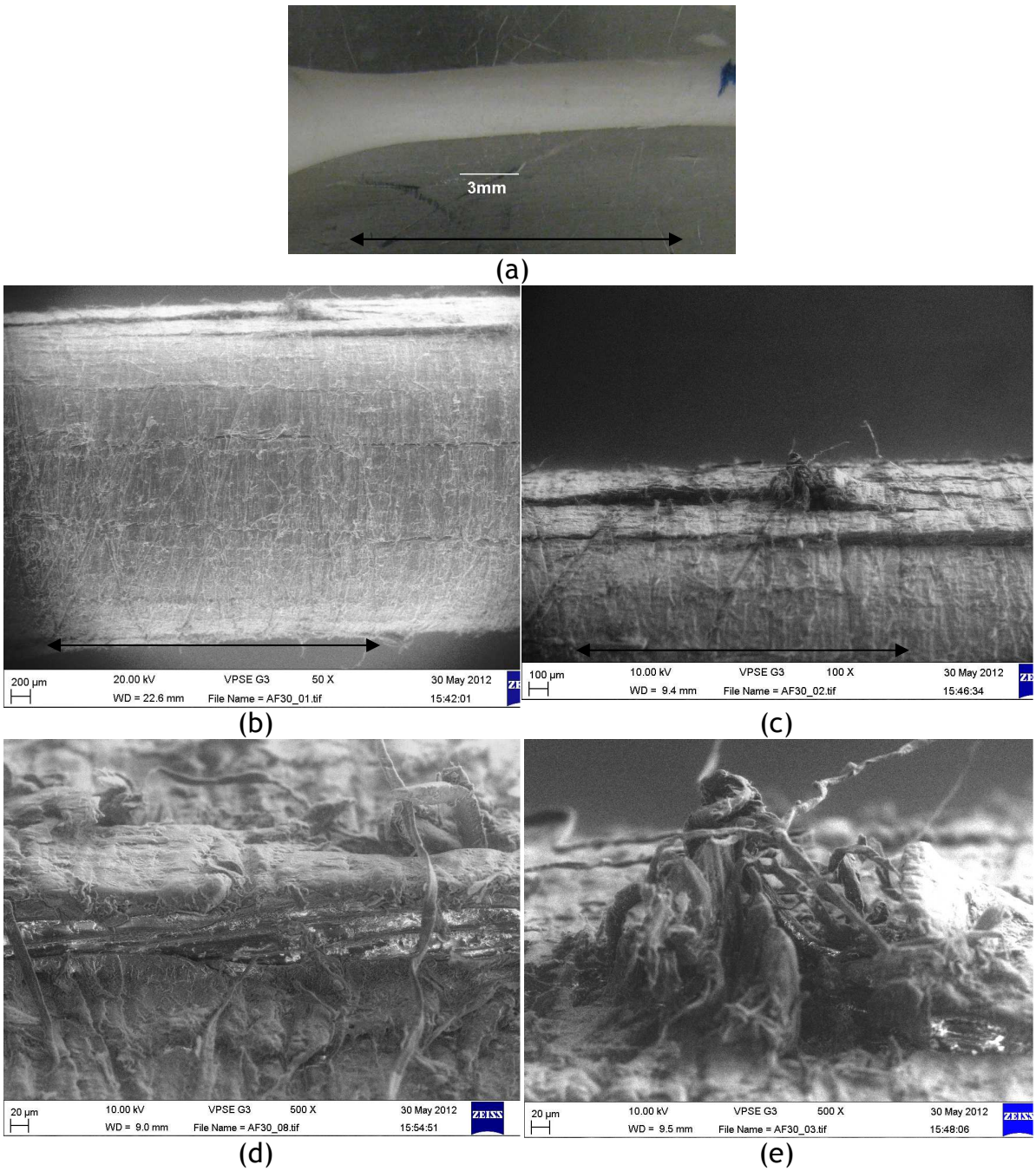

Figure 5.11 Fracture surfaces of in-phase fatigue specimens at 25A25T

(a) optical general view; SEM observation on (b) matrix crack parallel to main axial fibre orientation (c) fibre failure at the horizontal crack; (d) exposed TCP particles and (e) high magnification of fibre fracture (Marker bars= (a) 3mm; (b) 200µm; (c) 100 µm; (d & e)20 µm. Arrows indicate fibre direction which is horizontal throughout)

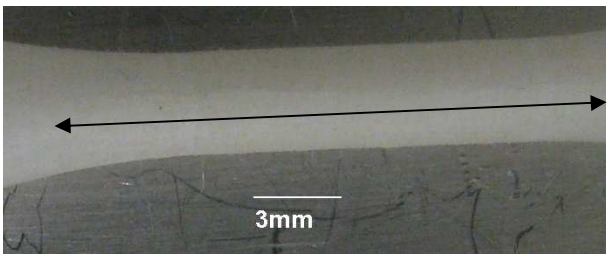

(a)

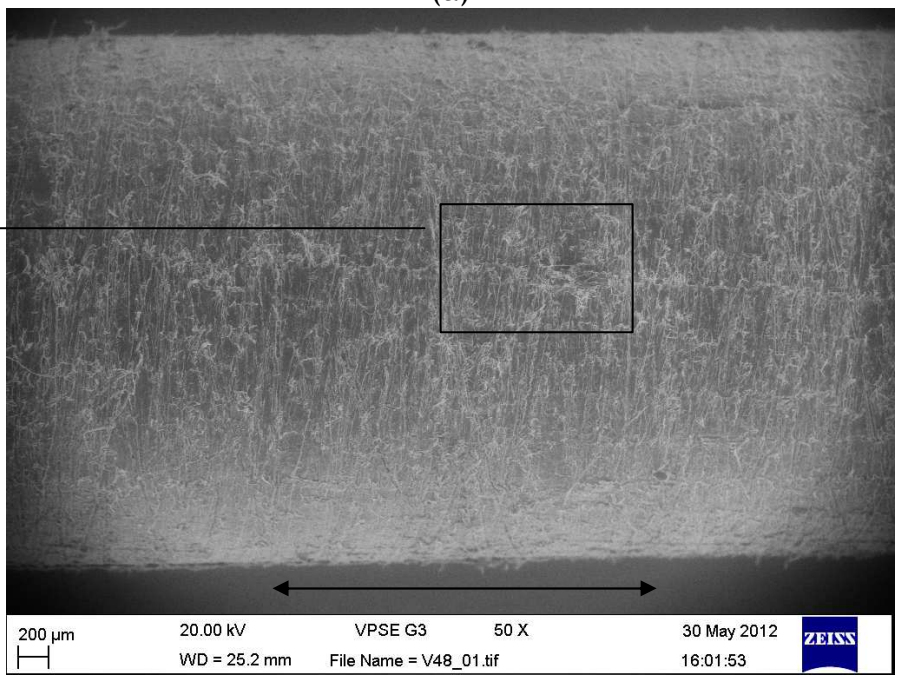

(b)

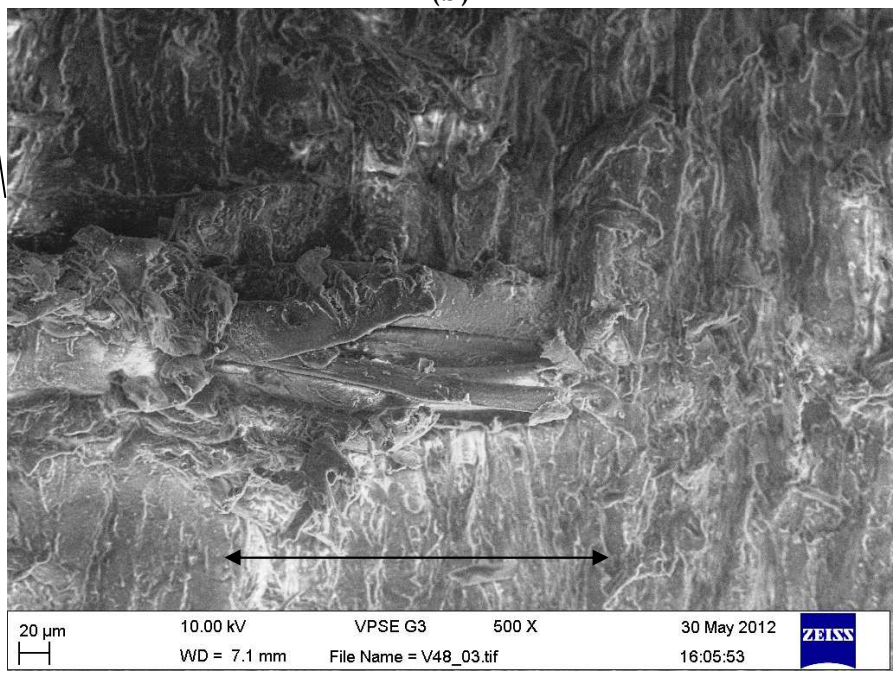

(c)

Figure 5.12 Fracture surfaces of 90° out-of-phase fatigue specimens at 25A25T

(a) matrix crack parallel to main axial fibre orientation (b) fibre failure at the horizontal crack shown in higher magnification in (c). (Marker bars= (a) 3mm; (b) 200 µm; (c) 20 µm. Arrows indicate fibre direction which was horizontal throughout)

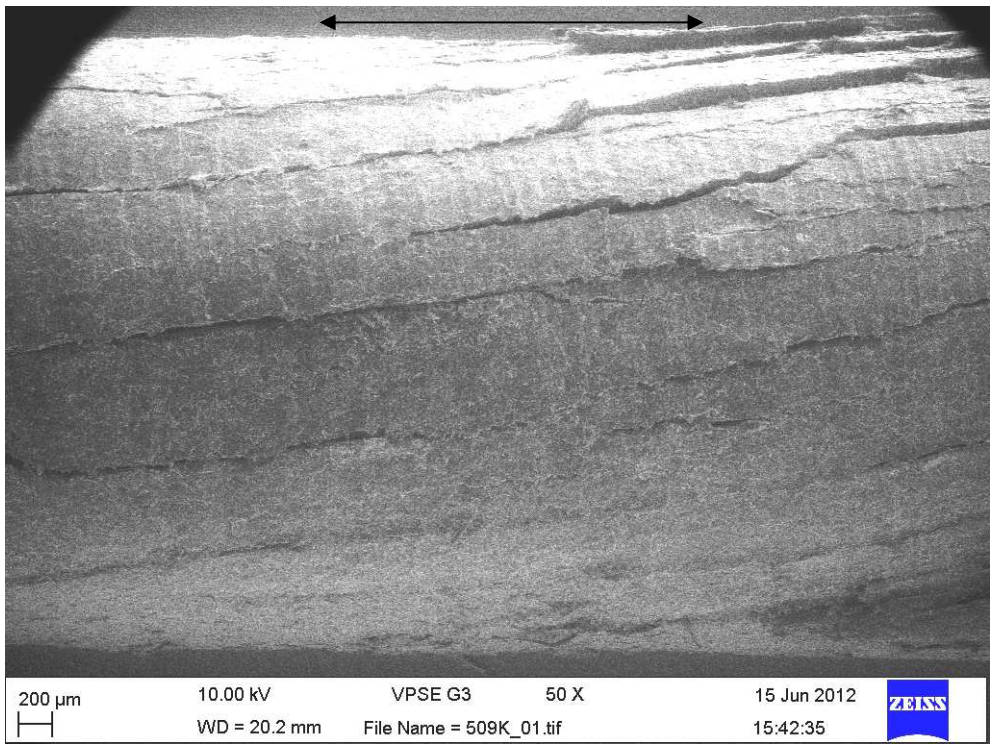

(a)

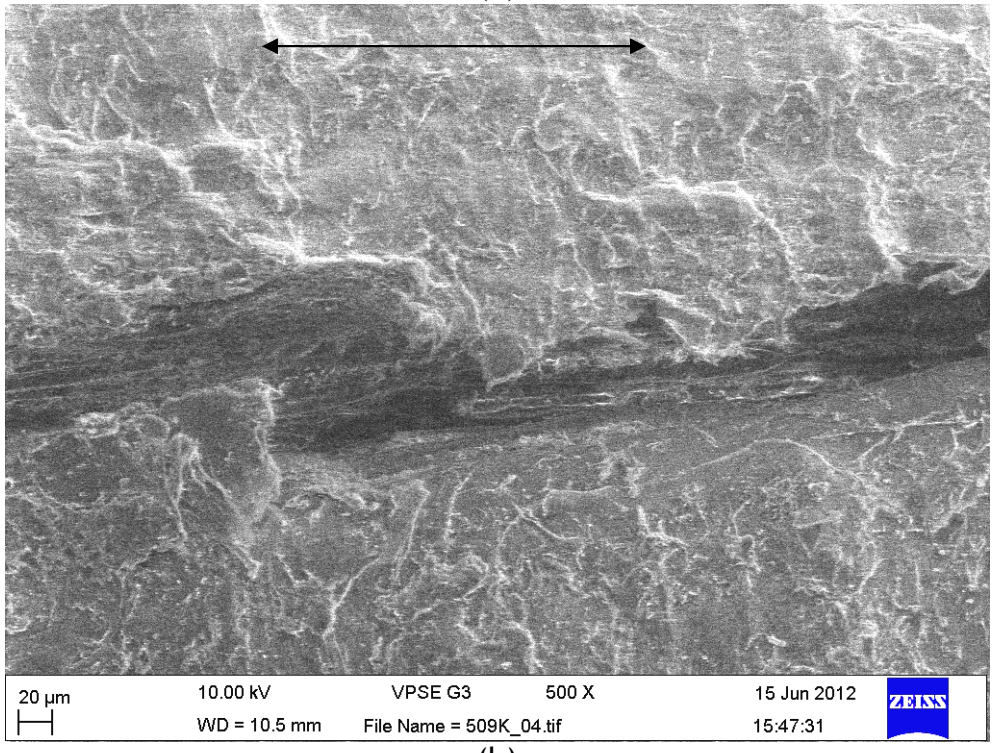

(b)

Figure 5.13 Fracture surfaces of in-phase fatigue specimens at 25A50T

(a) matrix crack parallel to main axial fibre orientation (b) exposed fibre at the interface failure at the horizontal crack. (Marker bars= (a) 200µm; (b) 20 µm, Arrows indicate fibre direction)

5.4 DISCUSSION

The yield stresses of the composite in this study under torsional, compression and tension is roughly in the ratio of 1:3:4. The literature suggests that yield stresses are associated with the onset of microcracking in materials (Wright et al., 1981; Yoshikawa et al., 1994), thus a lower yield stress in torsion indicates a lower threshold for microcracking formation under torsion in comparison to compression or tension. Cezayirlioglu et al. (1985) showed that the superposition of torsion on tension and compression lowers the yield stress of anisotropic materials such as cortical bone. They implied that superimposition of torsional loads decreased the microcracking threshold of the material thus suggesting that the addition of torsional stress to the axial testing would decrease the fatigue life of the materials. For continuous fibre reinforced composites under uniaxial fatigue loading, the composite failed in compressive loading rather than tensile due to kinking mode failure. This finding has been discussed in detail in Chapter 4. However to summarise, the first models for kinking failure in composite were developed by Argon (1972) and later Budiansky (1983), where they observed that the fibres in unidirectional fibre reinforced composites are not uniformly straight. Thus, they suggested that the local shear stresses in the composite develop from the fibre misalignment under the action of remote pure compressive loads. Therefore, it was implied that when these shear stresses exceeded the shear yield stress of the matrix, the fibre would undergo shear buckling and later lead to failure in compression. The compression strengths of polymers have been established in great detail. There are many factors that might influence the strength such as fibre mechanical properties, matrix shear properties, fracture energy of the fibre/matrix interface, volume fraction of the fibres and also initial misalignment of fibres. Among these parameters, induced local shearing stresses controlled by matrix shear properties and interfacial fracture energy, influence the failure mechanism and the failure strength of a composite. The presence of the shear stresses during the compressive loads on the specimen will induce further misalignment of the fibres that will initiate the failure mechanism.

In the literature, there are only a few reports on the effects of combined compression and torsional loading on continuous fibre composites. Jelf and Fleck (1994) performed a study on effect of constant value shearing stress of hollow tubes of carbon fibre/epoxy composites. The torque was applied to a given level, after which the compression stress was increased until failure occurred. They reported that the compressive strength reduced linearly with increasing values of the shear stress before failing under plastic microbuckling. They also observed that microbuckling occurs in the compression torsion test by the development of a single micro buckled band around the gauge section and is arrested by formation of an axial split after completing a circumferential propagation around the tube.

Superposition of torque on low (25A) as well as high (50A) levels of axial loading leds to reduction in the fatigue life of PLA-PLA-TCP composite and the magnitude of the reduction depended on the magnitude of the torsional loading (Figure 5.1).

In uniaxial fatigue, the torsional fatigue life was less than the axial fatigue life at the same proportion of the failure stress. For example, the fatigue lives for 25A and 25T are 1.3 $x10^6$ and 9 $x10^4$ cycles respectively. At higher stress levels, 50A and 50T alone give about $1x10^3$ and $6x10^2$ cycles respectively. Additional of 25T to 25A reduced the number of cycles to about $3x10^4$. For 25A25T in-phase biaxial fatigue (σ_{max}= 33.69 MPa, τ_{max} =17.47 MPa, I_F=0.21), the addition of 25T to 50A (giving σ_{max} = 65.51MPa, τ_{max} = 33.08 MPa, I_F=0.54) reduced the fatigue life to about $5x10^2$ cycles. At the same time, it was observed that adding 25A to 50T (σ_{max} = 36.99 MPa, τ_{max} = 20.77 MPa, If=0.41) further reduced the fatigue life to about $2x10^3$ cycles. 50A50T (σ_{max} = 67.37 MPa, τ_{max} = 34.93 MPa, I_F = 0.72) has a fatigue life of about $4x10^2$ which is two decades lower than 25A25T, indicating that the biaxial fatigue life of the material is governed by the axial and torsional stresses.

The reduction was statistically significant for all comparisons between the axial only and axial-torsional load cases, with exception of 50A versus 50A25T load case, thus implying that at high axial load levels (50A), effect of torsion is less significant compared to low load levels (25A) to the axial fatigue life of the

composite. This finding may suggest that the ratio of shear/normal stresses in an axial-torsional load case has to exceed a threshold if torsional loading is to play a dominant role in determining the fatigue life of the composite.

Using principal stress analyses (Gere and Timoshenko, 1991), the threshold value of shear/normal stress, represented by 50A25T load case, can be calculated and expressed in terms of maximum shear/maximum normal stress. The maximum shear to maximum normal stress ratio represents the contribution of shear stresses relative to normal stresses to causing failure in materials (Vashishth et al., 2001). The calculated value for maximum shear stress/maximum normal stress of 50A25T load case is equal to 50A fatigue. Therefore, even though failure was observed in 50A25T fatigue test, the damage was dominated by axial stresses not torsional. To reinforce this conclusion, the same analysis was also carried out for low axial loading (25A). The shear stress to normal ratio stress in 25A is 0.50, while in 25A25T is 0.52, further adding 50T, increased the ratio to 0.56, implying that dominant stress from torsional reduced the threshold in microcracking formation, thus reduced the fatigue resistant of the composite. A similar observation was reported for anisotropic materials by Vashishth et al. (2001) in their fatigue study of bovine bone.

Superposition of torsional on axial loading leads to dramatic reductions in fatigue life. At the same time, it was observed that increasing the phase angle, increases the fatigue life of the composite. Increasing the phase angle to 90° between the axial and torsional stress however increased the number of ranging from a factor approximately 3 for 50A50T and approximately 4 for 25A25T. Ton That (2000) studied effect of phase angle on biaxial fatigue of isotropic particulate reinforced composite and reported that the important role of phase angle depended on the relative levels of axial and torsional stresses, as well as maximum shear stress and the Tsai-Wu parameter. He showed that by increasing the phase angle would decrease the principal maximum stress and maximum shear. The full analysis for this study is shown in Appendix A4. Vashishth and co-workers (Vashishth et al., 2001; George and Vashishth, 2005) studied biaxial fatigue behaviour of cortical bone in respect to loading and phase angle. They reported that superposition of the torque caused significant reductions in fatigue life of bone, this effect decreased with increasing phase angle. They also

observed that during in-phase testing, the damage was a combination of mixed mode crack initiation and the propagation of tension, compression and torsional. For out-of-phase loading, only the torsional mode was significant affected, thus reducing the contribution of the mix-mode behaviour load that extends the fracture path. The second factor is the rotation of the principal planes. Damage normally takes place on principal planes that become the main site of damage. During the test, out-of phase loading creates principal plane rotation, so the damage is spread over a larger volume than in-phase, when the damage is more concentrated on a small volume, which leads to faster failure fracture. Detailed explanation on the effect of loading path is described in Section 2.3.5.1. Under load controlled testing as used in this study, the maximum shear strain for total loading cycles is less in out-of-phase than in-phase. Therefore slower damage will occur in out-of-phase loading and results in increasing in fatigue life. Literature showed similar effects was achieved when studied biaxial fatigue under load controlled conditions (Nishihara and Kawamoto, 1945; Grubisic and Simburger, 1976; Sonsiono and Grubisic, 1985; Sonsino, 2001).

Analysis of the fatigue damage parameters in biaxial fatigue are similar to those in uniaxial fatigue, with a gradual reduction in secant moduli and increases in energy absorbed as the loading progresses. Monitoring the secant modulus and energy absorbed trends provides good comparisons of degradation in mechanical properties of the composite due to the fatigue damage with affects of various combined loads conditions and phase angle. Combined in-phase loads had the highest modulus reduction and greatest energy absorption per load cycle value in comparison to higher phase angles such as 60° or 90°. It was observed in uniaxial fatigue damage changes in modulus and energy indicated the on-set of failure in the composite. When compared to damage variations in biaxial fatigue, the specimens absorbed several times more energy above the initial value than fully reversed uniaxial tension-compression fatigue for a given load regime. The number of load cycles at the initiation of failure is in inverse correlation, first with levels of combined load then with the phase angle. For example for 25A25T, the threshold occurs after more cycles in comparison to other combined load such as 25A50T or 50A25T, secondly higher phase angle increases the threshold as can be seen when comparing 0° to 90°, or 30° with 90° phase angles.

Analysis lines showed that principal maximum stress (σ_{1max}), maximum shear stress (τ_{12max}) and Tsai-Wu (I_{Fmax}) have different degrees of correlation with number of cycles to failure, with the Tsai-Wu criterion giving the best fit. However the value is still low to be conclusively meaningful. Echaabi et al. (1996) reviewed a number of failure criterion for fibre composites and preferred to use the maximum stress criterion, as it is simpler and extensively used by researchers. However, the drawback of this method is it has a tendency to overestimate the failure stress. Fatemi (1987, 1988) shown that while maximum stress criterion can give good correlation for brittle materials, but is unreliable for low cycle fatigue where cyclic plasticity is involved.

Tanaka et al. (1998) showed that while principal stress is more useful to use in tension/compression failure criterion, under static combined stresses, Tsai- Wu failure criterion showed better correlation when used in the presence of tension/compression and shear stresses. They suggest that the stress combination, between the axial and shear stresses superficially affected the final failure of the composite. Fujii et al. (1995) however showed that while the Tsai-Wu criterion showed a good correlation in biaxial tension-compression/ shear fatigue failure for low cycle fatigue, that is less than 10^4, however a non-conclusive result was obtained for high cycle fatigue. This current study has both low and high cycle fatigue.

Thus, the Tsai-Wu criterion is not always useful for fatigue strength. In this study, the calculated fatigue strength in uniaxial tension-compression at 25A is higher than 25T, yet the experimental results indicated that 25T is more damaging than 25A. Calculated Tsai-Wu criterion showed 50A to be higher than 50T, yet experimental results for 50T showed it has fewer cycles to failure compare to 50A. This finding is similar that being reported by Tanaka and co-workers earlier, which indicated that Tsai-Wu criterion works best with the present of shear, as a shear parameter is used in the third part of the criterion equation. Thus, when only biaxial loading data was considered, a better best fit line achieved, increased R^2 from 0.71 to 0.88, presenting better estimation for fatigue failure for biaxial condition, this finding is similar with to the conclusion of Amijima et al. (1991). At same time, further examination of the Tsai-Wu criterion need to be examined under biaxial and multi-axial fatigue loading or

other method need to be use in order to describe better fatigue failure in this study.

The role of torsional loading in biaxial fatigue failure was also investigated by considering the fracture surfaces. Monotonic tensile, compression and torsional loading produced drawn split fibres, transverse buckled fibres and spiral cracks (Figures 4.3 to 4.7). These images were used as references images for all subsequent analyses involving biaxial fatigue (Figure 5.11 to 5.13). Figure 4.24 demonstrated that contributions of tensile and compressive loads are clearly evident on the fracture surface for a fully reversed axial load case (±25% of UTS) with the specimen forming kink bands due to transverse strains that lead to buckling. At ±50% of USS, the specimens failed with spiral splits parallel with the fibres, with fractured fibres and exposed TCP particles that indicated final failure due to the weak PLA-PLA-TCP interface. Superimposition of fully reversed in-phase at the same load level, 25A25T increased formation of spiral cracks with the disappearance of transverse fibre buckling as seen in compression and fully reversed uniaxial fatigue. This indicated that the final failure is occurred due to shear failure, and it occurred before formation of kink bands that might lead to compression buckling. This finding is consistent with the finding that at low stress level of 25T, the specimen has lower fatigue life in torsion compared to axial loading. The results of phase differences on the fatigue damage can be seen in Figure 5.12 for 90° out-of-phase. Less damage was observed with fewer longitudinal cracks in comparison to the in-phase. However, as the specimens displayed shear mode failure, it can be assumed that at the combined stress level, 25A25T, the fatigue live is dominated by shear both in-phase and out-of-phase. The resulting profile for combined axial and in-phase torsional loading at higher torque (25A50T) indicated that while the final failure is still dominated by the shear properties, more damage can be seen with a number of cracks parallel to the fibres (Figure 5.13). The dominance of the shear stress in the biaxial loading is due to the direction of the stress relative to the weaker part of the composite being applied as discussed in Chapter 4. In axial loading, the tensile or compression stresses are taken by the fibres, which is the strongest component of the composite. In torsion, there are two kinds of stresses generated, which are tensile stress and compressive stresses. During the loading, the compression will act to initiate twist by generate shear at

approximately 45° to the fibre direction and caused failure on the matrix which is the weakest part of the composite. Once the matrix fails, this will act as the weakest point in the composite for further crack propagation. Thus, it is often seen that shear strength of unidirectional fibre reinforced composite is lower than the axial strength.

Ritchie et al. (1985) suggested that the fracture surface of in-phase combined stress loading failure mechanism is mixed mode crack propagation as a result from stress loading on different axial and shear planes produced complex fracture surfaces of various helical shapes through the material structure or thickness. In out-of-phase loading on the other hand, they observed a transition from mode III to mode I fracture, as the crack was unable to penetrate the interior of the specimens. Jayaraman and Ditmars (1989) studied the differences in the fractures surface of iron under pure tension testing with preliminary cracks. They reported that the primary crack is perpendicular to the axis of the specimen, which contains the maximum shear planes. During in-phase loading, the principle axes and maximum shear stress are at a fixed orientation, however during out-of-phase, these two planes rotate through each cycle. Socie (1987) proposed that the direction and magnitude of the principal stresses change throughout each cycle during out-of-phase loading. This resulting in lower values of principal stress, maximum shear stress and Tsai-Wu values as calculated in Appendix A4. Thus in respect to this study, it is logical to assume that there is competing axial and shear failure mechanisms present during the biaxial testing. For example, for 25A25T in-phase the combination of the axial and shear stresses leads to reduction in the fatigue life when compared to 25A, however it is still in the region of the fatigue life of uniaxial 25T. While, the combination of the mixed mode crack of fibre kinking and shearing and rubbing might be present, however the shear stress produced during this testing might exceed the critical value in the torsional shear reduction that caused the reduction in shear secant modulus earlier than the threshold in the axial secant modulus. Therefore the final fracture failure of the specimens is controlled by the shear rather than axial as observed above.

On the microscopic scale, at 25A25T in-phase have similar number of longitudinal surface cracks as the fully reversed 50T uniaxial fatigue test. Under

pure torsional surface fracture, crazing was observed. Crazing normally begins with microvoid formation under tension, therefore it is sensitive to mutiaxial stress (Petrie, 1988). As the specimens are subjected to tension as well as shear, it is possible similar mechanisms occurred in the specimens when in tension and shear loading regions. As the cycles progress, the strain in the materials will increase, thus microvoids coalesce and form a continuous fracture surface. The fracture surface mode is controlled by the state of stress within the materials which influence the deformability of the material. Thus the change from uniaxial to biaxial state of stresses may alter the deformability of the specimen. SEM observation of the uniaxial and biaxial fatigue fracture agreed with this theory. The fracture surface of the biaxial loaded specimens contained more micro damage features, such as numerous fatigue striations, than were seen in uniaxial fatigue.

5.5 CONCLUSIONS

The fatigue life of biaxial fatigue loading is significant by influenced by superimposition of torque on the axial loading. In-phase loading produces more damage than out-of-phase loading. Fractography examinations also revealed that biaxial failure is dominated by the shear mechanism and fatigue–striated features were observed at stress levels of 25A as well as at 50A.

CHAPTER 6 - EFFECT OF COMPOSITE DEGRADATION ON FATIGUE PROPERTIES

6.1 INTRODUCTION

Most of the potential application of degradable composites in the field of biomaterials are not only subjected in cyclic loading, but are used in media that cause the material to degrade physically as well as mechanically. Therefore it is necessary to understand the effect of degradation on the strength retention of the composite in static as well as cyclic condition in order to ensure better design parameters for intended applications. The degradation rate of resorbable polymers depends on many variables, including manufacturing techniques and micro- and microstructural of the composite as well as environmental factors. To investigate this, a degradation study was carry out in phosphate buffered saline (PBS) solution for up to 20 weeks. Degradation was accessed by recording changes in wet and dry masses of the samples (giving information on fluid uptake and mass of the sample degraded), changes in pH of the saline solution, changes in modulus and strength in tensile, shear, fatigue life, secant modulus and energy absorbed in axial as well as in torsional.

6.2 METHODS

The specimens used for degradation study were compressed moulded at 150°C using the methods describe in section 3.2.3. The specimen were immersed in saline solution for up to 20 weeks as described in section 3.2.6, which at each immersion point, the specimens then were dried and wet as well as dried weight measured. Uniaxial fatigue testing was carried out at ±25% UTS (25A) and ±25% USS (25T) of the non-degraded specimen strength. Fatigue damage analysis was carried as describe in section 3.3.3 for fatigue life, reduction in secant modulus and increase in energy absorbed and fracture surface. All quasi-static and fatigue properties for the degradation samples then were compared with results from non-degraded specimens.

6.3 RESULTS

6.3.1 Weight and pH change

Figure 6.1 shows the change in pH of the PBS with degradation time. The pH stayed constant throughout the 20 weeks degradation period showing the buffering effect from the tricalcium phosphate on the pH of the acidic solution produced during the PLA degradation.

The fluid uptake of samples of PLA_{96} fibres in PLA_{70} matrix with TCP filler after immersion in PBS for up to 20 week is shown in Figure 6.2. There was gradual increase through the 20 weeks in vitro study period. However, the increase between each measurement period was not statistically significant. Figure 6.3 shows the percentage decrease in sample mass after drying, representing the mass of sample that has been lost by degradation following immersion in PBS with standard deviation. Compared to the initial mass loss in the first 8 weeks, the subsequent decreases in mass were not statistically significant until week 20. It can be seen that the fluid absorption and weight loss is relatively small with less than 2% and 1% respectively for all four periods of immersion. These compare well with the data from Bleach (2001), who reported that self-reinforced PLA filled TCP composite has slow degradation, increasing by less than 2% for fluid absorption and minimal weight change with less than 1% mass loss between 1 and 24 weeks.

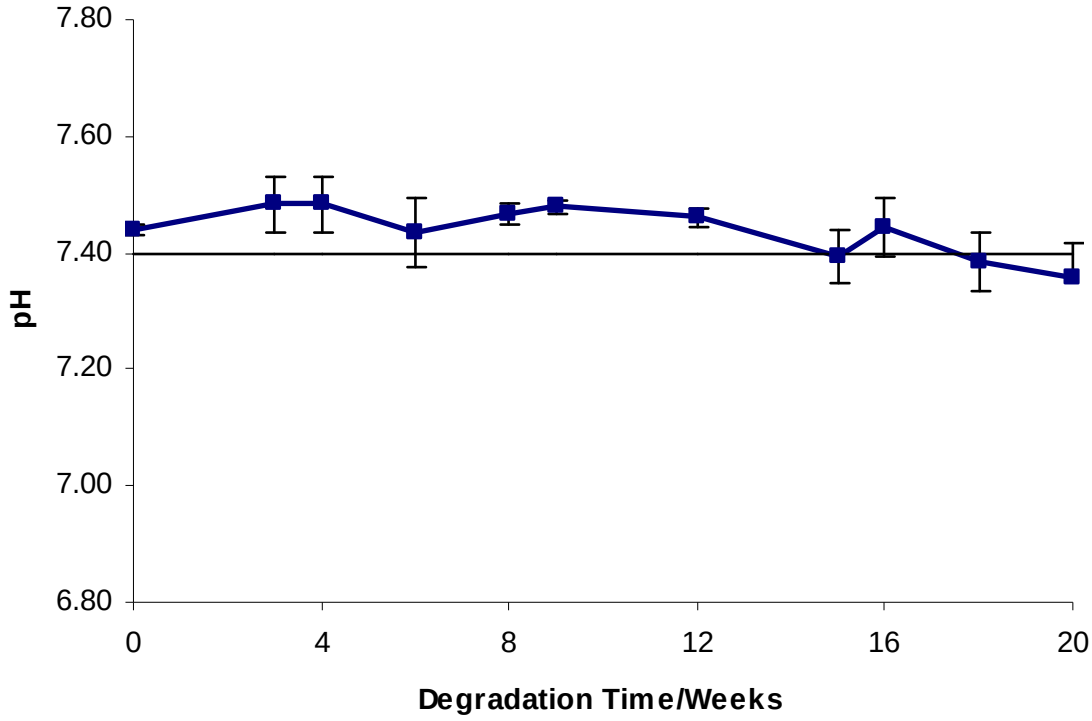

Figure 6.1 Change in pH of PBS versus degradation time for PLA-PLA-TCP composite. PBS was changed every three weeks (error bar indicate standard deviation, n=3-5).

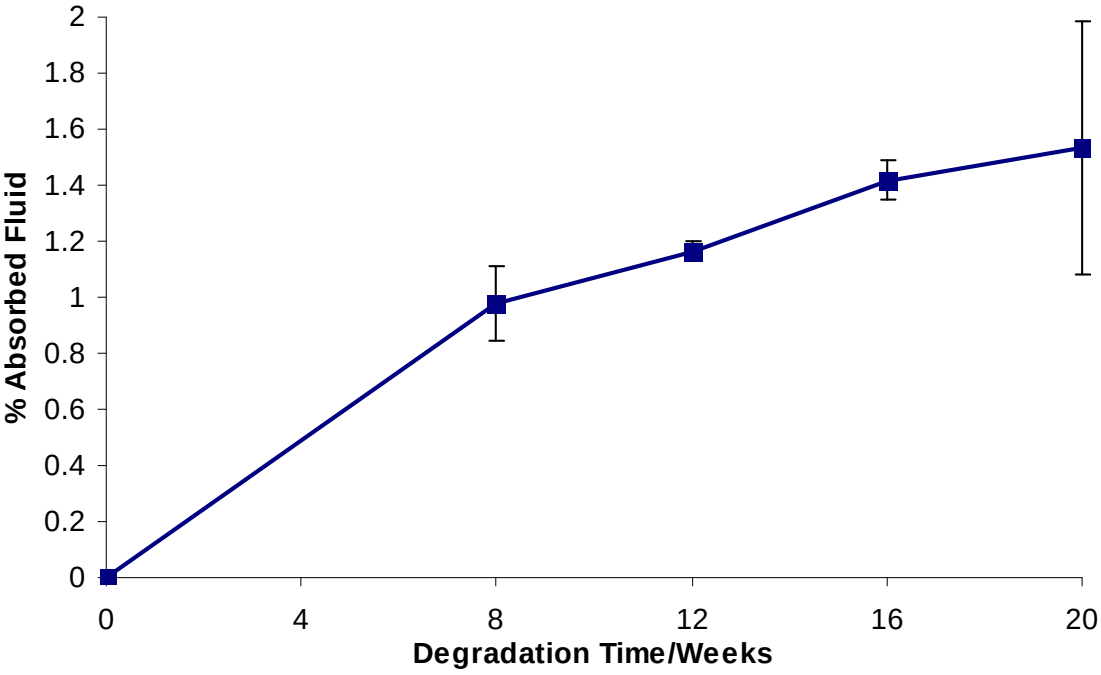

Figure 6.2 Percentage mass increase due to absorbed fluid versus degradation time for PLA-PLA-TCP composite (error bar indicate standard deviation, n=3-5)

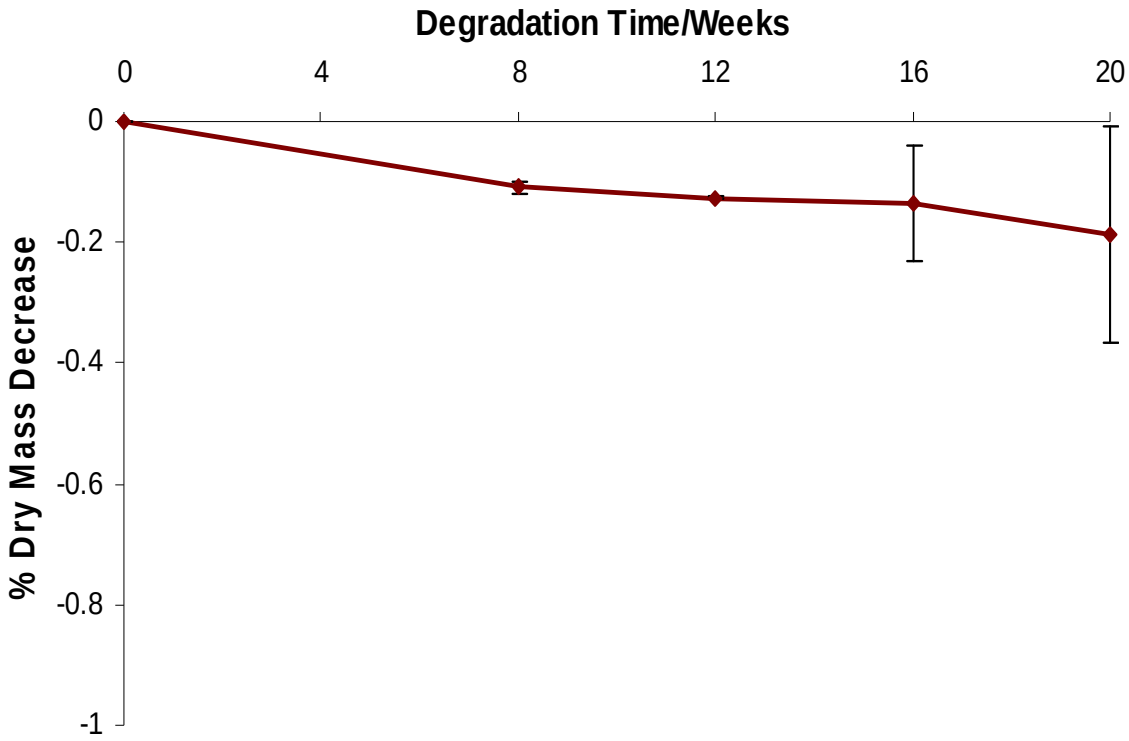

Figure 6.3 Percentage dry mass decrease versus degradation time for PLA-PLA-TCP composite (error bar indicate standard deviation, n=3-5)

6.3.2 Monotonic test

Table 6.1 and Figures 6.4 and 6.5 show how the axial modulus, ultimate tensile stress, shear modulus and ultimate shear stress changed over the 20 weeks degradation. In comparison to the non-degraded specimens, the tensile modulus remains virtually unchanged for the first 8 weeks of degradation, after which time the modulus decreased significantly at week 12 ($p<0.05$) and week 16 ($p<0.01$). After 20 weeks of degradation, the modulus of the degraded samples was significantly ($p<0.01$) reduced approximately by 20% compared to the non-degraded specimens. The shear modulus however remained virtually unchanged during the 20 weeks degradation period. This finding is consistent with those reported by Bleach et al. (2000) for a similar composite.

The ultimate tensile stresses showed a constant rate of strength loss throughout the 20 weeks degradation. Initially, when compared to the non-degraded specimens, the strength of the degraded specimens remained unchanged for the first 8 weeks of immersion, followed by a slight reduction after week 12. The strength started to reduce significantly ($p<0.01$) after week 16 and 20 but was

still comparable to that of cortical bone. At the end of the 20 weeks degradation, the strength of the composite was 62% of the initial value. In comparison to the axial properties, the effect of the degradation on the torsional properties was minimal. No significant loss was observed in shear strength throughout the 20 weeks degradation period, similar to the trend in the shear modulus shown earlier. Full statistical analysis is shown in Tables 6.2 and 6.3.

Table 6.1 Axial and torsional moduli and strength properties of PLA-PLA-TCP composite degraded for up 20 weeks. Values are means of 5 samples (standard deviation).

	Axial		Torsional	
Degradation Time/weeks	Axial Modulus/ GPa	Ultimate Tensile Strength (MPa)	Shear modulus/GPa	Ultimate Shear Strength/MPa
0	6.47 (0.65)	144.00 (11.58)	1.37 (0.16)	26.49 (4.96)
8	6.37 (0.07)	124.37 (11.52)	1.31 (0.04)	28.72 (2.77)
12	5.77 (0.02)	116.96 (19.28)	1.24 (0.07)	26.88 (4.65)
16	5.22 (0.13)	98.78 (2.58)	1.28 (0.01)	27.71 (4.85)
20	4.99 (0.05)	89.55 (2.46)	1.27 (0.05)	24.98 (2.22)

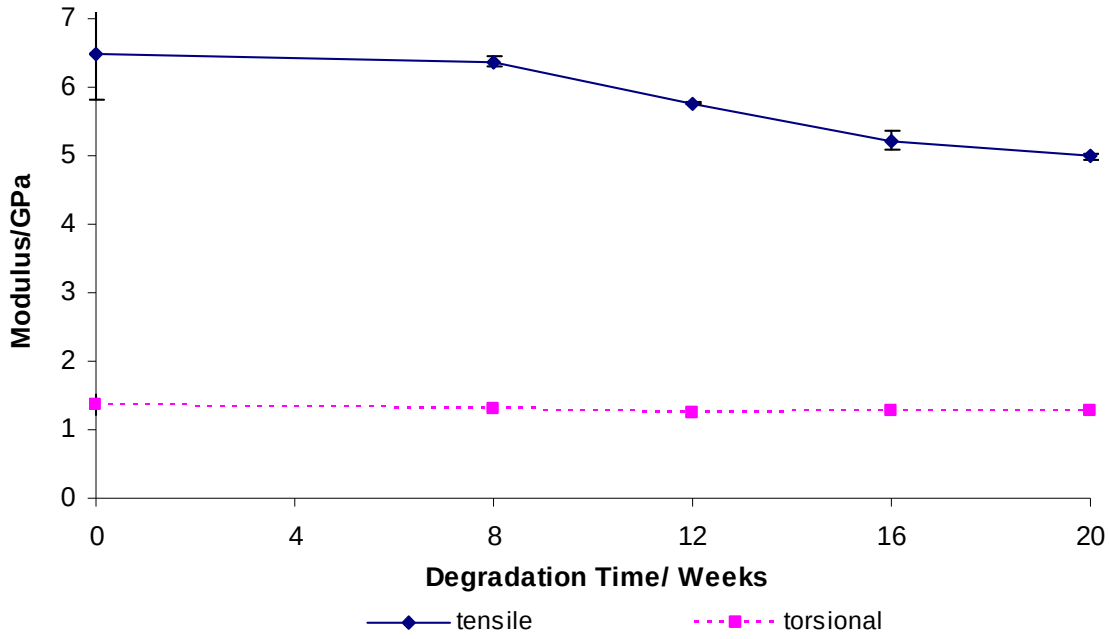

Figure 6.4 Modulus versus degradation time (all tested at 37˚C in saline) for PLA-PLA-TCP composite (error bar indicate standard deviation, n=3-5)

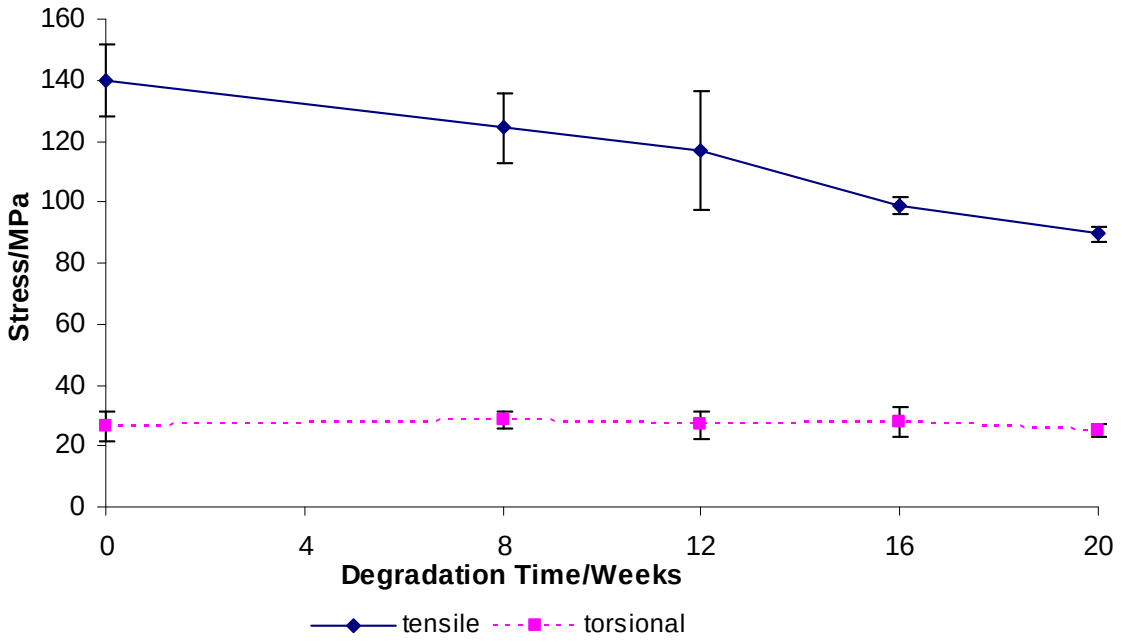

Figure 6.5 Tensile and torsional ultimate strength versus degradation time (all tested at 37˚C in saline) for PLA-PLA-TCP composite (error bar indicate standard deviation, n=3-5)

Table 6.2 Levels of significance for tensile modulus and ultimate strengths over the 20 weeks degradation period

Tensile modulus						Tensile strength					
	0	8	12	16	20		0	8	12	16	20
8	n.s					8	n.s				
12	*	*				12	n.s	n.s			
16	**	*	*			16	**	*	n.s		
20	**	**	*	*		20	**	**	**	*	

Note: n.s = p>0.05, * = 0.05>p>0.01, ** = 0.01>p>0.001, *** = p<0.001

Table 6.3 Levels of significance for shear modulus and ultimate shear strengths over the 20 weeks degradation period

Shear modulus						Shear strength					
	0	8	12	16	20		0	8	12	16	20
8	n.s					8	n.s				
12	n.s	n.s				12	n.s	n.s			
16	n.s	n.s	n.s			16	n.s	n.s	n.s		
20	n.s	n.s	n.s	n.s		20	n.s	n.s	n.s	n.s	

Note: n.s = p>0.05, * = 0.05>p>0.01, ** = 0.01>p>0.001, *** = p<0.001

6.3.3 Fatigue Life

The fatigue testing on the degraded specimens were carried out at ±25% UTS and ±25% USS of the non-degraded specimen. Due to the reduction in mechanical properties, ±25% UTS for non-degraded specimens now equated to about 38% UTS after 20 weeks degradation. Figure 6.6 shows the fatigue life for ±25% UTS at 37°C after different degradation periods up to 20 weeks in saline solution. The fatigue lives of the degraded specimens are fairly unaffected at the beginning of the degradation period. Compared to the fatigue lives for non-degraded specimens, the fatigue lives after 8 and 12 weeks in saline showed non-significant reductions in the number of cycles to failure. However, the number of cycles was significantly reduced ($p<0.01$) to 298,899 cycles after 16 weeks and by week 20, the fatigue lives showed a further significant reduction ($p<0.01$) to 197,145 cycles.

The fatigue lives of non-degraded and degraded specimens tested at ±25% USS are shown in Figure 6.7. The torsional fatigue lives of the degraded specimens were retained up to week 8. Small reductions in fatigue lives were observed at week 12 to the end of 20 weeks degradation period but none was statistically

significant. This indicated that torsional fatigue is less affected by the degradation activity compared to axial fatigue. In summary, the degradation in number of fatigue lives results is similar with the alteration in static properties with respect to the effect of the degradation activity after immersion in saline solution. While the modulus and tensile strength drop slightly faster compared to axial fatigue life, the shear modulus and ultimate shear strength was minimal so the results for the shear fatigue are as expected. This leads to the conclusion that immersion in saline solution at 37°C affects the axial fatigue behaviour of the self-reinforced PLA composite more than the torsional.

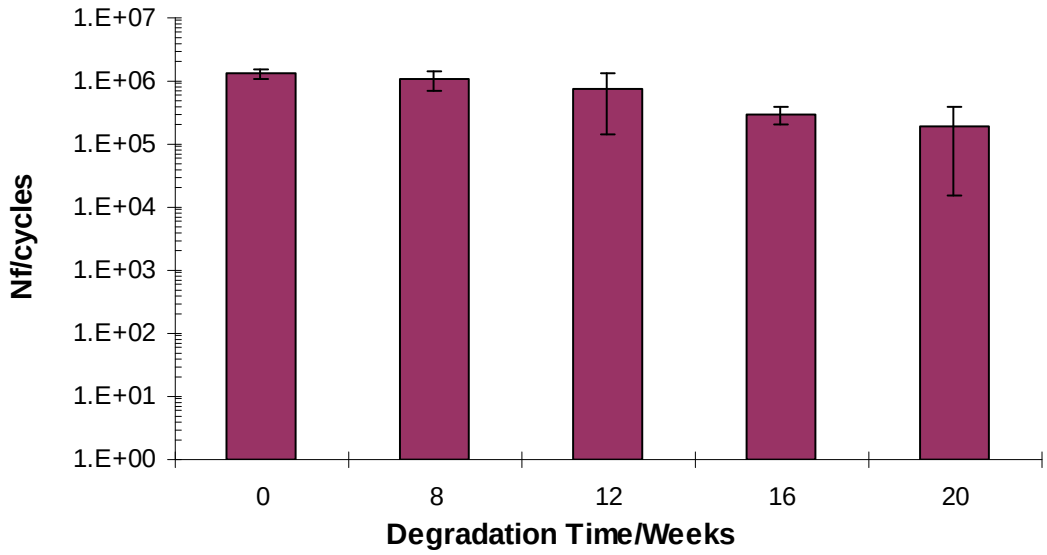

Figure 6.6 Fatigue lives of non-immersed and immersed specimens tested at ±25% UTS fully reversed tension-compression for PLA-PLA-TCP composite (error bar indicate standard deviation, n=3-5)

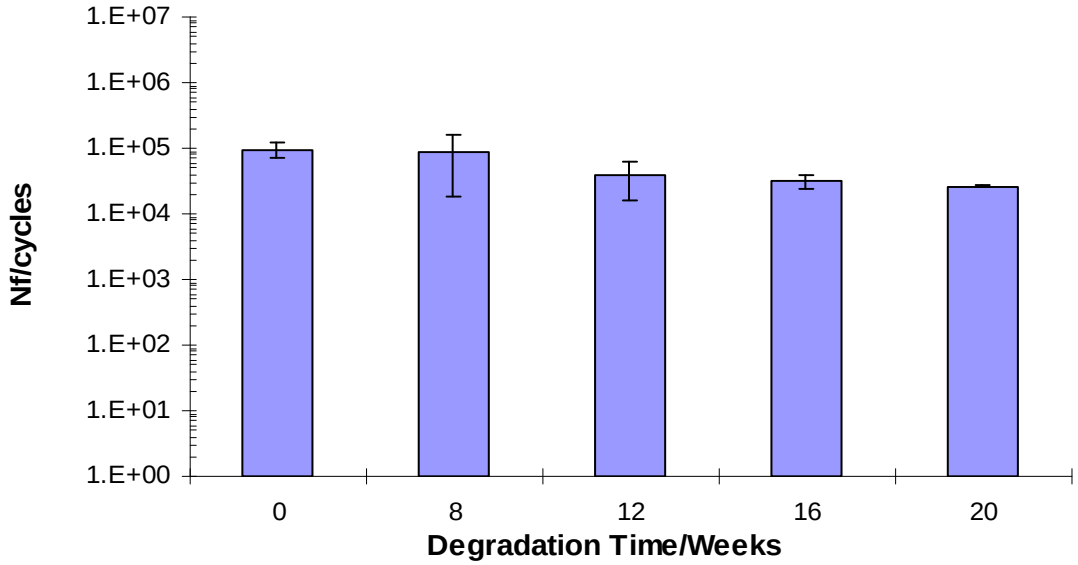

Figure 6.7 Fatigue lives of non-immersed and immersed PLA-PLA-TCP tested ±25% USS fully reversed torsional for PLA-PLA-TCP composite (error bar indicate standard deviation, n=3-5)

6.3.4 Analysis of Fatigue Damage

The variations in secant modulus and dissipated energy during ±25% UTS fatigue of 8, 12, 16 and 20 weeks degraded specimens, together with non-degraded specimens, are shown in Figure 6.8. It can be seen that the non-degraded materials have higher modulus and lower dissipated energy compared to the degraded specimens throughout the fatigue process indicating that they have higher fatigue resistance. In comparison with the non-degraded specimens, specimens that underwent 8 to 12 weeks immersion showed similar behaviour. The modulus showed slow reduction till 10^5 cycles, before the reduction become accelerated. Similar behaviour was observed in the energy absorbed pattern. The energy absorbed increased gradually before becoming apparent after 10000 cycles.

The modulus for 16 and 20 weeks degraded specimens reduced in a similar gradual rate but the modulus reduction become more apparent earlier than for the first 2 immersion periods, which were after 10^5 and 10^4 cycles respectively. The initial values of secant modulus observed after these last two degradation periods were also slightly less than after the 8 and 12 weeks degradation periods. Having said that, the reduction in the secant modulus showed a similar trend to the tensile modulus obtained from quasi-static testing, with exception of the secant modulus in week 8. While for quasi-static testing, there was no

change in modulus up to week 8, in fatigue tests, the secant modulus reduced slightly but not significantly from week 0 to week 8 of the degradation period. This is probably due to the effect of compression loading as the fatigue tests were carried out in fully reversed tension-compression direction and the static modulus was only tested in tensile loading. As number of cycles progress, increases in specimen damage were observed through increased of energy absorbed. The damage in the structure of the specimens become more apparent as early as 100,000 and 50,000 cycles for specimens immersed for 16 and 20 weeks respectively.

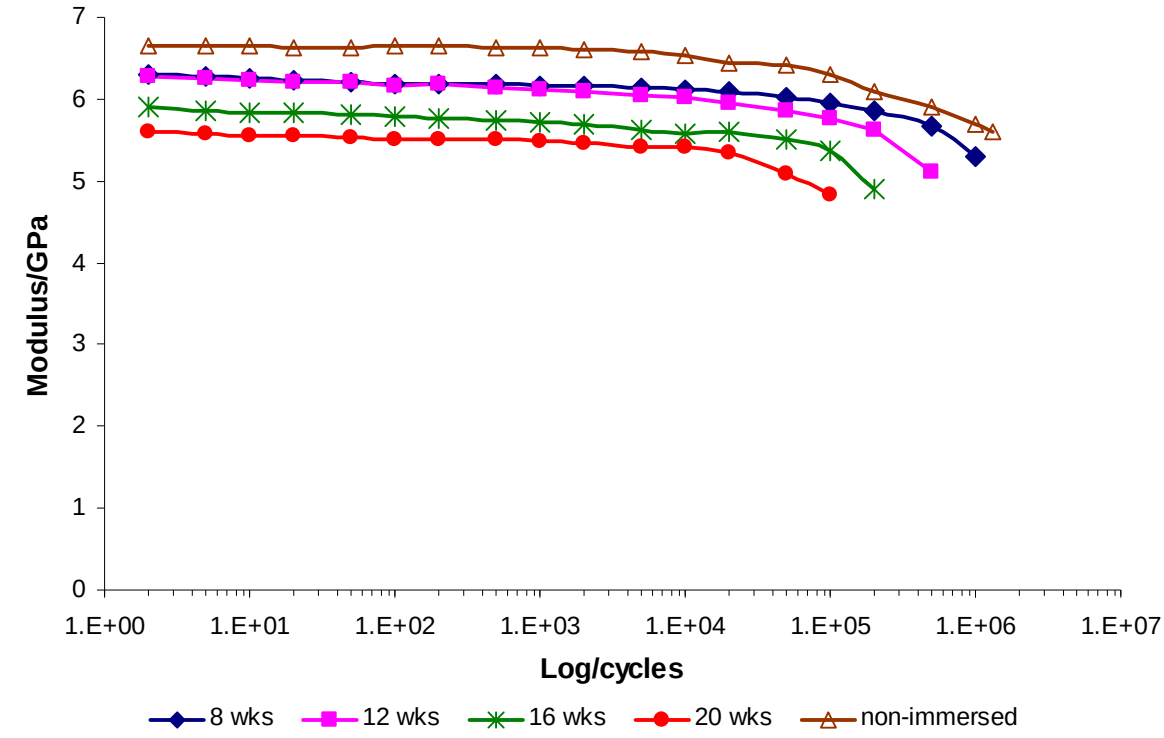

(a)

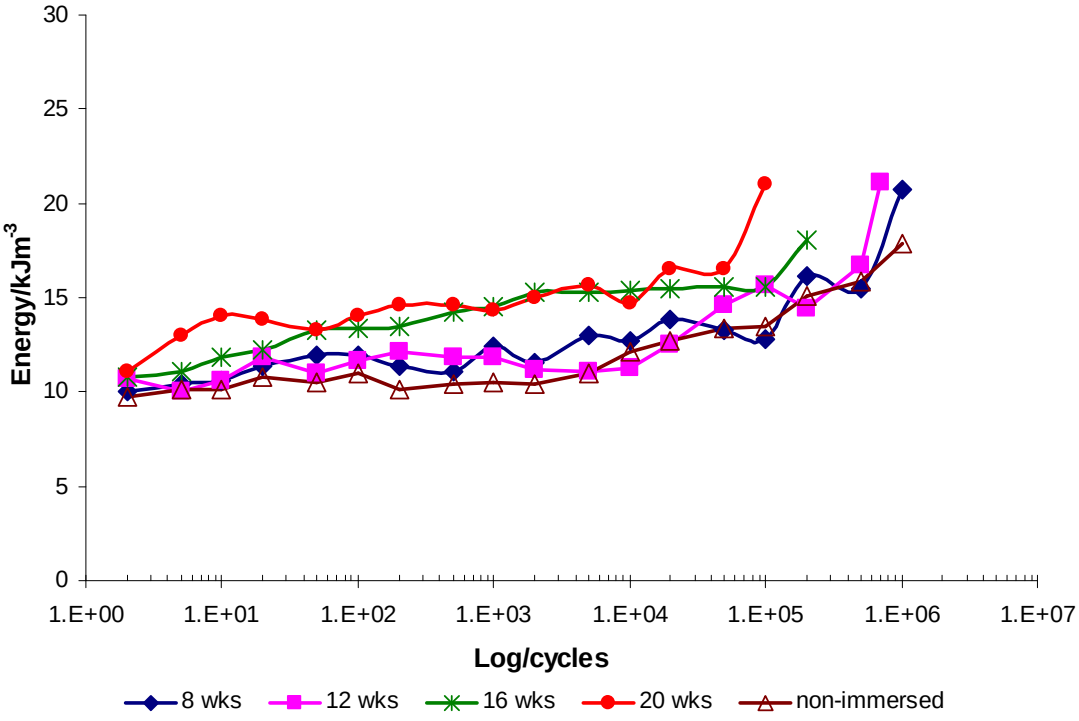

(b)

Figure 6.8 Fully reversed tension-compression ±25% UTS uniaxial fatigue of non-immersed and immersed specimens: comparison a) axial secant modulus b) axial energy absorbed

The fatigue damage characteristics of ±25% USS fatigue after 8, 12, 16 and 20 weeks degradation are illustrated in Figure 6.9. All the degraded specimens have lower initial secant modulus and higher energy absorbed values compared to the non-degraded specimens indicating that more damage was experienced by the specimen's structure during the fatigue test. This indicates the effect of *in vitro* degradation on the materials structure as well as mechanical activity during the test. The modulus of the specimens for 8 and week 12 weeks degradation was retained up to 1000 cycles and the reduction became more apparent thereafter. This result showed that severe damage had already initiated at this stage, in parallel with the increased energy absorbed at the same time point. The fatigue damage in specimens after 12 weeks degradation period was slightly accelerated compared to 8 weeks as indicated by higher level of energy absorbed as early from 2000 cycles. However, when compared to the 16 weeks and 20 weeks degraded specimens, the reduction in the mechanical properties due to the fatigue damage after 20 weeks degradation is slower than after 16 weeks degradation time. Specimens soaked for 20 weeks managed to retain their modulus up to 10,000 cycles to failure before the damage become obvious. The amount of the energy absorbed in the 20 weeks degraded specimen was increased after 2000 cycles, indicating the damage in the composite system had started but the composite still mange to retain its stiffness.

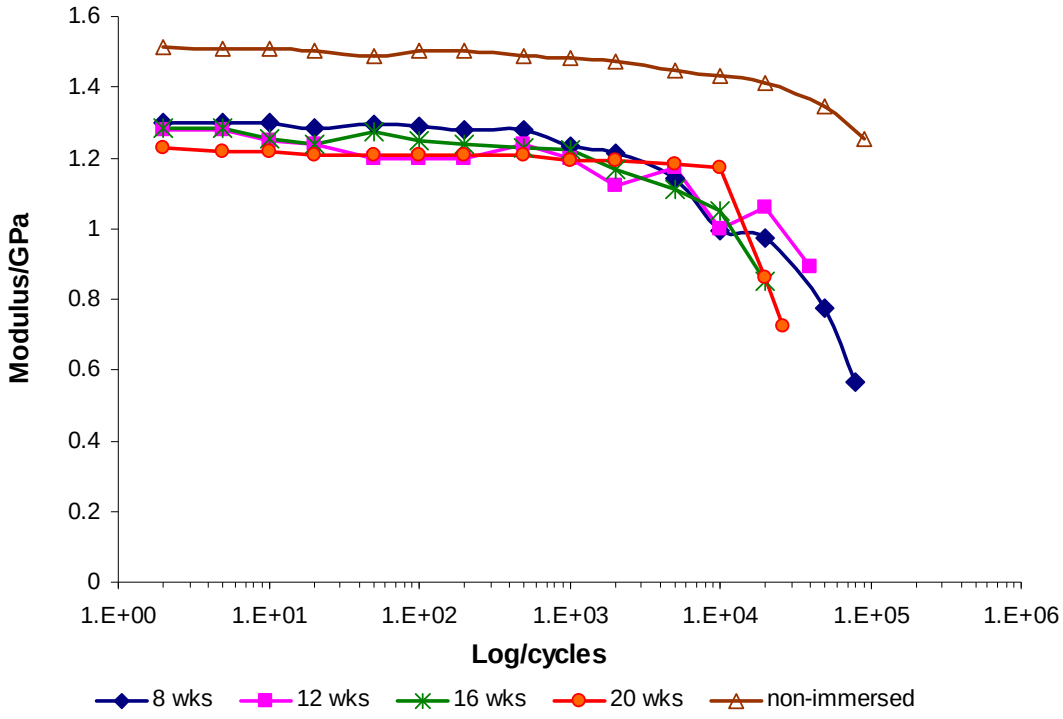

(a)

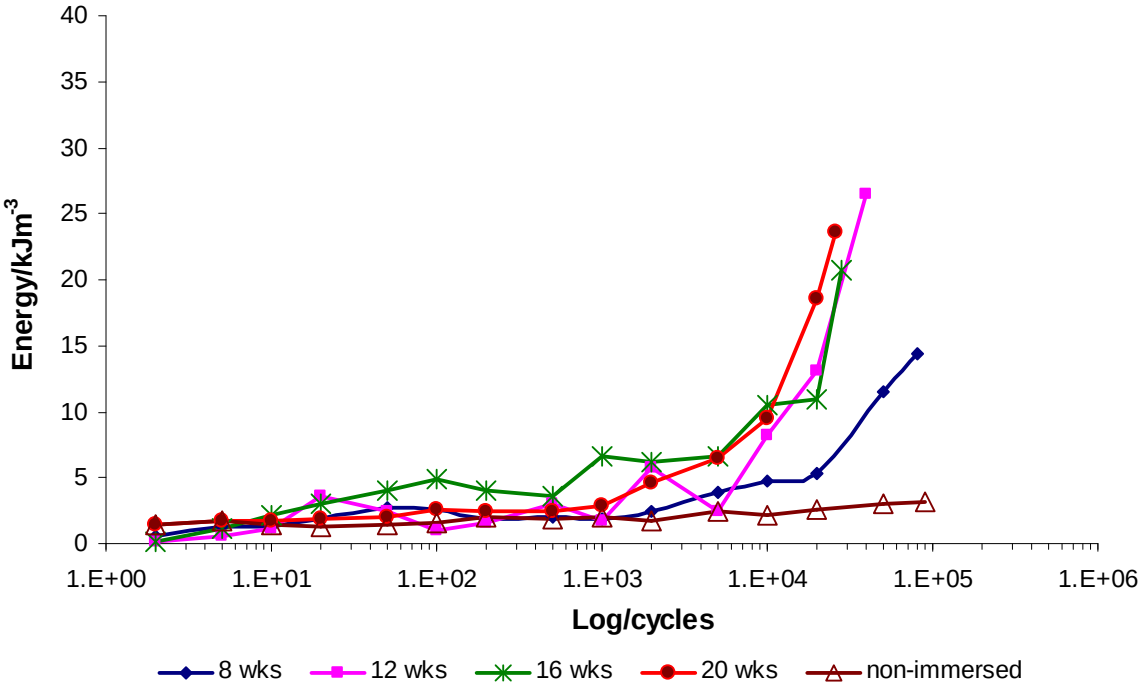

(b)

Figure 6.9 Fully reversed torsional ±25% USS uniaxial fatigue of non-immersed and immersed specimens: comparison a) torsional secant modulus b) torsional energy absorbed

6.3.5 Fractography

Figure 6.10 shows the surface fracture after 8 weeks immersion and tested at ± 25% UTS fatigue. In parallel with the strength and fatigue result, the specimen fractured in a similar manner to the non-degraded specimen shown in Figure 4.19 in Chapter 4. Figure 6.10a shows that the fibres fractured with staggered fracture surfaces in bundles indicating slow crack propagation. Figure 6.10b shows that good adhesion between the fibre and the matrix can be seen indicating that the matrix is still mainly intact after 8 weeks immersion in saline which could be the reason for good strength retention achieved, while the presence of tricalcium phosphate on the fibres surfaces indicated some degradation had occurred in the matrix-fibre interface region (Figure 6.10c).

After 16 weeks degradation, the degradation or loss of material between the fibre bundles has become more apparent (Figure 6.11a), indicating that the matrix degraded faster than the fibres, and the reduction in strength is due to loss of matrix. Figure 6.11b shows split damage to the single fibre inside the specimen resulting from the fatigue damage, indicating an increase in brittleness of the fibre due to degradation. The specimen failed in the compression region as indicated by the buckled fibres at the end of the fatigue test (Figure 6.11c).

Further degradation periods caused more material loss and damage to the specimen structure as indicated by reduced fatigue lives. This result is supported by the fractography study of the fractured surface after 20 weeks of degradation as shown in Figure 6.12a. In comparison to the non-degraded specimen and 8 weeks immersion specimens, 20 weeks soaking in saline solution caused further loss of the matrix, as the fibres fractured as individual strands rather than in bundles, indicating severe degradation at the interface (Figure 6.12b). Closer inspection at the bottom of the failure surface showed clear gaps between the fibre/matrix with fewer TCP particles attached to the fibres in comparison to Figure 6.10c, indicating reduced adhesion at the fibre/matrix interface. This further supported the argument that more damage occurred in amorphous materials such as the matrix at the longest degradation periods.

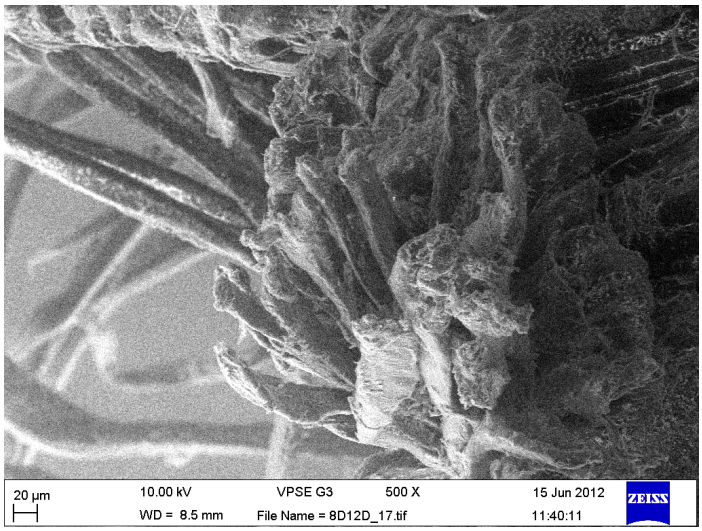

a)

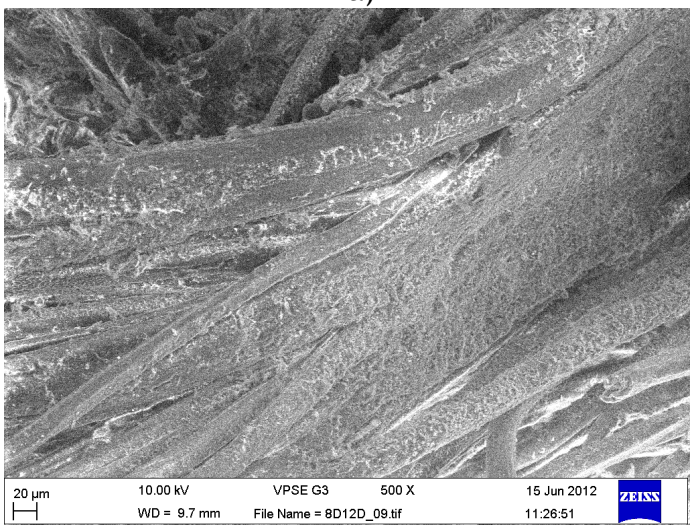

(b)

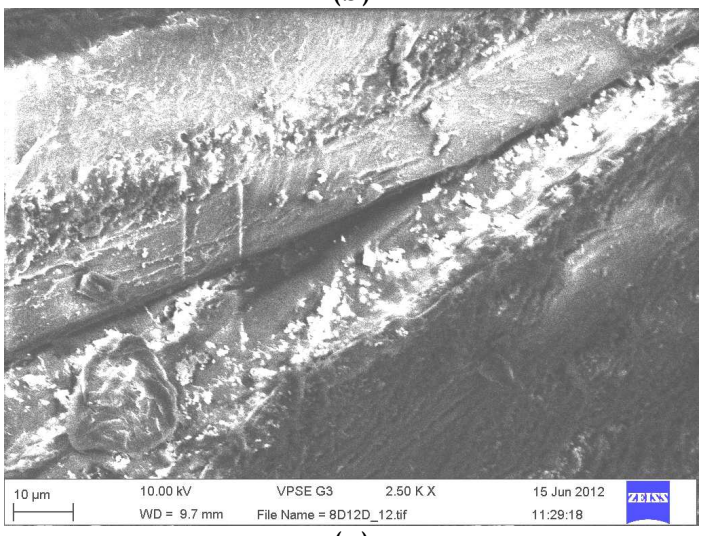

(c)

Figure 6.10 Fracture surfaces of 8 weeks immersed specimens subjected to tension-compression ±25% UTS fatigue

a) drawn fibres with staggered fracture surfaces in bundles; (b) matrix around the fibres and (c) TCP particles on the fractured matrix/fibres interfaces (scale bars= (a)&(b) 20µm and (c) 10µm)

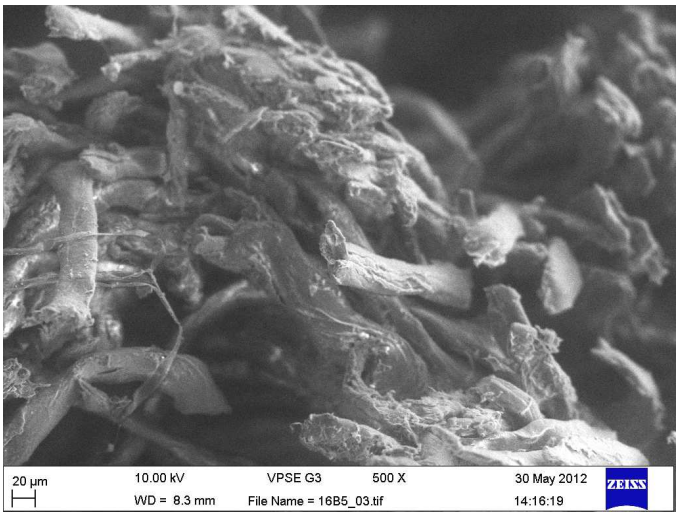

(a)

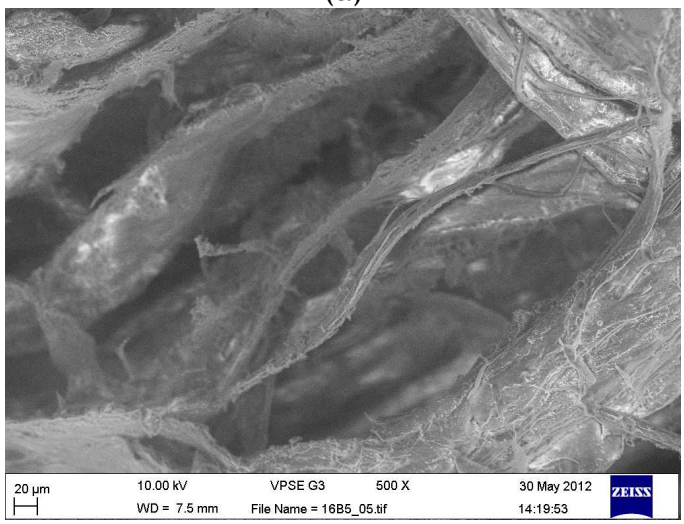

(b)

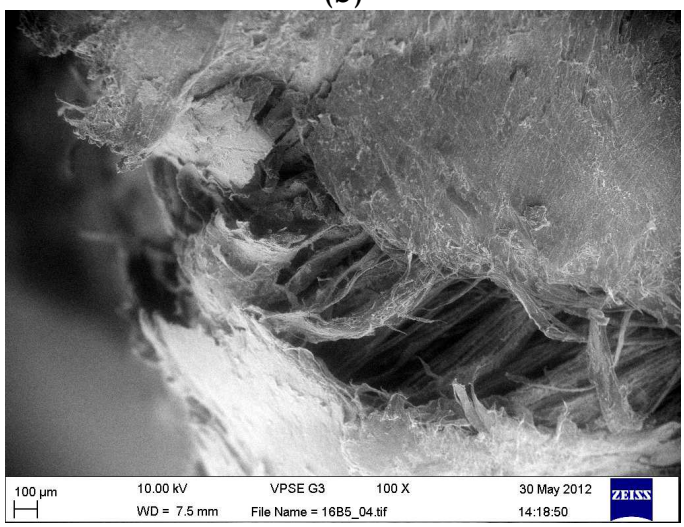

(c)

Figure 6.11 Fracture surfaces of 16 weeks immersed specimens subjected to tension-compression ±25% UTS fatigue

(a) degradation of materials between the bundles of fibre near the specimen surface; (b) split of fibres inside the specimen (c) buckled fibres (scale bars= (a)&(b) 20µm and (c) 100µm)

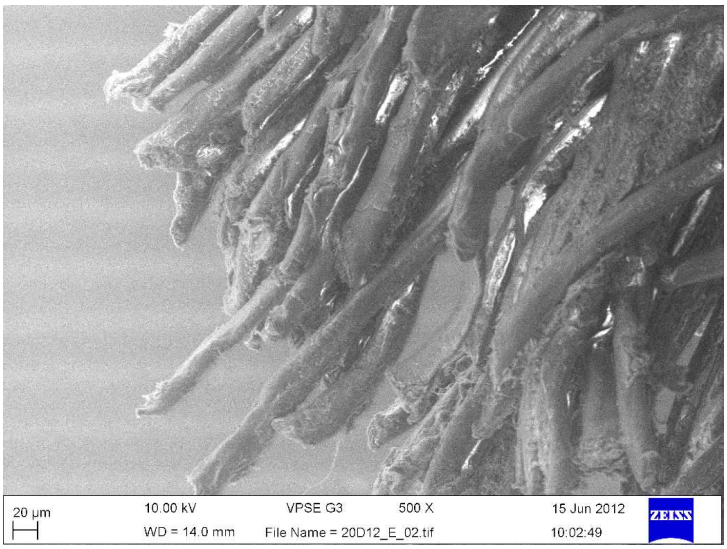

(a)

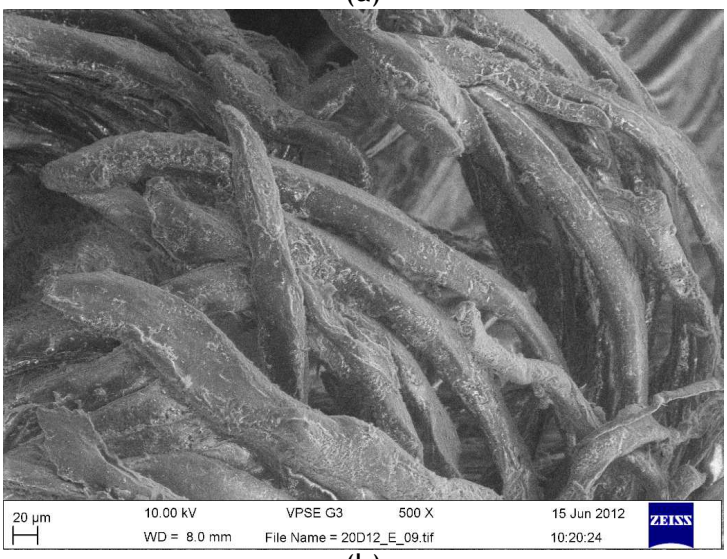

(b)

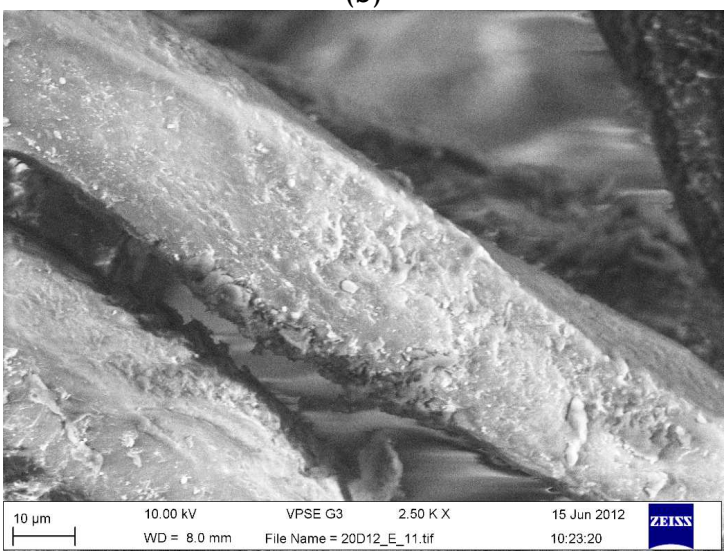

(c)

Figure 6.12 Fracture surfaces of 20 weeks immersed specimens subjected to tension-compression ±25% UTS fatigue

a) fibre fracture at beginning of facture path; (b) buckled fibres and (c) closer view of fracture fibre (scale bars = (a) &(b) 20µm; (c) 10 µm)

Figures 6.13 and 6.14 show the fatigue damage observed at ±25% USS after immersion in saline solution for 8 and 20 weeks respectively, similar to the non-degraded specimens (Figure 4.26). The materials did not fracture into two separate pieces at the end of fatigue testing indicating the ductile nature of the fibres. The failure mechanism is splitting parallel to the fibre direction as shown in Figures 6.13b and 6.14b, exposure of the TCP particles suggest that the filler particles had detached from the drawn PLA fibre and final fracture occurred due failure of the fibre-matrix interface. The fracture surface was similar to the non-degraded specimens as discussed in detail in Chapter 4 and reviewed by Jelf and Fleck (1994). However, the fracture surface of 8 weeks degraded specimen appeared rougher and with visible vertical cracks formation (Figure 6.13b) in comparison to specimen degraded at 20 weeks. The differences in physical appearance probably due the water uptake during the immersion that caused the matrix to swell and after 20 weeks degradation, the outer machined surface layer of the specimen has eroded away leaving behind a smoother surface.

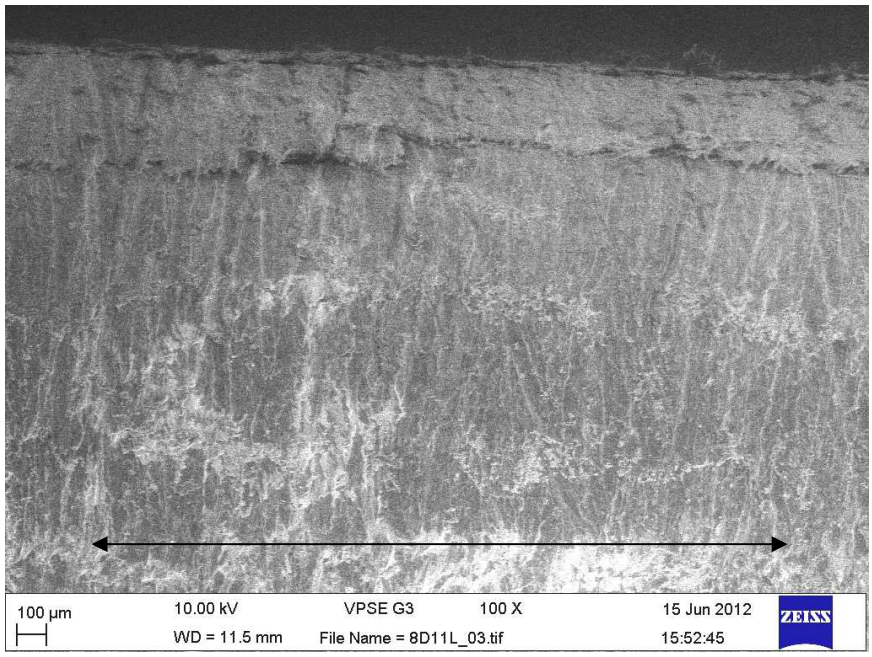

(a)

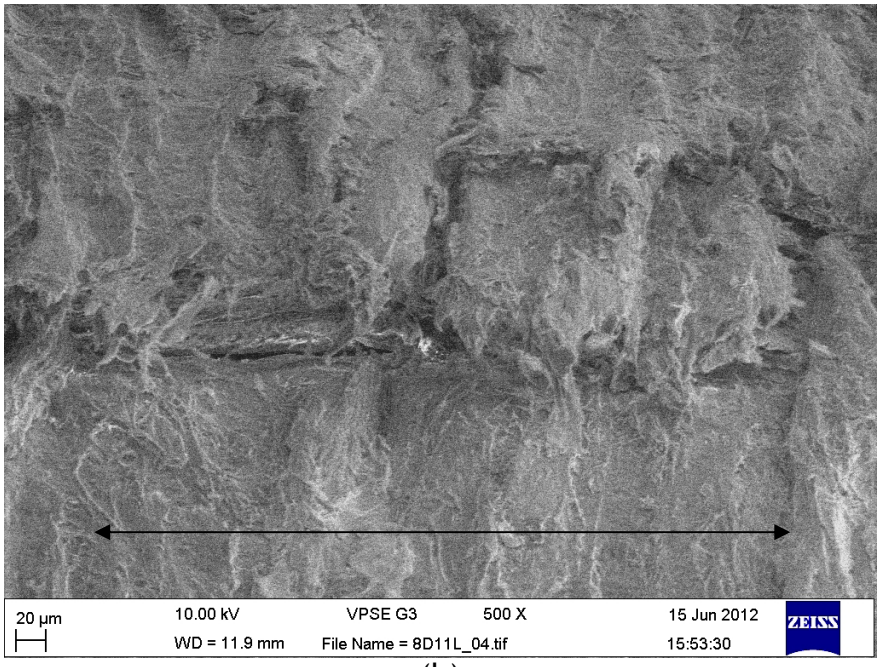

(b)

Figure 6.13 Fracture surface of 8 weeks immerse subjected to torsion ±25% USS fatigue

(a) general view of matrix crack parallel to main axial fibre orientation, (b) vertical crack with exposed TCP particles (scale bars = (a) 100µm; (b) 20µm. Arrow indicate fibre direction)

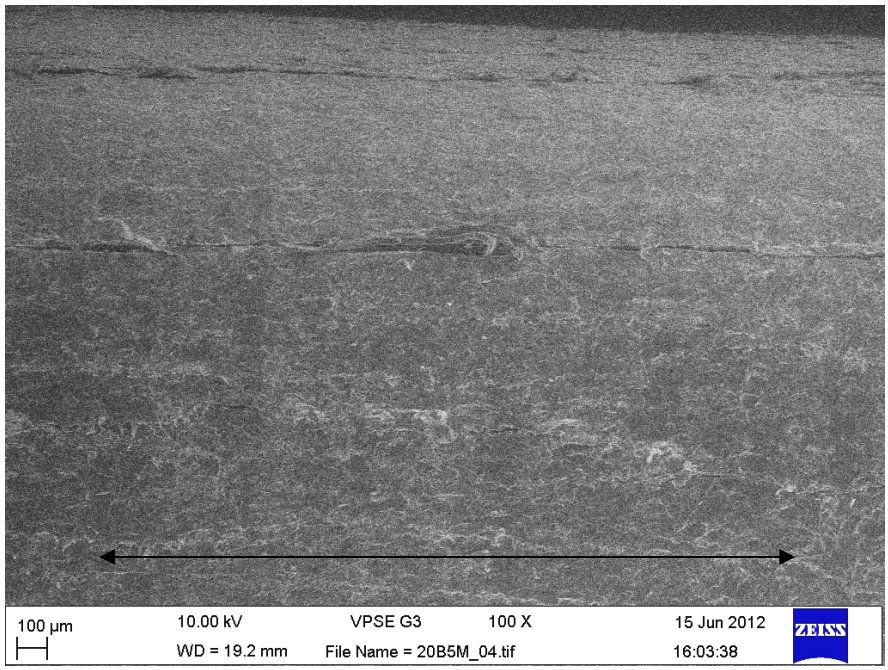

(a)

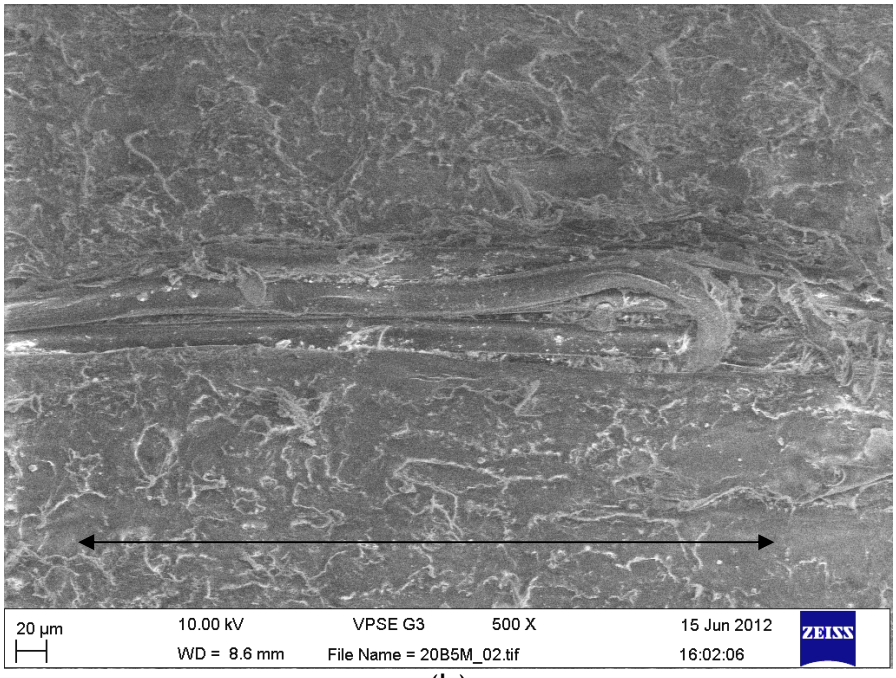

(b)

Figure 6.14 Fracture surface of 20 weeks immerse subjected to torsion ±25% USS fatigue

(a) general view of matrix crack parallel to main axial fibre orientation, (b) fibre fractured of with exposed TCP particles (scale bars = (a) 100µm; (b) 20µm. Arrow indicate fibre direction)

6.4 DISCUSSION

Polymer degradation is the first step of the erosion process and can be estimated by measuring the reduction in mechanical properties. The complete loss of the polymer is known to take substantially longer than the loss of the tensile or shear strength. During the first phase, aqueous solution penetrates the polymer, followed by hydrolytic degradation, converting the very long polymer chains into shorter water-soluble fragments, which can be regarded as a reverse polycondensation process. For example, PLA becomes soluble in water for molecular weight Mn below $\approx$ 20,000(g/mol) (Zhang et al., 2008).

In practice, when the PLA matrix starts to degrade, the pH of the buffer solution will be slightly acidic due to the release of the acidic degradation products from the poly-α-hydroxyacids during the hydrolysis process (Li and Vert, 1999; Middleton and Tipton, 2000). Niemala (2010) and Nimela et al. (2005) showed that with addition of osteoconductive filler materials such as bioactive glass (BaG) and β-tricalcium phosphate the pH values of the buffer solution remained neutral for longer. A similar finding was shown in this study (Figure 6.1). This is thought to be a neutralizing effect produced when tricalcium phosphate releases phosphates ions into the surrounding saline solution during the degradation process. The phosphates ions help to neutralize the acidic degradation product by binding with the hydrogen ions from the solution and acting as an alkali (Ara et al., 2002; Schiller et al., 2003). Bleach et al. (2002) showed a similar neutralizing effect when immersing similar PLA-PLA-calcium phosphates composites in SBF solutions during their in vitro degradation study. Additional similar findings have also been reported for other osteoconductive bioceramics in bioresorbale polymer composites (Kikuchi et al., 2002; Maquet et al., 2004; Li and Chang, 2005 and Zhou et al., 2009).

Niemelä and co-workers (2005, 2007 and 2010) showed that the addition of the osteoconductive filler materials such as BaG and TCP increased the water absorption in PLA based composites in the early stages of their 110 weeks degradation study of unfilled and filled self-reinforced composite. This was thought to be due to the porous surface of the filler. They argued that the interface between the matrix polymer and fillers particles allows the water to

penetrate the structure. However, the presence of osteoconductive filler reduces the degradation rate when compared to the unfilled polymer.

As all specimens in this study were reinforced with approximately 12 wt.% tricalcium phosphate, the effect of filler content on the physical properties was not being investigated, the issue is well reported elsewhere. The preliminary results showed that water absorbed and dry mass loss in this study was minimal for the 20 weeks degradation period (Figure 6.2). When compared the progress of mass loss to the water uptake (Figure 6.3), the polymer mass seem to decrease slower than the water uptake. This lag normally occurs in degradable polymers in vitro (Li et al., 1999; Bleach et al., 2000) as well as in vivo (Matsusue et al., 1992). This phenomenon is caused by a delay in the leaching out of low molecular weight fragments produced during hydrolysis as degradation occurred preferentially in the centre of the polymer (heterogeneous degradation). Although the fibre and calcium phosphate reinforcements should help in the diffusion process of hydrolysis products to the surface of the composite, this was not large enough to produce any significant changes until around eight weeks of degradation.

The slow physical degradation results indicated that the composites were still in the first phase of hydrolytic degradation even after 20 weeks. As this occurs in the amorphous regions, there was no apparent loss in the physical properties, as the crystalline regions hold the structure together, as well as minimum water intake and reduction in dry mass occurred. Niemelä (2005) discussed that first phase degradation of self-reinforced poly-L-D-lactide with L:D dimer ratio 96/4 composite lasting approximately about 52 weeks. They reported that there was no significant increase in water absorption in both unfilled self reinforced composite (1% water intake) and filled 20 wt.% of TCP-polymer composite (5% water intake) in the first 20 weeks of degradation. By 52 weeks, the water absorbed had increased to 4% and 11% respectively. The dry mass of both composites remained unchanged until after week 52, thereafter the mass loss increased, water absorption decreased rapidly indicating that the composite was entering the second stage of hydrolytic degradation where the crystalline regions started to fragment. Recently, Han et al. (2012) reported similar results

when studying water absorption and mass loss during in vitro degradation of semicrystalline PLLA composite.

Niemelä et al. (2008) reported faster water absorption and mass loss rate when using PLA based polymer with L:D dimer ratio 70/30, after approximately 48 weeks in comparison to PLA 96/4. The different alteration time in the physical properties of PLA 96/4 and PLA 70/30 are due to the different amounts of the amorphous and crystalline regions in the polymer. Previous studies by Li (1991), Vert et al. (1991) and recently Daculsi et al. (2011) summarized that PLA 70/30, being an amorphous material has greater tendency for fast degradation as it has few crystalline regions holding the polymer structure as in comparison to semicrystalline poly-l-dl-lactide (96/4), that is the material used for the fibres.

Strength retention of the composite during the degradation process is a major factor in designing an implant for bone fixation in order to ensure primary stability of the fracture. Cancellous bone normally heals within 8-12 weeks, although the healing process can be delayed for many reasons. A tibial fracture wills typically take 16 weeks to heal but again the healing process can be delayed by many factors (Kenwright et al., 1991; Richardson et al., 1994). Therefore, good strength retention of the composite in longer degradation environment duration is desirable for slower fracture healing (Claes et al., 1996).

The modulus and strength retention in vitro of PLA-PLA-TCP composite from tensile and torsion tests are presented in Figure 6.4 and 6.5 respectively. The composite was able to retain its initial tensile strength and stiffness up to approximately 12 weeks immersion in PBS. Bleach et al. (2000) showed in their early degradation study of similar composites, there was initial increase in the flexural modulus after one week's degradation in SBF followed by slight reduction at week 4 followed by non-significant reduction up to week 12. This phenomenon possibly due to leaching of the low monomer or low molecular weight fragments that act as a plasticizer, so their removal would increase the flexural modulus. Contrary to this finding, Felfel et al. (2011) reported a sudden decrease in flexural and compressive strength after 3 days immersion in PBS which could have been the due to plasticisation of the fibre/matrix interface by

the soaking media in their degradation study of phosphate glass fibre reinforced PLA composite. Ton That et al. (2000) showed similar finding attributed to the same reason. They reported that soaking the HA/HDPE composite in saline made the materials more ductile, yet at the same time reduced the ultimate strength of the composite in the first 12 weeks of degradation study. Theocaris et al. (1983) discussed that the presence of saline in polymers can act as internal plasticiser, which allows the polymer chains to flow and slip over each other more easily, thus reducing the modulus and increasing ductility. Nevertheless, since the pattern of degraded properties is similar, it can be assumed that a similar phenomenon occurred in this study.

Compared to the non-immersed specimens, the tensile strength of 20 weeks immersed specimens were reduced by nearly 40%, while the axial modulus was reduced by about 20%. While significant reductions were observed after 20 weeks immersion, their altered strength is still comparable to that of cortical bone. The shear modulus and strength virtually remained unchanged throughout the degradation period. It is promising that the tensile modulus and strength of the PLA-PLA-tricalcium phosphate composite are retained over 20 weeks degradation as they remain stiff and strong enough to give sufficient support to the bone during healing period. This finding is consistent with the mechanical results reported by Bleach et al. (2000).

In an another study, Ignatius et al. (2001) reported similar finding when studying the degradation behaviour of injection moulded composite pins made poly (L, DL-lactide) filled with 10% and 30% tricalcium phosphate. While the composite with 10% tricalcium phosphate showed slower loss of strength and the mechanical properties remained nearly constant for 26 weeks after immersion in phosphate buffer, the composite pins with 30% tricalcium phosphate degraded quickly from start of the immersion period in a linear manner. They argued that accelerated strength retention loss was not due to faster hydrolysis of the matrix but rather decreased adhesion between the matrix and filler particles, confirmed by significant water intake and swelling during the degradation. This is similar to the results reported by Suwanprateeb et al. (1997) who showed that the water uptake in HA reinforced PE increased with increasing filler content.

In the study mentioned earlier by Niemelä and co-workers (2005, 2010), it was also reported that the shear and bending strengths were nearly unchanged up to 30-36 weeks in PBS immersion. The longer strength retention is probably due to the porous structure of polymer/filler. They assumed that during degradation, the pores become interconnected and allow acidic degradation products to diffuse away from the internal structure. Retention of this by-product can cause local acidic environment in the internal structure of specimen which act as catalyzer for further degradation (Niemelä, 2005; Li, 1999; Middleton and Tipton, 2000). Similar strength retention behaviour in other self-reinforced composites has been reported (Niemelä et al., 2004; Niiranen et al., 2004) confirming the theory that porous structure seems advantageous in maintaining strength retention in PLA based composites.

All 8, 12, 16 and 20 week degraded specimens have comparable fatigue behaviour. This is reflected by similar trends in modulus degradation and energy absorbed as shown in Figures 6.8 and 6.9. Fractography revealed that the significant reduction in axial strength is due to matrix loss and failure of the PLA matrix-TCP interface. With increased degradation periods, the fibres fracture as single fibres (Figures 6.11 to 6.14) rather than in bundles as occurred in non-degraded specimens (Figure 4.24a). As the matrix is made of a more amorphous PLA, the matrix material probably degraded faster compared to the more crystalline fibres. The amount of TCP particles was also reduced on the fracture surfaces of 20 weeks degraded specimen compared to non-degraded. This suggested TCP particles were easily detached from PLA chains subsequently reducing the fatigue life of the immersed composite and have probably started degrading themselves.

Analysis of the damage characteristics also showed that at 20 weeks, the specimen has higher energy absorbed compared to non degraded specimens which is as expected. However, the amount of energy absorbed in torsion for 20 week specimens was also higher than non immersed specimen despite no significant differences obtained in shear strength during quasi-static testing.

While the reduction in fatigue lives is not statistically significant, the internal damage at the interface is substantially higher as reflected by higher energy

absorbed per load cycle. As the immersion lengthens, decreases in specimen dry mass and water uptake were observed. As more of the polymer was hydrolysed, the ability of oligonomers to leach out of the composite was increased. More water thus was able to enter the composite, resulting in increased hydrolysis rate. The PLA_{70} matrix tends to decrease faster than the fibres, which might also influence the integrity of the fibre-matrix interface. Nielsen and Landel (1994) argue that under loading, energy is dissipated at interface of the fibre/matrix and if this interface is altered or destroyed by the absorption of the water into the composite, the damping will increase. Previously, Nielsen and Lee (1972) reported that the storage modulus of polystyrene filled glass bead composite was increased when the composite was soaked in water. The increase in damping was attributed to weakening of the interface adhesion, which provides friction between the polymer and particles and thus controls the interfaces. This occurred due to crack formation in the matrix as a result of stresses around the glass beads. Thus, it is likely that similar effects played a role in increasing the energy absorbed in this study in axial as well as in torsional loading, which act as an indicator of the damage sustained by the composite as a direct result of degradation.

In torsional loading, the fatigue lives are less affected by the degradation in comparison to the axial fatigue, as expected considering there was no significant reduction found during the quasi-static tests. As mentioned in Chapter 4, the interface strength can be influenced by the type of mechanical test that is conducted, which in this case was the direction of the load with respect to the fibre. Therefore, the interface has more significant effects on the compressive or tensile strength of the composite compared to the shear strength. This is because the direction of the load in tension or compression is parallel to the fibres, while for shear test, the load that been applied was perpendicular to the fibre direction. This is one possible reason why the degradation has less effect on the shear strength in static and consequently shear fatigue lives. However, as the hydrolytic degradation of the polymeric materials did alter the interface strength of the composite, the energy absorbed in shear fatigue for degraded specimen is higher, indicating more damage occurred in the degraded specimens' structure when compared to non-degraded specimens.

6.5 CONCLUSIONS

The physical appearance of the PLA-PLA-tricalcium phosphate only showed slight changes after 20 weeks of the degradation period due to slow degradation process by the composite. While the mechanical properties show significant alteration from 16 weeks in PBS immersion till end of degradation period, the axial strength are still comparable to those of cortical bone. Thus, it can be concluded that the composite has a good strength retention as it still able to load bearing. The shear strength and stiffness given from the torsional test however remained unchanged, similar to those reported in literature, indicating that torsional properties were less affected by degradation compared to the axial.

The fatigue behaviour of the degraded samples was significantly affected by 20 weeks of degradation. This might be attributed to the strength being reduced to 60% of the initial value of non-degraded specimens. Therefore, stress loading of fatigue test for weeks 20 degraded specimen were equivalent to 40% UTS of non-degraded strength. The number of cycles to failure of the degraded specimens followed the trend with the S-N curve established in Figure 4.8 previously.

CHAPTER 7 - GENERAL DISCUSSION, CONCLUSIONS AND FUTURE WORK

7.1 GENERAL DISCUSSION

Self-reinforced PLA-PLA-TCP was produced using a pre-pregging process. In order to give high filler content in the final composite, a much higher volume fraction of TCP had to be incorporated into PLA_{70} matrix since the presence of the PLA_{96} fibres decreased the total percentage of the filler. In this study, 67 wt.% TCP was used in PLA_{70} matrix, but due to the quantities of the fibres used, this only give approximately 12% wt. as determined by ashing. As the composite was developed with bone fixation in mind, the low amount of CaP was questionable whether it will help in improving bioactivity. However, Bleach et al. (2001) showed the bioactivity of similar self-reinforced composite with 12 wt.% (5.5 vol.%) of HA or tricalcium phosphate showed significant bioactivity in a human cell culture study.

In order to study the effect of the moulding temperature on the composite strengths in static as well as in cyclic loading, two moulding temperature were used, that is 140 and 150°C. Increases in axial moduli and yield and ultimate strengths were found for the higher moulding temperature but no significant effects were observed in the torsional properties. The increased mechanical properties are thought due to better interaction between the matrix-fibre interfaces at the higher temperature. This is because the higher temperature moulding allowed better impregnation of the fibres bundles by the matrix. Further evidence was shown in Figure 4.2 where increased consolidation and fewer gaps were observed in materials moulded at 150°C. Based on this result, a compression moulding temperature of 150°C was used to investigate the effect of biaxial loading and degradation activities on the fatigue properties of the composite.

The quasi-static results also demonstrated that PLA-PLA-TCP composite is stronger in tension than in compression and torsion. This finding is however expected for the type of continuous fibre reinforced composite. The torsion and tensile behaviour of the composite is also more ductile than the compressive. In general, the compressive failure of the continuous fibre reinforcement

composite is due to the buckling that caused by kink band formation in the composite resulted from compressive stress (Jelf and Fleck, 1992; Budiansky, 1983; Argon 1972). When a compressive load is applied, the stress is taken by the fibres and transferred to the matrix through shear at the interface. With increase of the stress, the fibres start to flex and the matrix starts to stretch away from the fibres and trigger the kink bands formation inside the specimen that led to buckling. There are many factors that can contribute to the formation of the kink bands, but the most common is misalignment of the fibres during the fabrication. As the composite in this study were produced by hand-lay up technique, such possibility of the variation in the fibre waviness is highly present.

Uniaxial fatigue results showed that the composite moulded at 150°C (T150) had increased fatigue lives compared to that moulded at 140°C (T140) when tested at 25A, 50A and 75A of individual ultimate strengths. Torsional fatigue lives were unaffected by the moulding temperature. This finding is expected considering the results from the earlier quasi-static tests to failure. S-N curves for both moulding parameters were established in Figure 4.9. As the cycles to failure for the lowest load level used still showed failure, a fatigue endurance limit for the unidirectional self-reinforcement PLA-PLA–TCP composite cannot be identified. However, as no failure were observed for two specimens (T150) when tested at 25A, there may be a fatigue endurance limit below 34.9 MPa for samples moulded at 150°C.

The fatigue surfaces fracture from the uniaxial fatigue loaded is also differ for specimens moulded at moulding temperature of 140°C (T140) in comparison to moulding temperature of 150°C (T150). It was observed that for T140, the specimen failed via delamination buckling while for T150, the specimen failed due to fibre microbuckling. The delamination fracture surface indicated poor matrix-fibre interfaces strength, while by increasing the moulding temperature, better interaction was achieved in T150 thus increase the interface strengths and change the fracture failure mode. This finding is similar to that discussed by Madzukar and Drzal (1992) that showed that compressive strength and failure mode are sensitive to the matrix-fibre interfaces.

Superposition of the torque on axial loading reduced the fatigue life of the composite as shown in Figure 5.1. At equal stress levels, the failure was dominated by the shear failure as torsional loading lead to lower fatigue resistant in comparison to the axial. Increasing phase angle increased the fatigue lives. The difference is due to the loading path as shown in Chapter 2, where under load-controlled test, both in-phase and out-of-phase loading has maximum applied strain. George and Vashishth (2005) and Ton That (2000) both showed that maximum shear strain for total loading cycles for out-of-phase is lower than in-phase loading, thus less damage occurred during out-of-phase loading.

The presence of the calcium phosphate in the composite lead to slow degradation of the material, due to neutralization of acidic end group, thus reducing the amount of autocatalysis that occurred (van der Meer et al., 1996). Further evidence was shown in Figure 6.1, where the pH value of saline solution remained unchanged for the 20 weeks degradation period of the tricalcium phosphate filled specimens. Bleach et al. (2001) showed with unfilled but similar specimens, the pH decreased with degradation time.

The high initial tensile and compression moduli and strengths of the specimen moulded at 150°C indicated that this composite shows promise for use in fracture fixation. The composite showed significant decreases in tensile modulus and ultimate strength ($p<0.01$) by 20 weeks, however the degraded properties are still comparable to cortical bone, showing that not only the degradation process of the composite is slow but it also has the potential to use where when longer degradation times are required, such as tibia fractures where average the healing time is 16 weeks.

The fatigue properties of the degraded specimens decreased with increasing degradation period. Even though the fatigue tests were carried out at the low level stress of 25A for non-degraded specimens, the degradation process reduced the quasi-static properties of the composite. At 20 weeks degradation period, the 25% UTS test value is equivalent to 40% UTS of the degraded specimen, thus explaining the decrease in the number of cycle to failure. Fatigue lives given by degraded specimens shows a similar trend to uniaxial S-N curves that were established earlier.

7.2 CONCLUSIONS

1. S-N curves for axial and torsional loading were established in which the fatigue limits appears to be less than 25% of the ultimate stress (34MPa). PLA-PLA-TCP composite moulded at 150°C was shown to be more fatigue resistant than materials moulded at 140°C.

2. The ultimate strengths are highest in tension followed by compression then torsion. The material is ductile in torsion as well as in tension.

3. Microscopy examination revealed that higher mechanical properties in quasi-static and fatigue testing with higher moulding temperature are due to better interaction and adhesion between the fibre and matrix.

4. Numbers of cycles to failure in the unidirectional fibre reinforced composite are dominated by the compression loading behaviour, which is a typical type of failure for continuous fibre reinforced composite agreeing with the literature.

5. Fractography analysis revealed that the composite failure is initiated by the fibre kinking mechanism that led to fibre buckling.

6. Superposition of the torque on axial loading considerably reduces the fatigue life of self-reinforced PLA-PLA-TCP composite. Out-of-phase loading is less damaging than in-phase loading, which agrees with analysis of combined stress. S-N curves in terms of principal stress; maximum shear stress and Tsai-Wu criteria were plotted. The Tsai-Wu criterion was found to have the best fit.

7. Failure in fully reversed fatigue appears to be dominated by the lower torsional properties. The weak PLA fibre-matrix interfaces and PLA matrix–TCP interfaces are also responsible for failure in axial as well as torsional fatigue.

8. Fractography examinations showed that biaxial failure was dominated by shear mechanism and that fatigue-striated features were observed.

9. The threshold number of cycles at which damage starts to accumulate in the composite was shown to be load dependent. For biaxial fatigue, the threshold is also further influenced by the phase difference.

10. The composite showed slow degradation, it absorbs about 1.4% by weight of saline solution and has insignificant dry mass loss, less than 0.2% by the end of 20 weeks degradation.

11. The PLA-PLA-TCP composite showed good strength retention over 20 weeks. Even though there is significant reduction in modulus and ultimate strength at week 20, the strength is comparable to the cortical bone showing promise for use in longer fracture fixation applications.

12. The fatigue lives of the degraded composite decrease with increasing the degradation period showing the influence of the material degradation on the cyclic properties.

7.3 FUTURE WORK

1. Further work should be carried out to optimize the manufacturing procedure since the pre-preg produced is currently still of variable quality. A different solvent other than acetone could be studied. The fibres used are thought to be slightly weakened during the pre-pregging process as they are slightly soluble in the acetone, however this may help in promoting a bond between the fibres and matrix. Nevertheless, higher initial mechanical properties could be achieved if a solvent were found that did not partially dissolve the fibres during the manufacturing.

2. Further combination of different stress levels should be carried out at different phase angle in order to establish better estimations of the multiaxial S-N curve.

3. Longer degradation studies should be carried out on the composite, with possibility of investigating the fatigue properties up to one or two years.

4. Biaxial fatigue studies should be carried out on the degraded material to study the effects of the superimposed loading stress as well as phase angle on the fatigue behaviour of the degraded composite.

5. Further mechanical tests such as creep should be used to characterize the mechanical properties of the composite for non-degraded as well as after degraded samples.

6. Cell culture work should be carried out for the specimens that undergone degradation in order to fully understand the *in vitro* biological response of the bioactive composite.

7. Further investigation need to be carried out on how the composite could be manufactured into useful devices for the intended applications.

8. Different fibre orientation and effect of laminar lay-up should be investigated in respect of the effect on the mechanical properties in static and cyclic conditions.

9. Finally, in-vivo study would be needed before clinical application.

REFERENCES

Abu Bakar, M. S., Cheng, M. H. W., Tang, S. M., Yu, S. C., Liao, K., Tan, C. T., Khor, K. A. & Cheang, P. 2003. Tensile properties, tension-tension fatigue and biological response of polyetheretherketone-hydroxyapatite composites for load-bearing orthopedic implants. *Biomaterials,* 24**,** 2245-2250.

Adden, S. & Horst, P. 2006. Damage propagation in non-crimp fabrics under bi-axial static and fatigue loading. *Composites Science and Technology,* 66**,** 626-633.

Alcock, B., Cabrera, N. O., Barkoula, N. M., Loos, J. & Peijs, T. 2006. The mechanical properties of unidirectional all-polypropylene composites. *Composites Part A: Applied Science and Manufacturing,* 37**,** 716-726.

Ali, M., French, T., Hastings, G., Rae, T., Rushton, N., Ross, E. & Wynn-Jones, C. 1990. Carbon fibre composite bone plates. Development, evaluation and early clinical experience. *Journal of Bone & Joint Surgery, British Volume,* 72-B**,** 586-591.

Al-Shawi, A. K., Smith, S. P. & Anderson, G. H. 2002. The use of a carbon fiber plate for periprosthetic supracondylar femoral fractures. *The Journal of Arthroplasty,* 17**,** 320-324.

Ambrose, C. G. & Clanton, T. O. 2004. Bioabsorbable implants: review of clinical experience in orthopedic surgery. *Ann Biomed Eng,* 32**,** 171-7.

Amijima, S., Fujii, T. & Hamaguchi, M. 1991. Static and fatigue tests of a woven glass fabric composite under biaxial tension-torsion loading. *Composites,* 22**,** 281-289.

An, Y. H., Woolf, S. K. & Friedman, R. J. 2000. Pre-clinical in vivo evaluation of orthopaedic bioabsorbable devices. *Biomaterials,* 21**,** 2635-2652.

Anderson, J. 2004. *Inflammation, wound healing and the foreign body response, Biomaterials Science: An Introduction to Materials in Medicine.,* San Diego, Elsevier Press.

Andersons, J., Lomonov, V., Mikelsons, M. & Tamužs, V. 1994. Strength and durability of mixed glass-fibre-reinforced laminates. *Mechanics of Composite Materials,* 30**,** 22-29.

Andrews, E. H. & Walker, B. J. 1971. Fatigue fracture of polyethylene. *Proceeding of the Royal Society* 325**,** 57-79.

Ara, M., Watanabe, M. & Imai, Y. 2002. Effect of blending calcium compounds on hydrolytic degradation of poly(DL-lactic acid-co-glycolic acid). *Biomaterials,* 23**,** 2479-2483.

Arata, J., Ishikawa, K., Sawabe, K., Soeda, H. & Kitayama, T. 2003. Osteosynthesis in digital replantation using bioabsorbable rods. *Annals of Plastic Surgery,* 50**,** 350-353.

Argon, A. S. 1972. Fracture of Composites. *Treatise on Materials Science and Technology,* 1**,** 106-114.

ASTM Standard E466-07 Standard Practice for Conducting Force Controlled Constant Amplitude Axial Fatigue Tests of Metallic Materials

Avérous, L. 2008. Chapter 21 - Polylactic Acid: Synthesis, Properties and Applications. *In:* Mohamed Naceur, B. & Alessandro, G. (eds.) *Monomers, Polymers and Composites from Renewable Resources.* Amsterdam: Elsevier.

Avinc, O. & Khoddami, A. 2009. Overview of poly(lactic acid) (PLA) fibre. *Fibre Chemistry,* 41**,** 391-401.

Avinc, O. & Khoddami, A. 2010. Overview of Poly(lactic acid) (PLA) fibre. *Fibre Chemistry,* 42**,** 68-78.

Aydin, E., Planell, J. A. & Hasirci, V. 2011. Hydroxyapatite nanorod-reinforced biodegradable poly(l-lactic acid) composites for bone plate applications. *Journal of Materials Science: Materials in Medicine,* 22**,** 2413-2427.

Azimi, H. R., Pearson, R. A. & Hertzberg, R. W. 1996. Fatigue of rubber-modified expoxies: effect of particles size and volume fraction. *Journal Materials Science,* 31**,** 3777-3789.

Baslé, M. F., Rebel, A., Grizon, F., Daculsi, G., Passuti, N. & Filmon, R. 1993. Cellular response to calcium phosphate ceramics implanted in rabbit bone. *Journal of Materials Science: Materials in Medicine,* 4**,** 273-280.

Basu, S., Waas, A. M. & Ambur, D. R. 2006. Compressive failure of fiber composites under multi-axial loading. *Journal of the Mechanics and Physics of Solids,* 54**,** 611-634.

Behravesh, E., Yasko, A. W., Engel, P. S. & Mikos, A. G. 1999. Synthetic biodegradable polymers for orthopaedic applications. *Clinical Orthopaedics & Related Research,,* 367**,** S118-29.

Bergsma, J. E., Rozema, F. R., Bos, R. R. M., Boering, G., de Bruijn, W. C. & Pennings, A. J. 1995c. In vivo degradation and biocompatibility study of in

vitro pre-degraded as-polymerized polylactide particles. . *Biomaterials,* 16**,** 267-274.

Bergsma, J. E., Rozema, F. R., R.R.M., B., van Rozendaal, A. W. M., de Jong, W. H., Teepema, J. S. & Joziasse, C. A. P. 1995d. Biocompatibility and degradation mechanisms of predegraded and non-predegraded poly(lactide) implants: an animal study. *Journal of Materials Science: Materials in Medicine,* 6**,** 711-724.

Bernstein, M., Gotman, I., Makarov, C., Phadke, A., Radin, S., Ducheyne, P. & Gutmanas, E. Y. 2010. Low Temperature Fabrication of β-TCP–PCL Nanocomposites for Bone Implants. *Advanced Engineering Materials,* 12**,** B341-B347.

Blacher, S., Maquet, V., Jerome, R., Pirard, J. P. & Boccaccini, A. R. 2005. Study of the connectivity properties of Bioglass (R)-filled polylactide foam scaffolds by image analysis and impedance spectroscopy. *Acta Biomaterialia,* 1**,** 565-574.

Black, J. 1988. *Orthopedic Biomaterials in Research and Practice,* New York, Churchill Livingstone.

Black, J. 1992. *Biological performance of biomaterials,* New York, Marcel Dekker.

Blaker, J. J., Gough, J. E., Maquet, V., Notingher, I. & Boccaccini, A. R. 2003. In vitro evaluation of novel bioactive composites based on Bioglass®-filled polylactide foams for bone tissue engineering scaffolds. *Journal of Biomedical Materials Research Part A,* 67A**,** 1401-1411.

Bleach, N. C. 2001. *Optimisation of Degradable Bioactive Polymer Composites.* Phd, Queen Mary, University of London.

Bleach, N. C., Nazhat, S. N., Tanner, K. E., Kellomäki, M. & Törmälä, P. 2002. Effect of filler content on mechanical and dynamic mechanical properties of particulate biphasic calcium phosphate—polylactide composites. *Biomaterials,* 23**,** 1579-1585.

Boccaccini, A. R. & Blaker, J. J. 2005. Bioactive composite materials for tissue engineering scaffolds. *Expert Review Medical Devices,* 2**,** 303-317.

Boccaccini, A. R., Notingher, I., Maquet, V. & Jerome, R. 2003. Bioresorbable and bioactive composite materials based on polylactide foams filled with and coated by Bioglass (R) particles for tissue engineering applications. *Journal of Materials Science: Materials in Medicine,* 14**,** 443-450.

Bohner, M., Lemaitre, J. & Ring, T. A. 1996. Effects of Sulfate, Pyrophosphate, and Citrate Ions on the Physicochemical Properties of Cements Made of β-Tricalcium Phosphate-Phosphoric Acid-Water Mixtures. *Journal of the American Ceramic Society,* 79**,** 1427-1434.

Bonfield, W., Grynpas, M., Tully, A. E., Bowman, J. & Abram, J. 1981. Hydroxyapatite reinforced polyethylene- a mechanically compatible implant material for bone replacement. *Biomaterials,* 2**,** 185-186.

Borden, M. 2006. Biomaterials, Absorbable. *Encyclopedia of Medical Devices and Instrumentation.* John Wiley & Sons, Inc.

Bos, R. R. M., Rozema, F. R., Boering, G., Nijenhuis, A. J., Pennings, A. J. & Verwey, A. B. 1989. Bio-absorbable plates and screws for internal fixation of mandibular fractures. A study in six dogs. *International Journal of Oral and Maxillofacial Surgery,* 18**,** 365-369.

Boskey, A. L. 2004. The Organic and Inorganic Matrices. *In:* Hollinger, J. O., Einhorn, & T. A., D., B. A. and Sfeir, C., (eds.) *Bone Tissue Engineering.* Washington CRC Press.

Bouvier, S., Haddadi, H., Levée, P. & Teodosiu, C. 2006. Simple shear tests: Experimental techniques and characterization of the plastic anisotropy of rolled sheets at large strains. *Journal of Materials Processing Technology,* 172**,** 96-103.

Bradley, J. S., Hastings, G. W. & Johnson-Nurse, C. 1980. Carbon fibre reinforced epoxy as a high strength, low modulus material for internal fixation plates. *Biomaterials,* 1**,** 38-40.

Brand, R. & Claes, L. E. 1989. The law of bone remodelling. *Journal of Biomechanics,* 22**,** 185-187.

Brauer, D., Rüssel, C., Vogt, S., Weisser, J. & Schnabelrauch, M. 2008. Degradable phosphate glass fiber reinforced polymer matrices: mechanical properties and cell response. *Journal of Materials Science: Materials in Medicine,* 19**,** 121-127.

Brauer, D. S., Rüssel, C., Vogt, S., Weisser, J. & Schnabelrauch, M. 2007. Fabrication and in vitro characterization of porous biodegradable composites based on phosphate glasses and oligolactide-containing polymer networks. *Journal of Biomedical Materials Research Part A,* 80A**,** 410-420.

Brown, M. W. & Miller, K. J. 1973. A theory for fatigue failure under multiaxial stress-strain conditions. . *Proceedings of the Institution of Mechanical Engineers,* 187**,** 745-755.

Brown, M. W. & Miller, K. J. 1982. Two Decades of Progress in the Assessment of Multiaxial Low-Cycle Fatigue Life. *Low cycles fatigue life prediction.* ASTM STP

Bruck, S. D. 1980. *Properties of biomaterials in the pysiological environment,* Boca Ranton, FL., CRC Press.

Budiansky, B. 1983. Micromechanics. *Computers & Structures* 16**,** 3-12.

Budiansky, B., Fleck, N. A. & Amazigo, J. C. 1998. On kink-band propagation in fiber composites. *Journal of the Mechanics and Physics of Solids,* 46**,** 1637-1653.

Buggy, M. & Carew, A. 1994. The effect of thermal ageing on carbon fibre-reinforced polyetheretherketone (PEEK). *Journal of Materials Science,* 29**,** 1925-1929.

Bureau, M. N., Perrin, F., Denault, J. & Dickson, J. I. 2002. Interlaminar fatigue crack propagation in continuous glass fiber/polypropylene composites. *International Journal of Fatigue,* 24**,** 99-108.

Burr, D. B., Martin, R. B., Scaffler, M. B. & Radin., E. L. 1985. Bone Remoddeling in Response to in vivo Fatigue Damage. *Journal of Biomechanics,* 18**,** 189-197.

Caler, W. E. & Carter, D. R. 1989. Bone creep-fatigue damage accumulation. *Journal of Biomechanics,* 22**,** 625-635.

Callister, W. D. 2000. *Materials Science and Engineering, An Introduction*, John Wiley and Sons, Inc.

Cao, W. & Hench, L. L. 1996. Bioactive materials. *Ceramics International,* 22**,** 493-507.

Capiati, N. J. & Porter, R. S. 1975. The concept of one polymer composites modelled with high density polyethylene. *Journal of Materials Science,* 10**,** 1671-1677.

Caprino, G. 2003. Short-fibre thermoset composites. *In:* Harris, B. (ed.) *Fatigue in composites.* Cambridge,UK: Woodhead Publishing Ltd.

Caprino, G. & D'Amore, A. 1998. Flexural fatigue behaviour of random continuous-fibre-reinforced thermoplastic composites. *Composites Science and Technology,* 58**,** 957-965.

Carter, D. R. & Caler, W. E. 1985. A cumulative damage model for bone fracture. *Journal of Orthopaedic Research,* 3**,** 84-90.

Carter, D. R., Caler, W. E., Spengler, D. M. & Frankel, V. H. 1981. Uniaxial fatigue of human cortical bone. The influence of tissue physical characteristics. *Journal of Biomechanics,* 14**,** 461-470.

Carter, D. R. & Hayes, W. C. 1977. Compact bone damage: A microscopic examination. *Clinical Orthopaedics and Related Research,* 127**,** 265-274.

Cezayirlioglu, H., Bahniuk, E., Davy, D. T. & Heiple, K. G. 1985. Anisotropic yield behavior of bone under combined axial force and torque. *Journal of Biomechanics,* 18**,** 61-69.

Charnley, J. 1975. Fracture of femoral prostheses in total hip replacement. A clinical study. *Clinical Orthopaedics and Related Research,* 111**,** 105-20.

Chen, A. S. & Matthews, F. L. 1993. A review of multiaxial/biaxial loading tests for composite materials. *Composites,* 24**,** 395-406.

Chen, A. S. & Matthews, F. L. 1994. Static and cyclic biaxial bending of CFRP panels. *Composites Science and Technology,* 52**,** 267-273.

Choi, D. & Kumta, P. N. 2007. Mechano-chemical synthesis and characterization of nanostructured β-TCP powder. *Materials Science and Engineering C,* 27**,** 377-381.

Chou, P. M., Mariatti, M., Zulkifli, A. & Sreekantan, S. 2012. Evaluation of the flexural properties and bioactivity of bioresorbable PLLA/PBSL/CNT and PLLA/PBSL/TiO2 nanocomposites. *Composites Part B: Engineering,* 43**,** 1374-1381.

Claes, L. E., Ignatius, A. A., Rehm, K. E. & Scholz, C. 1996. New bioresorbable pin for the reduction of small bony fragments: design, mechanical properties and in vitro degradation. *Biomaterials,* 17**,** 1621-1626.

Cool, S. M., Kenny, B., Wu, A., Nurcombe, V., Trau, M., Cassady, A. I. & Grondahl, L. 2007. Poly(3-hydroxybutyrate-co-3-hydroxyvalerate) composite biomaterials for bone tissue regeneration: In vitro performance assessed by osteoblast proliferation, osteoclast adhesion and resorption, and macrophage proinflammatory response. *Journal of Biomedical Materials Research Part A,* 82A**,** 599-610.

Correa, E., Gamstedt, E. K., París, F. & Mantič, V. 2007. Effects of the presence of compression in transverse cyclic loading on fibre–matrix debonding in unidirectional composite plies. *Composites Part A: Applied Science and Manufacturing,* 38**,** 2260-2269.

Cotton, J. R., Winwood, K., Zioupos, P. & Taylor, M. 2005. Damage Rate is a Predictor of Fatigue Life and Creep Strain Rate in Tensile Fatigue of Human Cortical Bone Samples. *Journal of Biomechanical Engineering,* 127**,** 213-219.

Cotton, N. J., Egan, M. J. & Brunelle, J. E. 2008. Composites of poly(DL-lactide-co-glycolide) and calcium carbonate: In vitro evaluation for use in orthopedic applications. *Journal of Biomedical Materials Research Part A,* 85A**,** 195-205.

Couque, H., Albertini, C. & Lankford, J. 1993. Failure mechanisms in a unidirectional fibre-reinforced thermoplastic composite under uniaxial, in-plane biaxial and hydrostatically confined compression. *Journal of Materials Science Letters,* 12**,** 1953-1957.

Creighton, C. J. & Clyne, T. W. 2000. The compressive strength of highly-aligned carbon-fibre/epoxy composites produced by pultrusion. *Composites Science and Technology,* 60**,** 525-533.

Currey, J. D. 1998. Mechanical properties of vertebrate hard tissues. *Proceeding of the Institute of Mechanical Engineers, ,* 212H**,** 399-411.

Curtis, D. C., Davies, M., D.R., M. & Slater, B. 1991. Fatigue behaviour of continuous carbon fibre reinforced PEEK. *In:* O'Brien, T. K. (ed.) *Composite Materials: Fatigue and Fracture.* Philadelphia: ASTM STP 1110, ASTM.

Daculsi, G. 1998. Biphasic calcium phosphate concept applied to artificial bone, implant coating and injectable bone substitute. *Biomaterials,* 19**,** 1473-1478.

Daculsi, G., Goyenvalle, E., Cognet, R., Aguado, E. & Suokas, E. O. 2011. Osteoconductive properties of poly(96L/4D-lactide)/beta-tricalcium phosphate in long term animal model. *Biomaterials,* 32**,** 3166-3177.

Daniel, I. M., Cho, J.-M., Werner, B. T. & Fenner, J. S. 2011. Characterization and Constitutive Modeling of Composite Materials Under Static and Dynamic Loading. *AIAA Journal,* 49**,** 1658-1664.

Daniel, I. M. & Ishai, O. 1994. *Engineering mechanics of composite materials,* N.Y., Oxford University Press, Inc.

Dartee, M., Lunt, J. & Shafer, A. 2000. Natureworks PLA: sustainable performance fiber. *Chem.Fibers Int,* 50**,** 546.

Davalos, J. F., Qiao, P., Wang, J., Salim, H. A. & Schlussel, J. 2002. Shear moduli of structural composites from torsion tests. *Journal of Composite Materials,* 36**,** 1151-1173.

Davies, J. E. 1999. Bone Engineering. *Proceeding of Bone Engineering Workshop.* Toronto, Canada: Em Squared Incorporated.

De Santis, R., Guarino, V. & Ambrosio, L. 2009. Bone tissue engineering. *In:* Planell, J. A. (ed.) *Bone repair materials.* Cambridge, England: Woodhead Publishing Limited.

Deng, S., Ye, L., Mai, Y.-W. & Liu, H.-Y. 1998. Evaluation of fibre tensile strength and fibre/matrix adhesion using single fibre fragmentation tests. *Composites Part A: Applied Science and Manufacturing,* 29**,** 423-434.

Descamps, M., Richart, O., Hardouin, P., Hornez, J. C. & Leriche, A. 2008. Synthesis of macroporous β-tricalcium phosphate with controlled porous architectural. *Ceramics International,* 34**,** 1131-1137.

Dieter, E. 1988. *Mechanical Metallurgy*, Mc Graw Hill Book Company.

Dillon, G. & Buggy, M. 1995. Damage development during flexural fatigue of carbon fibre-reinforced PEEK. *Composites,* 26**,** 355-370.

Dobb, M. G. & Robson, R. M. 1990. Structural characteristics of aramid fibre variants. *Journal of Materials Science,* 25**,** 459-464.

Dong, C. X., Zhu, S. J., Mizuno, M. & Hashimoto, M. 2011. Fatigue Behavior of HDPE Composite Reinforced with Silane Modified TiO2. *Journal of Materials Science & Technology,* 27**,** 659-667.

Dorozhkin, S. V. 2010. Amorphous calcium (ortho)phosphates. *Acta Biomaterialia,* 6**,** 4457-4475.

Dorozhkin, S. V. 2012. Biphasic, triphasic and multiphasic calcium orthophosphates. *Acta Biomaterialia,* 8**,** 963-977.

Dorozhkin, S. V. & Epple, M. 2002. Biological and medical significance of calcium phosphates. *Angew Chem Int Ed Engl,* 41**,** 3130-46.

Downes, R. N., Vardy, S., Tanner, K. E. & Bonfield, W. Year. Hydroxyapatite-polyethylene composite in ophthalmic surgery. *In:* Bonfield, W., Hastings, G. W. & Tanner, K. E., eds. Bioceramics 4. Proc. 4th Int. Symp. on Ceramics in Medicine, 1991 London, UK. London, UK: Butterworth–Heinnemann Ltd.

Ducheyne, P. & Qiu, Q. 1999. Bioactive ceramics: the effect of surface reactivity on bone formation and bone cell function. *Biomaterials,* 20**,** 2287-2303.

Dumitriu, S. & Dumitriu, D. 1994. Biocompatibility of Polymers. *In:* Dumitriu, S. (ed.) *Polymeric Biomaterials.* N.Y.: Marcel Dekker.

Dunn, A. S., Campbell, P. G. & Marra, K. G. 2001. The influence of polymer blend composition on the degradation of polymer/hydroxyapatite biomaterials. *Journal of Materials Science-Materials in Medicine,* 12**,** 673-677.

Echaabi, J., Trochu, F. & Gauvin, R. 1996. Review of failure criteria of fibrous composite materials. *Polymer Composites,* 17**,** 786-798.

Edgren, F., Asp, L. E. & Joffe, R. 2006. Failure of NCF composites subjected to combined compression and shear loading. *Composites Science and Technology,* 66**,** 2865-2877.

Ehrenfried, L. M., Farrar, D. & Cameron, R. E. 2009. Degradation Properties of Co-Continuous Calcium−Phosphate−Polyester Composites. *Biomacromolecules,* 10**,** 1976-1985.

Ehrenfried, L. M., Patel, M. H. & Cameron, R. E. 2008. The effect of tri-calcium phosphate (TCP) addition on the degradation of polylactide-co-glycolide (PLGA). *J Mater Sci Mater Med,* 19**,** 459-66.

Eling, B., Gogolewski, S. & Pennings, A. J. 1982. Biodegradable materials of poly(-lactic acid). 1. Melt-spun and solution-spun fibres. *Polymer,* 23**,** 1587-1593.

Ellä, V., Kellomäki, M. & Törmälä, P. 2005. In vitro properties of PLLA screws and novel bioabsorbable implant with elastic nucleus to replace intervertebral disc. *Journal of Materials Science: Materials in Medicine,* 16**,** 655-662.

Ellyin, F. 1988. Recent Developments in Predicting Multiaxial Fatigue Failure *Resource Mechanical,* 25**,** 1-23.

Ellyin, F., Golos, K. & Xia, Z. 1991. In-phase and out-of-phase multiaxial fatigue. *Transactions of the ASME,* 113**,** 112-119.

Ellyin, F. & Martens, M. 2001. Biaxial fatigue behaviour of a multidirectional filament-wound glass-fiber/epoxy pipe. *Composites Science and Technology,* 61**,** 491-502.

Evans, F. G., Behiri, J. C., Currey, J. D. & Bonfield, W. 1990. Microhardness and Young Modulus's in cortical bone exhibiting a wide range of mineral volume fraction in a bone analogue. *Journal Materials Science Materials Medicine: Materials in Medicine,* 1**,** 38-43.

Evans, F. G. & Lebow, M. 1957. Strength of human compact bone under repetitive loading. *Journal of Applied Physiology,* 10**,** 127-130.

Fahami, A., Nasiri-Tabrizi, B. & Ebrahimi-Kahrizsangi, R. 2012. Synthesis of calcium phosphate-based composite nanopowders by mechanochemical process and subsequent thermal treatment. *Ceramics International,* 38**,** 6729-6738.

Fambri, L., Pegoretti, A., Fenner, R., Incardona, S. D. & Migliaresi, C. 1997. Biodegradable fibres of poly(L -lactic acid) produced by melt spinning. . *Polymer* 38**,** 79-85.

Fang, Y., Agrawal, D. K., Roy, D. M., Roy, R. & Brown, P. W. 1992. Ultrasonically accelerated synthesis of hydroxyapatite. *Journal of Materials Research,* 7**,** 2294-2298.

Fatemi, A. & Kurath, P. 1988. Multiaxial Fatigue Life Predictions Under the Influence of Mean-Stresses. *Journal of Engineering Materials and Technology,* 110**,** 380-388.

Fatemi, A. & Socie, D. F. 1988. A Critical Plane Approach to Multiaxial Fatigue Damage including out-of-phase loading. *Fatigue & Fracture of Engineering Materials & Structures,* 11**,** 149-165.

Fawaz, Z. & Ellyin, F. 1994. Fatigue Failure Model for Fibre-Reinforced Materials under General Loading Conditions. *Journal of Composite Materials,* 28**,** 1432-1451.

Felfel, R. M., Ahmed, I., Parsons, A. J., Walker, G. S. & Rudd, C. D. 2011. In vitro degradation, flexural, compressive and shear properties of fully bioresorbable composite rods. *Journal of the Mechanical Behavior of Biomedical Materials,* 4**,** 1462-1472.

Feng, J. T., Sui, J. H., A.N., C. & Cai, W. 2009. Effect of Multi-Walled Carbon Nanotubes on the Biodegradable Behaviour of Poly (L-Lactide) in vitro. *International Journal of Modern Physics B,* 23**,** 1503-1509.

Fernando, G., Dickson, R. F., Adam, T., Reiter, H. & Harris, B. 1988. Fatigue behaviour of hybrid composites. *Journal of Materials Science,* 23**,** 3732-3743.

Ferry, J. D. 1970. *Viscoelastic properties of polymers,* New York, Wiley.

Fitzer, E., Hüttner, W., Claes, L. & Kinzl, L. 1980. Torsional strength of carbon fibre reinforced composites for the application as internal bone plates. *Carbon,* 18**,** 383-387.

Fleck, N. A. 1997. Compressive Failure of Fiber Composites. *In:* John, W. H. & Theodore, Y. W. (eds.) *Advances in Applied Mechanics.* Elsevier.

Fleck, N. A., Deng, L. & Budiansky, B. 1995. Prediction of Kink Width in Compressed Fiber Composites. *Journal of Applied Mechanics,* 62**,** 329-337.

Fleck, N. A., Kang, K. J. & Ashby, M. F. 1994. Overview no. 112: The cyclic properties of engineering materials. *Acta Metallurgica et Materialia,* 42**,** 365-381.

Folkes, M. J., Kalay, G. & Ankara, A. 1993. The effect of heat treatment on the properties of peek and APC2. *Composites Science and Technology,* 46**,** 77-83.

Found, M. S., Fernando, U. P. & Miller, K. J. 1985. Requirement of a New Muliaxial Fatigue Testing Facility. *In:* Miller, K. J. & M.W., B. (eds.) *Multiaxial Fatigue.* Philadephia: ASTM STP 1983.

Frantzén, J., Pälli, A., Kotilainen, E., Heino, H., Mannerström, B., Huhtala, H., Kuokkanen, H., Sándor, G. K., Leino, K., Röyttä, M., Parkkola, R., Suuronen, R., Miettinen, S., Aro, H. T. & Haimi, S. 2011. In vivo and in vitro study of a polylactide-fiber-reinforced β-tricalcium phosphate composite cage in an ovine anterior cervical intercorporal fusion model. *International Journal of Biomaterials*, 2011, 1-11.

Friedenstein, A. Y. 1968. Induction of bone tissue by transitional epithelium. *Clinical Orthopeadics and Related Research,* 59**,** 21-37.

Friedrich, K. & Karsch, U. A. 1981. Failure processes in particulate filled polypropylene. *Journal of Materials Science,* 16**,** 2167-2175.

Friedrich, K. & Karsch, U. A. 1982. Fatigue crack growth and fracture in glass sphere-filled nylon 6. *Polymer Composites,* 3**,** 65-74.

Friedrich, K., Walter, R., Voss, H. & Karger-Kocsis, J. 1986. Effect of short fibre reinforcement on the fatigue crack propagation and fracture of PEEK-matrix composites. *Composites,* 17**,** 205-216.

Fujihara, K., Yoshida, E., Nakai, A., Ramakrishna, S. & Hamada, H. 2007. Influence of micro-structures on bending properties of braided laminated composites. *Composites Science and Technology,* 67**,** 2191-2198.

Fujii, T. & Lin, F. 1995. Fatigue Behavior of a Plain-Woven Glass Fabric Laminate under Tension/Torsion Biaxial Loading. *Journal of Composite Materials,* 29**,** 573-590.

Furukawa, T., Matsusue, Y., Kobayashi, M., Fujita, H. & Shikinami, M. 1998. Ultra-high strength hydroxyapatite/Poly(L-lactide) composite rods for internal fixation of bone fractures: In vivo study. *In:* LeGeros, R. & LeGeros, J. (eds.) *Bioceramics.* New York: World Sciencetific Publishing.

Furukawa, T., Matsusue, Y., Yasunaga, T., Shikinami, Y., Okuno, M. & Nakamura, T. 2000. Biodegradation behavior of ultra-high-strength hydroxyapatite/poly (l-lactide) composite rods for internal fixation of bone fractures. *Biomaterials,* 21**,** 889-898.

Gadaree, K. P. & Salee, G. 1983. Fatigue crack propagation in composites with spherical fillers—part 1. *Polymer Composites,* 4**,** 19-25.

Galois, L. G., Mainard, D. M. & Delagoutte, J. D. 2002. Beta-tricalcium phosphate ceramic as a bone substitute in orthopaedic surgery. *International Orthopaedics,* 26**,** 109-115.

Gamstedt, E. K. 2000. Fatigue in composite laminates – A qualitative link from micromechanisms to fatigue life performance *In:* Cardon, A. H., Fukuda, H., Reifsnider, K. L. & Verchery, G. (eds.) *Recent Developments in Durability Analysis of Composite Systems,.* Rotterdam,Netherlands: A. A. Balkema.

Gamstedt, E. K. & Berglund, L. A. 2003. Fatigue of thermoplastic composites. *In:* Harris, B. (ed.) *Fatigue in composites* Woodhead Publishing Limited.

Gamstedt, E. K., Berglund, L. A. & Peijs, T. 1999. Fatigue mechanisms in unidirectional glass-fibre-reinforced polypropylene. *Composites Science and Technology,* 59**,** 759-768.

Gamstedt, E. K. & Sjögren, B. A. 1999. Micromechanisms in tension-compression fatigue of composite laminates containing transverse plies. *Composites Science and Technology,* 59**,** 167-178.

Gamstedt, E. K. & Talreja, R. 1999. Fatigue damage mechanisms in unidirectional carbon-fibre-reinforced plastics. *Journal of Materials Science,* 34**,** 2535-2546.

Gao, C., Yu, L., Liu, H. & Chen, L. 2012. Development of self-reinforced polymer composites. *Progress in Polymer Science,* 37**,** 767-780.

Garland, B. D., Beyerlein, I. J. & Schadler, L. S. 2001. The development of compression damage zones in fibrous composites. *Composites Science and Technology,* 61**,** 2461-2480.

Garlotta, D. 2001. A Literature Review of Poly(Lactic Acid). *Journal of Polymers and the Environment,* 9**,** 63-84.

Garmendia, J., Olaizola, M., Etxeberria, I., Franco, J. C. & Mondragon, I. 1995. Influence of processing and testing conditions on the mechanical behaviour of sheet-moulding compound laminates. *Journal of Materials Science,* 30**,** 5287-5294.

George, W. T. & Vashishth, D. 2005. Influence of phase angle between axial and torsional loadings on fatigue fractures of bone. *Journal of Biomechanics,* 38**,** 819-825.

Gere, J. M. & Timoshenko, S. P. 1991. *Mechanics of Materials,* London, Chapman and Hall.

Gibson, L. J. 1985. The mechanical behaviour of cancellous bone. *Journal of Biomechanics,* 18**,** 317-328.

Gibson, L. J. & Ashby, M. F. 1997. Chapter 11: Cancellous bone. *In: Cellular Solids: Structure and Properties.* 2nd ed. Cambridge, UK: Cambridge University Press.

Gloria, A., Causa, F., De Santis, R., Netti, P. A. & Ambrosio, L. 2007. Dynamic-mechanical properties of a novel composite intervertebral disc prosthesis. *Journal of Materials Science-Materials in Medicine,* 18**,** 2159-2165.

Goel, A., Chawla, K. K., Vaidya, U. K., Chawla, N. & Koopman, M. 2009. Characterization of fatigue behavior of long fiber reinforced thermoplastic (LFT) composites. *Materials Characterization,* 60**,** 537-544.

Goldenberg, R. A. & Driver, M. 2000. Long-term results with hydroxylapatite middle ear implants. *Otolaryngology-Head and Neck Surgery,* 122**,** 635-642.

Grusibic, V. & Simburger, A. Year. Fatigue under combined out-of-phase multiaxial stresses. *In:* International Conference on Fatigue Testing and Design, 1976 London. Society of Environmental Engineers.

Gude, M., Hufenbach, W., Koch, I. & Protz, R. 2006. Fatigue failure criteria and degradation rules for composites under multiaxial loadings. *Mechanics of Composite Materials,* 42**,** 443-450.

Gude, M., Hufenbach, W., Koch, I. & Protz, R. 2006. Fatigue failure criteria and degradation rules for composites under multiaxial loadings. *Mechanics of Composite Materials,* 42**,** 443-450.

Guo, X., Zheng, Q. & Du, J. 1998. Biodegradation and mechanical properties of hydroxyapatite/ poly-DL-lactide composites for fracture fixation. *Journal of Wuhan University Technology,* 13**,** 9-15.

Gupta, B., Revagade, N. & Hilborn, J. 2007. Poly(lactic acid) fiber: An overview. *Progress in Polymer Science,* 32**,** 455-482.

Han, Y., Fan, Z., Lu, Z., Zhang, Y. & Li, S. 2012. In vitro degradation of poly[(L-lactide)-co-(trimethylene carbonate)] copolymers and a composite with poly[(L-lactide)-co-glycolide] fibers as cardiovascular stent material. *Macromolecular Materials and Engineering,* 297**,** 128-135.

Harmia, T. 1996. Fatigue behavior of neat and long glass fiber (LGF) reinforced blends of nylon 66 and isotactic PP. *Polymer Composites,* 17**,** 926-936.

Harper, E. J. 1998. Bioactive bone cements. *Proceedings of the Institution of Mechanical Engineers, Part H: Journal of Engineering in Medicine,* 212**,** 113-120.

Harper, E. J., Behiri, J. C. & Bonfield, W. 1995. Flexural and fatigue properties of a bone cement based upon polyethylmethacrylate and hydroxyapatite. *Journal of Materials Science: Materials in Medicine,* 6**,** 799-803.

Harris, B. 2003. A historical review of the fatigue behaviour of fibre-reinforced plastics. *In:* Harris, B. (ed.) *Fatigue in composite.* Cambridge, UK: Woodhead Publishing Ltd.

Harris, B., Gathercole, N., Reiter, H. & Adam, T. 1997. Fatigue of carbon fibre reinforced plastic under block loading conditions. *Composites,* 25A**,** 327-337.

Harris, B., Reiter, H., Adam, T., Dickson, R. F. & Fernando, G. 1990. Fatigue behaviour of carbon fibre reinforced plastics. *Composites,* 21**,** 232-242.

Hashin, Z. & Rotem, A. 1973. A Fatigue Failure Criterion for Fiber Reinforced Materials. *Journal of Composite Materials,* 7**,** 448-464.

Hasting, G. W. 1978. Carbon fibre composite for orthopaedic implants,. *Composites,* 9**,** 193-197.

Hayes, W. C. & Wright, T. M. 1977. An Empirical Strength Theory for Compact Bone. *Fracture,* 3**,** 1173-1177.

Heidemann, W., Jeschkeit, S., Ruffieux, K., Fischer, J. H., Wagner, M., Krüger, G., Wintermantel, E. & Gerlach, K. L. 2001. Degradation of poly(d,l)lactide implants with or without addition of calciumphosphates in vivo. *Biomaterials,* 22**,** 2371-2381.

Hench, L. L. 1996. Ceramic, glasses and glass-ceramics. *In:* Ratner, B. D., Hoffmann, A.S., Scihien, F.J., Lemons, J.E., (ed.) *Biomaterials Science : An*

Introduction to Materials in Medicine. San Diego, California, USA: Academic Press.

Hench, L. L. 1998a. Bioceramics. *Journal of the American Ceramic Society,* 81**,** 1705-1728.

Hench, L. L. 1998b. Biomaterials: a forecast for the future. *Biomaterials,* 19**,** 1419-1423.

Hench, L. L. 2005. The Skeletal Systems. *In:* Hench, L. L. & Jones, J. R. (eds.) *Biomaterials, Artificial Organs and Tissue Engineering.* England: Woodhead Publishing Ltd.

Hench, L. L. & Wilson, J. 1993. Introduction. *In:* Hench, L. L. & J. Wilson, J. (eds.) *An Introduction to Bioceramics.* Singapore: World Scientific Publishing Co.

Hench, L. L. & Wilson, J. 1993. An introduction to bioceramics. *In:* Hench, L. L. & Wilson, J. (eds.). Singapore: World Scientific Publishing Co.

Hertzberg, R. W., Manson, J. A. & Skibo, M. 1975. Frequency sensitivity of fatigue processes in polymeric solids. *Polymer Engineering & Science,* 15**,** 252-260.

Herztberg, R. W. & Manson, J. A. 1980. *Fatigue of engineering plastic,* New York, Academic Press.

Hine, P. J., Olley, R. H. & Ward, I. M. 2008. The use of interleaved films for optimising the production and properties of hot compacted, self reinforced polymer composites. *Composites Science and Technology,* 68**,** 1413-1421.

Hine, P. J., Ward, I. M., Olley, R. H. & Bassett, D. C. 1993. The hot compaction of high modulus melt-spun polyethylene fibres. *Journal of Materials Science,* 28**,** 316-324.

Hou, M., Ye, L. & Mai, Y.-W. 1996. Effect of Moulding Temperature on Flexure, Impact Strength and Interlaminar Fracture Toughness of CF/PEI Composite. *Journal of Reinforced Plastics and Composites,* 15**,** 1117-1130.

Hsiao, H. M. & Daniel, I. M. 1996. Effect of fiber waviness on stiffness and strength reduction of unidirectional composites under compressive loading. *Composites Science and Technology,* 56**,** 581-593.

Hsiao, H. M., Daniel, I. M. & Wooh, S. C. 1995. A New Compression Test Method for Thick Composites. *Journal of Composite Materials,* 29**,** 1789-1806.

Huang, J. & Best, S. M. 2007. Ceramic biomaterials. *In:* Boccaccini, A. R. & Gough, J. E. (eds.) *Tissue Engineering Using Ceramics and Polymers.* Cambridge: Woodhead Publishing Ltd.

Huang, J., Di Silvio, L., Wang, M., Tanner, K. E. & Bonfield, W. 1997b. *In vitro assessment of hydroxyapatite- and Bioglass (R)-reinforced polyethylene composites,* Oxford, Pergamon Press Ltd.

Huang, J., DiSilvio, L., Wang, M., Tanner, K. E. & Bonfield, W. 1997a. In vitro mechanical and biological assessment of hydroxyapatite-reinforced polyethylene composite. *Journal of Materials Science-Materials in Medicine,* 8**,** 775-779.

Huang, Y. H., Li, D. P., Shen, T. C., Zuo, H., Tian, J. & Zou, J. 2011. Biomechanical properties of poly-L lactic acid/beta-tricalcium phosphate absorbable materials during degradation in vivo. *Journal of Clinical Rehabilitative Tissue Engineering Research,* 15**,** 7851-7854.

Hull, D. 1981. *An introduction to composite materials,* Cambridge, England, Cambridge University Press.

Hull, D. & Clyne, T. W. 1996. *An introduction to composite materials,* Cambridge, England, Cambridge University Press.

Huskins, D. W. L., Leahy, J. C. & Mathias, K. J. 1999. Biomaterials: Defining the Mechanical Properties of Natural Tissues and Selection of Replacement Materials. *Journal of Materials Chemistry,* 9**,** 629-636.

Huttunen, M., Ashammakhi, N., Törmälä, P. & Kellomäki, M. 2006. Fibre reinforced bioresorbable composites for spinal surgery. *Acta Biomaterialia,* 2**,** 575-587.

Huttunen, M., Tormala, P., Godinho, P. & Kellomaki, M. 2008. Fiber-reinforced bioactive and bioabsorbable hybrid composites. *Biomed Mater,* 3**,** 8.

Hyon, S. H., Jamshidi, K. & Ikada, Y. 1998. Effects of residual monomer on the degradation of DL-lactide polymer. *Polymer International,* 46**,** 196-202.

Hyon, S.-H., Jamshidi, K. & Ikada, Y. 1997. Synthesis of polylactides with different molecular weights. *Biomaterials,* 18**,** 1503-1508.

Ignatius, A. A., Augat, P. & Claes, L. E. 2001. Degradation behavior of composite pins made of tricalcium phosphate and poly(L,DL-lactide). *Journal of Biomaterials Science, Polymer Edition,* 12**,** 185-194.

Inoue, A., Fujii, T. & Kawakami, H. 2000. Effect of loading path on mechanical response of a glass fabric composite at low cyclic fatigue under tension/torsion biaxial loading. *Journal of Reinforced Plastics and Composites,* 19**,** 111-123.

Jaakkola, T., Rich, J., Tirri, T., Närhi, T., Jokinen, M., Seppälä, J. & Yli-Urpo, A. 2004. In vitro Ca-P precipitation on biodegradable thermoplastic composite of poly(ε-caprolactone-co-dl-lactide) and bioactive glass (S53P4). *Biomaterials,* 25**,** 575-581.

Jaakkola, T., Rich, J., Tirri, T., Närhi, T., Jokinen, M., Seppälä, J. & Yli-Urpo, A. 2004. In vitro Ca-P precipitation on biodegradable thermoplastic composite of poly(ε-caprolactone-co-dl-lactide) and bioactive glass (S53P4). *Biomaterials,* 25**,** 575-581.

Jacobsen, S., Fritz, H. G., Degée, P., Dubois, P. & Jérôme, R. 1999. Polylactide (PLA)—a new way of production. *Polymer Engineering & Science,* 39**,** 1311-1319.

Jan, C. & Grzegorz, K. 2005. The study of lifetime of polymer and composite bone joint screws under cyclical loads and in vitro conditions. *Journal of Materials Science: Materials in Medicine,* 16**,** 1051-1060.

Jarcho, M. 1981. Calcium phosphate ceramics as hard tissue prosthetics. *Clinical Orthopaedics and Related Research,* No.157**,** 259-278.

Jayaraman, N. & Ditmars, M. M. 1989. Torsional and biaxial (tension-torsion) fatigue damage mechanisms in Waspaloy at room temperature. *International Journal of Fatigue,* 11**,** 309-318.

Jelf, P. M. & Fleck, N. A. 1992. Compression Failure Mechanisms in Unidirectional Composites. *Journal of Composite Materials,* 26**,** 2706-2726.

Jelf, P. M. & Fleck, N. A. 1994. The failure of composite tubes due to combined compression and torsion. *Journal of Materials Science,* 29**,** 3080-3084.

Jeon, K.-W., Shin, K.-B. & Kim, J.-S. 2011. Evaluation of tension-compression and tension-tension fatigue life of woven fabric glass/epoxy laminate composites used in railway vehicle. *International Journal of Precision Engineering and Manufacturing,* 12**,** 813-820.

Johnson, J. A., Provan, J. W., Krygier, J. J., Chan, K. H. & Miller, J. 1989. Fatigue of acrylic bone cement--effect of frequency and environment. *J Biomed Mater Res,* 23**,** 819-31.

Jones, J. R. & Hench, L. L. 2006. Biomaterials: Bioceramics. *In:* Webster, J. G. (ed.) *Encyclopaedia of Medical Devices and Instrumentation.* Hoboken: Wiley.

Joseph, R. & Tanner, K. E. 2005. Effect of Morphological Features and Surface Area of Hydroxyapatite on the Fatigue Behavior of

Hydroxyapatite−Polyethylene Composites. *Biomacromolecules,* 6**,** 1021-1026.

Juutilainen, T. & Patiala, H. 1995. Arthrodesisi in rheumatoid arthritis using absorbable screws and rods. *Scandinavian Journal of Rheumatolology,* 24**,** 228-233.

Kadel, N. J., Teitz, C. C. & Kronmal, R. A. 1992. Stress fractures in ballet dancers. *The American Journal of Sports Medicine,* 20**,** 445-449.

Kalita, S. J., Bhardwaj, A. & Bhatt, H. A. 2007. Nanocrystalline calcium phosphate ceramics in biomedical engineering. *Materials Science and Engineering: C,* 27**,** 441-449.

Kallela, I., Laine, P., Suuronen, R., Ranta, P., Iizuka, T. & Lindqvist, C. 1999. Osteotomy site healing following mandibular sagittal split osteotomy and rigid fixation with polylactide biodegradable screws. *International Journal of Oral Maxillofacial Surgery,* 28**,** 166-70.

Kanazawa, K., Miller, K. J. & Brown, M. W. 1977. Low-Cycle Fatigue Under Out-of-Phase Loading Conditions. *Journal of Engineering Materials and Technology,* 99**,** 222-228.

Kane, R. J., Converse, G. L. & Roeder, R. K. 2008. Effects of the reinforcement morphology on the fatigue properties of hydroxyapatite reinforced polymers. *Journal of the Mechanical Behavior of Biomedical Materials,* 1**,** 261-268.

Kar, N. K., Hu, Y., Barjasteh, E. & Nutt, S. R. 2012. Tension–tension fatigue of hybrid composite rods. *Composites Part B: Engineering,* 43**,** 2115-2124.

Karger-Kocsis, J. & Friedrich, K. 1988. Fatigue crack propagation in short and long fibre-reinforced injection-moulded PA 6.6 composites. *Composites,* 19**,** 105-114.

Katogi, H., Shimamura, Y., Tohgo, K. & Fujii, T. 2012. Fatigue Behavior of Unidirectional Jute Spun Yarn Reinforced PLA. *Advanced Composite Materials,* 21**,** 1-10.

Kawai, M., Yajima, S., Hachinohe, A. & Takano, Y. 2001. Off-axis fatigue behavior of unidirectional carbon fiber-reinforced composites at room and high temperatures. *Journal of Composite Materials,* 35**,** 545-576.

Kawakami, H., Fujii, T. J. & Morita, Y. 1996. Fatigue degradation and life prediction of glass fabric polymer composite under tension/torsion biaxial loadings. *Journal of Reinforced Plastics and Composites,* 15**,** 183-195.

Kellomäki, M., Niiranen, H., Puumanen, K., Ashammakhi, N., Waris, T. & Törmälä, P. 2000. Bioabsorbable scaffolds for guided bone regeneration and generation. *Biomaterials,* 21**,** 2495-2505.

Kellomäki, M., Tanner, K. E., Bonfield, W. & Törmälä, P. 1997. Reinforced polylactide-hydroxyapatite composites. *13th European Conference on Biomaterials, Göteborg, Sweden.* Göteborg, Sweden.

Kelly, A. 1970. Interface Effects and the Work of Fracture of a Fibrous Composite. *Proceedings of the Royal Society of London. Series A, Mathematical and Physical Sciences,* 319**,** 95-116.

Kenwright, J. & Gardner, T. 1998. Mechanical Influences on Tibial Fracture Healing. *Clinical Orthopaedics and Related Research,* 355**,** S179-S190.

Kenwright, J., Richardson, J., Cunningham, J., White, S., Goodship, A., Adams, M., Magnussen, P. & Newman, J. 1991. Axial movement and tibial fractures. A controlled randomised trial of treatment. *Journal of Bone & Joint Surgery, British Volume,* 73-B**,** 654-659.

Kihara, H., Shiota, M., Yamashita, Y. & Kasugai, S. 2006. Biodegradation process of α-TCP particles and new bone formation in a rabbit cranial defect model. *Journal of Biomedical Materials Research Part B: Applied Biomaterials,* 79B**,** 284-291.

Kihara, T., Hirose, M., Oshima, A. & Ohgushi, H. 2006. Exogenous type I collagen facilitates osteogenic differentiation and acts as a substrate for mineralization of rat marrow mesenchymal stem cells in vitro. *Biochemical and Biophysical Research Communications,* 341**,** 1029-1035.

Kikuchi, M., Koyama, Y., Takakuda, K., Miyairi, H., Shirahama, N. & Tanaka, J. 2002. In vitro change in mechanical strength of β-tricalcium phosphate/copolymerized poly-L-lactide composites and their application for guided bone regeneration. *Journal of Biomedical Materials Research,* 62**,** 265-272.

Kikuchi, M., Koyama, Y., Yamada, T., Imamura, Y., Okada, T., Shirahama, N., Akita, K., Takakuda, K. & Tanaka, J. 2004. Development of guided bone regeneration membrane composed of β-tricalcium phosphate and poly (l-lactide-co-glycolide-co-ε-caprolactone) composites. *Biomaterials,* 25**,** 5979-5986.

Kim, K. S., Nam, K. M., Kwak, G. J. & Hwang, S. M. 2004. A fatigue life model for 5% chrome work roll steel under multiaxial loading. *International Journal of Fatigue,* 26**,** 683-689.

King, A. I. & Evans, F. G. 1967. Analysis of fatigue strength of human compact bone by Weibull method. *In:* Jacobson, B. (ed.) *Digest of the International Conference on Medical and Biological Engineering.* Stockholm.

Kivrak, N. & Taş, A. C. 1998. Synthesis of calcium hydroxyapatite-tricalcium phosphate (HA-TCP) composite bioceramic powders and their sintering behavior. *Journal of the American Ceramic Society,* 81**,** 2245-2252.

Kmetty, Á., Bárány, T. & Karger-Kocsis, J. 2010. Self-reinforced polymeric materials: A review. *Progress in Polymer Science,* 35**,** 1288-1310.

Kobayashi, H. Y. L. S., Brauer, D. S. & Rüssel, C. 2010. Mechanical properties of a degradable phosphate glass fibre reinforced polymer composite for internal fracture fixation. *Materials Science and Engineering: C,* 30**,** 1003-1007.

Kobayashi, S. & Sakamoto, K. 2006. Experimental and Analytical Characterization of β-Tricalcium Phosphate Particle Reinforced Poly-L-Lactide Composites. *JSME International Journal Series A Solid Mechanics and Material Engineering,* 49**,** 314-320.

Kobayashi, S. & Sakamoto, K. 2009. Effect of hydrolysis on mechanical properties of tricalcium phosphate/poly-l-lactide composites. *Journal of Materials Science: Materials in Medicine,* 20**,** 379-386.

Koerten, H. K. & van der Meulen, J. 1999. Degradation of calcium phosphate ceramics. *Journal of Biomedical Materials Research,* 44**,** 78-86.

Kohn, J. & Langer, R. 2004. Bioresorbable and bioerodible materials. *In:* Ratner, B., Hoffman, A., Schoen, F. & Lemons, J. (eds.) *Biomaterials Science; An Introduction to Materials in Medicine.* 2 ed. San Diego, USA: Academic Press.

Kohri, M., Miki, K., Waite, D. E., Nakajima, H. & Okabe, T. 1993. In vitro stability of biphasic calcium phosphate ceramics. *Biomaterials,* 14**,** 299-304.

Kondo, N., Ogose, A., Tokunaga, K., Ito, T., Arai, K., Kudo, N., Inoue, H., Irie, H. & Endo, N. 2005. Bone formation and resorption of highly purified β-tricalcium phosphate in the rat femoral condyle. *Biomaterials,* 26**,** 5600-5608.

Kozey, V. V. 1993. Fibre strength-dominated failure mode in unidirectional composites under compression. *Journal of Materials Science Letters,* 12**,** 48-52.

Kruzic, J. J. & Ritchie, R. O. 2008. Fatigue of mineralized tissues: Cortical bone and dentin. *Journal of the Mechanical Behaviour of Biomedical Materials,* 1**,** 3-17.

Lacroix, F. V., Loos, J. & Schulte, K. 1999. Morphological investigations of polyethylene fibre reinforced polyethylene. *Polymer,* 40**,** 843-847.

Lacroix, F. V., Werwer, M. & Schulte, K. 1998. Solution impregnation of polyethylene fibre/polyethylene matrix composites. *Composites Part A: Applied Science and Manufacturing,* 29**,** 371-376.

Ladizesky, N. H., Ward, I. M. & Bonfield, W. 1997. Hydrostatic extrusion of polyethylene filled with hydroxyapatite. *Polymers for Advanced Technologies,* 8**,** 496-504.

Ladizesky, N. H., Ward, I. M. & Bonfield, W. 1997. Hydroxyapatite/high-performance polyethylene fibre composites for high load bearing bone replacement materials. *Journal of Applied Polymer Science,* 65**,** 1865-1882.

Lakes, R. S. 2003. Composite biomaterials. *In:* Park, J. B. & Bronzino, J. D. (eds.) *Biomaterials-Principles and Applications.* Bota Raton, Florida: CRC Press LLC.

Landrigan, M. D. & Roeder, R. K. 2009. Systematic error in mechanical measures of damage during four-point bending fatigue of cortical bone. *Journal of Biomechanics,* 42**,** 1212-1217.

Lang, R. W., Manson, J. A., Hertzberg, R. W. & Schirrer, R. 1984. Craze development in poly(methyl methacrylate) during stable fatigue crack propagation. *Polymer Engineering & Science,* 24**,** 833-842.

Lankford, J. 1995. Compressive failure of fibre-reinforced composites: buckling, kinking, and the role of the interphase. *Journal of Materials Science,* 30**,** 4343-4348.

Lasprilla, A. J. R., Martinez, G. A. R., Lunelli, B. H., Jardini, A. L. & Maciel, R. 2012. Poly-lactic acid synthesis for application in biomedical devices - A review. *Biotechnology Advances,* 30**,** 321-328.

Laurencin, C. T. & Lu, H. H. 2000. Polymer-ceramic composites for bone-tissue engineering. *In:* Davies, J. E. (ed.) *Bone Engineering.* Toronto, Canada: EM Inc.

Le Huec, J. C., Lesprit, E., Delavigne, C., Clement, D., Chauveaux, D. & Le Rebeller, A. 1997. Tri-calcium phosphate ceramics and allografts as bone substitutes for spinal fusion in idiopathic scoliosis as bone substitutes for spinal fusion in idiopathic scoliosis: comparative clinical results at four years. *Acta Orthopaedica Beligica,* 63**,** 202-11.

Lee, C. S., Hwang, W., Park, H. C. & Han, K. S. 1999. Failure of carbon/epoxy composite tubes under combined axial and torsional loading 2. Fracture morphology and failure mechanism. *Composites Science and Technology,* 59**,** 1789-1804.

Lee, C. Y., Prasad, H. S., Suzuki, J. B., Stover, J. D. & Rohrer, M. D. 2011. The correlation of bone mineral density and histologic data in the early grafted maxillary sinus: a preliminary report. *Implant Dentistry,* 20**,** 202-14.

Leenslag, J. W., Gogolewski, S. & Penning, A. J. 1984. Resorbable materials of poly(L -lactide). 5. Influence of secondary structure on the mechanical-properties and hydrolyzability of poly(L-lactide) fibres produced by a dry-spinning method. *Journal of Applied Polymer Science,* 29**,** 2829-2842.

LeGeros, R. Z. 2008. Calcium-phosphate based osteoinductive materials. *Chemical Reviews,* 108**,** 4742-4753.

Lemanski, S. L. & Sutcliffe, M. P. F. 2012. Compressive failure of finite size unidirectional composite laminates with a region of fibre waviness. *Composites Part A: Applied Science and Manufacturing,* 43**,** 435-444.

Lewis, G., Janna, S. & Carroll, M. 2003. Effect of test frequency on the in vitro fatigue life of acrylic bone cement. *Biomaterials,* 24**,** 1111-1117.

Li, B., Reis, L. & de Freitas, M. 2009. Comparative study of multiaxial fatigue damage models for ductile structural steels and brittle materials. *International Journal of Fatigue,* 31**,** 1895-1906.

Li, H. & Chang, J. 2005. In vitro degradation of porous degradable and bioactive PHBV/wollastonite composite scaffolds. *Polymer Degradation and Stability,* 87**,** 301-307.

Li, J., Zhang, Z.-p., Sun, Q., Li, C.-w. & Li, R.-s. 2011. A Simple Relationship Between Axial and Torsional Cyclic Parameters. *Journal of Materials Engineering and Performance,* 20**,** 1289-1293.

Li, S., Garreau, H. & Vert, M. 1990c. Structure-property relationships in the case of the degradation of massive poly(α-hydroxy acids) in aqueous media. *Journal of Materials Science: Materials in Medicine,* 1**,** 198-206.

Li, S. & Vert, M. 1999. Biodegradable polymers: Polyesters. *In:* Mathiowitz, E. (ed.) *Encylopaedia of Controlled Drug Delivery.* John Wiley and Sons.

Li, S. M., Garreau, H. & Vert, M. 1990a. Structure-property relationships in the case of the degradation of massive aliphatic poly-(α-hydroxy acids) in aqueous media. *Journal of Materials Science: Materials in Medicine,* 1**,** 123-130.

Li, S. M., Garreau, H. & Vert, M. 1990b. Structure-property relationships in the case of the degradation of massive poly(α-hydroxy acids) in aqueous media. *Journal of Materials Science: Materials in Medicine,* 1**,** 131-139.

Liang, J. Z., Li, R. K. Y. & Tjong, S. C. 1999. Tensile properties and morphology of PP/EPDM/glass bead ternary composites. *Polymer Composites,* 20**,** 413-422.

Limonov, V. A., Perevozchikov, V. G. & Tamuzh, V. P. 1988. Fatigue of laminated composites with various reinforcement systems. 1. Experimental results. *Mechanics of Composite Materials,* 24**,** 585-594.

Lin, F.-H., Chen, T.-M., Lin, C.-P. & Lee, C.-J. 1999. The Merit of Sintered PDLLA/TCP Composites in Management of Bone Fracture Internal Fixation. *Artificial Organs,* 23**,** 186-194.

Linnemann, B., Sri Harwoko, M. & Gries, T. 2003. Polylactide fibers (PLA). *Chemical Fibers International,* 53**,** 426-433.

Little, R. E. 1969. A note on the shear stress criterion for fatigue failure under combined stresses. *Aeronautical Quarterly,* 20**,** 57-60.

Liu, C. T. & Ravi-Chandar, K. 1996. Local Fracture and Crack Growth Behavior in a Particulate Composite Material. *Journal of Reinforced Plastics and Composites,* 15**,** 196-207.

Liu, Y., Lu, Y., Tian, X., Cui, G., Zhao, Y., Yang, Q., Yu, S., Xing, G. & Zhang, B. 2009. Segmental bone regeneration using an rhBMP-2-loaded gelatin/nanohydroxyapatite/fibrin scaffold in a rabbit model. *Biomaterials,* 30**,** 6276-6285.

Liu, Y. & Mahadevan, S. 2007. A unified multiaxial fatigue damage model for isotropic and anisotropic materials. *International Journal of Fatigue,* 29**,** 347-359.

Losken, H. W., van Aalst, J. A., Mooney, M. P., Godfrey, V. L., Burt, T., Teotia, S., Dean, S. B., Moss, J. R. & Rahbar, R. 2008. Biodegradation of Inion fast-

absorbing biodegradable plates and screws. *Journal of Craniofacial Surgery,* 19**,** 748-56.

Lu, H. H., El-Amin, S. F., Scott, K. D. & Laurencin, C. T. 2003. Three-dimensional, bioactive, biodegradable, polymer–bioactive glass composite scaffolds with improved mechanical properties support collagen synthesis and mineralization of human osteoblast-like cells in vitro. *Journal of Biomedical Materials Research Part A,* 64A**,** 465-474.

Lu, H. H., Tang, A., Oh, S. C., Spalazzi, J. P. & Dionisio, K. 2005. Compositional effects on the formation of a calcium phosphate layer and the response of osteoblast-like cells on polymer-bioactive glass composites. *Biomaterials,* 26**,** 6323-6334.

Madhukar, M. S. & Drzal, L. T. 1992. Fiber-Matrix Adhesion and Its Effect on Composite Mechanical Properties. III. Longitudinal (0°) Compressive Properties of Graphite/Epoxy Composites. *Journal of Composite Materials,* 26**,** 310-333.

Majola, A., Vainionpää, S., Rokkanen, P., Mikkola, H. M. & Törmälä, P. 1992. Absorbable self-reinforced polylactide (SR-PLA) composite rods for fracture fixation: strength and strength retention in the bone and subcutaneous tissue of rabbits. *Journal of Materials Science: Materials in Medicine,* 3**,** 43-47.

Manninen, M. J. & Pohjonen, T. 1993. Intramedullary nailing of the cortical bone osteotomies in rabbits with self-reinforced poly-l-lactide rods manufactured by the fibrillation method. *Biomaterials,* 14**,** 305-312.

Maquet, V., Boccaccini, A. R., Pravata, L., Notingher, I. & Jerome, R. 2003. Preparation, characterization, and in vitro degradation of bioresorbable and bioactive composites based on Bioglass (R)-filled polylactide foams. *Journal of Biomedical Materials Research Part A,* 66A**,** 335-346.

Maquet, V., Boccaccini, A. R., Pravata, L., Notingher, I. & Jerome, R. 2004. Porous poly(alpha-hydroxyacid)/Bioglass (R) composite scaffolds for bone tissue engineering. I: preparation and in vitro characterisation. *Biomaterials,* 25**,** 4185-4194.

Maquet, V., Martin, D., Scholtes, F., Franzen, R., Schoenen, J., Moonen, G. & Jerome, R. 2001. Poly(D,L-lactide) foams modified by poly(ethylene oxide)-block-poly(D,L-lactide) copolymers and a-FGF: in vitro and in vivo evaluation for spinal cord regeneration. *Biomaterials,* 22**,** 1137-1146.

Marquis, G. B. & Socie, D. F. 2003. 4.09 - Multiaxial Fatigue. *In:* Editors-in-Chief: , I. M., Ritchie, R. O. & Karihaloo, B. (eds.) *Comprehensive Structural Integrity.* Oxford: Pergamon.

Martin, R. B. 1999. Bone as a Ceramic Composite Material. *In:* Shackelford, J. F. (ed.) *Materials Science Forum.* New Zealand: Trans Tech Publications.

Martini, F. H. 1995. *Fundamentals of Anatomy and Physiology*, Prentice Hall.

Martini, F. H. 2004. *Fundamentals of Anatomy and Physiology,* New Jersey, USA, Prentice Hall.

Matheson, G. O., Clement, D. B., Mckenzie, D. C., Taunton, J. E., Lloyd-Smith, D. R. & Macintyre, J. G. 1987. Stress fractures in athletes. *The American Journal of Sports Medicine,* 15**,** 46-58.

Matsuda, S., Kishi, H. & Murakami, A. 2004. New processing of apataite fiber and some application for medical use. *Composites Science and Technology,* 64**,** 909-914.

Matsusue, Y., Yamamuro, T., Oka, M., Shikinami, Y., Hyon, S.-H. & Ikada, Y. 1992. In vitro and in vivo studies on bioabsorbable ultra-high-strength poly(L-lactide) rods. *Journal of Biomedical Materials Research,* 26**,** 1553-1567.

Maurus, P. B. & Kaeding, C. C. 2004. Bioabsorbable implant material review. *Operative Techniques in Sports Medicine,* 12**,** 158-160.

McEvily, A., Raymond, C. B. & Jonhston, T. L. Year. On the formation and Growth of Fatigue Cracks in Polymers, Fatigue -An Interdisciplinary Approach. *In:* Burke, J. J., Rees, N. L. & Weiss, V., eds. Proceeding of the 10th Sagamore Army Materials Research Conference, 1964. Syracuse University Press, 95-104.

McKinley, M. & O'Loughlin, V. D. 2008. *Human Anatomy,* New York, McGraw-Hill Higher Education.

Meer, S. A. T., Wijn, J. R. & Wolke, J. G. C. 1996. The influence of basic filler materials on the degradation of amorphous D- and L-lactide copolymer. *Journal of Materials Science: Materials in Medicine,* 7**,** 359-361.

Merten, H. A., Wiltfang, J., Grohmann, U. & Hoenig, J. F. 2001. Intraindividual comparative animal study of alpha- and beta-tricalcium phosphate degradation in conjunction with simultaneous insertion of dental implants. *Journal of Craniofacial Surgery,* 12**,** 59-68.

Middleton, J. C. & Tipton, A. J. 2000. Synthetic biodegradable polymers as orthopedic devices. *Biomaterials,* 21**,** 2335-2346.

Mishnaevsky Jr, L. & Brøndsted, P. 2009. Statistical modelling of compression and fatigue damage of unidirectional fiber reinforced composites. *Composites Science and Technology,* 69**,** 477-484.

Misra, S. K., Nazhat, S. N., Valappil, S. P., Moshrefi-Torbati, M., Wood, R. J. K., Roy, I. & Boccaccini, A. R. 2007. Fabrication and Characterization of Biodegradable Poly(3-hydroxybutyrate) Composite Containing Bioglass *Biomacromolecules,* 8**,** 2112-2119.

Moore, D. R. 1993. Long-Term Mechanical Properties of Aromatic Thermoplastic Continuous Fiber Composites: Creep and Fatigue. *In:* Kausch, H. H. (ed.) *Advance Thermoplastic Composite: Characterization and Processing* Munich: Hanser Publishers.

Morris, A. D. & Garrett, G. G. 1981. A comparative study of the static and fatigue behaviour of plain and steel fibre reinforced mortar in compression and direct tension. *International Journal of Cement Composites and Lightweight Concrete,* 3**,** 73-91.

Morris, S. 1974. PhD Thesis, University of Nothingham, UK, 1970. *In:* Broutman, L. J. & Krock, R. H. (eds.) *Composite Materials.* New York: Academics.

Muller, J. A., Vashishth, D. & Milgrom, C. 2003. Anisotropic analysis of in-vivo strain gauge data yield clues about fatigue fracture during normal activity. *Transactions of the 50th Annual Orthopaedic Research Society,2004*.

Mustafa, Z. 2005. *The testing of fibre reinforced composites for metacarpal fixation.* MSc Thesis, Queen Mary, University of London.

Mustafa, Z. & Tanner, K. E. 2012. Composites for Hard Tissue Repair. *In:* Nicolais, L. and Borzacchiello, A. (ed.) *Wiley Encyclopaedia of Composites.* John Wiley & Sons, Inc.

Nair, L. S. & Laurencin, C. T. 2007. Biodegradable polymers as biomaterials. *Progress in Polymer Science,* 32**,** 762-798.

Nakagawa, N., Saegusa, Y., Abe, S., Miura, Y. & Yoshiya, S. 2006. The effectiveness of RA wrist fusion using beta-TCP without autogenous iliac bone grafting: A report of four cases. *Hand Surgery,* 11**,** 71-75.

Narhi, T. O., Jansen, J. A., Jaakkola, T., de Ruijter, A., Rich, J., Seppala, J. & Yli-Urpo, A. 2003. Bone response to degradable thermoplastic composite in rabbits. *Biomaterials,* 24**,** 1697-1704.

Neo, M., Herbst, H., Voigt, C. F. & Gross, U. M. 1998. Temporal and spatial patterns of osteoblast activation following implantation of beta-TCP particles into bone. *Journal of Biomedical Materials Research,* 39**,** 71-6.

Neumann, M. & Epple, M. 2006. Composites of Calcium Phosphate and Polymers as Bone Substitution Materials. *European Journal of Trauma,* 32**,** 125-131.

Nielsen, L. E. & Landel, R. F. 1994. *Mechanical Properties of Polymers and Composites,* New York, Marcel Dekker.

Nielsen, L. E. & Lee, B.-L. 1972. Dynamic Mechanical Properties of Some Polystyrene Composites. *Journal of Composite Materials,* 6**,** 136-146.

Niemelä, T. 2010. *Self reinforced bioceramic and polylactide based composites.* Doctor of Science PhD, Tampere University of Technology.

Niemelä, T. & Kellomäki, M. 2007. Three composites of bioactive glass and PLA-copolymers: Mass loss and water absorption in vitro. *Key Engineering Materials,* 330-332. **,** 431-434.

Niemela, T., Kellomaki, M. & Tormala, P. 2004. In vitro degradation of osteoconductive poly-L/DL-lactide/b-TCP composites. *Key Eng Mater 2004,,* 54**,** 509−512.

Niemelä, T., Niiranen, H. & Kellomäki, M. 2008. Self-reinforced composites of bioabsorbable polymer and bioactive glass with different bioactive glass contents. Part II: In vitro degradation. *Acta Biomaterialia,* 4**,** 156-164.

Niemelä, T., Niiranen, H., Kellomäki, M. & Törmälä, P. 2005. Self-reinforced composites of bioabsorbable polymer and bioactive glass with different bioactive glass contents. Part I: Initial mechanical properties and bioactivity. *Acta Biomaterialia,* 1**,** 235-242.

Niiranen, H., Pyhältö, T., Rokkanen, P., Kellomäki, M. & Törmälä, P. 2004. In vitro and in vivo behavior of self-reinforced bioabsorbable polymer and self-reinforced bioabsorbable polymer/bioactive glass composites. *Journal of Biomedical Materials Research Part A,* 69A**,** 699-708.

Niiranen, H. & Törmälä, P. Year. Self-Reinforced Bioactive Glass-Bioabsorbable Polymer Composites. *In:* Neenan, T., Marcolongo, M. & Valentini, R. F., eds. Biomedical materials: drug delivery, implants, and tissue engineering, 1999. Materials Research Society, 267–272.

Nishihara, T. & Kawamoto, M. 1945. The strength of metals under combined alternating bending and torsion with phase difference. *Memoirs of College Engineering., Kyoto Imperial University,* 11**,** 85-112.

Nisitani, H. & Takao, K. 1977. Influence of Mean Stress on Crack Closure Phenomenon and Fatigue Crack Propagation. *Bulletin of the Japanese Society of Mechanical Engineers,* 20**,** 264-268.

Ogose, A., Kondo, N., Umezu, H., Hotta, T., Kawashima, H., Tokunaga, K., Ito, T., Kudo, N., Hoshino, M., Gu, W. & Endo, N. 2006. Histological assessment in grafts of highly purified beta-tricalcium phosphate (OSferion®) in human bones. *Biomaterials,* 27**,** 1542-1549.

Oonishi, H. & Oomamiuda, K. 1998. Degradation/resorption in bioactive ceramics in orthopedics. *In:* Black, J. & Hasting, G. (eds.) *Handbook of Biomaterials Properties.* London: Chapman & Hall.

Owen, M. J. & Rice, D. J. 1981. Biaxial strength behaviour of glass fabric-reinforced polyester resins. *Composites,* 12**,** 13-25.

Paris, P. C. 1962. *The growth of crack due to variations in loads.* PhD thesis, Lehigh University.

Park, J. & Lakes, R. S. 2007. *Biomaterials, An Introduction,* New York, Springer.

Park, M. S., Aryan, H. E., Ozgur, B. M., Jandial, R. & Taylor, W. R. 2004. Stabilization of Anterior Cervical Spine with Bioabsorbable Polymer in One- and Two-level Fusions. *Neurosurgery,* 54**,** 631-635.

Parker, E. R. 1957. *Brittle behaviour of Engineering Structures,* New York, John Wiley and Sons.

Parsons, W. B. 1939. *Engineers and Engineering in the Renaissance,* Baltimore.

Partio, E. K., Böstman, O., Hirvensalo, E., Vainionpää, S., Vihtonen, K., Pätiälä, H., Törmälä, P. & Rokkanen, P. 1992. Self-reinforced absorbable screws in the fixation of displaced ankle fractures: a prospective clinical study of 152 patients. *Journal of Orthopedic Trauma,* 6**,** 209-215.

Pattin, C. A. 1991. *Cyclic Mechanical Property Degradation during Fatigue Loading of Cortical Bone.* PhD Thesis, University of Stanford.

Pattin, C. A., Caler, W. E. & Carter, D. R. 1996. Cyclic mechanical property degradation during fatigue loading of cortical bone. *Journal of Biomechanics,* 29**,** 69-79.

Pegoretti, A. & Ricco, T. 2000. Fatigue Fracture of Neat and Short Glass Fiber Reinforced Polypropylene: Effect of Frequency and Material Orientation. *Journal of Composite Materials,* 34**,** 1009-1027.

Pegoretti, A. & Ricco, T. 2002. Crack growth in discontinuous glass fibre reinforced polypropylene under dynamic and static loading conditions. *Composites Part a-Applied Science and Manufacturing,* 33**,** 1539-1547.

Perevozchikov, V. G., Limonov, V. A., Protasov, V. D. & Tamuzh, V. P. 1988. Static and fatigue strength of unidirectional composites under the combined effect of shear stress and transverse tension-compression stresses. *Mechanics of Composite Materials,* 24**,** 638-644.

Petermann, J. 2004. *A Contribution to Evaluate and Predict the Strength and Life Time of Angle-Ply Laminates under Static and Cyclic Loads,* TU, Hamburg–Harburg.

Philips, D. C. & J.M., S. 1976. AERE Technical Report AERE G645. Automic Energy Authority, UK.

Pietrzak, W. S., Sarver, D. R. & Verstynen, M. L. 1997. Bioabsorbable polymer science for the practicing surgeon. *Journal Craniofacial Surgery,* 8**,** 87-91.

Piggott, M. R. 1995. The effect of fibre waviness on the mechanical properties of unidirectional fibre composites: A review. *Composites Science and Technology,* 53**,** 201-205.

Pihlajamäki, H., Bostman, O., Hirvensalo, E., Tormala, P. & Rokkanen, P. 1992. Absorbable pin of self reinforced poly l-lactide acid for fixation of fractures and osteotomies. *Journal of Bone and Joint Surgery,* 74B**,** 853-857.

Pihlajamäki, H., Kinnunen, J. & Böstman, O. 1997. In vivo monitoring of the degradation process of bioresorbable polymeric implants using magnetic resonance imaging. *Biomaterials,* 18**,** 1311-1315.

Pistner, H., Bendix, D. R., Mühling, J. & Reuther, J. F. 1993. Poly(L-lactide): a long-term degradation study in vivo. Part III. Analytical characterization. *Biomaterials,* 14**,** 291-298.

Pohjonen, T., Helevirta, P., Tormala, P., Koskikare, K., Patiala, H. & Rokkanen, P. 1997. Strength retention of self-reinforced poly-L-lactide screws. A comparison of compression moulded and machine cut screws. *Journal of Materials Science: Materials in Medicine,* 8**,** 311-320.

Pohjonen, T. & Törmälä, P. 1996. In vitro hydrolysis of self-reinforced polylactide composites. *Medical and Biological Engineering and Computing,* 34**,** 127-128.

Portier, L., Calloch, S., Marquis, D. & Geyer, P. 2000. Ratchetting under tension–torsion loadings: experiments and modelling. *International Journal of Plasticity,* 16**,** 303-335.

Potter, K., Khan, B., Wisnom, M., Bell, T. & Stevens, J. 2008. Variability, fibre waviness and misalignment in the determination of the properties of composite materials and structures. *Composites Part A: Applied Science and Manufacturing,* 39**,** 1343-1354.

Pouilles, J. M., Bernard, J., Tremollières, F., Louvet, J. P. & Ribot, C. 1989. Femoral bone density in young male adults with stress fractures. *Bone,* 10**,** 105-108.

Pruitt, L. & Suresh, S. 1992. Fatigue crack growth in unidirectional graphite-epoxy composites under cyclic compression. *Journal of Materials Science Letters,* 11**,** 1356-1360.

Quaresimin, M., Susmel, L. & Talreja, R. 2010. Fatigue behaviour and life assessment of composite laminates under multiaxial loadings. *International Journal of Fatigue,* 32**,** 2-16.

Quaresimin, M., Susmel, L. & Talreja, R. 2010. Fatigue behaviour and life assessment of composite laminates under multiaxial loadings. *International Journal of Fatigue,* 32**,** 2-16.

Raikin, S. M. & Ching, A. C. 2005. Bioabsorbable Fixation in Foot and Ankle. *Foot and Ankle Clinics,* 10**,** 667-684.

Ramani, S. V. & Williams, D. P. 1976. *Failure Mode in Composite,* New York, 115-140, Metallurgical Society of AIME.

Ranne, T., Tirri, T., Yli-Urpo, A., Narhi, T. O., Laine, V. J. O., Rich, J., Seppala, J. & Aho, A. 2007. In vivo behavior of poly(epsilon-caprolactone-CO-DL-lactide)/bioactive glass composites in rat subcutaneous tissue. *Journal of Bioactive and Compatible Polymers,* 22**,** 249-264.

Rao, V. & Drzal, L. T. 1991. The dependence of interfacial shear strength on matrix and interphase properties. *Polymer Composites,* 12**,** 48-56.

Ravi Chandran, K. S., Chang, P. & Cashman, G. T. 2010. Competing failure modes and complex S–N curves in fatigue of structural materials. *International Journal of Fatigue,* 32**,** 482-491.

Reed, A. M. & Gilding, D. K. 1981. Biodegradable polymers for use in surgery — poly(glycolic)/poly(lactic acid) homo and copolymers: 2. In vitro degradation. *Polymer,* 22**,** 494-498.

Reifsnider, K. L. 1990. Damage and damage mechanics. *In:* Reifsnider, K. L. (ed.) *Fatifue of composite materials.* Amsterdam: Elsevier.

Reinhart, T. J. & Clements, L. L. 1987. Introduction to composites. *Engineered Materials Handbook.* ASM International.

Reis, R. L., Cunha, A. M., Oliveira, M. J., Campos, A. R. & Bevis, M. J. 2001. Relationship between processing and mechanical properties of injection molded high molecular mass polyethylene + hydroxyapatite composites. *Materials Research Innovations,* 4**,** 263-272.

Revell, P. 1998. Bone structure. *In:* Hughes, S. P. F. & McCarthy, I. D. (eds.) *Science basic to orthopaedics.* London: W.B. Saunders.

Rey, C., Combes, C., Drouet, C. & Somrani, S. 2008. Tricalcium phosphate-based ceramics. *In:* Kokobo, T. (ed.) *Bioceramic and their clinical applications.* Cambridge, England: Woodhead Publishing Limited.

Rezwan, K., Chen, Q. Z., Blaker, J. J. & Boccaccini, A. R. 2006. Biodegradable and bioactive porous polymer/inorganic composite scaffolds for bone tissue engineering. *Biomaterials,* 27**,** 3413-3431.

Rich, J., Jaakkola, T., Tirri, T., Närhi, T., Yli-Urpo, A. & Seppälä, J. 2002. In vitro evaluation of poly(ε-caprolactone-co-DL-lactide)/bioactive glass composites. *Biomaterials,* 23**,** 2143-2150.

Richardson, J., Cunningham, J., Goodship, A., O'Connor, B. & Kenwright, J. 1994. Measuring stiffness can define healing of tibial fractures. *Journal of Bone & Joint Surgery, British Volume,* 76-B**,** 389-394.

Ritchie, R., McClintock, F., Nayeb-Hashemi, H. & Ritter, M. 1982. Mode III fatigue crack propagation in low alloy steel. *Metallurgical and Materials Transactions A,* 13**,** 101-110.

Ritchie, R. O. 1988. Mechanisms of fatigue crack propagation in metals, ceramics and composites: Role of crack tip shielding. *Materials Science and Engineering,* A103**,** 15-28.

Ritchie, R. O., McClintock, F., Tsehegg, E. K. & Nayeb-Hashemi, H. 1985. Mode III fatigue crack growth under combined torsional and axial loading. *In:* Miller, J. & Brown, M. (eds.) *Multiaxial Fatigue.* ASTM STP.

Roberts, M., Reiss, M. & Monger, G. 1993. *Biology: Principles and Processes*, Nelson.

Rokkanen, P. U., Bostman, O., Hirvensalo, E., Makela, E. A., Partio, E. K., Patiala, H., Vainionpa, S., Vihtonen, K. & Tormala, P. 2000. Bioabsorbable fixation in orthopaedic surgery and traumatology. *Biomaterials,* 21**,** 2607-2613.

Ryu, H. S., Youn, H. J., Sun Hong, K., Chang, B. S., Lee, C. K. & Chung, S. S. 2002. An improvement in sintering property of β-tricalcium phosphate by addition of calcium pyrophosphate. *Biomaterials,* 23**,** 909-914.

Kunz, S. C. & Beaumont, P. W. R. 1975. *Fatigue of Composite Materials STP 569,* Philadelphia, USA, ASTM Philadelphia, USA, 71-91.

Samat, N., Burford, R., Whittle, A. & Hoffman, M. 2009. The effects of frequency on fatigue threshold and crack propagation rate in modified and unmodified polyvinyl chloride. *Polymer Engineering & Science,* 49**,** 1299-1310.

Sanosh, K. P., Chu, M. C., Balakrishnan, A., Kim, T. N. & Cho, S. J. 2010. Sol-gel synthesis of pure nano sized β-tricalcium phosphate crystalline powders. *Current Applied Physics,* 10**,** 68-71.

Saringer, W., Nobauer-Huhmann, I. & Knosp, E. 2002. Cranioplasty with individual carbon fibre reinforced polymer (CFRP) medical grade implants based on CAD/CAM technique. . *Acta Neurochir,* 144**,** 1193-1203.

Sauer, J. & Richardson, G. 1980. Fatigue of polymers. *International Journal of Fracture,* 16**,** 499-532.

Saunders, L. 1998. Hapex^{TM} Progress Report. *mentioned in Ton That Thesis (2000).* London: Queen Mary, University of London.

Schadler, L. S., Laird, C. & Figueroa, J. C. 1992. Interphase behaviour in graphite-thermoplastic monofilament composites. *Journal of Materials Science,* 27**,** 4035-4044.

Schambron, T., Lowe, A. & McGregor, H. V. 2008. Effects of environmental ageing on the static and cyclic bending properties of braided carbon fibre/PEEK bone plates. *Composites Part B: Engineering,* 39**,** 1216-1220.

Schiller, C. & Epple, M. 2003. Carbonated calcium phosphates are suitable pH-stabilising fillers for biodegradable polyesters. *Biomaterials,* 24**,** 2037-2043.

Schmidt, F., Rheinfurth, M., Horst, P. & Busse, G. 2012. Effects of local fibre waviness on damage mechanisms and fatigue behaviour of biaxially loaded tube specimens. *Composites Science and Technology,* 72**,** 1075-1082.

Shikinami, Y., Matsusue, Y. & Nakamura, T. 2005. The complete process of bioresorption and bone replacement using devices made of forged

composites of raw hydroxyapatite particles/poly l-lactide (F-u-HA/PLLA). *Biomaterials,* 26**,** 5542-5551.

Shikinami, Y. & Okuno, M. 1999. Bioresorbable devices made of forged composites of hydroxyapatite (HA) particles and poly-L-lactide (PLLA): Part I. Basic characteristics. *Biomaterials,* 20**,** 859-877.

Shikinami, Y. & Okuno, M. 2001. Bioresorbable devices made of forged composites of hydroxyapatite (HA) particles and poly l-lactide (PLLA). Part II: practical properties of miniscrews and miniplates. *Biomaterials,* 22**,** 3197-3211.

Shinozaki, D. & Groves, G. W. 1973. The plastic deformation of oriented polypropylene: tensile and compressive yield criteria. *Journal of Materials Science,* 8**,** 71-78.

Shokrieh, M. M. & Lessard, L. B. 2003. Fatigue under multiaxial stress systems. *In:* Harris, B. (ed.) *Fatigue in Composites.* Cambride, UK Woodhead Publishing

Sin, L. T., Rahmat, A. R. & Rahman, W. A. W. A. 2012. 5 - Mechanical Properties of Poly(lactic Acid). *Polylactic Acid.* Oxford: William Andrew Publishing.

Sivashanker, S. 1998. Damage growth in carbon fibre–PEEK unidirectional composites under compression. *Materials Science and Engineering: A,* 249**,** 259-276.

Sivashanker, S., Fleck, N. A. & Sutcliffe, M. P. F. 1996. Microbuckle propagation in a unidirectional carbon fibre-epoxy matrix composite. *Acta Materialia,* 44**,** 2581-2590.

Slaughter, W. S. & Fleck, N. A. 1993. Compressive fatigue of fibre composites. *Journal of the Mechanics and Physics of Solids,* 41**,** 1265-1284.

Smith, E. W. & Pascoe, K. J. 1977. The role of shear deformation in the fatigue failure of a glass fibre-reinforced composite. *Composites,* 8**,** 237-243.

Smith, E. W. & Pascoe, K. J. 1989. Biaxial fatigue of glass–fibre reinforced composite. Part 1: fatigue and fracture behaviour. *In:* M. Brown, K. J. M. (ed.) *Biaxial and multiaxial fatigue EGF 3.* London: Mechanical Engineering Publications.

Socie, D. 1987. Multiaxial Fatigue Damage Models. *Journal of Engineering Materials and Technology,* 109**,** 293-298.

Socie, D. 1993. Critical Plane Approaches for Multiaxial Fatigue Damage Assessment. *In:* McDowell, D. L. & Ellis, R. (eds.) *Advances in Multiaxial Fatigue.* Philadephia: ASTM STP.

Socie, D. F., Kurath, P. & Kock, J. L. 1985. A Multiaxial Fatigue Damage Paremater. *Second International Conference on Multiaxial Fatigue.*

Sonsino, C. M. 2001. Influence of load and deformation-controlled multiaxial tests on fatigue life to crack initiation. *International Journal of Fatigue,* 23**,** 159-167.

Sonsino, C. M. & Grubisic, V. 1985. Mechanik von schwingbrüchen an gegossenen und gesinterten konstruktionswerkstoffen unter mehrachsiger beanspruchung. *Konstruktion,* 37**,** 261-269.

Sousa, R. A., Reis, R. L., Cunha, A. M. & Bevis, M. J. 2002. Structure development and interfacial interactions in high-density polyethylene/hydroxyapatite (HDPE/HA) composites molded with preferred orientation. *Journal of Applied Polymer Science,* 86**,** 2873-2886.

Sousa, R. A., Reis, R. L., Cunha, A. M. & Bevis, M. J. 2003. Processing and properties of bone-analogue biodegradable and bioinert polymeric composites. *Composites Science and Technology,* 63**,** 389-402.

Soutis, C. & Fleck, N. A. 1990. Static compression failure of carbon fibre t800/924c composite plate with a single hole. *Journal Composite Material,* 24**,** 536-558.

Suresh, S. 1998. *Fatigue of Materials,* Cambridge, UK, Cambridge University Press.

Susmel, L. & Petrone, N. 2003. Multiaxial fatigue life estimations for 6082-T6 cylindrical specimens under in-phase and out-of-phase biaxial loadings. *In:* Andrea Carpinteri, M. d. F. & Andrea, S. (eds.) *European Structural Integrity Society.* Elsevier.

Suuronen, R. 1993. Biodegradable fracture-fixation devices in maxillofacial surgery. *Int J Oral Maxillofac Surg,* 22**,** 50-7.

Suuronen, R., Pohjonen, T., Wessman, L., Tormala, P. & Vainionpaa, S. 1992. New generation biodegradable plate for fracture fixation: Comparison of bending strengths of mandibular osteotomies fixed with absorbable self-reinforced multi-layer poly-l-lactide plates and metallic plates - An experimental study in sheep. *Clinical Materials,* 9**,** 77-84.

Swanson, S. R., Messick, M. & Toombes, G. R. 1985. Comparison of torsion tube and Iosipescu in-plane shear test results for a carbon fibre-reinforced epoxy composite. *Composites,* 16**,** 220-224.

Szabo, G., Huys, L., Coulthard, P., Maiorana, C., Garagiola, U., Barabas, J., Nemeth, Z., Hrabak, K. & Suba, Z. 2005. A prospective multicenter randomized clinical trial of autogenous bone versus beta-tricalcium phosphate graft alone for bilateral sinus elevation: histologic and histomorphometric evaluation. *Int J Oral Maxillofac Implants,* 20**,** 371-81.

Tai, N. H., Ma, C. C. M. & Wu, S. H. 1995. Fatigue behaviour of carbon fibre/PEEK laminate composites. *Composites,* 26**,** 551-559.

Talreja, R. 1981. Fatigue of Composite Materials: Damage Mechanisms and Fatigue-Life Diagrams. *Proceedings of the Royal Society of London. A. Mathematical and Physical Sciences,* 378**,** 461-475.

Tanaka, T., Fujii, T. & Ishikawa, A. 1998. Damage Progression and Failure of Glass Fabric Composites Subjected to Tension/Tension and Tension/Shear Combined Stresses. *Journal of Thermoplastic Composite Materials,* 11**,** 82-96.

Tanaka, T., Fujii, T. & Kamada, M. 1996. Effect of Loading Path on the Stress-Strain Relation and Progressive Damage of a Polymer-Matrix Composite under Tension/Torsion Biaxial Loading. *Journal of Thermoplastic Composite Materials,* 9**,** 329-341.

Tang, H. C., Nguyen, T., Chuang, T. J., Chin, J. W., Wu, H. F. & Lesko, J. Year. Temperature Effects on Fatigue of Polymer Composites. *In:* Hui, D., ed. Composites Engineering, 7th Annual International Conference ICCE/7, July 2-8, 2000 Denver. 861-862 p.

Tanner, K. E. 2010. Hard tissue applications of biocomposites. *In:* Ambrosio, L. (ed.) *Biomedical Composites.* Cambridge, UK: Woodhead Publishers.

Tanner, K. E. 2012. *RE: Personal communications.*

Tanner, K. E., Downes, R. N. & Bonfield, W. 1994. Clinical-Applications of Hydroxyapatite Reinforced Materials. *British Ceramic Transactions,* 93**,** 104-107.

Teng, H. 1992. Effective longitudinal shear modulus of a unidirectional fiber composite containing interfacial cracks. *International Journal of Solids and Structures,* 29**,** 1581-1595.

Teoh, S. H. 2000. Fatigue of biomaterials: a review. *International Journal of Fatigue,* 22**,** 825-837.

Theocaris, P. S., Papanicolaou, G. C. & Kontou, E. A. 1983. Interrelation between moisture absorption, mechanical behavior, and extent of the boundary interphase in particulate composites. *Journal of Applied Polymer Science,* 28**,** 3145-3153.

Thompson, K. D. & Sheppard, S. D. 1992. Fatigue crack growth in notched and plain shafts subjected to torsion and axial loading. *Engineering Fracture Mechanics,* 43**,** 55-71.

Ton That, P. T., Tanner, K. E. & Bonfield, W. 2000a. Fatigue characterization of a hydroxyapatite-reinforced polyethylene composite. I. Uniaxial fatigue. *Journal of Biomedical Materials Research,* 51**,** 453-460.

Ton That, P. T., Tanner, K. E. & Bonfield, W. 2000b. Fatigue characterization of a hydroxyapatite-reinforced polyethylene composite. II. Biaxial fatigue. *Journal of Biomedical Materials Research,* 51**,** 461-468.

Toor, P. M. 1975. A unified engineering approach to the prediction of multiaxial fatigue fracture of aircraft structures. *Engineering Fracture Mechanics,* 7**,** 731-741.

Törmälä, P. 1992. Bioabsorbable surgical composite materials. *Advanced Materials,* 4**,** 589-591.

Törmälä, P. 1992. Biodegradable self-reinforced composite materials; Manufacturing structure and mechanical properties. *Clinical Materials,* 10**,** 29-34.

Törmälä, P., Kellomäki, M., Bonfield, W. & Tanner, K. E. 1997. *Bioactive and biodegradable composites of polymers and ceramics or glasses and method to manufacture such composites*. US Patent Application 08/921.

Tormala, P., Pohjonen, T. & Rokkanen, P. 1998. Bioabsorbable polymers: materials technology and surgical applications. *Proceedings of the Institution of Mechanical Engineers, Part H,* 212**,** 101-11.

Tormala, P., Rokkanen, P., Laiho, J. & Vainionpaa, S. 1988. *Materials for osteosynthesis devices, US Patent 4743257*.

Törmälä, P., Rokkanen, P., Vainionpää, S., Laiho, J., Heponen, V. & Pohjonen, T. 1990. *Surgical materials and devices. U.S. Patent 4 968 317*.

Törmälä, P., Vasenius, J., Vainionpää, S., Laiho, J., Pohjonen, T. & Rokkanen, P. 1991. Ultra-high-strength absorbable self-reinforced polyglycolide (SR-

PGA) composite rods for internal-fixation of bone-fractures-in vitro and in vivo study *Journal Biomedical Material Research,* 25**,** 1-22.

Totry, E., González, C. & Llorca, J. 2008. Influence of the loading path on the strength of fibre-reinforced composites subjected to transverse compression and shear. *International Journal of Solids and Structures,* 45**,** 1663-1675.

Tregub, A., Harel, H. & Marom, G. 1994. Thermal treatment effects on the crystallinity and the mechanical behaviour of carbon fibre-poly(ether ether ketone) composites. *Journal of Materials Science Letters,* 13**,** 329-331.

Tregub, A., Harel, H., Marom, G. & Migliaresi, C. 1993. The influence of thermal history on the mechanical properties of poly(ether ether ketone) matrix composite materials. *Composites Science and Technology,* 48**,** 185-190.

Tsai, S. W. & Wu, E. M. 1971. A General Theory of Strength for Anisotropic Materials. *Journal of Composite Materials,* 5**,** 58-80.

Unsworth, A. 1991. Tribology of human and artificial joints. *Proceeding of Institution of Mechanical Engineers. Part H, Journal of Engineering in Medicine,* 205**,** 163-72.

Vaccaro, A. R., Venger, B. H., Kelleher, P. M., Singh, K., Carrino, J. A., Albert, T. & Hilibrand, A. 2002. Use of a Bioabsorbable anterior cervical plate in the treatment of cervical degenerative and traumatic disk disruption. *Orthopedics,* 25**,** S1191-S1199.

Vallons, K., Duque, I., Lomov, S. V. & Verpoest, I. 2011. Loading direction dependence of the tensile stiffness, strength and fatigue life of biaxial carbon/epoxy NCF composites. *Composites Part A: Applied Science and Manufacturing,* 42**,** 16-21.

van den Oever, M. & Peijs, T. 1998. Continuous-glass-fibre-reinforced polypropylene composites II. Influence of maleic-anhydride modified polypropylene on fatigue behaviour. *Composites Part A: Applied Science and Manufacturing,* 29**,** 227-239.

Vargas, G. & Mujika, F. 2010. Determination of In-plane Shear Strength of Unidirectional Composite Materials Using the Off-axis Three-point Flexure and Off-axis Tensile Tests. *Journal of Composite Materials,* 44**,** 2487-2507.

Varma, H. K. & Sureshbabu, S. 2001. Oriented growth of surface grains in sintered beta tricalcium phosphate bioceramics. *Materials Letters,* 49**,** 83-85.

Vashishth, D., Tanner, K. E. & Bonfield, W. 2001. Fatigue of cortical bone under combined axial-torsional loading. *Journal of Orthopaedic Research,* 19**,** 414-420.

Vaughan, J. M. 1975. *The Physiology of Bones,* Oxford, Clarendon Press.

Vaughan, T. J. & McCarthy, C. T. 2011. Micromechanical modelling of the transverse damage behaviour in fibre reinforced composites. *Composites Science and Technology,* 71**,** 388-396.

Verheyen, C. C. P. M., De Wijn, J. R., Van Blitterswijk, C. A. & De Groot, K. 1992. Evaluation of hydroxylapatite/poly(l-lactide) composites: Mechanical behavior. *Journal of Biomedical Materials Research,* 26**,** 1277-1296.

Verheyen, C. C. P. M., de Wijn, J. R., van Blitterswijk, C. A., de Groot, K. & Rozing, P. M. 1993. Hydroxylapatite/poly(L-lactide) composites: An animal study on push-out strengths and interface histology. *Journal of Biomedical Materials Research,* 27**,** 433-444.

Verrier, S., Blaker, J. J., Maquet, V., Hench, L. L. & Boccaccini, A. R. 2004. PDLLA/Bioglass (R) composites for soft-tissue and hard-tissue engineering: an in vitro cell biology assessment. *Biomaterials,* 25**,** 3013-3021.

Vert, M. 2005. Aliphatic polyesters: great degradable polymers that cannot do everything. *Biomacromolecules,* 6**,** 538-46.

Vert, M., Christel, P., Garreau, H., Audion, M., Chavanaz, M. & Chabot, F. 1986. Totally bioresorbable composites systems for internal fixation of bone fractures. *In:* Chielleni, G. (ed.) *Polymers in medicine.* New York: Plenum Press.

Vert, M. & Guerin, P. 1991. Biodegrable aliphatic polyesters of the poly(hydroxy acid)type for temporary therapeutic applications *In:* Barbosa, M. A. (ed.) *Biomaterials Degradation: Fundamental Aspects and Related Clinical Penomena.* Amsterdam: Elsevier Science Publishers.

Vert, M., Li, S. & Garreau, H. 1991. More about the degradation of LA/GA-derived matrices in aqueous media. *Journal of Controlled Release,* 16**,** 15-26.

Vert, M., Li, S. & Garreau, H. 1992. New insights on the degradation of bioresorbable polymeric devices based on lactic and glycolic acids. *Clinical Materials,* 10**,** 3-8.

Vieira, A. C., Vieira, J. C., Ferra, J. M., Magalhães, F. D., Guedes, R. M. & Marques, A. T. 2011. Mechanical study of PLA–PCL fibers during in vitro

degradation. *Journal of the Mechanical Behavior of Biomedical Materials,* 4**,** 451-460.

Vogler, T. J. & Kyriakides, S. 2001. On the initiation and growth of kink bands in fibre composites: Part I. experiments. *International Journal of Solids and Structures,* 38**,** 2639-2651.

Wallbridge, N. & Dowson, D. 1982. The walking activity of patients with artificial hip joints. *Engineering in Medicine,* 11**,** 95-6.

Walsh, W. R., Vizesi, F., Michael, D., Auld, J., Langdown, A., Oliver, R., Yu, Y., Irie, H. & Bruce, W. 2008. β-TCP bone graft substitutes in a bilateral rabbit tibial defect model. *Biomaterials,* 29**,** 266-271.

Wang, L., Weng, L., Song, S. & Sun, Q. 2010. Mechanical properties and microstructure of polyetheretherketone-hydroxyapatite nanocomposite materials. *Materials Letters,* 64**,** 2201-2204.

Wang, M. 2003. Developing bioactive composite materials for tissue replacement. *Biomaterials,* 24**,** 2133-2151.

Wang, M., Porter, D. & Bonfield, W. 1994. Processing, characterisation and evaluation of hydroxyapatite –reinforced polyethylene composites. *British Ceramic Transaction,* 93**,** 91-95.

Ward, I. M., Bonfield, W. & Ladizesky, N. H. 1997. The development of load-bearing bone substitute materials. *Polymer International,* 43**,** 333-337.

Waris, E., Ashammakhi, N., Raatikainen, T., Törmälä, P., Santavirta, S. & Konttinen, Y. T. 2002. Self-reinforced bioabsorbable versus metallic fixation systems for metacarpal and phalangeal fractures: A biomechanical study. *The Journal of Hand Surgery,* 27**,** 902-909.

Waris, T., Pohjonen, T. & Törmälä, P. 1994. Self-reinforced absorbable polylactide (SR-PLLA) plates in craniofacial surgery. *European Journal of Plastic Surgery,* 17**,** 236-238.

Weatherholt, A. M., Fuchs, R. K. & Warden, S. J. 2012. Specialized Connective Tissue: Bone, the Structural Framework of the Upper Extremity. *Journal of Hand Therapy,* 25**,** 123-132.

Weaver, J. L. & Beatty, C. L. 1978. The effect of temperature on compressive fatigue of polystyrene. *Polymer Engineering & Science,* 18**,** 1117-1126.

Weibull, W. 1951. A statistical distribution function of wide applicability. *Journal of Applied Mechanics,* 18**,** 293-297.

Weng, J., Wang, M. & Chen, J. 2002. Plasma-sprayed calcium phosphate particles with high bioactivity and their use in bioactive scaffolds. *Biomaterials,* 23**,** 2623-2629.

Wilberforce, S. I. J., Finlayson, C. E., Best, S. M. & Cameron, R. E. 2011. A comparative study of the thermal and dynamic mechanical behaviour of quenched and annealed bioresorbable poly-l-lactide/α-tricalcium phosphate nanocomposites. *Acta Biomaterialia,* 7**,** 2176-2184.

Williams, D. F. 1982. *Biocompatibility in clinical practice,* Boca Raton, FL., CRC Press.

Williams, D. F. Year. Definitions in Biomaterials. *In:* Proceedings of a Concensus of the European Society for Biomaterials, 1987 Chester, England. Elsvier Science Publisher Ltd. N.Y.

Williams, D. F. 1999. *Williams Dictionary of Biomaterials, Liverpool University Press, Liverpool, 1999. ,* Liverpool, Liverpool University Press.

Wilson, L., Nolan, J. & Heywood-Waddington, M. 1992. Fracture of the femoral stem of the Ring TCH hip prosthesis. *Journal of Bone & Joint Surgery, British Volume,* 74-B**,** 725-728.

Wilson-Hench, J. 1987. Osteoinduction. *In:* Williams, D. F. (ed.) *Progress in biomedical engineering, Definitions in biomaterials.* Amsterdam: Elsevier.

Wiltfang, J., Merten, H. A., Schlegel, K. A., Schultze-Mosgau, S., Kloss, F. R., Rupprecht, S. & Kessler, P. 2002. Degradation characteristics of α and β tri-calcium-phosphate (TCP) in minipigs. *Journal of Biomedical Materials Research,* 63**,** 115-121.

Wright, T. M., Vosburgh, F. & Burstein, A. H. 1981. Permanent deformation of compact bone monitored by acoustic emission. *Journal of Biomechanics,* 14**,** 405-409.

Wright-Charlesworth, D. D., King, J. A., Miller, D. M. & Lim, C. H. 2006. In vitro flexural properties of hydroxyapatite and self-reinforced poly(L-lactic acid). *Journal of Biomedical Materials Research Part A,* 78A**,** 541-549.

Wu, C. H., Hara, K. & Ozawa, H. 1992. Enhanced osteoinduction by intramuscular grafting of BMP-beta-TCP compound pellets into murine models. *Archives of histology and cytology,* 55**,** 97-112.

Xiao, X. R. 1999. Modeling of Load Frequency Effect on Fatigue Life of Thermoplastic Composites. *Journal of Composite Materials,* 33**,** 1141-1158.

Xiao, X. R. & Al-Hmouz, I. 1998. Fatigue behaviour of angle-ply AS4/PEEK composite. *In:* Reifsnider, K. L., Dillard, D. A. & Cardon, A. H. (eds.) *Progress in durability analysis of composite systems.* Rottherdam: A A Balkema, 331-338.

Yamada, M., Shiota, M., Yamashita, Y. & Kasugai, S. 2007. Histological and histomorphometrical comparative study of the degradation and osteoconductive characteristics of alpha- and beta-tricalcium phosphate in block grafts. *Journal of Biomedical Materials Research. Part B Applied Biomaterials,* 82**,** 139-48.

Yamauchi, K., Takahashi, T., Funaki, K., Hamada, Y. & Yamashita, Y. 2010. Histological and histomorphometrical comparative study of β-tricalcium phosphate block grafts and periosteal expansion osteogenesis for alveolar bone augmentation. *International Journal of Oral and Maxillofacial Surgery,* 39**,** 1000-1006.

Yang, B., Kozey, V., Adanur, S. & Kumar, S. 2000. Bending, compression, and shear behavior of woven glass fibre–epoxy composites. *Composites Part B: Engineering,* 31**,** 715-721.

Yao, J., Radin, S., S. Leboy, P. & Ducheyne, P. 2005. The effect of bioactive glass content on synthesis and bioactivity of composite poly (lactic-co-glycolic acid)/bioactive glass substrate for tissue engineering. *Biomaterials,* 26**,** 1935-1943.

Yasunaga, T., Matsusue, Y., Furukawa, T., Shikinami, Y., Okuno, M. & Nakamura, T. 1999. Bonding behavior of ultrahigh strength unsintered hydroxyapatite particles/poly(L-lactide) composites to surface of tibial cortex in rabbits. *Journal of Biomedical Materials Research,* 47**,** 412-419.

Yerramalli, C. S. & Waas, A. M. 2003. A failure criterion for fibre reinforced polymer composites under combined compression–torsion loading. *International Journal of Solids and Structures,* 40**,** 1139-1164.

Yoshikawa, T., Mori, S., Santiesteban, A. J., Sun, T. C., Hafstad, E., Chen, J. & Burr, D. B. 1994. The effects of muscle fatigue on bone strain. *Journal of Experimental Biology,* 188**,** 217-233.

Younesi, M. & Bahrololoom, M. E. 2011. Effect of polypropylene molecular weight, hydroxyapatite particle size, and Ringer's solution on creep and impact behavior of polypropylene-surface treated hydroxyapatite biocomposites. *Journal of Composite Materials,* 45**,** 513-523.

Yuan, H., De Bruijn, J. D., Li, Y., Feng, J., Yang, Z., De Groot, K. & Zhang, X. 2001. Bone formation induced by calcium phosphate ceramics in soft tissue of dogs: a comparative study between porous alpha-TCP and beta-TCP. *J Mater Sci Mater Med,* 12**,** 7-13.

Zhang, X., Espiritu, M., Bilyk, A. & Kurniawan, L. 2008. Morphology behaviour of poly(lactic) acid during hydrolytic degradation. *Polymer Degradation and Stability,* 93**,** 1964-1970.

Zhou, H., Lawrence, J. G. & Bhaduri, S. B. 2012. Fabrication aspects of PLA-CaP/PLGA-CaP composites for orthopedic applications: A review. *Acta Biomaterialia,* 8**,** 1999-2016.

Zhou, Z., Yi, Q., Liu, X., Liu, L. & Liu, Q. 2009. In vitro degradation behaviors of Poly-l-lactide/bioactive glass composite materials in phosphate-buffered solution. *Polymer Bulletin,* 63**,** 575-586.

Zhou, Z. H., Ruan, J. M., Zhou, Z. C. & Shen, X. J. 2007. Bioactivity of bioresorbable composite based on bioactive glass and poly-L-lactide. *Transactions of Nonferrous Metals Society of China,* 17**,** 394-399.

Zijderveld, S. A., Schulten, E. A. J. M., Aartman, I. H. A. & Ten Bruggenkate, C. M. 2009. Long-term changes in graft height after maxillary sinus floor elevation with different grafting materials: radiographic evaluation with a minimum follow-up of 4.5 years. *Clinical Oral Implants Research*.

Zioupos, P., Currey, J. D. & Casinos, A. 2001. Tensile Fatigue in Bone: Are Cycles-, or Time to Failure, or Both, Important? *Journal of Theoretical Biology,* 210**,** 389-399.

APPENDICES

Appendix 1: Correction Factor for Axial and Torsional Test

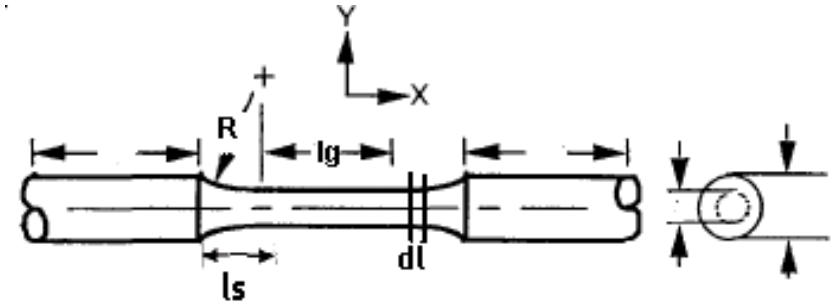

Figure A1 Specimen parameters

A1.1 Axial testing

As the test was carried out in saline solution, and with absent of immersable extensometer, therefore the strain were calculated from the relative movement of the grips. Thus, correction factor need to calculated for the difference between the cross-head separation gauge length strain

Strain
$$\varepsilon = \frac{\sigma}{\mathrm{E}} = \frac{\mathrm{P}}{\mathrm{AE}} \qquad \textbf{A.1}$$

Thus,

$$\frac{\delta}{L} = \frac{\mathrm{P}}{\mathrm{AE}} \qquad \textbf{A.2}$$

$$\therefore \quad \delta = \frac{\mathrm{P}L}{\mathrm{AE}} \qquad \textbf{A.3}$$

Where δ is deformation

$$\delta_{total} = \delta_{gauge} + 2\delta_{shoulder} \qquad \textbf{A.4}$$

For the gauge section:

$$\delta_g = \frac{Pl_g}{\pi r_g^2 E} \qquad \textbf{A.5}$$

With r_g=1.75mm, l_g = 13mm, will gives:

$$\delta_g = 4.24\frac{P}{\pi E} \qquad \textbf{A.6}$$

For the shoulder section:

The specimens used were cylindrical with the shoulder profile being part of a circle. If r is a point on the curve, the equation for a circle is:

$$A = \pi r^2 = \pi\left[(b+R) - \sqrt{(R^2 - l^2)}\right]^2 \qquad \textbf{A.7}$$

The –ve value is chosen for reasons of the geometry, therefore for a small slice

$$d\delta = \frac{Pdl}{A_S E} = \frac{Pdl}{\pi r_s^2 E}$$

Or

$$d\delta = \frac{P}{\pi E}\int_0^{l_s} \frac{dl}{\left[(b+R) - \sqrt{R^2 - l^2}\right]^2} \qquad \textbf{A.8}$$

By substituting values of R= 28mm, b =1.75 mm, and l_s= 9mm into equation A.8 gives:

$$\delta_s = 1.99\frac{P}{\pi E} \qquad \textbf{A.9}$$

Thus combining equation A.4, A.6 and A.9 gives

$$ratio\frac{\delta_g}{\delta_{total}} = 0.52 \qquad \textbf{A.10}$$

Therefore the gauge length strain, $\varepsilon = \frac{\delta_g}{l_g} = 0.49\frac{\delta_t}{l_g}$ where δ_{total} is measured by the machine displacement.

A1.2 For torsional testing

The total twist θ_{total},

$$\theta_{total} = \theta_{real(r)} = \theta_g + 2\theta_s \qquad \text{A.11}$$

Where θ_g is the torsion in gauge section and θ_s is the twist each of each of the shoulder section.

The section stress and strain are as followed:

$$\tau = \frac{2T}{\pi r^3} \text{ and } \gamma = \frac{r\theta}{l}$$

$$\text{lead to shear modulus, } G = \frac{2Tl}{\pi r^4 \theta} \qquad \text{A.12}$$

$$\text{therefore, } \theta = \frac{2Tl}{\pi r^4 G} \qquad \text{A.13}$$

$$\text{or } \frac{d\theta}{dl} = \frac{2Tl}{\pi r^4 G} \qquad \text{A.14}$$

<u>For gauge section</u>

From equation A.11,

$$\theta_g = \frac{2T}{\pi r^4 G} \qquad \text{A.15}$$

$$\theta_g = \frac{2T}{\pi G}\alpha_1 = \theta_a \qquad \text{A.16}$$

$$\text{where, } \alpha_1 = \frac{l_g}{r^4} \qquad \text{A.17}$$

For shoulder section:

$$r = (b + R) \pm \sqrt{(R^2 + l^2)} \qquad \textbf{A.18}$$

From the equation A.14, it can be deduced that:

$$\frac{d\theta}{dl} = \frac{2T}{\pi\left[(b+R) \pm \sqrt{R^2 - l^2}\right]^4 G}$$

this leads to $\theta_S = \frac{2T}{\pi G_S} \int_0^{l_0} \frac{2T}{\pi\left[(b+R) \pm \sqrt{R^2 - l^2}\right]^4 G} dl$ **A.19**

By substituting relevant values in to equation and intergrating it gives:

$$\theta_S = \frac{2T}{\pi G_s} \alpha_2 \qquad \textbf{A.20}$$

where $\alpha_S = \int_0^{l_0} \frac{2T}{\left[(b+R) \pm \sqrt{R^2 - l^2}\right]^4} dl$

Combining equation A.11, A.16 and A.20 gives:

$$\theta_{real(r)} = \frac{2T}{\pi G_s} (\alpha_2 + 2\alpha_2) \qquad \textbf{A.21}$$

The ratio of $\frac{\theta_r}{\theta_g}$ from equation (A.16) and (A.21) gives the correction factor of 1.72.

Appendix 2: Calculations of Euler Buckling Load

The critical force, P_c For built in end:

$$P_{critical} = 4\pi^2 \frac{EI}{l_b^2} \quad \textbf{A.22}$$

For pin joint,

$$P_{critical} = \pi^2 \frac{EI}{l^2} \quad \textbf{A.23}$$

Where E is the Young's Modulus, *l* is the length and the polar moment of inertia

$$\mathrm{I} = \frac{\pi r^4}{2}$$

The ASTM E466 dumbbell specimen has build-in ends, but since its gripping distance is over the gauge length and two shoulder sections, l_b is used and can be calculated from A1

By substituting the relevant value into equation A.23, the P critical value was found to be approximately 965N (≈100 MPa) for T150 composite

Appendix 3: Calculation of a Principal Stresses and Maximum Shear Stresses of Various Loading Conditions

For 25% UTS (25A) σ_{max} = 32.43 MPa

50% UTS (50A) σ_{max} = 64.87 MPa

25% USS (25T) τ_{max} = 6.48 MPa

50% USS (50T) τ_{max} = 12.97 MPa

The specimen is assured to have a diameter of 3.75mm and substituting these values in equation in section 3.3.7 to calculate the principal stress and the maximum shear stress

1. 25A25T(in-phase)

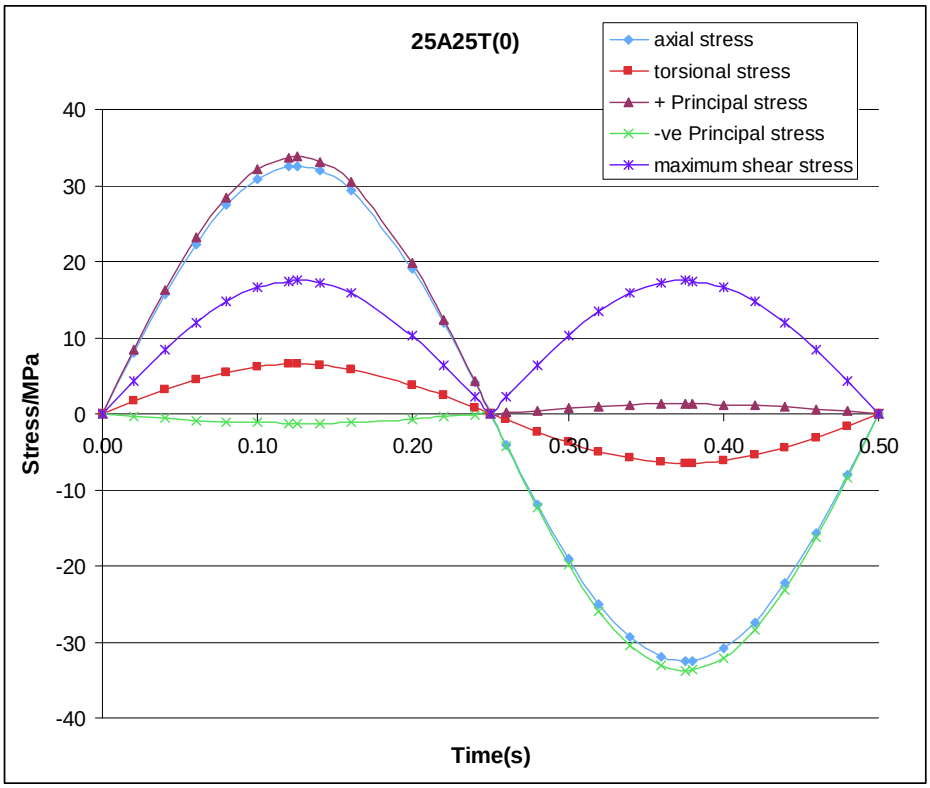

2. 25A50T(in-phase)

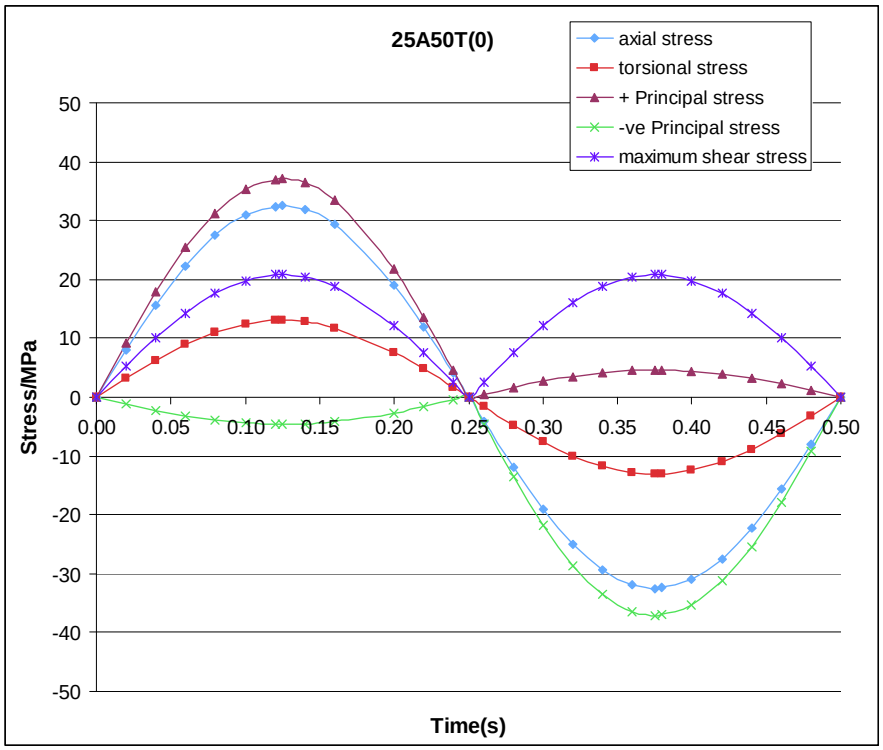

3. 50A25T(in-phase)

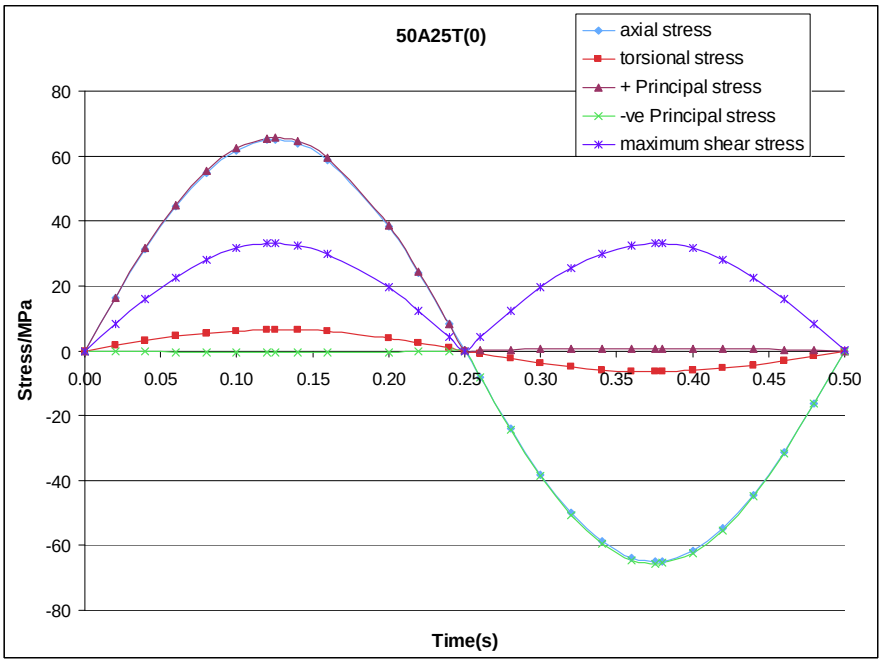

4. 50A50T(in-phase)

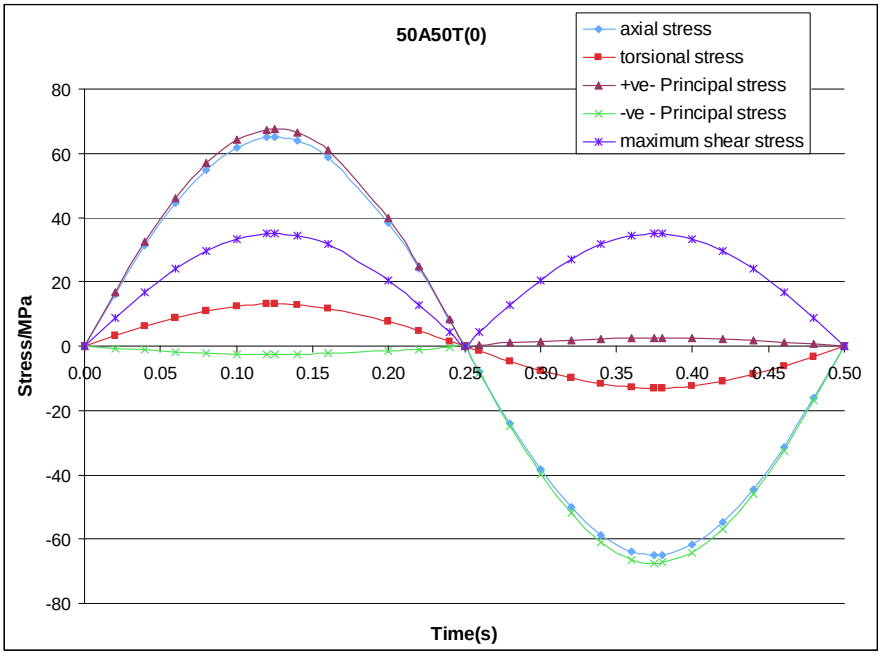

5. 25A25T (30° out-of-phase)

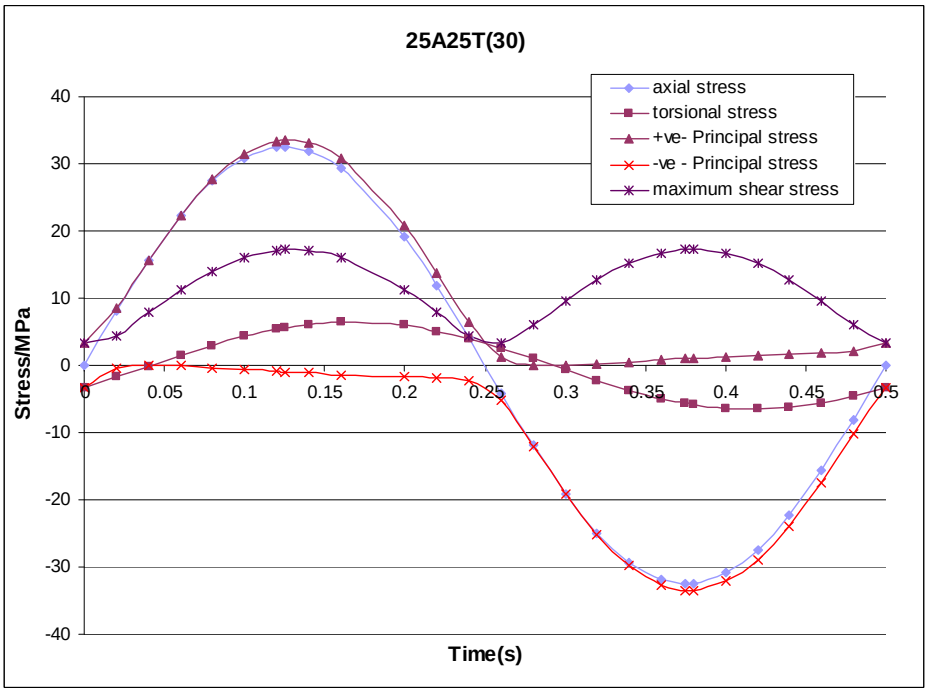

6. 25A25T (60° out-of-phase)

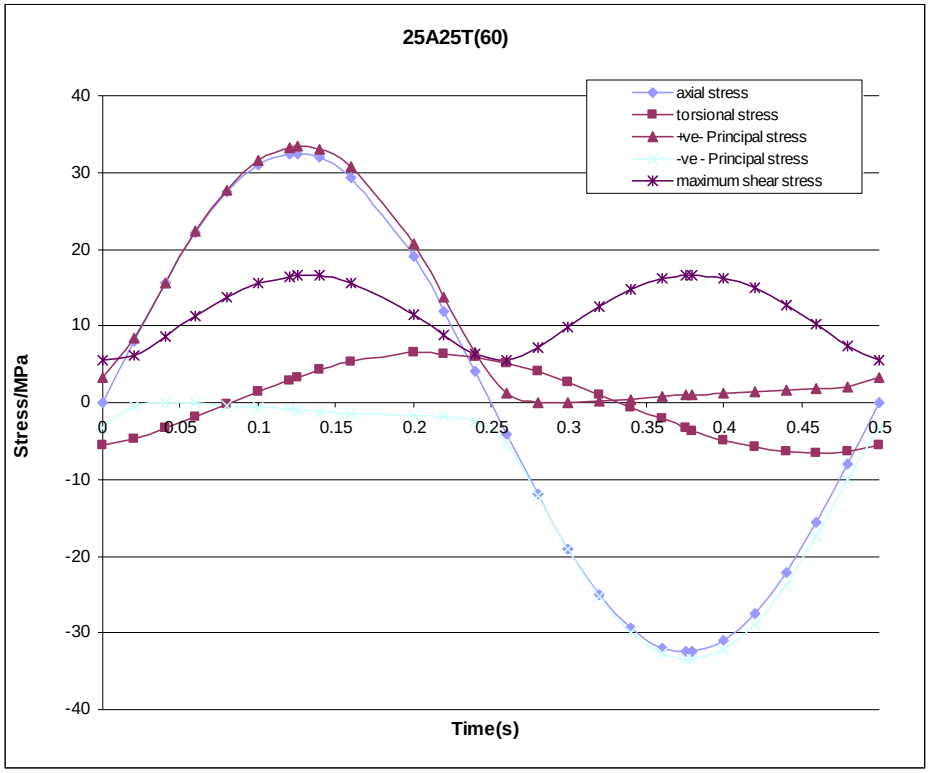

7. 25A25T (90° out-of-phase)

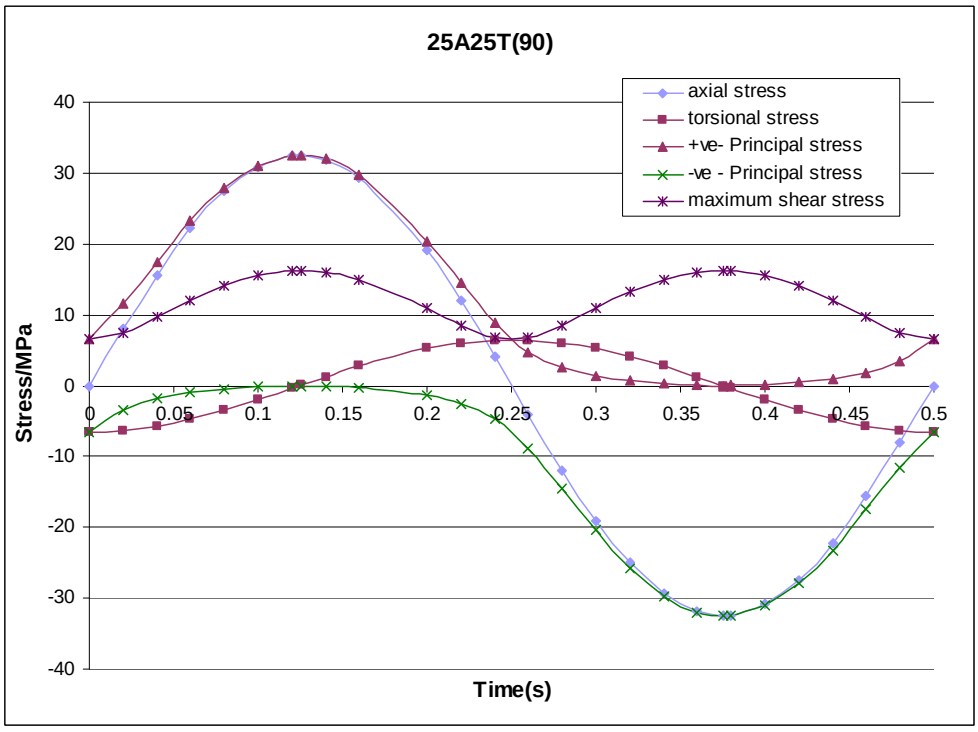

8. 50A50T (90° out-of-phase)

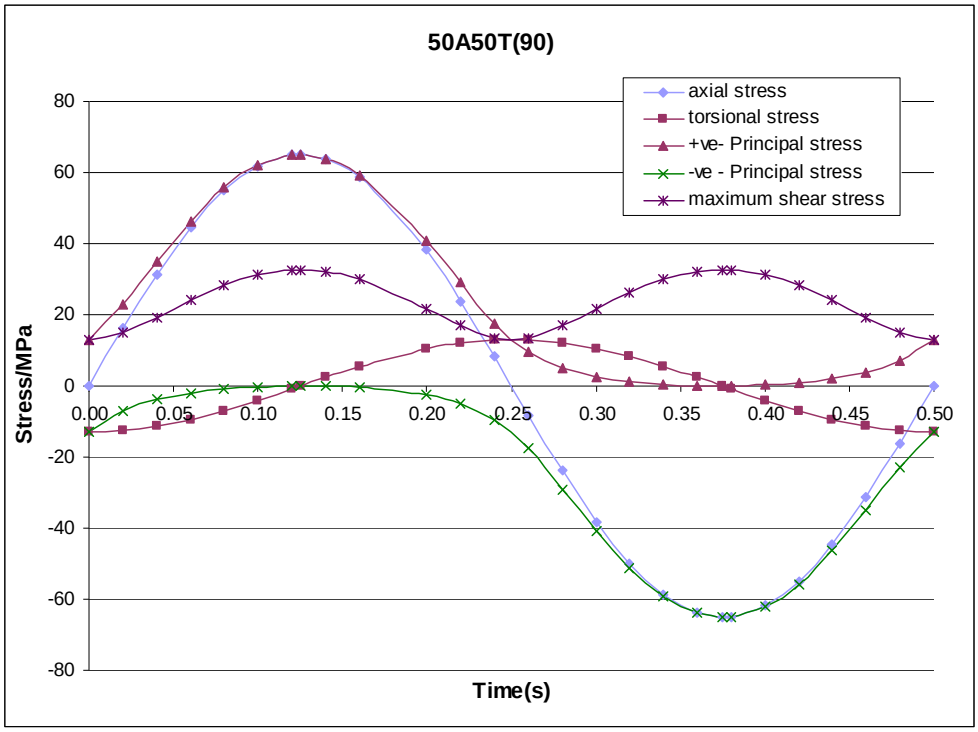

Appendix 4: Calculation of Tsai-Wu values of Various Loading Conditions

Using value of F_x, F_{XX} and F_{SS} constants in section 3.3.8, the maximum values of Tsai-Wu parameter are calculated and can be summarised

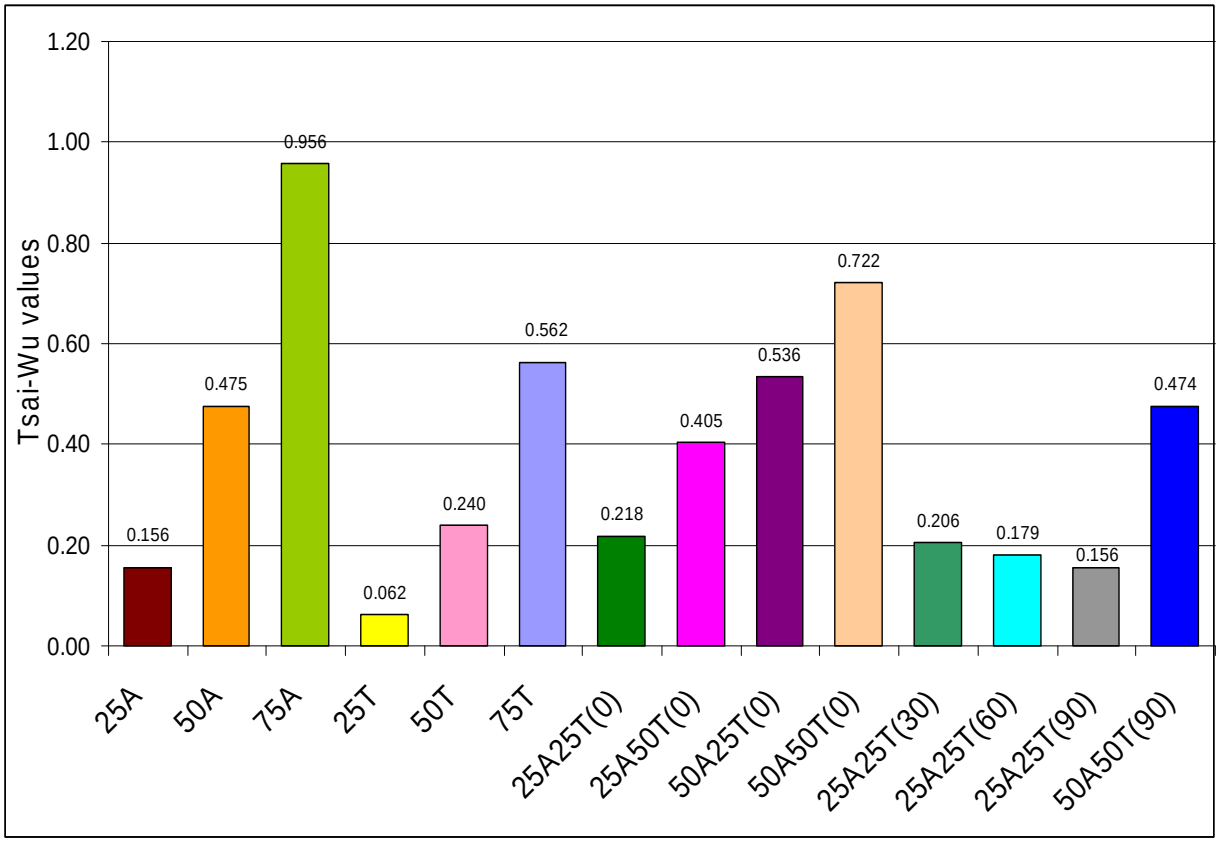

Figure A2 Maximum values of the Tsai-Wu parameter
For different loading conditions (biaxial phase angle showed in bracket)

PUBLICATIONS

Conferences Abstracts

1. **Fatigue Study of Self reinforcement PLA with bioactive ceramic** at UK Biomaterials Society Conference, Glasgow, 1st-2nd July 2010.

2. **Uniaxial Fatigue Characterisation of Tricalcium Phosphate Reinforced Polylactic Acid (PLA) Fibre Composite** at European Biomaterial Society (ESB) Conference, Tampere, Finland, 11-15th September 2010

3. **Biaxial Fatigue Study on self-reinforced PLA filled Tricalcium phosphate composite** at European Biomaterial Society (ESB) Conference, Dublin, Ireland, 4-8th September 2011.

4. **Effect of Degradation Time on the Uniaxial Fatigue Behaviour of Self-Reinforced Polylactic Acid-Calcium Phosphate Composite** at 9th World Biomaterials Congress, Chengdu, China, 2nd -6th June 2012.

Journals/ Books

1. Zaleha Mustafa and K.E.Tanner, Composite for Hard Tissue Repair, Encyclopaedia of Composites, 2nd Edition, Editors: Luigi Nicolais Assunta Borzacchiello, publisher John Wiley &Sons, Hoboken, New Jersey, 2012. ISBN 978-0-470-12828-2.

Uniaxial Fatigue Characterisation of Tricalcium Phosphate Reinforced Polylactic Acid (PLA) Fibre Composite

Z.Mustafa, K.E.Tanner

Department of Mechanical Engineering, University of Glasgow, James Watt Building (South), Glasgow G12 8QQ, UK

Email: zmustafa@eng.gla.ac.uk

Introduction:

The development of bioresorbable and simultaneously bioactive PLA-based composites has progressed from partially absorbable PLA composite reinforced with carbon fibres to totally absorbable composites reinforced with calcium phosphates, such as hydroxyapatite (HA)[1] and tricalcium phosphate (TCP), particles or fibres or bioactive glass particles[2] and with PLA fibres[3]. There are two major targets in the production of bioresorbable composites of degradable polymers filled with bioceramics or bioglasses, which are to increase the mechanical properties and to increase the bioactivity, allowing higher load bearing applications and achieving bone bonding to the implant interfaces thus accelerating the fracture healing. Most potential clinical applications are subjected to cyclic loading. This study investigates the quasi-static and fatigue properties of PLA reinforced with PLA fibres and TCP particles in uniaxial loading.

Materials and Methods:

Sheets of pre-preg were manufactured from drawn polylactide fibres (27 µm diameter) with L/D ratio 96/4 (PLA_{96}) in a matrix of polylactide with an L/D ratio of 70/30 (PLA_{70}) and tri-calcium phosphate filler particles with mean particle size of 4µm. The pre-preg was compressed moulded at 140°C into cylindrical rods and then machined into dumbbells to ASTM E466 standard, with gauge diameter of 3.5mm and gauge length of 20mm. The samples were tested in physiological environment (37ºC saline solution) using MTS Bionix 858 biaxial test system. Specimens were first subjected to monotonic tension to determine the ultimate tensile strength (UTS). Fatigue test were carried out at ±25%, ±50% and ±75% of UTS using sinusoidal loading at a frequency of 2Hz in load control. Testing was performed both in tension only and fully reversed tension-compression. Data from sets of 10 load cycles were collected in a logarithmic manner. Ten sets of force-extension data were collected per recorded load cycle and used to calculate stress and strain.

Result and Discussion:

The ultimate tensile strength was 103±4.8MPa. The tension only fatigue stress-strain curves for various cycles are shown in Figure 1. As the number of cycles increased, the creep increased and the material become more damaged, as reflected by the increasing size of the stress-strain loops and reduced modulus. From these graphs, the energy absorbed per load cycle and the secant moduli (Figure 2) were calculated. The damage become apparent after 10^4 cycles, thus before failure occurs.

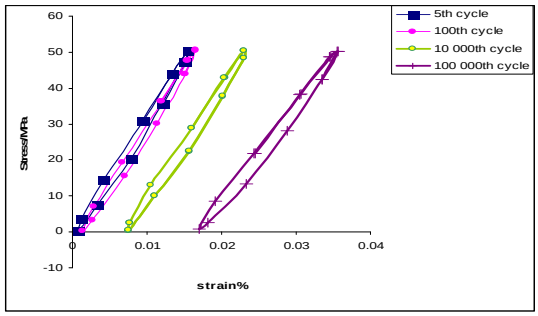

Figure 1: Stress-strain curves for axial tension fatigue

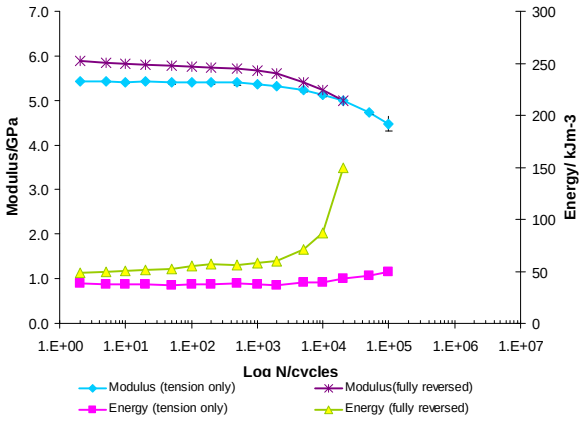

Figure 2: Dissipated energy for axial fatigue

Conclusions / Summary:

Based on monotonic and fatigue test of the degradable composite, it can be concluded that firstly, the fatigue damage accumulation was monitored by observing the increase in the dissipated energy and the reduction in the modulus. Secondly, the failure primarily occurred due to debonding between the fibres and the matrix.

References

1. Wright-Charlesworth *et al.* (2006) *J. Biomed. Mater. Res.*, 78A, 541-549.
2. Cool *et al.* (2007) *J. Biomed. Mater. Res.*, 82A, 599-610.

3. Bleach *et al*. (2002) *Biomaterials*, 23, 1579-1585.

Acknowledgment

The authors would like to thank Malaysian Government and Universiti Teknikal Malaysia Melaka for providing financial support for this study

Biaxial Fatigue Study of Self -Reinforced PLA filled Tricalcium Phosphate Composite

Zaleha Mustafa[1] and K.E Tanner[1]
[1]School of Engineering, University of Glasgow, United Kingdom
z.mustafa.1@research.gla.ac.uk

INTRODUCTION

The development of bioresorbable and simultaneously bioactive PLA-based composites has progressed from partially absorbable PLA composite reinforced with carbon fibres to totally absorbable composites reinforced with calcium phosphates, such as hydroxyapatite (HA)[1] and tricalcium phosphate (TCP), particles or fibres or bioactive glass particles[2] and with PLA fibres[3]. Most potential clinical applications are subjected to cyclic loading. For example, $1x10^6$ cycles per annum estimated for finger joints while in hips, ranging from 0.5 to 2 $x10^6$ cycles per annum. Thus, if self reinforced PLA is going to be used in such dynamically loaded implants, its fatigue behaviour needs to be study. This study investigates the fatigue behaviour of PLA reinforced with PLA fibres and TCP particles both in biaxial direction.

EXPERIMENTAL METHODS

Sheets of pre-preg were manufactured from drawn polylactide fibres (27 μm diameter) with L/D ratio 96/4 (PLA_{96}) in a matrix of polylactide with an L/D ratio of 70/30 (PLA_{70}) and tri-calcium phosphate filler particles with mean particle size of 4μm. The pre-preg was compression moulded using a hydraulic press into cylindrical rods. The sample then machined into dumbbells with gauge diameter of 3.5mm and gauge length of 13mm. The samples were tested in physiological environment (37ºC saline solution) using MTS Bionix 858 biaxial test system. Specimens were first subjected to monotonic tension and torsion to determine the ultimate tensile strength (UTS) and ultimate shear stress (USS). Uniaxial fatigue test were carried out at 25%, 50% and 75% of ultimate tensile and shear strength using sinusoidal loading at frequency of 2 Hz. Biaxial fatigue tests were then performed various combination of level of axial and torsional loading. Data from sets of 10 load cycles were collected in a logarithmic manner to allow energy absorbed per cycle and tangent modulus to be calculated in both axial and torsional directions.

RESULTS AND DISCUSSION

Uniaxial fatigue results showed that the torsional fatigue has lower number cycles to failure than axial fatigue (Figure 1). Superposition of torque on axial loading considerably reduces the fatigue life of composite (Figure 2). With progressive cycling, fatigue damage was observed by the reduction in modulus and the increase in dissipated energy both calculated from the hysteresis loop. Microscopy was used to study the fracture mechanism, which revealed evidence of interfacial failure.

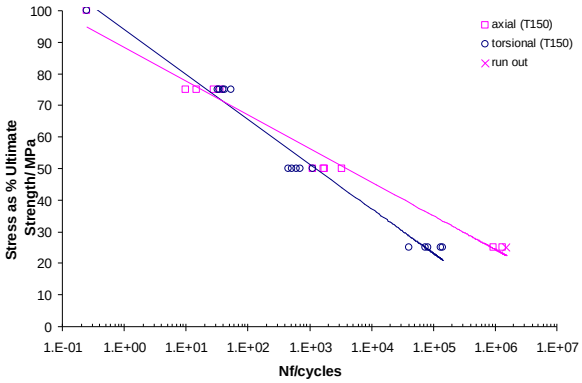

Figure 1: S-N curves for SR- PLA- TCP (37º in saline solution)

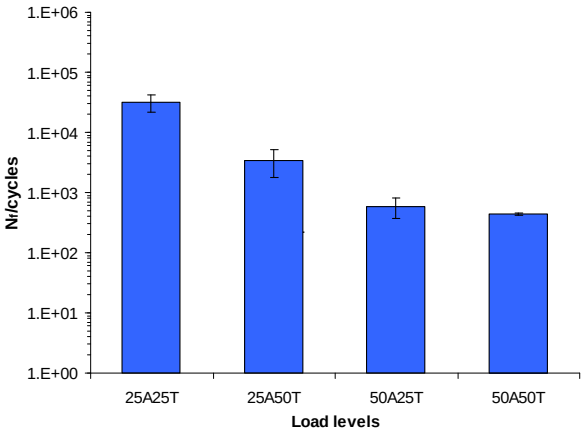

Figure 2: Biaxial fatigue lives of SR PLA-TCP composites (in- phase)

CONCLUSIONS

The fatigue damage accumulation was monitored by observing the increase in the dissipated energy and the reduction in the

modulus. Failure primarily occurred due to debonding between the fibres and the matrix

REFERENCES

1. Wright-Charlesworth *et al*. (2006) *J. Biomed. Mater. Res.*, 78A, 541-549.
2. Cool *et al*. (2007) *J. Biomed. Mater. Res.*, 82A, 599-610.
3. Bleach *et al*. (2002) *Biomaterials*, 23, 1579-1585.

ACKNOWLEDGMENTS

The authors would like to thank Malaysian Government and Universiti Teknikal Malaysia Melaka for providing financial support for this study

Effect of degradation time on the Uniaxial Fatigue Behaviour of Self- Reinforced Polylactide-Calcium Phosphate Composites

Zaleha Mustafa, [a] K.Elizabeth Tanner[a]
[a] Biomedical Engineering Department, School of Engineering, University of Glasgow, Glasgow, G12 8QQ, United Kingdom
Fax: 00 44 141 3304343; Tel: 0044 141 3308265;
E-mail: z.mustafa.1@research.gla.ac.uk

Introduction:

The development of bioresorbable and simultaneously bioactive PLA-based composites has progressed from partially absorbable PLA composite reinforced with carbon fibres to totally absorbable composites reinforced with calcium phosphates, such as hydroxyapatite (HA)[1] and tricalcium phosphate (TCP), particles or fibres or bioactive glass particles[2] and with PLA fibres[3].There are two major targets in the production of bioresorbable composites of degradable polymers filled with bioceramics or bioglasses, which are to increase the mechanical properties and to increase the bioactivity, allowing higher load bearing applications and achieving bone bonding to the implant interfaces thus accelerating the fracture healing. Most potential clinical applications are subjected to cyclic loading. This study investigates the effect of the degradation on the quasi-static strength and fatigue properties of PLA reinforced with PLA fibres and TCP particles.

Materials and Methods:

Sheets of pre-preg were manufactured from drawn polylactide fibres (27 µm diameter) with L/D ratio 96/4 (PLA_{96}) in a matrix of polylactide with an L/D ratio of 70/30 (PLA_{70}) and tri-calcium phosphate filler particles with mean particle size of 4µm. The pre-preg was compressed moulded into cylindrical rods and then machined into dumbbell with gauge diameter of 3.5mm and gauge length of 13mm. Samples then were degraded in saline solution for up to 20 weeks. Degradation rate was assessed by measuring changes in tensile modulus and strength as well as changes in wet mass, dry mass and pH of the solution. Uniaxial fatigue test were carried out at 25% of ultimate tensile and shear strength using sinusoidal loading at frequency of 2 Hz in environmental chamber. Data from sets of 10 load cycles were collected in a logarithmic manner. Ten sets of force-extension data were collected per recorded load cycle and used to calculate stress and strain.

Result and Discussion:

Result showed that sharp increased in fluid absorbed in the first period of the degradation time following with steady increased (Figure 1). Quasi testing result showed the mechanical strength decreased as degradation progressed (Figure 2). Increasing of fluid absorbed and reduction of the mass reduced the fatigue life of the composite (Figure 3). With progressive cycling, fatigue damage was observed by the reduction in modulus and the increase in dissipated energy both calculated from the hysteresis loop. Microscopy was used to study the fracture mechanism, which revealed evidence of interfacial failure.

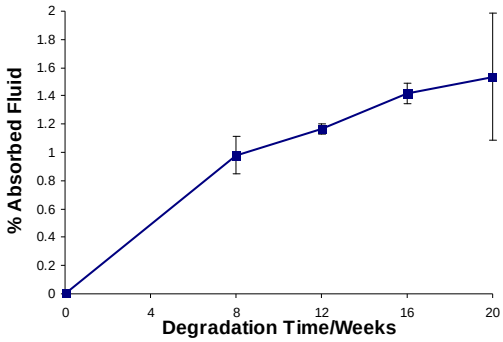

Figure 1: Percentage absorbed fluid versus degradation time

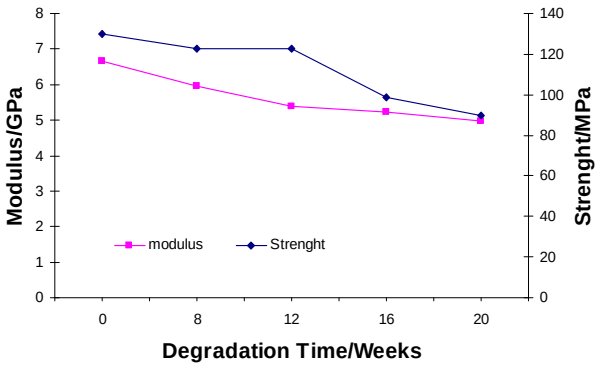

Figure 2: Axial modulus and strength versus degradation time

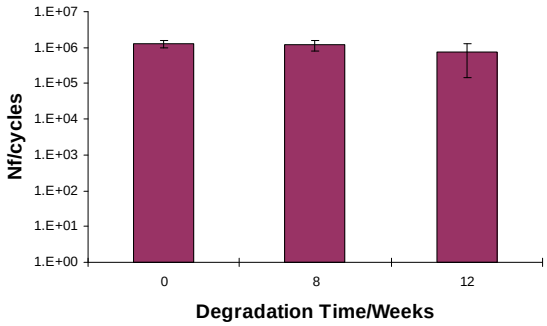

Figure 3: ±25% UTS fatigue lives of immersed specimens

References

1. Wright-Charlesworth *et al*. (2006) *J. Biomed. Mater. Res.*, **78A**, 541-549.
2. Cool *et al*. (2007) *J. Biomed. Mater. Res.*, **82A**, 599-610.
3. Bleach *et al*. (2002) *Biomaterials*, **23**, 1579-1585.

Acknowledgments

The authors would like to thank Malaysian Government and Universiti Teknikal Malaysia Melaka for providing financial support for this study.

COMPOSITES FOR HARD TISSUE REPAIR

ZALEHA MUSTAFA AND
K. ELIZABETH TANNER
University of Glasgow,
Glasgow, UK

INTRODUCTION

The materials requirements for composites for biomedical applications include all the usual mechanical property requirements for general engineering composites of stiffness, strength, toughness, and so on. However, there are additional biological requirements, the materials have to be biocompatible, that is, not produce a disadvantageous biological response in the required application [1,2] including in the case of degradable materials the degradation products must also be biocompatible. An additional desirable property is that the material should be bioactive, that is, it should produce a beneficial response in the appropriate application [1,2]. Bioactive means that the body's cells react beneficially with the material, and in the case of hard tissue applications, the bone cells, instead of producing a layer of fibrous tissue between the patient's own bone and the implant, produce new bone directly on the implant. This direct bone–implant contact leads to a mechanically stronger interface and thus a stronger and more durable bone–implant structure.

From a mechanical point of view, bone has two major functions, to provide a stiff skeleton against which the muscles can contract to provide locomotion and secondly to protect the major organs such as the brain, protected by the skull, and the heart and lungs, protected by the rib cage (Fig. 1). Biologically, bone provides a store of calcium and phosphate ions that are essential for biological function, while the marrow is the source for red and white blood cells [3]. At the macroscopic scale, there are two types of bone. The first type of bone is known as cortical, which is a nearly solid material, making up the outer surfaces of all bones, with a porosity of <3% in normal people [3]. The second type of bone is porous, is called either *cancellous* or *trabecular bone*, being a foam of bone made up of small struts called *trabeculae*. Cancellous bone is found throughout the middle of bones such as the ribs and the skull and at the end of long bones below the joint surface. The porosity ranges from 30% to 90%, depending on the position in the body, age, and activity level of the person. Both cortical and cancellous bones become more porous with age and conditions, such as osteoporosis that particularly affects postmenopausal women. At the structural and microstructural levels, cortical and cancellous bones have different structures in the form of osteons in cortical bone and trabeculae in cancellous bone. At the nanostructural level, all bone material is a composite of collagen, a natural polymer, filled with a calcium phosphate mineral, thus a particulate-reinforced composite. There are three major types of bone cells, osteoblasts that deposit new bone, osteocytes that are present throughout mature bone, and osteoclasts that resorb old and damaged bone. The properties of bone as a composite material are

Figure 1. Section through a proximal femur (thigh bone) showing cortical (lower walls) and cancellous bone (center of the femoral head).

discussed in greater detail in the articles titled ***Composite Rocket Propellants*** and ***Structure and Biomechanics of Biological Composites*** elsewhere in this handbook. Hard tissue implants could either be going into or on to the shaft of bones and, thus, can contact cortical or cancellous bone or both. Young's modulus of cortical bone is 7–25 GPa, while that for cancellous bone is 100–1000 MPa and their strengths are 50–150 and <50 MPa, respectively; all these mechanical properties depend on age, gender, activity level, and pathology in addition to the usual composite mechanical testing parameters of orientation and test velocity [4,5].

The major uses of hard tissue implants are as joint replacement to treat problems such as osteoarthritis, in fracture fixation where the bone ends need to be held stationary relative to each other until the fracture has healed, filling of bony defects, such as after a tumor has been removed, and, the newest application, tissue engineering. For applications such as joint replacement, the material needs to retain its properties for the rest of the patient's life, while for fracture fixation or tissue engineering scaffolds, the material should degrade once the function of the implant has been taken over by newly formed tissue [1,2]. In tissue engineering, cells are removed, usually from the patient themselves, grown up in the laboratory to increase the number of biologically active cells and then seeded into a scaffold that is then implanted back into the patient [6]. The scaffold material needs to be an open-celled foam of a degradable material so that the cells can be distributed throughout the scaffold material, body fluids can flow through to the cells to provide nutrients and remove waste products, and finally the scaffold material needs to

degrade at the same rate as new material is produced by the body. The earliest composite implants used in the 1970s and 1980s were nondegradable, but in the last 30 years, degradable materials have been investigated and been used clinically.

Considering composites that have been developed specifically for biomedical applications, a range of matrix materials and fillers have been tested individually and been shown to be biocompatible. However, virtually no coupling agents have undergone biocompatibility testing and, therefore, most biomedical composites avoid the use of coupling agents and rely solely on mechanical interlocking to bond the filler and the matrix. Currently, most composites used in biomedical applications are either particulate-filled polymers or drawn polymer fibers in a polymer matrix; a few more recent applications use bioactive glass (BG) fibers. Most polymers used for the matrix phase are biocompatible, but only a few are bioactive and being polymers all are lower modulus than cortical bone. However, many calcium phosphate ceramic, glass, or glass–ceramic fillers are bioactive, particularly in bony applications, as well as having higher moduli; thus, their use should increase stiffness and bioactivity of the composite and can increase the strength.

The testing of biomedical composites includes the usual mechanical tests to assess the mechanical behavior of the material including fatigue tested at a frequency and in an environment that models the human body. Additionally, there are four groups of biological testing required with increasing levels of complexity and cost, two types of *in vitro* tests that are performed in the laboratory, *in vivo* tests performed in animals, and finally clinical trials. The first of the *in vitro* tests is soaking in a solution that mimics the appropriate body fluid to assess both how the material will break down after implantation and how the material's properties change with time. While accelerated tests can be performed at raised temperature, most biomaterials testing is performed at body temperature (37°C), owing to the sensitivity of polymers to temperature effects, particularly in terms of their degradation behavior. In many applications, saline is the appropriate solution, but for potentially bone-bioactive materials, a simulated body fluid (SBF), such as that developed by Kokubo *et al.* [7] that is chemically very close to blood plasma, will be used. If a bone-bioactive material is placed in one of these solutions, a layer of apatite will be deposited on the surface, as would happen on implantation in the body, whereas a bioinert material does not produce this response. The second type of *in vitro* test uses cells and either the cells are grown in an elutant of the material, produced by soaking the material in a cell culture medium, or the cells are grown on the material surface. The elutant tests are to check for cytotoxicity, while the culturing of cells on the material is to assess the direct interaction of cells with the material, including how the cells attach to the material and whether their grown rate is increased or decreased by this contact with the material. The type of cell grown will depend on the potential application of the material and for bone applications is commonly either a line of bone cancer cells or bone cells taken from human hip joints at total hip replacement. Assuming that the new material has passed these tests as being biocompatible and even bioactive the last set of tests before human use is implantation in an animal, thus is know as *in vivo* testing. Finally, a clinical trial will be performed before the new material or device is released for general use. The costs of both *in vivo* testing and clinical trials are high and are highly controlled by national regulations. In the United States, approval is given by the Food and Drug Administration (FDA), while in Europe, approval is shown by a CE mark [8].

PRODUCTION OF BIOACTIVE COMPOSITES

All the techniques used for conventional composite materials production and polymerization are applicable to biomaterials production, although the number of potential matrix and filler materials are constrained by biocompatibility requirements. Biomedical composite based on thermoplastics and thermosets can be produced by conventional composite production methods such as compounding, extrusion, and injection molding and the application of preimpregation to produce "prepregs." In the production of fiber-reinforced composites, techniques such as filament winding have been used to produce devices including artificial intervertebral discs [9,10]. Selective laser sintering of both powders of composite materials and of the individual phases has been performed to produce custom built porous materials [11–13].

Nondegradable Bioactive Composites

The first composite material to enter clinical use was carbon-fiber-reinforced epoxy; it is extremely strong and light, with an elastic modulus close to that of bone, radiolucent, that is, allows X-rays to pass through it, enabling the bone below the implant to be monitored and most importantly biocompatible [14]. This material was used clinically as fixation fracture plates [15–17]. The devices were manufactured using layup of prepreg with compression molding to produce plates with fiber orientations of 0° in the outer layers and ±45° in the internal layers. The plates had a bending stiffness about 20% of the equivalent stainless steel plates, but showed 60% higher fatigue limit and angulation at failure. The plates were used to treat forearm fractures in 29 patients. The results showed that the patients treated with the carbon-reinforced epoxy composite plates were able to use their arms earlier in comparison with patients treated with the same size and shape metal plates. All the implants were removed after the fracture had healed. In another study, semirigid carbon-fiber-reinforced epoxy plates were used for cranioplasty, that is, the repair of defects in the skull, with a mean follow-up period of 3.3 years in five elderly female patients with severe osteoporosis and highly restricted mobility [18]. These patients had no adverse reactions to the plate, again supporting the use of carbon-reinforced epoxy in bone fixation. However, the major problem with carbon-fiber epoxy composites is that the implants cannot be bent to fit the patient in the operating theater, unlike the equivalent metal plates where plastic deformation is possible, thus restricting the use of these composite plates to the human forearm where the bones are close to straight

or to either preformed or low modulus implants as were used in the skull.

A different approach was taken Bonfield and colleagues, who proposed the use of high density polyethylene (HDPE) reinforced with hydroxyapatite (HA). Their philosophy was the "bone-analog" concept, that is, to produce a material with similar mechanical and biological properties to bone, consider the natural material, and try to reproduce it. In the HA–polyethylene (PE), the bone mineral was modeled by the HA and PE replaced the collagen, the HA providing stiffness and bioactivity, while the PE was responsible for ductility and toughness; at 40 vol% HA, the stiffness had increased from 0.94 to 4.29 GPa [19,20]. The first clinical application of this composite was as orbital floor implants and showed good biological responses [21,22]. Thereafter, the 40 vol% HA composite, HAPEX™, was used as the shaft of middle ear implants with the possibility of the supporting bone bonding with the HAPEX shaft, generating long-term stability of the implant; the high density of the composite was expected to improve the sound transfer through the implant shaft and the shaft could easily be trimmed intraoperatively to fit the individual patient. Goldenberg and Driver [23] reviewed the implant in 233 patients and found that the success rate was 66.8% defined by good hearing with only 6.3% implant extrusion occurred and 7.7% slippage. Meijer *et al.* [24], when reviewing some of the implants removed owing to reoccurrence of the original clinical problem, found good tissue cover, indicating better tissue acceptance than that occurred with previous implants of the same design, but manufactured using either Proplast or Plastipore.

Various attempts have been made to increase the mechanical properties of HAPEX. HAPEX was manufactured by compounding extrusion of spray-dried HA particles in HDPE. Joseph *et al.* [25,26] varied the molecular weight of the PE to produce an injection molding grade of HAPEX and found that increasing both the filler content of the composite and the molecular weight of the PE increased the viscosity of the melted composite. A similar effect was seen when using the nonsintered HA used in HAPEX rather than a sintered HA powder with the same mean particle size, but a specific surface area one-tenth of the nonsintered grade.

Ward and Bonfield and their colleagues attempted to produce HAPEX with higher and anisotropic mechanical properties by using hydrostatic extrusion [27,28]. Optimization of the extrusion ratio leads to a maximum flexural stiffness of 9 GPa and strength of 91 MPa in the longitudinal direction, although some slight reductions in the transverse properties were seen at the highest extrusion ratios.

A different approach to increase the mechanical properties was using very stiff drawn HDPE fibers as an additional filler in HA/HDPE composites [29,30]. They reported increases in stiffness and strength values to 17 GPa and 113 MPa respectively, suggesting that the mechanical performance of the composite can be further increased. Alternatively, Reis and colleagues [31–33] used the shear-controlled orientation injection molding (SCORIM) method by applying a macroscopic shear stress field at the melt/solid interface of the polymer during the molding cycle. This molding technique produced anisotropy in the HDPE and HDPE/HA composite and yielded stiffness values between 5 and 7 GPa. None of these higher modulus and anisotropic composites have progressed through to clinical applications, probably because of the complexity of applying the processing methods in a "clean" materials production environment as would be needed for clinical applications. This problem of ensuring that no contaminants enter during the production of medical grade composites has been a problem for many investigators.

Since these studies other authors have produced mineral-reinforced polymer composites, using either HA or to give a degradable mineral filler using tricalcium phosphate (TCP). HA ($Ca_{10}(PO_4)_6(OH)_2$) is stoichiometric version of bone mineral and, depending of the degree of crystallinity, either does not degrade or only degrades slowly, while TCP ($Ca_3(PO_4)_2$) degrades more quickly in the body and is commonly used as a filler with the aim of increasing bone repair due to the supply of calcium and phosphate ions. Polyetheretherketone (PEEK) is a high performance engineering polymer with good biocompatibility *in vivo*. The degradation rate of TCP depends on whether it has the α- or β-crystallographic structure and increasing the crystallinity decreases the degradation rate. Bioactive PEEK composites are produced usually by compounding of the polymer with calcium phosphates including HA or β-TCP. Petrovic *et al.* [34] studied bioactive PEEK filled with 5–40% β-TCP and reported proliferation normal human osteoblasts onto the composite. The finding leads to conclusion that the pure PEEK was nontoxic and has good biological interactions. Abu Bakar *et al.* [13] studied the use of HA/PEEK composites for bone substitution implants. The PEEK was reinforced with smooth thermal sprayed spherical HA particles via compounding followed by injection molding. The stiffness increased with the reinforcement volume up to the maximum tested of 40 vol% HA particles from 2.8 to 16.0 GPa; however, the ductility decreased and the strength reduced from 89 to 45.4 MPa. These composite were also laser sintered to produce porous implants that were tested *in vitro* and showed good biological responses. Wang *et al.* [35] successfully produced nanocomposites of PEEK–HA with 5 and 15 vol% of nanosized HA. The results showed the tensile strength increased with additional of the filler up to 15 vol%. The maximum strength was 93 MPa at 5 vol% and microscopic study showed that the HA particles are well bonded to the matrix.

Hao and colleagues [36–38] compounded 4 μm diameter HA particles into polyamide at 20 vol% or PE at 20 vol% and then selectively laser-sintered (SLS) powders of these composites to produce samples for mechanical testing and cell culture studies. The SLS process produced interconnecting open-celled pores and optimization of the process lead to material with flexural modulus measured using dynamic mechanical analysis (DMA) up to 580 MPa at 37°C. Cell seeding with an osteoblast cell line showed the material to be bioactive, with mineralization occurring after 28 days in culture without the addition of dexamethazone, which is normally

added to tissue culture medium to get cultured osteoblasts to mineralize.

Degradable Bioactive Composite Production

Biodegradable polymers and composites are used where the implant is no longer needed once the bone has healed, such as fracture healing and tissue engineering scaffolds. The most widely studied synthetic biodegradable polymers for hard tissue applications are the polyesters including poly(lactic acid) (PLA), poly(glycolic acid) (PGA), poly(hydroxybutyrate) (PHB), poly(lactic-*co*-glycolic acid) (PLGA), and poly(ε-caprolactone) (PCL). Degradation mechanisms of these polymers include surface and bulk erosion and the polymers have a range of degradation rates in the body. In the case of PLA, the polymer has two stereotactic forms known as L and D. The L form produces a highly crystalline bulk polymer with slow degradation rates, whereas the D form is less organized and thus has a faster degradation rate [40]. PHB copolymerizes with polyhydroxyvalerate (PHV) and increasing the PHV content decreases the stiffness, but increases the ductility of the bulk polymer. The processing route can be tailored to enhance the mechanical properties of the specimens. Poly-L-lactic acid (PLLA) usually has tensile strength and modulus of 50–70 MPa and 3–5 GPa, respectively, while PGA has a tensile modulus of 6–7 GPa and tensile strength of 60–100 MPa. To make degradable composites bioactive, inorganic components such as glasses, glass ceramics, and calcium phosphates are often used to produce composites; the fillers act to enhance the mechanical stiffness and strength as well as bioactivity.

The earliest biodegradable polymer composite was PHB reinforced with HA. Doyle *et al.* [41] studied bioactive PHB composite filled with HA; the modulus reached 11 GPa at 40 wt% filler. *In vitro* studies showed that the stiffness of the composite reduced to 5 GPa after four months of immersion in SBF and the degradation rate was controlled by the composition and processing condition. There was also no chronic inflammatory response reported after 12 months implantation, indicating that PHB has good compatibility properties.

Solvent casting is a simple method to produce degradable composites usually at room temperature and to produce for simple shapes such as flat sheets. The polymer is dissolved in an appropriate solvent at a concentration to give a suitable viscosity. The solution is cast onto a nonstick surface, such as glass, and allowed to dry slowly. The film can be removed once the solvent has evaporated. Composites are produced by mechanically mixing a filler into the solution to produce good dispersion of the filler and to prevent particle agglomeration. Misra *et al.* [42] adopted this method to produce PHB reinforced with 5 or 20 wt% Bioglass® 45S5. The addition of the Bioglass powder reduced the tensile modulus; however, DMA testing showed increases in the storage and loss moduli. It was suggested that difference was due to dewetting of the polymer–glass interface or agglomeration of the filler particles, leading to premature failure of the composite interface at higher stress levels than those used in DMA. The composite also show bioactivity when soaked in SBF solution.

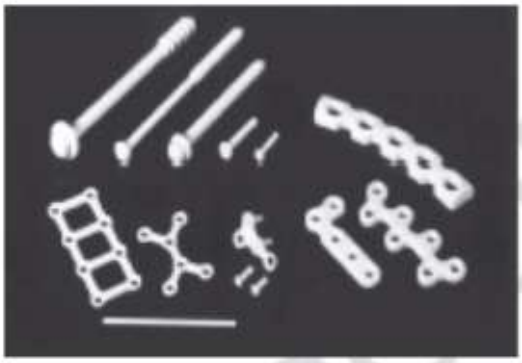

Figure 2. Screws, washers, a pin, and plates made of forged and then machined α-HA/PLLA composites. Source: From Shikinami and Okuno [43].

Shikinami and Okuno [43] successfully produced PLA/HA composites with strengths above that of cortical bone. They synthesized their own HA particles and mixed them into a PLLA/dichloromethane solution followed by precipitation. The composite was processed via extrusion and forging before it was finally machined into fracture fixation devices (Fig. 2). Increasing the HA content increases the modulus up to the maximum filler level of 50 wt% HA with the bending strength reported of 270 MPa exceeding that of cortical bone and modulus up to 12 GPa. The bending strength remained above 200 MPa for the first 25 weeks in phosphate-buffered saline (PBS) solution; thereafter, it was gradually decreased to 120 MPa after 52 weeks (Fig. 3).

Wright-Charlesworth *et al.* [44,45] produced 0–40 wt% HA in PLLA using compounding extrusion and injection molding. The addition of HA, as expected, increased the stiffness, but at the same time, decreased the strength of the PLLA with less drawing of the polymer matrix between the particles during the failure process. Soaking in PBS solution at 37°C showed that increasing the HA content decreased the degradation rate. As most with degradable composites, the strength seems to decrease faster than stiffness for all compositions. The ideal fracture fixation implant stiffness should reduce faster than the strength to allow gradual load transfer from the implant to the healing bone, while retaining strength to prevent refracture.

Melt spinning can produce PLLA fibers with tensile strength and modulus up to 1800 MPa and 9.3 GPa, respectively [46]. Solution spinning to manufacture PLLA fibers can lead to 560–2300 MPa tensile strength and 9.6–16 GPa tensile modulus [47,48]. As with any other fiber, these fibers can be used to increase the mechanical properties of composites. Tormala and colleagues used high temperature and pressure to sinter PLLA fibers to produce a composite with reinforcing elements and binding matrix with the same chemical composition. Tormala and colleagues [49–51] manufactured sintered self-reinforced, absorbable polyglycolide (SR-PGA), and injection molding PGA rods with 1.5–3.2 mm diameter presented bending moduli of 10–12 and 7 GPa, respectively. The bending strengths were 280 and 218 MPa

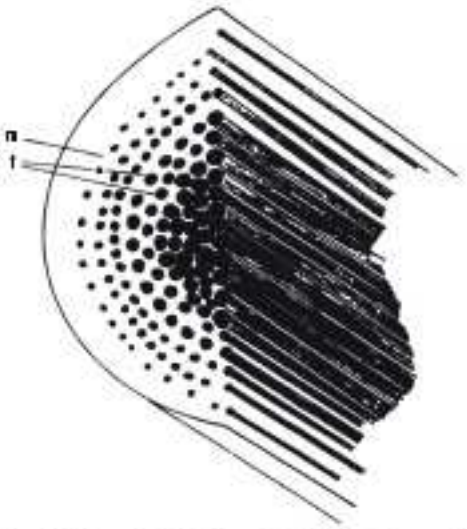

Figure 3. A schematic illustration of self-reinforced composite consisting of matrix (m) reinforced with parallel reinforcing lamenta (f). *Source*: From Törmälä *et al.* [49].

with shear strengths of 192 and 95 MPa, respectively. Degradation studies also showed that the strength of the specimens could be retained more than eight weeks. These self-reinforced implants were developed through to clinical application. However, the company developed to exploit the fiber-reinforced composite technology has subsequently concentrated on different PLA, PGA, and trimethylene carbonate (TMC) copolymers.

Triphasic composites of PLA–PLA–TCP were produced with flexural strength of 65–80 MPa and flexural modulus more than 7 GPa [52,53]. The composites were produced by producing a prepreg of PLA_{96}, that is, 96% PLLA, fibers in a PLA_{70} (70% PLLA and 30% PLDLA) matrix that was reinforced with HA or TCP. The strength was maintained up to 12 weeks soaking in buffered saline and, thereafter, lost stiffness and strength slowly. The presence of the calcium phosphates also increased the bioactivity of the materials when assessed by soaking in PBS solution and also slowed the degradation, compared to PLLA/PLDLLA composite prepared in the same manner, but without any calcium phosphate. The pH also remained near neutral for longer as the TCP degradation chemically buffered the lactic acid produced as the PLA degraded and furthermore slowed the degradation.

Bone Tissue Engineering Scaffolds

Until recently, materials were implanted into the body and the body was required to provide cells to the new implant surface. However, tissue engineering has been developed where cells are taken, commonly from the patient's own body, seeded into a porous scaffold and allowed to grow before being reimplanted back into the body [5]. The space for *in vitro* cell growth allows faster cell division than in the body and thus an increase in cell number. One of the earliest applications was for cartilage defects where cells are taken from a nonload bearing area of joint cartilage and expanded up and then replaced in a damaged load bearing area of cartilage. Scaffolds are designed to boost tissue repair rate by providing a large surface area to support revascularization, that is, restoration of the vascular system to allow the supply of nutrients and removal of waste products from the new tissue, and by integration of the regenerating tissue within the system. A scaffold needs to be open-celled porous with mechanical properties such that the implant will not collapse either on implantation or during use, until the newly formed tissue has taken over the mechanical function of the implant. In the case of bone tissue engineering, the scaffolds also need to be bioactive in addition to the usual biocompatible requirement. There are a range of methods to produce porous scaffolds such as thermally induced phase separation (TIPS), solvent casting with particulate leaching, sintering, microsphere templating, and others.

TIPS can be used to produce scaffolds with very high porosities up to 97% and very good pore interconnectivity that are usually used for tissues such as nerve, muscle, tendon, and ligament [54,55]. In this method, the polymer is dissolved and glass or ceramic powder then added into the polymer solution. For example, to produce high porosity PLDLLA/Bioglass composite scaffolds, the mixture was transferred into a flask and sonicated, followed by quenching in liquid nitrogen for 2 h at −196°C. The frozen mixture was later held at −10°C; the solvent was sublimated at −10°C and then at 0°C for 48 h, followed by drying at room temperature in a vacuum oven until the weight is constant. Maquet and colleagues [54–58] using the TIPS method successfully produced structure with tubular macropores of 100 μm, interconnected with micropores 10–50 μm in diameter. After adding 40 wt% Bioglass, the pore volume decreased from 9.5 to 6.7 cm^3/g, with no apparent change observed in the overall pore morphology. Both the PLDLLA/Bioglass composites and the unfilled PLDLLA foams maintained their structural integrity up to 16 weeks.

Another method to produce scaffolds is by solvent casting and particle leaching. In addition to the solvent, polymer, and filler particles, a further material is added that is not soluble in the polymer solvent, but is soluble in another liquid such as water, or can be melted out, and this material is known as the porogen. After the evaporation of the polymer solvent, the porogen is removed, leaving behind spaces previously occupied by the granules. Salt and sugar are commonly used as they are easily obtained, dissolve quickly in water, and any residuals are nontoxic. Dunn *et al.* [59] used salt leaching to manufactured scaffolds of 10 wt% HA in a blend of PCL and poly(DL-lactic acid-co-glycolic acid) at 10:90 or 40:60 PCL: Degradation testing was performed in PBS and serum-containing media, showing the pH decrease despite the present of HA in the composite. In a study by Li and Chang [60], porous scaffold of poly(β-hydroxybutyrate-co-β-hydroxyvalerate) (PHBV) reinforced with 0–40 wt% Wollastonite has been

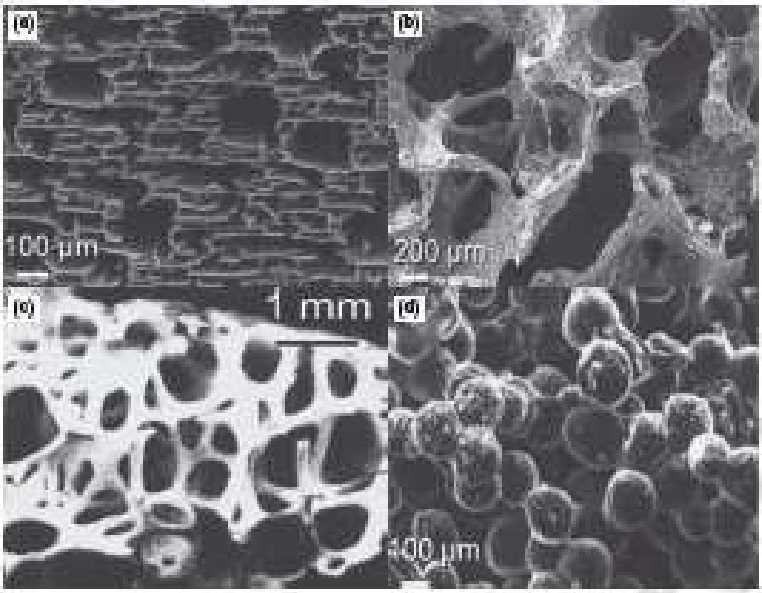

Figure 4. Typical morphologies of porous polymer foams produced by different techniques and structure of cancellous bone: (a) Thermal induced phase separation, (b) solvent casting and particle leaching, (c) cancellous bone, and (d) microsphere—sintering. Source: Part (a), from Maquet *et al.* [98]; part (b), from Wang *et al.* [38]; part (c), from Gibson [64]; part (d), from Lu *et al.* [82].

produced with porosity between 73% and 80% using the porogen method. The composite was found to be bioactive when soaked in SBF and the contact angle decreased with increasing amount of Wollastonite, making the materials to be more hydrophilic and thus increasing cell attachment. Wang *et al.* [38] used sugar leaching to manufacture porous scaffolds of PLLA reinforced with 20 wt% plasma-sprayed calcium phosphates. The spherical particles of CaP had smooth amorphous surfaces with crystalline cores. The surface layer dissolved easily when soaked in SBF or after ultrasonication in distilled water. The composite scaffold was expected to be highly bioactive as the amorphous calcium phosphate dissolved and then reprecipitated on the internal and external surfaces of the scaffold, giving a large number of potential nucleation sites on the scaffold surface.

Polymeric scaffolds also can be produced using a microsphere sintering process. Microspheres of a ceramic and polymer composite are synthesized using emulsion/solvent evaporation technique, followed by sintering the composite microspheres to produce 3D porous scaffolds. Lu *et al.* [81–83] successfully produced 3D composites of degradable polymers and BG using this method. First, PLA–PGA copolymer (polylactide-co-glycolide, PLAGA) Bioglass composite microspheres were produced through a water–oil–water emulsion technique and then compressed and heated to sinter the spheres together. This resulted in an interconnected porous structure with an average porosity of 40% with 90 μm pore diameter. The mechanical properties reported were close to those of cancellous bone. Furthermore, cell culture studies show a good response to the materials. This method was further developed by Yao and colleagues [83] to produce porous 3D scaffolds of PLGA/BG. They showed the materials have a very good bioactivity response and promoting osteogenesis of marrow stromal cells. Figure 4a,b and d shows various typical microsphere-sintered 3D structure produced by different methods in comparison to cancellous bone (Fig. 4c).

MECHANICAL PROPERTY TESTING

Mechanical testing of biomedical composites uses the same standards as composites for other applications. However, because of the cost of the materials, the size of the samples is commonly reduced. Samples need to be tested in both the "as produced and sterilized" that is ready-to-use state. In addition, samples should be tested after soaking in physiological solutions at 37°C for varying times to give partially degraded samples, particularly with degradable composites, although some changes have been seen in nondegradable materials after soaking with fluid intake, leading to some plasticization of the polymeric phase. Among the standards tests performed are tensile, compressive, impact, creep fatigue, and microhardness testing. The results of typical tensile test studies have been discussed throughout this article. The classic failure mode of particulate-filled polymers has been described by Friedrich and Karsch [66] where debonding of the polymer matrix from the filler surface is followed by drawing of polymer fibrils between the filler particles. While their studies were applied to tensile testing, the same failure mode is also seen after impact, fatigue, and creep loading.

Dynamic mechanical analysis (DMA) including temperature effects (DMTA) has been popular as small specimens can be used and, with the costs and difficulties of producing biomedical composites, such studies have benefits. A

typical flexion DMA test sample is $1 \times 2 \times 25$ mm^3, while compression samples are small cubes or cylinders a few millimeters in height. Nazhat *et al.* [4067–69] in a series of studies used DMA to investigate the mechanical properties of different composites. In their first study [68], they compared the storage modulus (E') measured using DMA with Young's modulus (E) of HA/PE composites and found a linear correlation given by

$$E' = 0.98E + 0.95 \ (R^2 = 0.998). \qquad (1)$$

In subsequent studies, Nazhat with various coauthors investigated various composites developed by Blaech *et al.* [68], Bleiker *et al.* [69], and Misra *et al.* [42]. Zhang *et al.* [70] used DMA to optimize the processing parameters for selective laser-sintered HA in polyamide and showed that for a given scan speed optimizing the laser power could increase the modulus by a factor of 1.5 (Fig. 6a). In all these DMTA studies, the transition temperatures seen for the nonreinforced polymer are also seen in the composite (Fig. 6b).

Younesi and Bahrololoom [71] studied the effect of molecular weight, particle size, and Ringer's solution on the impact properties of surface treated of polypropylene-filled HA composite. Their samples were notched Izod specimens of $64 \times 10.2 \times 6.4$ mm^3. About 6.4 mm was used instead of the standard specimen thickness of 3.2 mm to give higher bending resistance. Samples were tested both dry and after soaking in Ringer's solution for 30 days. Impact tests were carried out using drop weight impact testing that was performed by Zhang and Tanner [72,73] using 4-mm-thick 60 mm square samples, and they showed that increasing the molecular weight from 50,000 to 250,000 increased the total energy absorbed by a factor of 1.8 while adding 40 vol% spray-dried HA reduced the total energy absorbed by a factor of 12. They further found that replacing the spray-dried HA with a sintered HA with the same particle size but one-tenth the specific surface area increased the total energy absorbed by a factor between 1.5 and 2.0 depending on the volume fraction of filler.

The classic biomaterial to undergo fatigue testing is bone cement, given that the major failure of bone cement is due to the one million or so load cycles applied per year [74]. Most bone cements are polymethylmethacrylate with various amounts of fillers in the form of radiopacifiers and antibiotics, and these are considered too low filler concentrations to be described as a composite material. Ton That *et al.* [75,76] studied the fatigue behavior of HA-reinforced PE in fully reversed axial tension compression and fully reversed torsion using cylindrical dumbbell, which were machined according to the ASTM E466 standard. Fatigue tests were then carried out using sinusoidal loading at a frequency of 2 Hz at various loading levels, in saline solution at 37°C. *S–N* curves were established, showing that in tension–compression fatigue, the cycles to failure range from 1000 cycles at ±13 MPa to more than one million cycles at ±4.4 MPa. In torsion mode, the fatigue cycles range from 100 cycles at 75% of the ultimate shear stress to more than one million cycles for the 25% of the ultimate shear stress loading level.

In general, polymers have poor creep resistance which results in poor service life. Some of the early studies by Suwanprateeb *et al.* [77–79] are on HA-reinforced HDPE. While conventional creep testing is extremely time consuming, isochronous testing allows a large amount of initial data to be collected [81]. Here, a small stress is applied for a short time, say 100 s, the strain at the end of this time is measured and then the stress is removed for four times the original loading time (400 s); a higher stress is applied for 100 s and again the strain is measured at the end of the loading time. This load unload process is applied for gradually increasing stress levels (Fig. 6a) and finally an isochronous stress–strain curve is plotted. While allowing a large amount of data to be collected in a relatively short time, isochronous testing also allows the choice of the most appropriate stress levels for long-term creep testing. Isochronous creep testing can also allow various factors to be compared. They found that adding 20 and then 40 vol% HA halved the creep strain for a given stress level (Fig. 6b). They showed that 40 vol% HA in PE can sustain static tensile loads of up to 6 MPa in saline

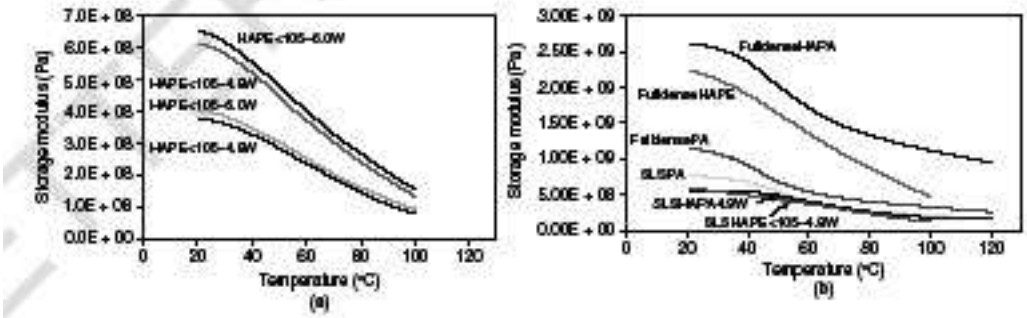

Figure 6. DMA analysis of (a) of SLS HA–PE composite manufactured with powder size of either <105 μm and >105 μm and laser power of 4.8 or 6.0 W and (b) comparison of storage modulus of fully dense and sintered HAPE, HAPA, and PA samples. *Source:* From Zhang *et al.* [35].

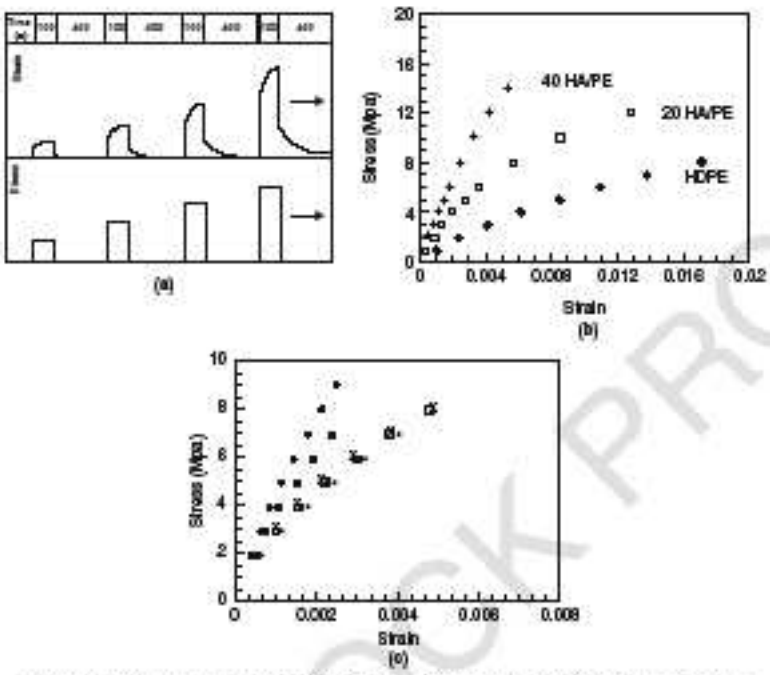

Figure 6. Isochronous creep testing of HA PE composites showing (a) strain and stress variations with time in isochronous testing, (b) the effect of adding 20 and 40 vol% HA to HDPE, and (c) the effect of soaking 40 vol% HAPE for ◦ noninmersed; ◦ 7 days; * 30 days; ×90 days; and □ 180 days. *Source:* From Suwanprateeb *et al.* [77,78].

solution. The importance of soaking samples before testing were considered by Suwanprateeb *et al.* [78] who showed that despite the nondegradability of PE, soaking in saline at 37°C caused the absorption of 0.1 wt% of liquid, which had minimal effects on the creep behavior, whereas with 40 vol% HA 1 wt% liquid was absorbed that nearly doubled the isochronous creep strain for a given stress (Fig. 6c).

Younesi and Bahrololoom [80] studied the creep behavior of the surface treated of polypropylene-filled HA composited in Ringer's solution. The samples were tested at dry and wet conditions, which undergo soaking time for 30 days in Ringer's solution. The test was carried out at 35% of their corresponding ultimate tensile strength (UTS) in physiological environment. They found that the creep resistance increased by decreasing the HA particle size, as this increased the contact surface between particles and the matrix. The decrease in friction reduces the motion and slippage between the polymers chains and thus reduces the deformation between the matrices, resulting in stronger composite. These findings are supported by Siaitova *et al.* [81], who reported that adding nanoparticles filler reduces the strain in the primary as well as secondary creep stage by restricting the movement of polymer chain restrict, thus producing higher creep resistance properties.

Degradation testing for the biodegradable composites is most often carried out in the same manner as nondegraded composite. Bleach *et al.* [52] showed that after 10 weeks soaking samples of PLLA fibers in a TCP/poly(L,DL-lactide) matrix absorbed less water and showed less mass loss than the samples prepared in the same manner but without the TCP. They hypothesized that the presence of the TCP chemically buffered the acid produced by the breakdown of the PLA and thus slowed the degradation. Kikuchi *et al.* [82] conducted three-point bending tests on copolymerized PLLA (CPLA) and TCP/CPLA composites. They reported that in the first four weeks of soaking in saline solution, bending strength of pure CPLA was constant, but declines rapidly thereafter. Niemelä [83] used shear testing to characterise self-reinforced poly-L-lactide (SRPLA) and TCP/SRPLA composites after *in vitro* hydrolysis. Results showed that all SRPLA rods retained their initial shear strength virtually unchanged up to 90–36 weeks, but thereafter the composite strength decreased rapidly. After 52 weeks of degradation testing, the composite appeared to have 16% of initial shear strength in comparison to TCP/SRPLA that managed to retain about

60–70% of the initial value. Kobayashi and Yamadi [84] used conventional tensile testing to study the strain rate dependancy of mechanical properties of β-TCP/(PLLA). They used rectangular specimens of the produced using injection molding technique and then immersed in SBF for 8, 16, and 24 weeks before testing. They found that the modulus and strength increased with strain rate, but that soaking reduced these increases.

Suwanprateeb *et al.* [85] used flexural testing to study the influence of three-dimensional printing fabrication technique for bioactive HA/bis-GMA (bisphenol A-glycidyl methacrylate) based composite.

In the field of tissue engineering, among other parameters that need to be considered in scaffold fabrications is that they should have appropriate and controllable mechanical properties, for example, elastic constants and compressive strength to provide sufficient temporary support for cells to enable tissue regeneration. Lu *et al.* [86] developed a three-dimensional porous composite of PLAGA and 45S5 BG (PLAGA–BG composite) scaffold for bone tissue. Compression testing showed that adding the BG granules to the composite yielded higher compressive modulus than PLAGA alone. Blaker *et al.* [87] performed similar compression testing to study the mechanical properties of highly porous PDLLA/Bioglass produced by TIPS technique. Compression tests were performed axially and transversely from 2 to 300 kPa. They also used DMA to establish the storage modulus (E'), loss modulus (E''), and mechanical loss tangent (tan δ). Results indicated that mechanical anisotropy was controlled by the direction of the macropores.

Microhardness studies, using a Vickers diamond indenter, were carried out by Sousa and colleagues [82] to investigate the structure development and interfacial interaction of preferred orientation in HDPE/HA composite. In the latter study, they investigated the influence of the processing on the mechanical performance of HA-reinforced biodegradable starch-based blends and HDPE [93].

IN VITRO BIOACTIVITY AND BIOCOMPATIBILTY TESTING

The biocompatibility of materials is an essential property for their use inside or in contact with the human body. Materials must to be nontoxic but should act as a substrate to promote cell spreading and growth in certain applications, while in other applications, the surface should prevent cell attachment. The second requirement is bioactivity. *In vitro* bioactivity testing was initiated by Kokubo *et al.* [7] who showed that materials that are bone bioactive *in vivo* will develop a hydroxy-carbonate apatite (HCA) layer when placed in a SBF, which has similar ion levels as those of blood plasma. This work was extended by Hench [88,89] who defined a bioactivity index based on the inverse of the time to get the entire surface of the biomaterial covered with an HCA layer (Fig. 7). Hench compared various formulations of Bioglass particles to find the highest bioactivity formulation. In composites work, Huang *et al.* [90] used this technique to compare 20 and 40 vol% Bioglass in PE and showed that after seven days the HCA layer had covered almost all the surface of the composite, while with only 20 vol% Bioglass very little of HCA layer has progressed beyond from the particles onto the PE (Fig. 6). Maquet *et al.* [56] manufactured foams of PDLLA reinforced with Bioglass particles as bone tissue scaffolds. The *in vitro* bioactivity results showed the rate of apatite deposition both on the surface and throughout the foams increased with increasing Bioglass content. At the same time, they also found some apatite deposition on the nonfilled PDLLA foams.

In vitro evaluation of the biocompatibility usually provides initial screening often using cell lines to minimize the variability in terms of metabolism, distribution, absorption and to maximize the cell response to possible toxicity reaction that may have. The results of *in vitro* testing of bioactive materials can indicate whether the material increases the response of the cells to the material, that is, it is bioactive as well as whether the material is biocompatible. Two types of cells are used: immortalized cell lines are obtained from either malignant tumors or where a cell line has been transformed and primary cells are obtained from people or animals and then grown up. The immortalized cells can be grown up and divided and grown up again an infinite number of times (each step being called a passage) so that they are convenient to use, but they are pathological cells. In contrast, primary bone cells are commonly harvested from discarded femoral heads after hip replacement, and so are considered normal cells but suffer from variability depending on age, gender, etc. of the individual from which they are taken. Furthermore, they can only be used for a limited number of passages

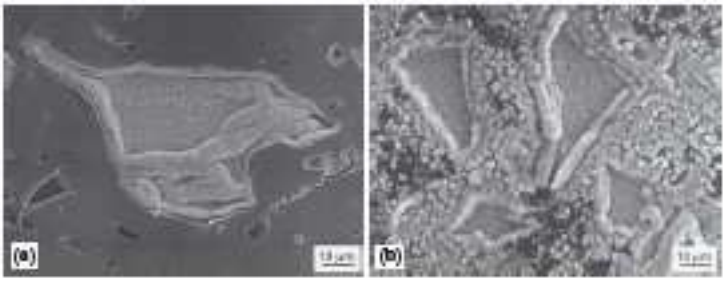

Figure 7. The formation of HCA layers on (a) 20% and (b) 40% Bioglass/HDPE composite after seven days in SBF. Source: From Huang *et al.* [90].

as they differentiate from their cell type after a number of passages. A wide range of materials have been investigated both for bioactivity and biocompatibility; some of these studies are described below.

Ehmer and coworkers [91,92] produced a porous material using a methacrylate-modified oligolactide polymer network and phosphate-based glasses in the system P_2O_5–CaO–MgO–Na_2O–TiO_2. These glasses were used to reinforce 10 wt% methacrylic acid 2-hydroxyethylester (pHEMA) copolymer at ~1:3.0 polymer-to-glass weight ratio. The porous structure was produce through the salt leaching method. *In vitro* cell culture testing was carried out using the MC3T3-E1 osteoblast cell line. They reported that the materials was nontoxic and biocompatible.

The foams produced by Maquet *et al.* [56] were later tested by Blaker *et al.* [93] *in vitro* cell culture using the osteosarcoma (bone cancer) line MG-63 for up to eight days. In cell culture studies, the osteosarcoma cells were deposited on the outer layer of the foam. They reported that the highest cell count was from 6 wt% Bioglass foams, but overall good attachment to the materials was found.

In vitro testing using three different cell lines, macrophages, osteoblasts, and osteoclasts, were used to study the biocompatibility of the PHBV composite filled with 40–60 wt% HA or TCP [94]. The three cell lines used cover those cells that are involved in the inflammatory response to materials, bone deposition, and bone resorption, respectively. The results showed that the addition of bioactive calcium phosphates enhances the cell response. In the macrophage study, they found low inflammatory responses with the reinforced materials with a slightly higher response with the nonfilled PHBV. The osteoblast study, that is, using cells involved in bone deposition, showed that plain HA or PHBV filled with HA produced more calcium and more mineralization than unfilled PHBV or when filled with TCP. In the osteoclast-like cells study, the cells attached to the composite were seen to be active but unable to resorpt the materials. In contrast, resorption pits were observed on samples of bone.

IN VIVO BIOCOMPATIBILITY TESTING

Full *in vivo* biocompatibility testing involves tests such as irritation, intracutaneous reactivity, systemic toxicity (acute toxicity), subchronic toxicity, genotoxicity (affects later generations), hemocompatibility (i.e., blood compatibility), chronic toxicity, carcinogenicity (cancer causing), biodegradation, and immune response [2]. If an entirely new material is developed, it will need to undergo the full set of tests; however, for composite biomaterials, usually the individual component materials have been tested. Therefore, for a composite that has undergone *in vitro* testing, the *in vivo* test is usually to assess the response to the material when in a body and under mechanical loading. The *in vivo* study allows long-term investigation of the biofunctionality in the complex biological environment before proceeding with clinical testing. As it involves animal implantation testing, it has to comply all aspects of legal rules and ethics on animal experimentation of the country concerned.

Shikinami and Okuno [43] successfully developed high modulus HA/PLLA rods, which was later used by Furukawa and colleagues [95,96] for *in vivo* testing in rabbits both subcutaneously and in the femoral medullary cavity. The HA was either calcined, to increase the crystallinity, or noncalcined. The subcutaneous implantation was used to observe the materials degradation behavior. After 52 weeks, the reduction of the molecular weight was reported to be less than 10%; however, the bending strength remained high enough to provide sufficient mechanical support to the system. In their second study, initial intermedullary implantation was studied between 2 and 26 weeks. They reported a fibrous layer surrounding the implants of nonreinforced PLLA, while the reinforced composite exhibited bone contact by two weeks and the amount of contact gradually increased. More bone contact was observed in 40 wt% than that in 30 wt% HA composites and those composites filled with the uncalcined HA. In the third paper [97], they reported that after four years *in vivo* testing the diameter of the rods has reduced to 77% of their original cross section. While after six or seven years, in some sections there was no material remaining; it was also observed that bone had replaced the lost composite. *In vivo* studies very rarely run beyond even one year because of the short life span of rabbits; thus, over seven years in these studies are probably unique.

Nurhi *et al.* [98] evaluated biological reaction to the bioactive composite and the biologic behavior of a poly(ε-caprolactone-co-DL-lactide) composite filled with 40 or 60 wt% BG implanted in the long bones of rabbits for 8 and 16 weeks. In eight weeks, the implants were covered with fibrous capsule and no direct contact with bone was observed. After 16 weeks, the capsule had thinned in all samples with bone ingrowth observed, indicating that the materials is compatible with the bone tissue. Similar findings were later reported by Ranna and coworkers [99] when implanted in rat subcutaneous tissue.

A large animal model, the sheep, was used to test a tissue engineering scaffold manufactured using supercritical processing of a PLLA β-TCP composite with similar structure as that of cancellous bone [100]. The rationale for a large animal model includes the fact that the mechanical loading is more physiological. Histology and microcomputed tomography were used to assess the bone ingrowth into the implant. Controls were an empty hole and porous HA, and it was found that with the composite at 2 and 4 months, there was fibrous layer surrounding the composite implant that was replaced with bone contact by 12 months, in comparison with the HA implant filled with new bone more quickly.

Liu *et al.* [101] developed a hybrid scaffold of gelatin/nanohydroxyapatite (nHAP) by incorporating human BMP-2 (rhBMP-2) to enhance bone regeneration. Microscopy showed the scaffold to have 3D porous structure and DNA assay test revealed that the structure was noncytotoxic and could promote cell proliferation. *In vivo* testing carried out in a rabbit model indicated good healing of the skull defect after 12 weeks of implantation (Fig. 8).

Figure 8. Comparison of healing after 12 weeks of radial bone defect: (a–c) with no implant in defect, (d–f) with gelatin/nHAP/fibrin scaffold without rhBMP-2 in the defect, and (h–j) gelatin/nHAP/fibrin scaffold with rhBMP-2 repaired the defect. *Source*: From Liu *et al.* [101].

CLINICAL USES

As discussed earlier, the first clinical use of composites was in the form of carbon-fiber-reinforced epoxy resin as fracture fixation plates [15–17]. While Downes *et al.* [21,22] used HA/HDPE composite for orbital floor implants and this material then progressed to extensive use in the shaft of middle ear implants as HAPEX [23,24]. Since 1990, the numbers of publications on fracture fixation in the human hand using bioabsorbable devices have increased. SR-PLLA pins (diameter 1.5 or 2.0 mm) [104] were used in clinical studies for the fixation of small fragment fractures and osteotomies. It was reported that in 27 patients, uneventful recovery of the function was accomplished in four fractures of the metacarpal and three of the proximal phalanx [103]. Arnia *et al.* [102] reported that in 26 cases of digital replantation using intramedullary SR-PLLA rods, no cases of nonunion or infection occurred. However, in one patient transient bone resorption occurred. They summarized that the intramedullary bioabsorbable rods gave stable, simple, and effective osteosynthesis in digital replantation. Bioabsorbable pins and screws can be used to stabilize fusions. Rokkanen *et al.* [106] wrote that in rheumatoid arthritis patients, bioabsorbable polymers (such as PLLA) with slow degradation are preferred. SR-PLLA pins with cross section of 1.5–2.0 mm were observed to provide stable fixation for 18 interphalangeal, metacarpophalangeal, and carpometacarpal arthrodeses when tested in patients with rheumatoid arthritis [104]. No complications were observed and the authors concluded that the results were comparable with earlier studies on use of metal implants. Furthermore, in the same study, 18 wrist joints were fused uneventfully with 2.2 mm SR-PLLA pins and only one patient reported a superficial infection postoperatively.

Park *et al.* [105] evaluated the clinical use of PLDLLA 70/30 bioresorbable implants in the cervical spine, that is, the neck (Fig. 9). The devices were implanted in 26 patients with an average age of 50.7 years. The patients underwent fusion one or two invertebral discs with allograft and fitted with 1-mm-macropore bioabsorbable plate and screws and followed up for up to two years. At average 14 months after the surgery, 96.2% of the patients achieved good radiographic fusion with no apparent sign of soft tissue reaction. Vacarro *et al.* [106] used the same plate and screw on nine patients with degenerative and traumatic disc herniations. In 77% patients, a solid fusion was seen when radiographically examined after six months. Clinical evaluation was repeated at 32 months of follow-up, and no soft tissue inflammatory or clinical complications were recorded.

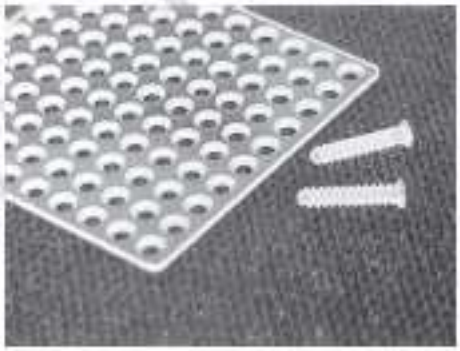

Figure 9. Macropore bioabsorbable sheet and screw of 70:30 PLLDLA polymer. *Source*: From Park *et al.* [104].

Composites have been developed that have been used in patients since the 1970s; the early composites, such as carbon-reinforced epoxy [15–17], were used in a few patients and then were either too complex to use or had insufficient advantages over similar devices manufactured of more conventional metal implants. One composite material, HAPEX, did enter extensive clinical use but owing to low mechanical properties could only be used in the orbital floor or middle ear implants. However, it did show that

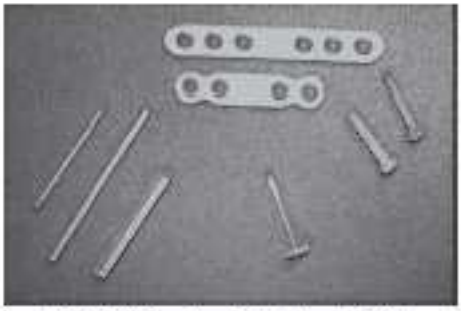

Figure 10. Self-reinforced poly-L-lactide (SR-PLLA) and self-reinforced poly-L/DL-lactide (SR-P(L/DL)LA) miniplates, pins (diameter 1.5, 2.0, and 3.2 mm), tacks, and screws (diameter 2.0 and 1.5 mm) for bone fixation in the hand. *Source:* From Wurie *et al.* [107].

the use of composites allowed bioactivity to be combined with the ductility of polymeric phases.

The conventional composite production techniques such as the development of prepregs and then compression molding have been applied to biomaterials and have allowed the production of composites with higher mechanical properties [49–53]. Self-reinforced PLA composites have entered extensive clinical use (Fig. 10).

The latest developments in composites are as bioactive scaffolds for bone tissue engineering. There are a series of new composites under development and in various stages of testing from *in vitro* through to clinical trials. It is hoped that in the next few years some of these will come into general use.

Composites based on the application of conventional materials production techniques to biologically compatible materials have been used since the 1970s. Their application is gradually increasing because of the benefits of modulus compatibility with the materials they are replacing and the bioactivity of the some of the individual materials used in the composite manufacture. Both degradable and nondegradable materials can be manufactured depending on the starter materials. Optimization of the filler content and processing regime should be used to optimize both the mechanical and biological properties. The applications can run from low modulus porous degradable scaffolds containing bioactive molecules used for tissue engineering to high modulus (for a composite) nondegradable implants owing to permanently replace a lightly load bearing bone. Currently, no composite material has been used successfully to replace a major load bearing bone, but that is only a matter of time.

REFERENCES

1. Williams DF. Williams dictionary of biomaterials. Liverpool: Liverpool University Press; 1999.
2. Anderson J. An introduction to materials in medicine. San Diego (CA): Elsevier Press; 2004. pp. 296–304.
3. Martini FH. Fundamentals of anatomy and physiology. Singapore: Prentice Hall; 2007.
4. Benfield W, Grynpas MD. Nature 1977;270:453–454.
5. Currey JD. Proc Inst Mech Eng [H] J Eng Med 1998; 212-H:309–412.
6. El Haj AJ, Cartmell SH. Proc Inst Mech Eng [H] J Eng Med 2010;224-H:1623–1632.
7. Kokubo T, Kushitani H, Sakka S, *et al.* J Biomed Mater Res 1990;24:721–734.
8. Alcock B. In: Ambrosio L, Tanner KE, editor. Biomaterials for spinal applications. Cambridge: CRC Woodhead; 2012. Chapter 2. In press.
9. Gloria A, Causa F, De Santis R, *et al.* J Mater Sci Mater Med 2007;18:2159–2168.
10. Gloria A, De Santis R, Ambrosio L, *et al.* J Biomater Appl 2011;25:705–810.
11. Sovalani MM, Hao L, Zhang Y, *et al.* Proc Inst Mech Eng [H] J Eng Med 2007;221-H:873–886.
12. Tan KH, Chua CK, Leong KF, *et al.* Biomaterials 2003; 24:3115–3123.
13. Abu Bakar MS, Cheang P, Khor KA. Mat Sci Eng A 2003;348:85–93.
14. Suringer W, Nohauer-Huhmann I, Knosp E. Acta Neurochir 2002;144:1193–1203.
15. Hastings GW. Composites 1978;9:193–197.
16. Bradley JS, Hasting GW, Johnson-Nurse C. Biomaterials 1980;1:38–40.
17. Ali MS, French TA, Hasting GW, *et al.* J Bone Joint Surg Br 1990;72-B:886–891.
18. Al-Sharvi AK, Smith SP, Anderson GH. J Arthroplasty 2002;17:320–324.
19. Benfield W, Grynpas M, Tully AE, *et al.* Biomaterials 1981;2:188–196.
20. Wang M, Porter D, Benfield W. Br Ceram Trans 1994;93:91–96.
21. Downes RN, Vardy S, Tanner KE, *et al.* In: Benfield W, Hastings GW, Tanner KE, editors. Bioceramics 4 - proceedings of the fourth international symposium on ceramics in medicine. Oxford: Pub Butterworth-Heinemann Ltd; 1991. pp. 239–246.
22. Tanner KE, Downes RN, Benfield W. Br Ceram Trans 1994;93:104–107.
23. Goldenberg RA, Driver M. Otolaryngol Head Neck Surg 2000;122:835–842.
24. Meijer ACW, Segenhout HM, Albers FWJ, *et al.* ORL 2002;64:173–179.
25. Joseph R, McGregor WJ, Martyn MT, *et al.* Biomaterials 2002;23:4295–4302.
26. Joseph R, McGregor WJ, Martyn MT, *et al.* Polym Eng Sci 2002;42:326–335.
27. Ladizesky NH, Ward IM, Benfield W. Polym Adv Technol 1997;8:496–504.
28. Ward IM, Benfield W, Ladizesky NH. Polym Int 1997;43:333–337.
29. Benner M, Saunders LS, Ward IM, *et al.* J Mater Sci 2002;37:325–334.
30. Ladizesky NH, Pirhonen EM, Appleyard DB, *et al.* Compos Sci Technol 1998;58:419–434.
31. Reis RL, Cunha AM, Oliveira MJ, *et al.* Mater Res Innov 2001;4:263–272.
32. Sousa RA, Reis RL, Cunha AM, *et al.* J Appl Polym Sci 2002;86:2866–2872.

97. Hasegawa S, Ishii S, Tamura J, *et al*. Biomaterials 2006;27:1327–1332.
98. Narhi TO, Jansen JA, Jaakkola T, *et al*. Biomaterials 2003;24:1697–1704.
99. Ranta T, Tirri T, Yli-Urpo A, *et al*. J Biomat Compat Polym 2007;22:249–264.
100. van der Pol U, Mathieu L, Zeiter S, *et al*. Acta Biomaterialia 2010;6:3782–3792.
101. Liu Y, Lu Y, Tian X, *et al*. Biomaterials 2009;30:6276–6286.
102. Arata J, Ishikawa K, Sawabe K, *et al*. Ann Plast Surg 2003;50:350–355.
103. Bokkanen PU, Böstman O, Hirvensalo E, *et al*. Biomaterials 2000;21:2607–2613.
104. Juutilainen T, Patiala H. Scand J Rheumatol 1998; 24:228–231.
105. Park MS, Aryan HE, Ozgur BM, *et al*. Neurosurgery 2004;54:631–636.
106. Vaccaro AR, Sahni D, Pahl MA, *et al*. Spine 2006; 31:2091–2094.
107. Waris E, Ashammakhi N, Kaarela O, *et al*. J Hand Surg 2004;29B(6):600–606.

FURTHER READING

Johnson AJW, Herschler BA. Acta Biomate 2011;7:16–30. DOI: 10.1016/j.actbio.2010.07.012.
Tanner KE. Proc Inst Mech Eng [H] 2010;224-H:1359–1372. DOI: 10.1243/09544119JEIm823.
Tanner KE. In: Wuisman PIJM, Smit TH, editors. Degradable polymers for skeletal implants. Cambridge: Pub Nova; 2009. pp. 73–93.
De Santis R, Guarino V, Ambrosio L. Composite materials for bone repair. In: Planell JA, Best SM, Lacroix D, *et al*., editors. Bone repair biomaterials. Cambridge: Pub Woodhead CRC; 2009. Chapter 9.

COMPOSITES FOR SPACE LAUNCHERS

Massimo Mazzola and
Marco Biagioni
AVIO s.p.a., Torino, Italy
Luca Mazzola
University "Roma Tre",
Roma, Italy

INTRODUCTION

Composites on Launch Vehicle: History

In the beginning of the space era, the necessary requirements of lightness and strength for launch of vehicle structures were fulfilled using light-weight metallic alloys based on technology developed by the aircraft industry.

The first rockets developed during and after World War II (WWII) were essentially based on aluminum alloys. The first rocket that opened the space rocket era, the German A4 or V2 Rocket, had a structure based on a metallic framework covered with a light-metal fuselage, whereas heavier parts were mounted on steel frames. Propellant tanks were made out of aluminum–magnesium alloys.

Similar architectures have been used on the vehicles that have been developed subsequently and relied for many years on the same materials.

Glass-fiber-reinforced composites were known since the 1930s. Fiberglass was made almost by accident in 1930, when an engineer became intrigued by a fiber that was formed during the process of applying letters in a glass milk bottle. Commercialization of this new fiber was started in 1937 by Owens Corning Fiberglass Company. It was soon understood that aircraft industries were likely customers for this new type of material, because it would have permitted the creation of new aircraft design and innovative concepts.

One company, Douglas Aircraft, bought the first roll of fiberglass to realize specific tools for aircraft manufacturing using phenolic resin, which was the only suitable adhesive available at that time. Not long afterwards, unsaturated polyester resins became available, and they became the preferred resins because of the relative ease in curing compared with phenolics. High performance resin systems became available with the invention of epoxies in 1938.

During WWII, the use of composites increased not only for aircraft manufacturing tools but also for some applications for aircraft's structural or semi structural parts. One of the first applications was on engine ducts. They are the last parts to be designed, so that their design could be adapted to the design of other parts. This led to very complex shapes that were very difficult to realize in metal but were quite easy for composites. Other WWII applications included engine nacelles and radomes, because they assured structural strength and radar transparency. Some applications on airplane wings were also recorded at that time.

At the Wright-Patterson Air Force Base in 1943, exploratory projects were launched to build structural aircraft parts from composite materials. This resulted in the first plane with GFRP fuselage being flown on the base one year later.

From the mid-1950s, glass-fiber-reinforced composite materials have been introduced in the aerospace industry starting from the use on gliders by the Japanese. Glass fibers are strong but not stiff enough to be used in high speed aircraft, so their utilization in rocket structures was even more difficult. At that time, the search for stiffer fiber-reinforced composites started in several countries. Laboratory scale production of high strength carbon fibers was reported in 1962 at Royal Aircraft Establishment, Farnborough, UK. In the United States, Union Carbide developed high modulus continuous carbon fibers in 1968. High strength graphite fibers were developed at the Governmental Industrial Research Institute of Osaka, Japan in 1969. Before the end of the 1960s, full scale commercial production of carbon fibers (PAN based) had started. Very high modulus boron fibers were also introduced during this period. High strength, low density organic fibers, Kevlar 49, were also marketed by Dupont., USA during